Neogene to Quaternary tectonics of the Garlock Fault and the Eastern California shear zone in the northern Mojave Desert, California

By

William Michael Rittase
B.S. University of North Carolina at Chapel Hill, 2004
M.S. University of Nevada, Las Vegas, 2007

Submitted to the graduate degree program in Geology and the Graduate Faculty of the University of Kansas in partial fulfillment of the requirements for the degree of Doctor of Philosophy.

_____
Chairperson, Dr. J. Douglas Walker

_____
Dr. Michael H. Taylor

_____
Dr. Daniel Fritz Stockli

_____
Dr. Anthony W. Walton

_____
Dr. Xingong Li

Date Defended: November 29, 2012

The Dissertation Committee for William Michael Rittase
certifies that this is the approved version of the following dissertation:

Neogene to Quaternary tectonics of the Garlock Fault and the Eastern California shear zone in the northern Mojave Desert, California

_____

Chairperson, Dr. J. Douglas Walker

Date Approved: December 12, 2012

ABSTRACT

This study investigates the late Tertiary and Quaternary tectonic, structural and sedimentologic history of the central Garlock fault (GF) in Pilot Knob Valley (PKV) and southwestern Searles Valley, and its interactions with the cross-cutting Eastern California shear zone (ECSZ). The interaction of these two active, orthogonally striking strike-slip fault systems has long been somewhat of a tectonic enigma. However, this work provides considerable insight into how the kinematic and structural relationships between these structures have evolved since ~5 Ma. This in turn, furthers our understanding of how the North American-Pacific transform plate margin evolves over thousand to million-year timescales.

The first contribution of this dissertation is the idea that the central GF is shown herein to have experienced large temporal variations in strain release since the late Pleistocene. A long-term, late Pleistocene slip rate of 5-7 mm/yr (e.g., McGill and Sieh, 1993) is comprises a ca. 13.2-4 ka period of low slip (4.3-5.1 mm/yr) followed by a recent, ca. 4-0 ka, period of elevated slip rate (10.2-14.3 mm/yr). Evidence for elevated slip rates in the late Holocene are from a 3.5-3.2 ka alluvial fan deposit offset 43-50 m against a shutter ridge. Two soil profile development index values and an optically stimulated luminescence age from the deposit establish robust age control. High-resolution, Earthscope™ airborne LiDAR imagery, a boulder levee on the upstream late Holocene deposit, elevation profiles of the site and three hand-excavated trenches establish tight control on fault displacement magnitudes. Periods of elevated strain release on the GF are correlated with higher strain release rates on the San Andreas fault and shortening in the Los Angeles basin, but are anti-phased with the ECSZ (e.g., Dolan et al., 2007).

A second contribution of this dissertation is the stratigraphic reorganization of late Cenozoic sedimentary rocks in PKV and Searles Valley, and the tectonic implications for the

GF, Searles Valley fault and the newly identified Marine Gate fault. Here, a 1000+ m package of exposed Pliocene and Pleistocene strata have been uplifted and tilted to the northeast. Based on new age and provenance data, we adopt the name Pilot Knob Formation to describe much of these rocks north of the GF and east of the Christmas Canyon gate. The Pilot Knob Formation comprises three distinct lithologic members, from oldest to youngest, the Eagle Crags Member, Randsburg Wash Member and Slate Range Member. The Eagle Crags Member is a ~5-3.7 Ma conglomerate, sandstone, siltstone, claystone and evaporite derived from the Eagle Crags volcanic field to the south of PKV. The Randsburg Wash Member is a ~3.7-3.1 Ma siltstone, claystone and evaporite deposit that grades laterally into a sandstone and is locally interbedded with a rockfall deposit. The Slate Range Member is a ~3.1-0.3 Ma sandstone and conglomerate that grades, in the eastern study area, into a siltstone, claystone and evaporite deposit. Sediments comprising the Slate Range Member are derived from the Slate Range north of PKV. Outcrop relations within the Pilot Knob Formation reveal three stages for the post-Miocene tectonic development of PKV. An initial ~5-3.1 Ma stage characterized by an active sinistral-oblique-normal Marine Gate fault and GF, resulting in a transtensional pull-apart basin in northern PKV. A second, 3.1-1.2 Ma, stage of minimal transtension or transpression, corresponding to a cessation of sinistral slip on the Marine Gate fault at ca. 2.5 Ma, and a continuation of sinistral slip on the GF. Finally, a 1.2 Ma-present stage of significant N-S shortening across the northern PKV, as evidenced by uplifted and incised Pilot Knob Formation and younger sediments. Together, these three tectonic stages record the development and evolution of the Panamint Valley fault, located ~20 km east of PKV, since ~3.5-3 Ma.

A third contribution of this dissertation involves quantifying the magnitude of modern N-S shortening in PKV and relating it to decreased slip on nearby strands of the ECSZ (e.g.,

Panamint Valley fault and Paradise fault zone). New detailed neotectonic mapping, Earthscope™ airborne and ground-based LiDAR imagery, and chronology of Quaternary deposits exposed along the GF and Marine Gate fault, including (1) three ^{10}Be terrestrial cosmogenic nuclide (TCN) depth profiles and (2) one soil description, place bounds on the vertical components of recent deformation. A $40.4^{+17.8}_{-10.0}$ ka ^{10}Be TCN profile age for a 16-m-high terrace tread adjacent to the GF (site PKV-1) suggests a differential incision (uplift) rate of 0.40 ± 0.13 mm/yr. A $55.2^{+13.3}_{-11.0}$ ka ^{10}Be TCN profile age from a 12.5-m-high tread located 4.5 km west on the GF (site PKV-5) suggests a differential incision (uplift) rate of 0.23 ± 0.05 mm/yr. A 25.5-m-high terrace adjacent to the southern Slate Range (site PKV-3) was dated using a soil profile development index (PDI) technique. A soil PDI age estimate of ~162 ka brackets the maximum age of uplift, and suggests a minimum uplift rate of ~0.16 mm/yr here. Using these ages and assuming dips on the GF between 90° and 80° to the north, resultant shortening magnitudes of 0-2.2 m and 0-2.8 m at sites PKV-5 and PKV-1, respectively, and 0-0.04±0.01 mm/yr at PKV-5 and 0-0.07±0.02 mm/yr at PKV-1 are estimated. At PKV-3, we estimate the dip of the newly recognized Marine Gate fault to be 70-80° to the south, resulting in 4.4-8.7 m of N-S shortening, suggesting a 0.03-0.05 mm/yr shortening rate. The shortening rate estimated at PKV-1 corresponds to 2-4% of Panamint Valley fault slip rate. Shortening at PKV-1 and PKV-3 can be summed to partially integrate 0.08-0.12 mm/yr shortening between the GF and Slate Range, or approximately 3-7% of Panamint Valley fault slip rate. The presence of numerous active reverse faults between PKV-1 and PKV-3 suggests that this is a minimum estimate.

A fourth contribution of this dissertation is a 1:12,000 scale geologic map of the central GF, northern Blackwater fault, southern Searles Valley fault and the Marine Gate fault. covering approximately 280 km².

Additional contributions of this work include: (1) quantification of the thermal history of the southern Slate Range through apatite and zircon (U-Th[SM])/He thermochronometry, and (2) enhancement of a Mojave-wide soil calibration tool developed and used by Eric Kirby and Eric McDonald that will be useful for future tectonic-geomorphic applications, dating climate-induced surficial processes and archeological dating.

ACKNOWLEDGEMENTS

For the most part, I have thoroughly enjoyed (...hmmm, is that *really* what I want to say?) the rigor and process, as well as the tangential opportunities and experiences afforded to me, of working toward my dissertation at Kansas. I feel that I have developed a more thorough appreciation of my strengths and weaknesses, that I will learn from and call upon in future endeavors. I also feel like I've spent *way* too much time in the Ridgecrest - Trona vicinity of California, to want to travel back there anytime soon! Thirteen months to be exact... I've also spent many a long day, and sleepless nights slaving away in the KU cosmogenic lab, surrounded by *immer kaputt* fume hoods and murky concoctions of lethal acids boiling away at scalding temperatures. Thus, I desire to share the conclusion of this work and my success with the following people:

First, and of greatest importance to me, is my family - father, mother, sister and brother. Next, of course, is my advisor, Dr. J. Douglas Walker, for whom many thanks is owed for his tireless support and passion over the past 6 years. His wisdom and guidance were critical to this work. I also wish to thank my committee, consisting of: Dr. Michael H. Taylor, Dr. Daniel Fritz Stockli, Dr. Anthony A.Walton and Dr. Xingong Li. I have gained valuable experiences from each of you; whether it be from courses and field trips taken, TA assignments with them, or ideas gleamed from their finely tuned noggins. I owe tremendous gratitude to Dr. Eric Kirby, for whom the second chapter would not have been possible. He has been a critical source of ideas and guidance throughout this project, and is a co-PI on the NSF grant that supported me. In a way, he has been a *de facto* committee member of mine. A huge "thank you" is given to Dr. Eric McDonald for his field teachings of desert soil processes and how to recognize them. Obviously, the neotectonic aspect of my project was greatly dependent upon his experienced help, and I'm

humbled to have worked with him. Plus, he is a lot of fun to be around and work with, too. Speaking of people who are a lot of fun to be around... I need to thank Dr. John Gosse, for his excellent help with the terrestrial cosmogenic aspect of this research. I learned a lot from my opportunities to be in the field with him. I also must thank him for allowing me to crash in his bed in Bern, Switzerland when I stayed out too late and couldn't make my train back to the hotel that was located some distance outside of town. I'm truly sorry for farting on you in my sleep - hope you kept the window open, LOL! I owe a warm "thank you" to Dr. Frank Monastero and Dr. Andy Sabin, of the Geothermal Program Office at China Lake Naval Air Weapons Station. Without these two, I would never have gained access to the base. There were several shit-heads out there that didn't appreciate what I was trying to do. I also thank both gentlemen for their exceptional enthusiasm (and financial assistance) for my research. While I'm on GPO and China Lake, I'd be remiss if I didn't acknowledge Steve Alm. Now a fellow Geohawk working with Doug, Steve has been a great help over the 5 years that I've traveled to China Lake for field work. It was unbelievable the number of different permitting obstacles he helped me through - thanks, thanks, thanks! I appreciate the help of AJ Herrs with the ground-based LiDAR acquisition and processing – I wouldn't have been able to do it all myself. I have been rescued numerous times by the awesome KU Geology Office staff and student workers - Jenna Coker (for taking care of my plants while away for field work), Yolanda, Gwethalyn (super helpful and all-around awesome person!), Liz, Maria and Sarah. I thank Dr. Bob Goldstein, the former department chair, for forgiving me after the occasional *faux pas* and for the delightful travel stories to Europe that you would freely share. I thank Dr. Don Steeples for his friendship and the chance to TA for him. I thank Dr. Steve Hasiotis for being a great friend, as well as his cheerful help to make me a better scientist. The same can be said for Dr. Gene Rankey (the word of the

day is "fertig"). I thank Dr. Diane Kamola for the awesome KU Colorado Plateau field trip my first semester at KU, and for helping me track down my advisor from time to time. I need to thank Dr. Andreas Möller for his help with various isotopic questions, his friendship and killer sense of dry humor! It is with regret, that I must mention here, how I still miss your wife Dr. Beate Mocek, who provided me with endless entertainment and support in the cosmo lab. I was lucky to have known her while I could, and I have fulfilled a secret promise to her, which would make her smile... in her dark, witty Germanic way. Up next is the super-duper *grande señor jefe* Dr. Luis González. A most wonderful and cheerful of Puerto Ricans, who always ran for cover when I'd come down to office to stir up trouble (just kidding, of course). My time at Kansas was innumerably bettered by my friends in the department and outside. I'd like to thank Zhaoqi Li for allowing me to travel with him to China in 2011. And finally, I have been truly blessed to have finally gotten the chance to know Pei-Ling Lin, my girlfriend. Thanks for ignoring me in the hallway those previous 4 years (by the way)! But being with you this past year has been one of the best things to have happened to me in life. :-)

TABLE OF CONTENTS

LIST OF FIGURES

LIST OF TABLES

LIST OF APPENDICES

LIST OF PLATES

This Page Intentionally Left Blank

DISSERTATION

CHAPTER 1

DISSERTATION INTRODUCTION

Active continental transform margins are intriguing places to study for a variety of reasons. They serve as an analog for understanding processes that shaped extinct margins throughout the world. These margins are far from simple in terms of their geometry, mechanics, kinematics and strain. This second aspect is a function of the naturally existing heterogeneities within the lithosphere (e.g., rock type, existing tectonic structures, thermal properties). In theory, transform faults should neither create nor destroy crust. But where changes in strike and/or stopovers occur, localized regions of transpression and transtension will dominate. Currently, the southwestern USA Cordillera is dominated by dextral transform faulting in California and western Nevada. Here, deep pullapart basins (i.e., Death Valley and Salton Trough) are located in close proximity and along the same structures that are responsible for great convergence (i.e., Avawatz Mountains and Transverse Ranges). In this dissertation, it is shown that Pilot Knob Valley is a hybrid of transtension and transpression. A third intriguing aspect of transform margins is that their geometry greatly affects strain-release cycles over geologic time. A multi-stranded and parallel transform system, as is found in California and western Nevada, is thought to be more conducive towards transient strain accumulation and release cycles (Rockwell et al., 2000; Dolan et al., 2007) than would a single-fault transform system (e.g., Dead Sea transform).

OVERVIEW OF THE DISSERTATION

This thesis is presented in four chapters. The first chapter is organized in a way to "lightly" acquaint the reader with the importance of strike-slip faults in local and regional tectonic context,

and to serve as an introduction to the subsequent three chapters that cover specific aspects of this study of the Garlock fault. One plate and several appendices present supplementary information that fosters greater understanding of the data and ideas presented in this dissertation, too.

Chapter two discusses the results of a study on an offset late-Holocene alluvial channel in Pilot Knob Valley and the implications for time-variant slip rates. Plate 1 is supplementary to this study and directly addresses a concern raised by Dr. Mike Oskin as to the relation of the late Holocene debris flow and the shutter ridge, and the relative age of the bevel on the shutter ridge. Appendix A serves to date the shutter ridge and provide a published control point for the soil PDI chronofunction. Appendix B presents data from a Mojave-wide soil PDI chronofunction developed by Eric Kirby and Eric McDonald and applied to two soil pits excavated into the late Holocene alluvial deposit. Appendix C contains OSL data that provides a quantitative age constraint on the late Holocene unit.

Chapter three discusses the results of a study of the Pliocene and Pleistocene sedimentation patterns in Pilot Knob Valley and the implications for basin development and the structural and kinematic evolution of the Garlock fault and Marine Gate fault. Appendix D is supplementary to chapter three and presents five tephrochronologic samples that bracket deposition of the newly named Pilot Knob Formation.

Chapter four discusses the results of a study on the uplift and north-south shortening in northern Pilot Knob Valley during the late Pleistocene and Holocene. This chapter explores the modern interaction of the Eastern California shear zone with the Garlock fault and the role of north-south shortening across it.

A full-size geologic map of the study area cannot be included herein due to dissertation figure size limitations, but this data will serve as a future stand-alone publication with GSA

Maps and Charts. Appendix E presents the current results of ongoing (U-Th[Sm])/He thermochronology work in the southern Slate Range that has been, more or less, a "post doc" added on during the 5th year of this dissertation project per request of the Geothermal Program Office at China Lake. This data will be expanded into a future manuscript by this author.

REFERENCES

Dolan, J.F., Bowman, D.D., and Sammis, C.G., 2007, Long-range and long-term fault interactions in southern California: Geology, v. 35, p. 855-858, doi: 10.1130/G23789A.1.

Rockwell, T.K., Lindvall, S., Herzberg, D., Murbach, D., Dawson, T., and Berger, G., 2000, Paleoseismology of the Johnson Valley, Kickapoo, and Homestead Valley faults: Clustering of earthquakes in the Eastern California shear zone: Bull. Seis. Soc. Am., v. 90, p. 1,200-1,236.

CHAPTER 2

TEMPORAL VARIATIONS IN HOLOCENE SLIP-RATE ALONG THE CENTRAL GARLOCK FAULT, PILOT KNOB VALLEY, CALIFORNIA

William Rittase [1]

Eric McDonald [2]

Eric Kirby [3]

J. Douglas Walker [1]

John Gosse [4]

Joel Spencer [5]

[1] University of Kansas

[2] Desert Research Institute, University of Nevada Reno

[3] Pennsylvania State University

[4] Dalhousie University

[5] Kansas State University

ABSTRACT

Average geologic slip rates along the Garlock fault (GF), in eastern California, during the Late Pleistocene and Early Holocene exceed present-day rates inferred from geodetically constrained block models by a factor of 2–3. New evidence from neotectonic mapping along the central GF in Pilot Knob Valley argues for a period of rapid slip rate during the late Holocene. Truncation of a late Holocene alluvial fan deposit against a shutter ridge composed of older alluvium requires a minimum of 36-42 m of displacement since deposition of the fan; maximum allowable displacement is 43-50 m. Soil profile development indices (PDI) from two depth profiles and optically stimulated luminescence (OSL) ages bracket debris flow deposition on the fan between 3.5-4.2 ka. Together, these data indicate that late Holocene slip rates along the central GF have ranged between 8.6-14.3 mm/yr, with a preferred rate of 10.2-14.3 mm/yr. Our results, in conjunction with previous estimates of displacement over the past 15 ka, require significant temporal variations in strain release along the GF. Thus, our results support hypotheses that suggest alternating periods of activity and quiescence along the various components of the North America-Pacific transform boundary.

INTRODUCTION

The temporal evolution of strain accumulation and release along intracontinental fault systems reflects a complicated interplay among far-field loading due to relative plate motions, short-term changes in postseismic static stress (e.g., Stein et al., 1992; Stein, 1999), mechanical interactions between fault strands (e.g., Nicol et al., 1997) and variations in rheology of crustal material (Furlong, 1993). Recent high-resolution records of fault behavior provide mounting evidence that such interactions give rise to time-dependent slip histories along fault networks

(e.g., Rockwell et al., 2000; Nicol et al., 2006), yet the exact nature of these interactions remains obscure. In eastern California, recent studies of slip rate and paleoearthquakes along N-NW trending dextral faults reveal slip and paleoseismic histories that are strongly variable in time and appear to reflect clusters of co-seismic events (Rockwell et al., 2000; Oskin et al., 2008; Ganev et al., 2010); such behavior has been variously attributed to alternations in activity among a conjugate fault system comprising the eastern California shear zone (ECSZ) and the Garlock fault (GF) or between such faults and the plate boundary (e.g. San Andreas-Los Angeles Basin) (Dolan et al., 2007). Although the irregular paleoseismic records along the GF (e.g., McGill and Rockwell, 1998; Dawson et al., 2003) are consistent with the expectation that the GF should exhibit time-variable slip, current estimates of the slip rate along the GF rely on markers of Late Pleistocene and Early Holocene age (McGill and Sieh, 1993; McGill et al., 2009; Ganev et al., 2012) and thus only provide average values over timescales ranging from 8 – 14 ka.

Here we utilize newly acquired, high-resolution topographic data from airborne laser swath mapping (ALSM) to reconstruct the slip history along the central segment of the GF over intervals of time that more closely approach those of paleoseismic clusters. Along the southern margin of the Slate Range, in Pilot Knob Valley, sinistral displacement of a shutter ridge truncates a Late Holocene alluvial fan across the trace of the fault. We use optically stimulated luminescence (OSL) dating and the degree of soil development to place absolute age estimates on the deposition of the fan. Our results require that slip-rates along the GF must have varied by a factor of two between the early and late Holocene. If all slip was released co-seismically, our results imply that past seismic events must have been strongly clustered in time.

GEOLOGIC SETTING

Transcurrent deformation along the North America-Pacific transform plate boundary is accomplished by dextral slip along the San Andreas fault system and distributed shear along a network of dextral faults in the Mojave Desert and east of the Sierra Nevada (Fig. 2.1) that comprise the ECSZ. Embedded within this deforming crust is the GF, a 250 km long sinistral strike-slip fault that cuts across the northwest-trending ECSZ and terminates against the San Andreas system near Fort Tejon, California (Fig. 2.1). The nature of the interaction between distributed shear in eastern California and slip along the GF, however, remains enigmatic. The ECSZ accommodates approximately 10-14 mm/yr (~25%) of the relative motion between the Pacific plate and stable North America (Bennett et al., 1999 and 2003). Budgets of geologic slip rates determined over late Pleistocene timescales (~50 – 100ka), however, are spatially variable; north of the GF, the sum of slip rates across the Death Valley, Hunter Mountain and Owens Valley fault systems could be as high as 8 – 10 mm/yr (Frankel et al., 2007), whereas rates south of the GF in the Mojave Desert appear to be 4 – 8 mm/yr (Oskin et al., 2008). Moreover, fault systems of the ECSZ terminate both north and south of the GF (Oskin and Iriondo, 2004; Numelin et al., 2007) and do not appear to significantly disrupt the western and central segments of the fault system (e.g., McGill and Sieh, 1991).

Despite the continuity of the GF, shear associated with the ECSZ clearly passes across the fault (Savage et al., 1990; Miller et al., 2001). This shear could be accommodated by progressive rotation of the GF (Savage et al., 2001; Gan et al., 2003; Guest et al., 2003), or it may be accommodated by oscillating strain release along interacting, conjugate fault networks (e.g., Peltzer et al., 2001). The latter hypothesis finds support in recent compilations of paleoseismic records (Rockwell et al., 2000) that appear to show that ECSZ faults exhibit

moment release that is anti-phased with respect to faults in the LA basin (Dolan et al., 2007). Understanding the nature of interaction among the ECSZ, the GF and the San Andreas is thus a key goal of refined slip histories along each of these systems.

McGill and Sieh (1991) divided the GF into three structural segments based on changes in strike and the occurrence of stepovers: (1) a western segment striking NE, west of Koehn Lake; (2) an ENE-striking central segment between Koehn Lake and the Quail Mountains; and (3) an E-striking eastern segment east of the Quail Mountains. The three different orientations of these segments, with respect to the current regional stress field, facilitate higher slip rates to the west decreasing to perhaps zero in the east (e.g., Bennett et al., 2003; Mead and Hager, 2005; Chuang and Johnson, 2011).

McGill and Sieh (1993) proposed a 5-7 mm/yr Holocene slip rate for the central GF based on a ~13.2 ka (11,200 ^{14}C yr B.P. preferred age, calibrated with U-Th time scale [e.g., Bard et al., 1990]) highstand shoreline that is offset ~90 m in western Pilot Knob Valley-southern Searles Valley. Dawson and others (2003) revisited an earlier paleoseismological study (McGill and Rockwell, 1998) at Iron Canyon/El Paso Peaks near US-395 and documented 6 "well-resolved" events on the central GF since ~7 ka. They noted an irregular clustering of surface-rupturing earthquakes with 215 - 3300 year intervals. Four events occurred during the last 2 ka and the oldest two are bracketed between ~4 and ~7 ka. An intervening ~3 ky interval between events 4 and 5 shows no evidence for surface-rupturing earthquakes in the trench. Apparent clustering of paleo-earthquakes directly suggests the possibility of irregular slip histories for nearby sections of the GF.

Along the western GF, where slip-rates are expected to be higher, McGill and others (2009) used displaced Late Pleistocene and Holocene alluvial fans to reconstruct slip rates of 5.3-10.7

mm/yr at Clark Wash (Fig. 2.1). A 5.3-9 mm/yr slip rate may be a more appropriate estimate at Clark Wash based on subjective underweighting of maximum channel offset probabilities (S. McGill 2009, personal communication). Clark and Lajoie (1974) also suggested a 4.5-6.1 mm/yr Holocene slip rate for the western GF in Koehn Lake, but their evidence and site location are less ideal than at Clark Wash for capturing all slip.

Together, these studies suggest that the average rate of slip of the central and western GF segments since ~13.2 ka is 5-9 mm/yr. However, geodetic strain accumulation rate estimates of 0-3 mm/yr (Bennett et al., 2003) are much lower than geologic slip rates, and suggest a complicated strain release cycle. An important task is to thus identify younger offset surfaces and deposits that may record temporal clustering of coseismic events, to bridge the gap between geodetic and existing geologic slip rate estimates for the GF. Here we test the hypothesis of a time-dependent GF strain release history using our new, higher slip-rate estimate from a late Holocene offset in Pilot Knob Valley.

SITE DESCRIPTION AND DATA

We studied fault displacement of alluvial deposits and surfaces along the GF in Pilot Knob Valley. Along the southern flank of the Slate Range, left-lateral offsets of numerous generations of alluvial fan surfaces provide constraints on the slip history of the GF (e.g., Helms et al., 2003). We focus on a site located at 117° 12’ 7” W, 35° 33’ 36” N (Fig. 2.2A). The site is located 6 km east of where McGill and others (1993) studied the offset Searles Lake shoreline, and thus our site affords the opportunity to compare slip rates determined over different time intervals. Three small drainages comprise the study area. The western-most and eastern-most washes are active and are labeled “W_a” and “E_a”, respectively (see Table 2.1 for unit descriptions). An older, now

abandoned, channel branches off "W_a" and is labeled "W_i". This inactive channel contains a late Holocene alluvial fan deposit labeled "$Qa3_b$". The $Qa3_b$ deposit is truncated by the GF, and is juxtaposed against a shutter ridge composed of ca. 30 ka alluvium (Fig. 2.2; Appendix A). Notably, a prominent channel levee atop the $Qa3_b$ surface runs nearly orthogonal to the GF and can be traced to within 1-2 meters of the north-facing scarp (Fig. 2.2b).

Deposition of $Qa3_b$ is interpreted to predate most, if not all, of the present-day width of the shutter ridge. Four lines of evidence support this interpretation. First, original bar and swale surfaces that represent the paleo-flow directions during fan deposition are aligned perpendicularly to the shutter ridge. We observe no deflection of bar-and-swale features around the eastern extent of the shutter ridge, as would be expected if the shutter ridge were present during deposition. Second, we observe no decrease in fan slope that would indicate ponding of sediments north of the shutter ridge (Fig. 2.2D, profile A-A'). Third, the relief between bar and swale is up to about 1 m and bars contain abundant clasts > 1-cm in diameter, features associated with deposition during high channel flow and not ponding. If the shutter ridge formed a barrier to flow, one would expect ponding of sediment up against the toe of the north-facing scarp. Fourth, the $Qa3_b$ terrace tread extends, at a minimum, 6 m west of the prominent debris levee and likely to the western channel wall, based on soil excavation pits and surface profiles (Fig. 2.2D, profile B-B'). These relationships indicate that the $Qa3_b$ deposit filled the entire width of the valley and does not represent a younger inset surface or a diachronous tread (e.g., Cowgill, 2007).

Given these relationships, we infer that most of the displacement of the shutter ridge occurred after deposition of the $Qa3_b$ deposit. However, the northeastern corner of the shutter ridge, south of the fault, exhibits an erosional bevel. Because the modern gully, inset against the

$Qa3_b$ deposit, deflects around the nose of the shutter ridge, the original depositional extent of the $Qa3_b$ deposit is somewhat uncertain. The modern gully is only 1-2 meters wide, and so has not strongly modified the original extent of the $Qa3_b$ surface north of the fault. To test whether relict patches of the $Qa3_b$ surface are present beneath colluvium adjacent to the scarp, we hand-excavated renches in two locations across the eroded bevel downstream of the GF. Our observations reveal that all material in the shutter ridge is compositionally distinct from the $Qa3_b$ deposit (Plate 1), and thus we infer that the beveled northeast corner of the shutter ridge is a relatively recent erosional modification. We also excavated a third trench located next to the $Qa3_b$ levee in which we observed $Qa3_b$ deposits overlain by colluvial material derived from the shutter ridge, indicating that $Qa3_b$ was deposited prior to emplacement of the shutter ridge at this location. Overall, we infer that the shutter ridge was not present during deposition of unit $Qa3_b$, and that displacement must have accumulated since $Qa3_b$ deposition.

These relationships allow us to place relatively precise bounds on the amount of slip represented by the width of the shutter ridge. At a minimum, lateral separation between the $Qa3_b$ channel levee (representing the westernmost surface associated with the $Qa3_b$ deposit) and the unbeveled portion of the downstream terrace riser is 36 m (Fig. 2.2). A more likely estimate of 42 m is obtained by considering the western extent of the $Qa3_b$ surface to extend to the western channel wall of W_i (Fig. 2.2). The easternmost preserved extent of the shutter ridge provides a maximum constraint on displacement of 43 – 50 m, when considering the same two markers north of the fault (Figure 2.2). Notably, Helms and others (2003) document a 47-m offset of the eastern E_a channel wall, which is consistent with our maximum restoration (50 m) of the W_i and E_a channels. This might imply minimal lateral erosion of channel walls following $Qa3_b$ deposition.

To evaluate the age of the $Qa3_b$ surface, we employ two techniques; characterization of the degree of soil development (relative to independently dated deposits of Late Holocene age) and direct dating of the burial of fine-grained silt lenses within the deposit.

The depositional morphology atop the deposit (i.e., prominent bar-and-swale, incipient pavement development with loosely packed clasts, and only light varnish and rubification) is suggestive of a relatively young age (e.g., Helms et al., 2003, McDonald et al., 2003). Relative age information provided by local and regional soil characteristics indicate that the $Qa3_b$ deposit is late Holocene in age (Appendix B). The profiles described for the $Qa3_b$ (CLK-1 and CLK-2) are strongly similar for soils formed in several late Holocene deposits dated at between 2.5 and 4.2 ka and that developed under similar soil forming conditions (e.g. climate, parent material). Common characteristics of late Holocene soils include a general horizon sequence of a weak to moderately developed Av (vesicular) horizon, weakly developed Bwk or Bky horizons, stage I carbonate morphology, weakly developed desert pavement, and PDI (profile development index) values of 1.8 to 4.2. By comparison, soils formed on alluvial deposits that are older than about 8 ka have moderately to strongly developed Av, Bwk, Btk, Bky, and Bty horizons, moderate to well developed desert pavement, and PDI values ranging from 7.9 to 44.1 (Appendix B).

A coarse silt lens within the $Qa3_b$ deposit was sampled (OSL-PKV-2) and dated at 3.88±0.36 ka (herein rounded to 3.5-4.2 ka) using OSL dating techniques (Fig. 2.2A) (Appendix C for detailed sample discussion). Soil moisture content and high-resolution gamma spectrometry were used to calculate environmental dose rate. Sample OSL-PKV-2 displayed luminescence characteristics consistent with young, partially bleached alluvial sediments. Additionally, the degree of development for CLK-1 and CLK-2 soils formed on the $Qa3_b$ deposit supports an OSL age of 3.5 to 4.2 ka for deposition of unit $Qa3_b$ (Appendix C).

TECTONIC SIGNIFICANCE

Our results demonstrate that 36-50 m of sinistral displacement has occurred on the central GF in Pilot Knob Valley since 3.5-4.2 ka. These data require slip rates during the late Holocene to have been between 8.6 and 14.3 mm/yr. Our preferred reconstruction of 43 – 50 m implies that slip rates were likely higher, in the range of 10.2-14.3 mm/yr. Notably, minimum allowable slip rate at this site only overlaps the previously determined maximum slip rates for the GF determined over ~14 ka timescales (e.g., McGill and Sieh, 1993). Chuang and Johnson (2011) used a viscoelastic block model to estimate a 9-11 mm/yr geodetic slip rate on the GF incorporating time-dependent deformation processes (e.g., earthquake cycle stages, co-seismic displacements and frequency). The discrepancy between our new late-Holocene geologic slip-rate estimate and low geodetic strain accumulation rates of 0-3 mm/yr (Bennett et al., 2003) may indicate, (1) that the GF is late in its earthquake cycle, or (2) active strain accumulation has recently focused on the ECSZ. Additionally, comparison of our results with these previous estimates allows determination of interval rates from the Late Pleistocene through Holocene time.

In southern Searles Valley-western Pilot Knob Valley, the late Pleistocene highstand shoreline of Searles Lake is displaced by 82-105 m (90 m preferred) across two strands of the GF (McGill and Sieh, 1993). The shoreline is dated to between 12-15.8 ka, on the basis of calibrated radiocarbon ages, 13.2 ka preferred. An incised stream channel at the site is offset 68 m across the two strands and represents an absolute minimum displacement rate of ~5 mm/yr.

Our results imply that a significant fraction of the total post-13.2 ka displacement (e.g., McGill and Sieh, 1993) along the central GF accumulated in the past 3.5-4 ka. Our preferred

interpretation is that 43-50 m of shoreline offset accrued in the past 3.9 ka, implying that the remainder (40–47 m) had accrued at some time within the interval 13.2-3.9 ka. The interval slip rates implied by these data suggest rates of 4.3-5.1 mm/yr during 13.2-3.9 ka (Fig. 2.3), and our data suggest a two- to three-fold increase in slip rate along the GF during the late Holocene (Fig. 2.3).

Assuming all slip is released co-seismically, our results also imply greater seismic strain release in the past 3.5-4.2 ka. This may have been accomplished through greater co-seismic displacements than commonly considered, or by more frequent, smaller seismic events that are not recorded in the paleoseismic record. Here we consider both of these possibilities.

McGill and Sieh (1991) measured offset geomorphic features along the central and eastern GF and plotted surface displacement as a function of along-strike distance. In Pilot Knob Valley, they argued for a clustering of offsets at 2-4 m per event. Presumably, a 3 m coseismic average displacement would require 30 events to accrue the 90-m shoreline offset observed in western Pilot Knob Valley by McGill and Sieh (1993). Approximately 14-17 events of equal magnitude would generate the 43-50 m of slip observed on the late Holocene $Qa3_b$ deposit (this study). At Iron Canyon (Fig. 2.1), 45 km west of our Pilot Knob Valley site, Dawson and others (2003) documented six paleoseismic events since 7 ka. Of these, four surface-rupturing events occur post-2 ka, with the oldest two surface-rupturing events at 5.1 and 7 ka. Because the Iron Canyon paleoseismic trench covers slightly more than one half of the time interval recorded by offset Searles Lake shorelines, there should be, at minimum, 15 events exposed at Iron Canyon, if 3 m slip per event is true. There may be unique conditions at Iron Canyon that under represent the expected paleoseismic record.

If coseismic displacements are closer to 5 m, then expected paleoseismic events from a 90-m-displaced shoreline and a 43-50-m-displaced late Holocene deposit drops to 18 and 9-10 events, respectively. Although larger slip magnitudes significantly reduce the gap between expected and observed paleo-seismicity at Iron Canyon, there are still 2 events missing from the expected 90-m-offset shoreline and at least 2-3 events missing from the offset late Holocene alluvial deposit. Field evidence supports the possibility of 5-m coseismic events in Pilot Knob Valley. Figure 12 in McGill and Sieh (1991) depicts a gully and a terrace riser offset 5.0±0.7 and 5.6±1 m, respectively. Our field observations, however, suggest that these features were displaced in one event. Figure 12 shows only one of two identically offset stream gullies. Both streams have only one beheaded, downstream gully, and one currently incising downstream channel. If this offset were generated via two 2.5-m coseismic events, then two beheaded channels should be present on both gullies. The offset terrace riser at this site is also herein interpreted to result from one rupture event as the "Qt2" terrace (see Figure 12, McGill and Sieh, 1991) is not stepped, but rather is a continuous, 6-m-wide surface. That the modern stream channel (their "Qal") is actively incising across both sides of the GF, a stepped "Qt2" terrace surface is expected for two events. Although the precise location of Figure 11 in McGill and Sieh (1991) cannot be readily determined to within ~200 m (no latitude-longitude coordinates were given), the presence of a multi-stranded GF in the immediate vicinity suggests that coseismic slip may be greater than the 3±0.5 m recorded here if the other strands broke during the most recent event.

Finally, our results carry implications for the interaction of the GF with both the ECSZ and the San Andreas system. Time-variant slip-rate histories have been documented on the San Andreas fault, and in the LA basin and the ECSZ south of the GF (e.g, Dolan et al., 2007).

Within this framework, the GF plays a central role in that it may serve to link slip in ECSZ faults to the plate boundary. The fact that strain release along the GF may be strongly clustered in time provides the potential for irregular loading of plate-boundary faults.

CONCLUSIONS

Displacement along the GF in Pilot Knob Valley is recorded by the truncation of a Late Holocene fan surface. The degree of soil development and direct dating by OSL brackets $Qa3_b$ deposition between 3.5-4.2 ka. Displacement of a shutter ridge by 36-50 m across this deposit indicates a late Holocene GF slip rate of 8.6-14.3 mm/yr. Our preferred reconstruction implies 43-50 m of displacement, and thus a preferred slip rate of 10.2-14.3 mm/yr. When compared with displaced late Pleistocene Searles Lake shorelines at a nearby site, our results reveal strongly time-variant slip histories that range from 4.3-5.1 mm/yr during the interval between 13.2-3.9 ka, followed by a post-3.9 ka period of higher strain release. These large fluctuations of slip during the Holocene are likely linked to time-variant loading from faults in the ECSZ (e.g., Rockwell et al., 2000; Dolan et al., 2007).

TABLES

TABLE 2.1 - UNIT DESCRIPTIONS FOR PKV STUDY AREA

Unit Label	Age Estimate (ka)	Description
Qa	0 – 0.1	Modern wash – no degradation of surface
Qa2	0.1 – 0.5	Not cut by last earthquake rupture
$Qa2_b$	0.5 – 1	Cut by most recent earthquake rupture
$Qa3_b$	3.5 – 4.2	Well preserved bar and swale, minimal pavement development on flat surfaces, no varnish on tops of clasts or rubification on bottoms, incipient soil development (stage I carbonate)

FIGURES

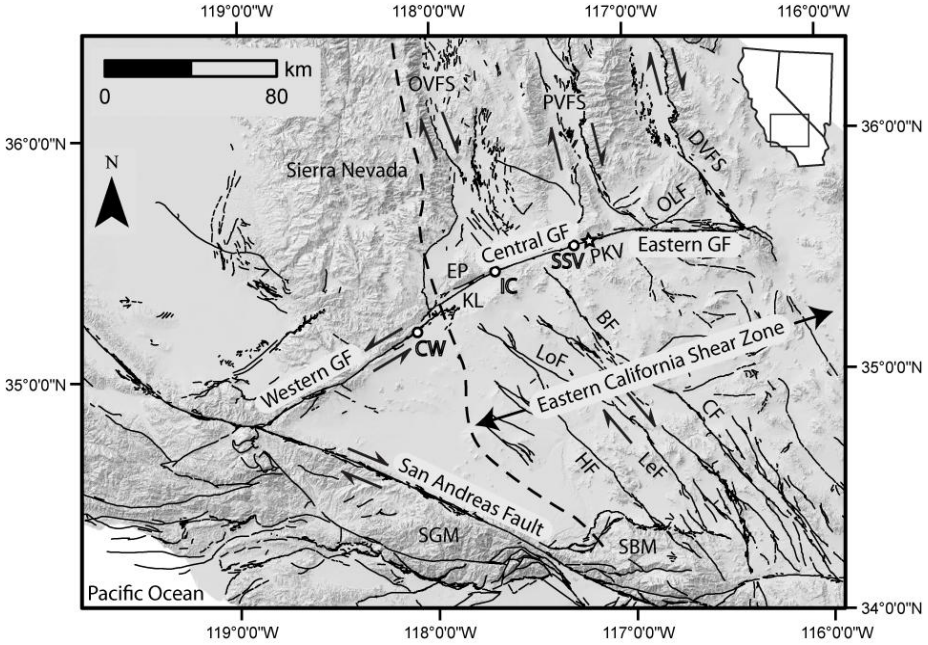
119°0'0"W
118°0'0"W
117°0'0"W
116°0'0"W
36°0'0"N
35°0'0"N
34°0'0"N
km
0
80
N
OVFS
PVFS
DVFS
OLF
Sierra Nevada
Central GF
Eastern GF
SSV
PKV
EP
IC
KL
CW
BF
LoF
Western GF
Eastern California Shear Zone
CF
HF
LeF
San Andreas Fault
SGM
SBM
Pacific Ocean

Figure 2.1 – Shaded-relief Quaternary fault map of southern California. Inset map of California-Nevada with rectangular box locates image. Arrows indicate sense of strike-slip motion. White star shows location of offset late Holocene debris flow (this study). White circles show locations of existing Garlock fault slip-rate and paleoseismic studies -- CW, Clark Wash (McGill et al., 2009); IC, Iron Canyon (McGill and Rockwell, 1998 and Dawson et al., 2003); SSV, Southeast Searles Valley (McGill and Sieh, 1993). Heavy dashed line locates the Eastern California shear zone. BF, Blackwater fault; CF, Calico fault; DVFS, Death Valley fault system; EP, El Paso Mountains; GF, Garlock fault; HF, Helendale fault; KL, Koehn Lake; LeF, Lenwood fault; LoF, Lockhart fault; OLF, Owl Lake fault; OVFS, Owens Valley fault system; PKV, Pilot Knob Valley; PVFS, Panamint Valley fault system; SBM, San Bernardino Mountains; and SGM, San Gabriel Mountains.

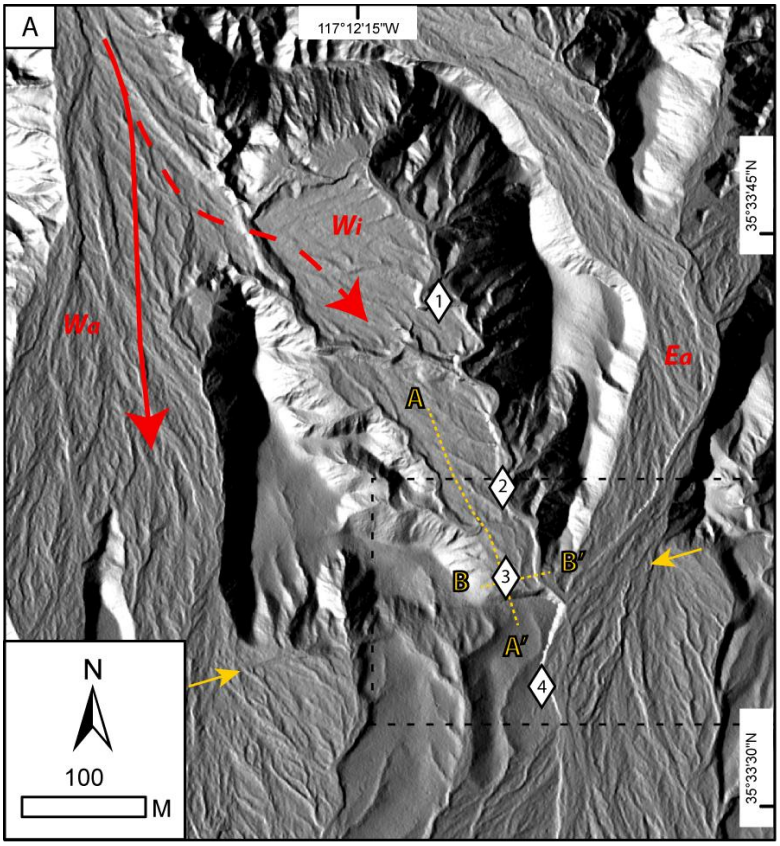
A
117°12'15"W
35°33'45"N
35°33'30"N
Wa
Wi
Ea
1
2
3
4
A
A′
B
B′
N
100
M

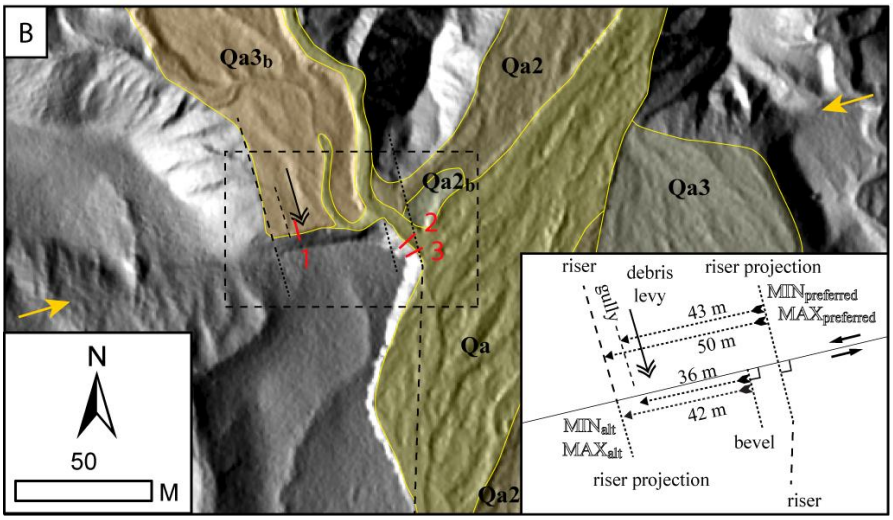
B
Qa3b
Qa2
Qa2b
Qa3
Qa
Qa2
1
2
3
N
50
M
riser
debris
levy
gully
riser projection
43 m
50 m
36 m
42 m
MINpreferred
MAXpreferred
MINalt
MAXalt
bevel
riser projection
riser


C
3

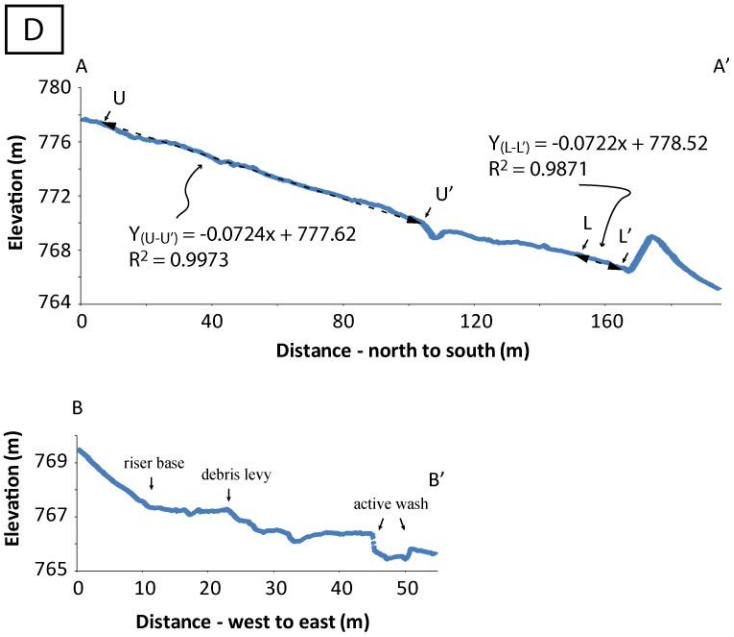
D
A
A′
780
776
772
768
764
U
U′
L
L′
Y(L-L′) = -0.0722x + 778.52
R2 = 0.9871
Y(U-U′) = -0.0724x + 777.62
R2 = 0.9973
Elevation (m)
0
40
80
120
160
Distance - north to south (m)

B
B′
769
767
765
riser base
debris levy
active wash
Elevation (m)
0
10
20
30
40
50
Distance - west to east (m)

Figure 2.2 – (A) A 0.5-m-resolution Earthscope hillshade image of the 50-m truncation site and surrounding surfaces in northern PKV. Small yellow arrows locate the GF. Red arrows indicate sediment transport direction for the modern (solid line) and abandoned (dashed line) stream channels. Wa and Wi are the active and inactive western channels, respectively, and Ea is the active eastern channel. Surfaces and deposits at the northern mouth of the abandoned channel are commensurate with those close to the shutter ridge, suggesting channel abandonment 3.5-4.2 ka. White diamonds indicate: (1) OSL-PVK-2 OSL sample site (see Appendix C), (2 & 3) soil profile sites CLK-2 and CLK-1 (see Appendix B), respectively, and (4) TCN-PKV-2 ^{10}Be cosmogenic profile site (see Appendix A). Dotted box shows location of figure 2.2B. Dark yellow lines show downstream and cross-stream elevational transects found in figure 2.2D. (B) Close-up image of offset debris flow with inset box highlighting offset interpretations. Dotted box shows location of inset box. Red lines and numbers indicate hand-dug trench locations (see Plate 1). Stippled area east of debris levy (double-headed black arrow) is an erosionally modified Qa3b deposit. (C) Southward-looking field photo of rocky debris flow levy (dashed double-headed dark yellow arrow) oriented orthogonally to the shutter ridge. (D) Elevation profiles U-U' and L-L' of upstream debris flow intesecting the north-facing shutter ridge and a channel surface cross section, respectively. A consistent gradient on the ground surface 10 m in front of the shutter ridge (i.e. L-L') suggests no ponding of sediments in front of the shutter ridge.

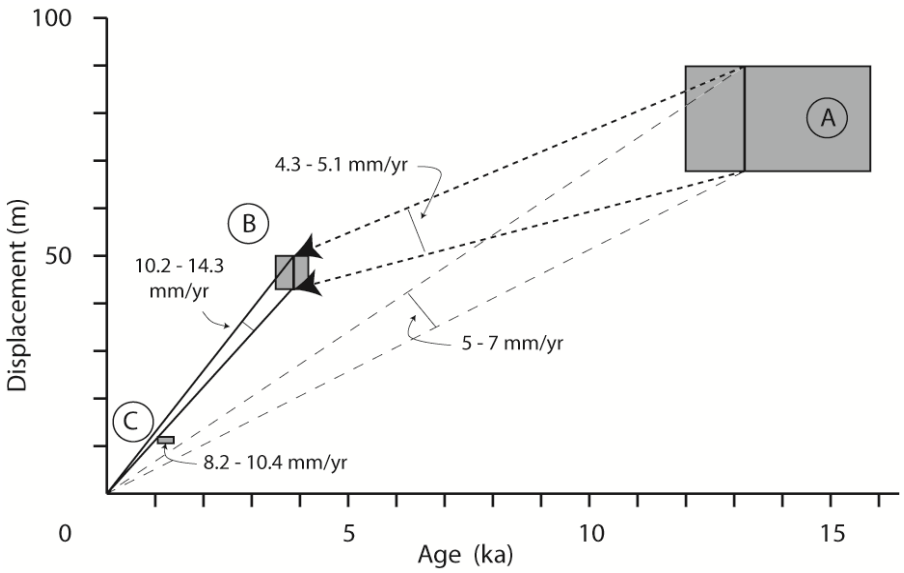
100
50
0
Displacement (m)
5
10
15
Age (ka)
A
B
C
4.3 - 5.1 mm/yr
10.2 - 14.3
mm/yr
5 - 7 mm/yr
8.2 - 10.4 mm/yr

Figure 2.3 – Compilation graph comparing variably displaced geomorphic features along the central GF. (A) A 90-m and 68-m offset of a late Pleistocene shoreline and incised channel, respectively, in SE Searles Valley 6 km west of our study area (table 3 in McGill and Sieh, 1993). Preferred age of 13.2 ka is used to calculate slip rate (B) A 3.5-4.2 ka debris flow offset 43-50-m (this study). Preferred age of 3.9 ka is used to calculate slip rate. (C) Slip rate estimate for the two most recent earthquakes at Iron Canyon 45 km west of study area (McGill and Sieh, 1991; McGill and Rockwell, 1998; Dawson et al., 2003). 2010 AD is zero on the abscissa used to compute slip rates, not radiocarbon age (i.e. 1950 AD).

REFERENCES CITED

Bard, E., Hamelin, B., Fairbanks, R.G., and Zindler, A., 1990, Calibration of the C-14 time scale over the past 30,000 years using mass-spectrometric U-Th ages from Barbados corals: Nature, 345, p. 405-410.

Bennett, R.A., Davis, J.L., and Wernicke, B.P., 1999, Present-day pattern of Cordilleran deformation in the western United States: Geology, v. 27, p. 371-374, doi: 10.1130/0091-7613(1999)027<0371:PDPOCD>2.3.CO;2.

Bennett, R.A., Wernicke, B.P., Niemi, N.A., Friederich, A.M., and Davis, J.L., 2003, Contemporary strain rates in the northern Basin and Range province from GPS data: Tectonics, v. 22, 1008, doi: 10.1029/2001TC001355.

Chuang, R., and Johnson, K.M., 2011, Reconciling geologic and geodetic fault-slip-rate discrepancies in southern California: consideration of non-steady mantle flow and lower crustal fault creep: Geology, v. 39, p. 627-630, doi: 10.1130/G32120.1.

Clark, M.M., and Lajoie, K.R., 1974, Holocene behavior of the Garlock fault: Geological Society of America Abstracts with Programs, v. 6, p. 156-157.

Cowgill, E., 2007, Impact of riser reconstructions on estimation of secular variation in rates of strike-slip faulting: Revisiting the Cherchen River site along the Altyn Tagh fault, NW China: Earth and Planetary Science Letters, v. 254, p. 239-255,

doi: 10.1016/j.epsl.2006.09.015.

Dawson, T.E., McGill, S.F., and Rockwell, T.K., 2003, Irregular recurrence of paleoearthquakes along the central Garlock fault near El Paso Peaks, California: J. Geophys. Res., v. 108, p. 2356, doi: 10.1029/2001JB001744.

Dolan, J.F., Bowman, D.D., and Sammis, C.G., 2007, Long-range and long-term fault interactions in southern California: Geology, v. 35, p. 855-858, doi: 10.1130/G23789A.1.

Frankel, K.L., Brantley, K.S., Dolan, J.F., Finkel, R.C., Klinger, R.E., Knott, J.R., Machette, M.N., Owen, L.A., Phillips, F.M., Slate, J.S., and Wernicke, B.P., 2007, Cosmogenic 10Be and 36Cl geochronology of offset alluvial fans along the northern Death Valley fault zone: Implications for transient strain in the Eastern California shear zone: J. Geophys. Res., v. 112, B06407, doi: 10.1029/2006JB004350.

Furlong, K.P., 1993, Thermal-rheologic evolution of the upper mantle and the development of the San Andreas fault system: Tectonophysics, v. 223, p. 149-164, doi: 10.1016/0040-1951(93)90162-D.

Gan, W., Zhang, P., Shen, Z., Prescott, W.H., and Svarc, L.J., 2003, Initiation of deformation of the Eastern California shear zone: constraints from Garlock fault

geometry and GPS observations: Geophys. Res. Letts., v. 30, 1496, 4 pp., doi: 10.1029/2003GL017090.

Ganev, P.N., Dolan, J.F., Frankel, K.L., and Finkel, R.C., 2010, Rates of extension along the Fish Lake Valley fault and transtensional deformation in the Eastern California shear zone - Walker Lane belt: Lithosphere, v. 2, p. 33-49, doi: 10.1130/L51.1.

Ganev, P.N., Dolan, J.F., McGill, S.F., and Frankel, K.L., 2012, Constancy of geologic slip rate along the central Garlock fault: implications for strain accumulation and release in southern California: Geophys. J. Int., v. 190, p. 745-760.

Guest, B., Pavlis, T.L., Golding, H., and Serpa, L., 2003, Chasing the Garlock: A study of tectonic response to vertical axis rotation: Geology, v. 31, p. 553-556, doi: 10.1130/0091-7613(2003)031<0553:CTGASO>2.0.CO;2.

Helms, J.G., McGill, S.F., and Rockwell, T.K., 2003, Calibrated, late Quaternary age indices using clast rubification and soil development on alluvial surfaces in Pilot Knob Valley, Mojave Desert, southeastern California: Quatern. Res., v. 60, p. 377-393, doi: 10.1016/j.yqres.2003.08.002.

McDonald, E.V., McFadden, L.D., and Wells, S.G., 2003, Regional response of alluvial fans to the Pleistocene-Holocene climatic transition, Mojave Desert, California, *in*

Paleoenvironments and Paleohydrology of the Mojave and Southern Great Basin Deserts, edited by Y. Enzel, S.G. Wells, and N. Lancaster: Geol. Soc. Am. Special Paper 368, p. 189-205.

McGill, S., and Sieh, K., 1991, Surficial offsets on the central and eastern Garlock fault associated with prehistoric earthquakes: J. Geophys. Res., v. 96, p. 21,597-21,621, doi: 10.1029/91JB02030.

McGill, S., and Sieh, K., 1993, Holocene slip rate of the central Garlock fault in southeastern Searles Valley, California: J. Geophys. Res., v. 98, p. 14,217-14,231, doi: 10.1029/93JB00442.

McGill. S., and Rockwell, T., 1998, Ages of late Holocene earthquakes on the central Garlock fault near El Paso Peaks, California: J. Geophys. Res., v. 103, p. 7,265-7,279, doi: 10.1029/97JB02129.

McGill, S.F., Wells, S.G., Fortner, S.K., Kuzma, H.A., and McGill, J.D., 2009, Slip rate of the western Garlock fault, at Clark Wash, near Lone Tree Canyon, Mojave Desert, Californa: Geol. Soc. Am. Bull., v. 121, p. 536-554, doi: 10.1130/B26123.1.

Meade, B.J., and Hager, B.H., 2005, Block models of crustal motion in southern California constrained by GPS measurements: Journal of Geophysical Research,

v. 110, 19 pp., doi: 10.1029/2004JB003209.

Miller, M.M, Johnson, D.J., Dixon, T.H., and Dokka, R.K., 2001, Refined kinematics of the Eastern California shear zone from GPS observations, 1993-1998: Journal of Geophysical Research, v. 106, 18 pp.

Monastero, F.C., Sabin, A.E., and Walker, J.D., 1997, Evidence for post-early Miocene initiation of movement on the Garlock fault from offset of the Cudahy Camp Formation, east-central California: Geology, v. 25, p. 247-250, doi: 10.1130/0091- 7613(1997)025<0247:EFPEMI>2.3.CO;2.

Nicol, A., Walsh, J.J., Watterson, J., and Underhill, J.R., 1997, Displacement rates of normal faults: Nature, v. 390, p. 157-159, doi: 10.1038/36548.

Nicol, A., Walsh, J., Berryman, K., and Villamor, P., 2006, Interdependence of fault displacement rates and paleoearthquakes in an active rift: Geology, v. 34, p. 865-868, doi: 10.1130/G22335.1.

Numelin, T., Kirby, E., Walker, J.D., and Didericksen, B., 2007, Late Pleistocene slip on a low-angle normal fault, Searles Valley, California: Geosphere, v. 3, p. 163-176, doi: 10.1130/GES00052.1.

Oskin, M., and Iriondo, A., 2004, Large-magnitude transient strain accumulation on the

Blackwater fault, Eastern California shear zone: Geology, v. 32, p. 313-316, doi: 10.1130/G20223.1.

Oskin, M., Perg, L., Shelef, E., Strane, M., Gurney, E., Singer, B., and Zhang, X., 2008, Elevated shear zone loading rate during an earthquake cluster in eastern California: Geology, v. 36, p. 507-510, doi: 10.1130/G24814A.1.

Peltzer, G., Crampe, F., Hensley, S., and Rosen, P., 2001, Transient strain accumulation and fault interaction in the Eastern California shear zone: Geology, v. 29, p. 975-978, doi: 10.1130/0091-7613(2001)029<0975:TSAAFI>2.0.CO;2

Rockwell, T.K., Lindvall, S., Herzberg, D., Murbach, D., Dawson, T., and Berger, G., 2000, Paleoseismology of the Johnson Valley, Kickapoo, and Homestead Valley faults: Clustering of earthquakes in the Eastern California shear zone: Bull. Seis. Soc. Am., v. 90, p. 1,200-1,236.

Savage, J.C., Lisowski, M., and Prescott, W.H., 1990, An apparent shear zone trending north-northwest across the Mojave Desert into Owens Valley, Eastern California: Geophysical Research Letters, v. 17, p. 2,113-2,116.

Savage, J.C., Gan, W., and Svarc, J.L., 2001, Strain accumulation and rotation in the Eastern California shear zone: Journal of Geophysical Research, v. 106, 21 pp.

Smith, G.I., and Ketner, K.B., 1970, Lateral displacement on the Garlock fault, Southeastern California, suggested by offset sections of similar metasedimentary rocks: U.S. Geologic Survey Professional Paper 700-D, p. D1-D9.

Stein, R.S., King, G.C.P., and Lin, J., 1992, Change in failure stress on the southern San Andreas fault system caused by the 1992 magnitude = 7.4 Landers earthquake: Science, v. 258, p. 1328-1332, doi: 10.1126/science.258.5086.1328.

Stein, R.S., 1999, The role of stress transfer in earthquake recurrence: Nature, v. 402, p. 605-609, doi: 10.1038/45144.

CHAPTER 3

LATE CENOZOIC SEDIMENTATION PATTERNS OF THE PILOT KNOB FORMATION IN PILOT KNOB VALLEY, CALIFORNIA, AND THE TECTONIC EVOLUTION OF THE CENTRAL GARLOCK FAULT AND MARINE GATE FAULT

William M. Rittase [1]

J. Douglas Walker [1]

Eric Kirby [2]

Elmira Wan [3]

Joe Andrew [1]

[1] University of Kansas

[2] Pennsylvania State University

[3] U.S.G.S. Tephrochronology Lab, Denver, CO

ABSTRACT

In Pilot Knob Valley, active inversion of a Pliocene-mid Pleistocene basin presents the opportunity to understand the spatial and temporal development of an enigmatic basin astride a major transform boundary in California. Here, a ~1000-m-thick package of exposed Late Cenozoic strata has been uplifted and tilted to the northeast. Based on new age and provenance data, we adopt the name Pilot Knob Formation, as will be formally proposed in the publication from this dissertation chapter, to designate much of this exposed stratigraphy north of the Garlock fault (GF) and east of Christmas Canyon gate. Post-Miocene development of Pilot Knob Valley is strongly influenced by the sinistral GF, the newly identified Marine Gate fault and dextral Eastern California shear zone.

The Pilot Knob Formation consists of three lithofacies members, from base to top: (1) rocks derived from Eagle Crags to the south; (2) Randsburg Wash playa-lacustrine rocks; and (3) an upper member derived from the Slate Range. Tephrochronologic data from four Pilot Knob Formation ash samples suggests deposition of Randsburg Wash Member rocks between 3.7-3.1 Ma and the Slate Range Member between 1.2-0.6 Ma. A fifth tephrochronologic sample from lacustrine-distal alluvial sediments south of the GF near Christmas Canyon places deposition of strata tentatively assigned to the Pilot Knob Formation facies at ~3.1 Ma.

Two variations of a 3-stage tectonic model for northern Pilot Knob Valley explain changing provenance patterns. In the preferred model, prior to ~3.1 Ma the western PKV paleo-low lay north of the current GF adjacent to the southern Slate Range and connected to Searles Valley. The Marine Gate fault cuts adjacent to the southern face of the Slate Range and southern Searles Valley with up to 7.5 km of sinistral oblique-normal slip between ~5-2.5 Ma. Eagle Crags Member deposition may continue after 3.7 Ma west of the Randsburg Wash-Searles

Valley spillway, but these rocks have been eroded away. By ~3.7 Ma, northward progradation of Eagle Crags sandstone and conglomerate waned and playa-lacustrine sediments were deposited north of the GF and east of the Randsburg Wash-Searles Valley spillway. At ~3.1 Ma, southward progradation of Slate Range sandstone and conglomerate across the GF began to the east of the Randsburg Wash-Searles Valley spillway. Continued sinistral slip of 1-3 km on the Marine Gate fault is inferred between 3.1-2.5 Ma from the fault juxtaposition of playa-lacustrine rocks of the Randsburg Wash Member against basement rocks in Slate Range. By 1.2 Ma, uplift of the Slate Range and southward progradation of Slate Range Member rocks increased with coarser sandstone and conglomerate reaching south across the GF. Concomitantly, the Marine Gate fault adjacent to the Slate Range and along southern Searles Valley is reactivated as an en echelon series of reverse faults. The alternative model suggests that the proximity of Randsburg Wash Member rocks to the southwest Slate Range front is not a consequence of pre-2.5 Ma sinistral translation along the Marine Gate fault, but rather a consequence of significant post-2.5 Ma reverse faulting on the Marine Gate fault. In both models, the Pilot Knob Formation records deposition along a continuously active main GF with a growing component of contractional strain through time.

INTRODUCTION

Pilot Knob Valley (PKV) forms an arcuate 45 km by 6 km, east-west elongated depression between the Slate Range to the north and Eagle Crags to the south (Fig. 3.1). The modern strand of the central Garlock fault (GF) cuts ENE-WSW across the northern third of the valley and demarks the locus of uplift and basin inversion between it and the Slate Range. This recent uplift provides the opportunity to study important PKV sedimentation patterns through the

Pliocene and Pleistocene that record changes in structural configuration in the region. Tectonic structures responsible for the sedimentologic development and evolution of PKV are: (1) the sinistral GF; (2) a newly identified secondary GF strand, herein referred to as the Marine Gate fault; (3) an intersecting Searles Valley fault to the north in Searles Valley; and (4) the intersecting strands of the Eastern California shear zone (ECSZ) to the west and east of PKV. Because of its proximity to these intersecting faults, PKV is in a critical location for understanding the Miocene-early Pleistocene spatial-temporal relations between the GF and ECSZ.

Because PKV lies entirely within the Naval Weapons Air Station at China Lake, where public access is restricted, much of the late Cenozoic geology of the valley was incompletely known prior to this study. Mapping of the Lava Mountains to the west, Searles Valley to the northwest, and Slate Range to the north by G.I. Smith (1964, 2009) and Smith and others (1968), respectively, covered our study area at a reconnaissance level only; no modern geochronological dating of sediments was presented in these studies. Clark (1973) surveyed Holocene ground ruptures and displacement along the GF through the study area. McGill (1991, 1993) mapped late Pleistocene and Holocene offsets along the GF through PKV in much greater detail. Helms and others (2003) investigated clast rubification as a potential Mojave Desert soil geochronometer. However, no comprehensive sedimentologic and tectonic map existed for the northern PKV until this study.

This report aims to: (1) redefine the stratigraphy of PKV sedimentary rocks through detailed mapping of facies assemblages and provenance associations (Fig. 3.2); (2) place age constraints on sedimentation in PKV to understand the temporal and spatial evolution of the basin's architecture; and (3) understand the influence from the GF, Marine Gate fault and ECSZ

fault on sedimentation in PKV, and thus infer their geometric and kinematic evolution from Pliocene to present.

GEOLOGIC BACKGROUND

This section discusses the major structures in the area as well as areas that could have been important sources of sediment for PKV.

Garlock Fault Origin(s) & Evolution

Identifying the timing and tectonic origins of the GF is not straightforward. Models for the initiation of the GF include: (1) a Cretaceous tear fault during flat-slab Farallon Plate subduction (Michael Wells, personal communication 2007), (2) reactivation of a lithospheric weakness during passage of the Mendocino triple junction and associated slab window (Glazner and Loomis, 1984), and (3) an intracontinental transform during Miocene basin and range extension (Davis and Burchfiel, 1973). The GF presumably became active during the mid-Miocene as Basin and Range-style extension initiated and migrated westward from the Death Valley-Lake Mead corridor. Because extension magnitudes were greater north of the fault relative to the Mojave block to the south, the GF behaved as an intracontinental transform fault accommodating differing magnitudes of crustal extension (Davis and Burchfiel, 1973).

Although the GF remains active as a sinistral strike-slip fault, it is overprinted by and embedded in the ECSZ. Development of the ECSZ is shown to have warped the trend of the central and eastern GF segments up to 20º and 50°, respectively, since ~5 Ma (Dokka and Travis, 1990; Gan et al., 2003 and Guest et al., 2003; Fig. 3.1). Single-stage models (e.g., Davis and Burchfiel, 1973; Guest et al., 2003; McGill et al., 2009) attempting to explain pre-ECSZ GF

activity do not account for post-ECSZ activity, and vice versa. The pre-ECSZ GF accommodates large magnitude extension to the north during the Miocene (Davis and Burchfiel, 1973). Development of the ECSZ reorients the regional stress field in eastern California. Thus, a syn-ECSZ GF is controlled by the same sigma-1 stress direction that drives dextral faults of the ECSZ to the north and south of it (Savage et al., 2001).

An important consequence of this change in GF orientation, coupled with a rotated stress field coinciding with development of the ECSZ, is that the tectonic role of the GF and how it slips are drastically different from those in the Miocene. Prior to development of the ECSZ, Basin and Range extension was east-west relative to a NE-SW trending GF, resulting in translational to transtentional motions (Wernicke and Snow, 1998; Snow and Wernicke, 2000; McQuarrie and Wernicke, 2005). However, the modern GF displays significant N-S contraction across the portions that lie within the ECSZ.

Marine Gate Fault

High-angle Quaternary faults were first mapped at a reconnaissance level along the southern flank of the Slate Range by Smith and others (1968), but were not discussed. They were portrayed as an east-west-oriented en echelon set of faults that project towards the GF near the Quail Mountains to the east. Because the purpose of their study was to identify the bedrock stratigraphy and pre-Quaternary geology of the Slate Range, the significance of these faults was largely ignored. Mapping in the Quail Mountains to the east-northeast of the PKV study area by J. Andrew (GSA Map & Chart, Andrew, 2007) identified rock types and a Mesozoic thrust fault that correlate well to the southern Slate Range. Separation between the Layton Well thrust fault in the SW corner of Slate Range and the thrust fault in the Quail Mountains is 18-20 km. In light

of this apparent separation, and new mapping herein, we propose the name Marine Gate fault to discuss this newly recognized structure.

Eastern California Shear Zone Development

Between 6-3 Ma, a significant portion of the dextral shear jumped inboard of the San Andreas fault system in southern California (Wernicke and Snow, 1998; Snow and Wernicke, 2000; McQuarrie and Wernicke, 2005). A precondition for this inboard migration of dextral shear is the opening of the Gulf of California around 6 Ma (Oskin and Stock, 2003a & b) and subsequent formation of the modern San Andreas fault system south of the ~35° N (Fig 3.1). Today, approximately 10-14 mm/yr of geodetically observed dextral strain passes through a diffuse zone between the Sierra Nevada-western Mojave Desert and Spring Mountains-Providence Mountains (Savage et al., 1990; Dixon et al., 1995; DeMets and Dixon, 1999; Dixon et al., 2000; Gan et al., 2000; McClusky et al., 2001; Miller et al., 2001; Bennett et al., 2003). The rheological structure of the lithosphere across this corridor south and north of the GF is debated (Bourne et al., 1998; Roy and Royden, 2000a, 2000b; Savage, 2000), but important to the strain localization processes ongoing in the ECSZ.

Faults of the ECSZ all apparently end prior to intersecting the GF. However, of these faults, the Panamint Valley Fault, more strongly influences the GF today than any other. A ~30° kink in the trace of the GF is observed at the intersection point with the Panamint Valley fault. The mechanism of strain transfer across the GF, and in particular, the mechanics of terminating slip at the end of Panamint Valley fault, plays an important role in sedimentation patterns along the GF and is discussed in further detail below.

Searles Valley Sedimentation & Tectonic Development

Searles Valley is a 15 km-wide, +30 km-long basin located immediately north of PKV. It is underlain by the Slate Range detachment and Searles Valley fault, which are two generations of a west-dipping low-angle normal fault that have their breakaway along the western Slate Range and along the crest of the central Slate Range (Didericksen, 2005; Numelin et al., 2007; Didericksen et al., *in prep*). Didericksen (2005) and Didericksen and others (*in prep*) interpreted the initiation of extension in Searles Valley around 14 Ma based on apatite (U-Th)/He cooling ages from Slate Range footwall rocks. They estimated a minimum of ~7.5 km of east-west extension in the Layton Pass section of the central Slate Range. Tectonically, Searles Valley lies astride an area of important strain transfer between the Searles Valley fault, the Manly Pass fault, the Panamint Valley fault, and the Ash Hill fault (Walker et al., 2005). The mechanical and kinematic linkages of these structures is shown to influence the development of proto- and modern-day PKV in following sections.

Modern Searles Valley is separated from PKV via a low-lying ridge of uplifted late Cenozoic sediments between the SW corner of Slate Range and the NE corner of the Lava Mountains. This topographic high was termed the Christmas Canyon Anticline by Smith (1991) (e.g., their Figure 1). It is pierced by the Randsburg Wash-Searles Valley spillway, which served as an important pluvial highstand overflow from Searles Lake into Lake Panamint via PKV. Alluvial and pluvial sedimentation patterns in Searles Valley record important tectonic and climatic variations during the past ~5 Ma.

A 930-m drill core (KM-3) for the Kerr-McGee Corporation near the center of Searles Valley revealed a 693 m section of lacustrine sediments deposited on top of 230 m of coarse alluvium, that in turn rests on quartz monzonite basement rock (Smith et al., 1983). The basal

alluvial unit was described by Smith and others (1983) as a pebbly arkosic sand and gravel unit. Several intervals are mostly poorly sorted coarse to very coarse sand, with clasts of quartz monzonite, porphyritic granite, dacite and andesite, up to 15 cm across. This deposit was suspected to be faintly bedded to massive, but is difficult to tell from a single core sample. Based on the plutonic clast assemblage, Smith and others (1983) attributed this deposit to having been "derived from the ancestral Argus Range to the west" and inferred a paleo-low to the east closer to Slate Range. However, the provenance of the dacite clasts is unknown.

The maximum age of deposition in Searles Valley is not well bracketed. Although no datable tuffs were recovered from the KM-3 core, exposures in northern Searles Valley suggest a mid- to late-Miocene age. Here, a late Tertiary volcanic flow caps beds of sediment that contain fossil snails on an east-sloping surface that predates extension in northern Searles Valley (Smith et al., 1968; Smith and Church, 1980). Based on the cooling ages of Slate Range footwall rocks (Didericksen, 2005; Didericksen et al., *in prep*), sedimentation may have begun as early as 14 Ma. Cessation of significant coarse sedimentation in the center of Searles Valley is estimated at ~3.18 Ma, based on paleomagnetic polarity data in the overlying lacustrine facies (Liddicoat et al., 1980).

Approximately 693 m of lacustrine sand, silt and evaporite referred to as the "mixed layer" depositionally overlie the coarse alluvial unit, and is divided into eight units defining major climatologic and sedimentologic shifts both regionally and locally (Smith et al., 1983). These lacustrine sediments are estimated to be ~3.18-0.13 Ma. With the exception of the upper, late Pleistocene and Holocene units, which were dated with ^{14}C and U-series techniques, all other unit age estimates come from paleomagnetic polarity data (Liddicoat et al., 1980; Smith et al.,

1983). These sediments are shown below to be potential subsurface equivalents of exposed sediments in the PKV study area.

Surface mapping by Smith (2009) defined the upper portion of the Searles Valley sediments younger than ~150 ka as the "Searles Lake Formation." He divided the Searles Lake Formation into seven units based on facies changes. These seven subunits, named Units A, AB, B, BC, C, CD and D, from oldest to youngest, correspond to different lacustrine sediments that interfinger with silts, sands and beach gravels around the Searles Lake margin. Unit A was estimated 150-32 ka based on ^{14}C and U-series dating of correlative subsurface borehole cuttings. Additionally, the Searles Lake Formation sits on top of the Christmas Canyon Formation of Smith (2009) and establishes its minimum age at 150 ka. The Christmas Canyon Formation is exposed across the northwestern PKV and provides important clues to the late Pleistocene tectonic and depositional history of the study area.

Slate Range

The Slate Range stretches approximately 45-km north-south between the Marine Gate fault and the Argus Range. Straw Peak, in the southern section of the range adjacent to PKV, rises to 1,700 m from around 700 m at the edge of the Panamint Valley and Searles Valley. Its general structure consists of an uplifted horst between Searles Valley and Panamint Valley that was initially exhumed in the middle Miocene and again during Pliocene-Pleistocene time (Didericksen, 2005; Didericksen et al., *in prep*). Smith and others (1968) suggested that the Slate Range was a north- to northwest-plunging anticline that exposes structurally deeper levels to the south near the GF. Evidence for Miocene extension and uplift includes (1) klippes in the central Slate Range consisting of back-tilted Miocene strata juxtaposed on basement rocks via

the Slate Range detachment and (2) footwall apatite (U-Th)/He cooling ages. Cross-cutting relations between the Slate Range detachment and a younger Searles Valley fault system, combined with younger (4 Ma) footwall apatite cooling ages, reveal a second stage of extensional faulting and uplift (Didericksen, 2005; Didericksen et al., *in prep*).

Active normal faults of the Searles Valley fault system have been documented as far south as South Canyon (Fig. 3.1) (Didericksen, 2005; see Figure 2 in Numelin et al., 2007; Didericksen et al., *in prep*). Smith and others (1968) mapped two northwest-striking normal faults cutting pre-Cenozoic bedrock with down-to-the-west displacement in the southwest corner of the Slate Range. They interpreted one strand as projecting southeastward to the GF and the other terminating against the Marine Gate fault. They assigned a Quaternary age of offset on these faults, which have subsequently been incorporated into the Searles Valley fault system (e.g., Didericksen, 2005; Didericksen et al., *in prep*).

The rock types exposed in the Slate Range provide important constraints on clast provenance in the PKV sediments. These bedrock units consist of: (1) Paleozoic and Triassic metasedimentary rocks in the southwestern corner; (2) a Middle Jurassic mixed plutonic suite of monzonite, hornblende diorite, leucogranite and granodiorite; (3) a Late Jurassic alaskite; (4) a Late Jurassic biotite granite; (5) a Late Jurassic meta-andesite and volcaniclastic assemblage, including a prominent meta-rhyolite in the southeastern Slate Range; and (6) Miocene volcanic and sedimentary rocks along the eastern flank in Panamint Valley (Dunne and Walker, 2004). For the purposes of this paper, the bedrock rock types in the Slate Range are not differentiated (Fig. 3.2a, b), except to show the extent of the meta-rhyolite unit, which is an important marker clast in the uplifted sediments in PKV.

Eagle Crags Volcanic Field

South of PKV lies the high-standing eroded remnant of an 18.7 to 12.4 Ma stratavolcano-caldera complex (Sabin, 1994) that occupies Eagle Crags, Pilot Knob and Robbers Mountain. Sabin (1994) mapped and identified a "series of intermediate to silicic tuffs, tabular flows, flow breccia, dikes, plugs and hypabyssal rocks ranging from tholeitic basalt to high-silica rhyolite" and termed this assemblage the Eagle Crags Volcanic Field (ECVF). This suite intrudes and nonconformably overlies Cretaceous plutonic and Paleozoic eugeoclinal rocks that crop out in southern PKV (Carr et al., 1992). Sabin (1994) suggested this suite of volcanism is neither bimodal, such as typical in Basin and Range extensional settings, nor is it arc-like, as are Jurassic and Cretaceous arc rocks to the west and north. Instead, Sabin (1994) interpreted the ECVF to be sourced via a heterogeneous magma chamber, which in turn, was sourced from tholeitic basaltic melts that assimilated granitic middle crust. Field relations suggest that a significant ECVF eruptive center lay just southwest of Myrick Spring (Sabin, 1994). The ECVF is an important source for PKV sediments.

PILOT KNOB VALLEY STUDIES

Approximately 1150-1300 m of sedimentary rock is exposed on a generally NE-tilted block between the GF and Slate Range (Figs. 3.3 and 3.4a and b) in western and central PKV. Based on regional stratigraphic correlations and new age data, we place these sediments into a newly defined Pilot Knob Formation (PKFm). In addition, we also mapped and recognized the presence of the late Pleistocene Christmas Canyon Formation described by Smith (2009). A brief description of each deposit follows below.

Pilot Knob Formation

We define the PKFm as consisting of three members: (1) a basal Eagle Crags Member, (2) a middle Randsburg Wash Member and (3) an upper Slate Range Member, based on clast compositions and facies assemblages (Fig. 3.5). The descriptions below are on rock types with complex transitions and relations. Thus, for ease of communicating depositional relationships among the units, the following unit labeling conventions are used in this study. A capitalized "QT" indicates a Quaternary-Tertiary formation age. A proceeding lower case "p" stands for the PKFm. The three PKFm members, Eagle Crags, Randsburg Wash and Slate Range Members, are abbreviated with "e", "r" and "s", respectively. The oldest units in each PKFm Member are designated by "1" with higher numbers indicating higher (younger) stratigraphic positions. Thus, unit QTpe1 indicates the oldest unit of the Eagle Crags Member of the Quaternary-Tertiary PKFm. Outcrop relations are shown on figure 3.2. Unit QTpe1 of the Eagle Crags Member is a basal sandstone and conglomerate with Eagle Crags provenance that is commonly exposed adjacent to the GF. The top of the Eagle Crags Member is unit QTpe2, a finer Eagle Crags-derived sandstone to siltstone-claystone deposit that fines upward and laterally from QTpe1 (Fig. 3.5). East of the Randsburg Wash-Searles Valley spillway, a thick siltstone-claystone-evaporite unit (QTpr1) composes most of the Randsburg Wash Member. A small rockfall deposit (unit QTpr4) with a Slate Range affinity is locally interbedded near the top of the Randsburg Wash Member. QTpr1 grades into a coarser sandstone and interbedded siltstone facies with Slate Range clasts (QTpr3) and mixed Slate Range-Eagle Crags clasts (QTpr2). A coarsening upward sequence into a Slate Range-derived sandstone and pebble conglomerate comprises unit QTps1 of the overlying Slate Range Member. QTps3 of the Slate Range Member is a brown gypsiferous siltstone and claystone that grades laterally and upward from QTps1 in the eastern

PKV study area. A coarse cobble and boulder conglomerate with Slate Range clasts and gentler dips comprises QTps2 and QTps4 of the Slate Range Member. QTps2 is differentiated from QTps4 from the presence of strong hematite and manganese-oxide (apparent) hydrothermal cementation. The base of QTps4 is diachronous and grades laterally into QTps1.

The PKFm was variously classified as Christmas Canyon Formation (units "ccg" and "Qcc"), 'Tertiary siltstone and sandstone' (unit "Ts"), and 'Tertiary or Quaternary sandstone and siltstone' (unit "QTs") by Smith (1964, 2009) and Smith and others (1968). The PKFm is thus separated out from units previously classified as Christmas Canyon Formation by Smith (1964, 2009) and Smith and others (1968). The PKFm is older than the Christmas Canyon Formation type section of Smith (1968), and displays a much greater degree of deformation due to the GF and ECSZ strain. Bedding within the Eagle Crags and Randsburg Wash members of the PKFm generally has steeper dips of 30-90º versus the 0-5º dip of the Christmas Canyon Formation. The contact between the Christmas Canyon Formation and the PKFm is an angular unconformity as seen in figure 2 of Smith (2009, p. 9).

Eagle Crags Member

The Eagle Crags Member forms the base of the exposed PKFm. Units QTpe1 and QTpe2 within this member contain detrital clasts from the Eagle Crags volcanic field to the south of the PKV. Where exposed, they are primarily a conglomerate, sandstone and siltstone-claystone deposit. The age of exposed Eagle Crags Member in the study area is inferred between ~5-3.7 Ma. These units are discussed below.

QTpe1 – Sandstone and conglomerate unit

Unit QTpe1 on figure 3.2 consists of fanglomerate and coarse sandstone with mixed mafic and intermediate volcanic clasts. Clasts are commonly rounded with imbrication showing paleoflow from the south. Sediment source is Eagle Crags, on the south side of PKV, as there are no similar rock types present in the southern Slate Range or east of Eagle Crags on the south side of the GF.

Bedding is typically crude east of the Randsburg Wash-Searles Valley spillway, where deposit is mostly coarse sand with pebble beds (Fig. 3.6a). Beds here are 5-10 cm thick and are normally graded. However, shearing associated with the GF distorts or obliterates bedding as much as ~50 m out from the fault locally. Between the Randsburg Wash-Searles Valley spillway and Christmas Canyon gate, the unit is a coarser-grained and well-bedded pebble to cobble conglomerate. Beds here are up to 30 cm thick and the deposit is locally clast-supported near Christmas Canyon gate. Clasts are up to 20 cm in diameter, but commonly 2-10 cm across. Up to 5% of the clasts are gray monzonite, possibly from Robbers Mountain (Carr et al., 1992) on the north flank of Eagle Crags. Metasedimentary clasts were not observed, but may be present in low abundances where plutonic clasts are present, as small outcrops of metasedimentary rocks are present near Robbers Mountain (Carr et al., 1992).

QTpe1 forms low-relief hills that are mantled by a lag of weathered-out clasts. The surface has a distinctive gray-blue hue from the more numerous dacitic clasts. Fresh exposures along cut banks are more salt-and-peppered to dark-gray colored. QTpe1 does not appear to show signs of oxidation during deposition (i.e. rubification of sediments) that is typical of arid alluvial fans. It is possible that much of the deposit exposed was low enough on the fan where salt precipitation and higher moisture contents dominate, possibly limiting reddening of the

sediments. However, the clast-supported fanglomerate section near Christmas Canyon gate is also not red, even though it appears to be more proximal deposit.

The unique provenance of QTpe1 helps to define the maximum depositional age at each location along the GF by palinspastically restoring locations to north of the eastern Eagle Crags contact with Granite Mountain (Fig. 3.7). Using a 5-7 mm/yr steady slip rate (e.g., McGill and Sieh, 1993) for the GF, and lateral distance from the eastern Eagle Crags contact with Granite Mountain (Fig. 3.7), we estimate that QTpe1 between Christmas Canyon gate and Randsburg Wash-Searles Valley spillway is ~5 Ma based on a ~30 km separation between deposit and source (e.g., Myrick Spring, Fig. 3.1). East of the spillway and along Slate Road, QTpe1 may be as old as ~4.5 Ma. The minimum age for QTpe1 cannot be established west of the spillway because much of the section has been eroded. However, east of the spillway, a minimum age of ~3.7 Ma is estimated for both QTpe1 and QTpe2 based on a ~3.6 Ma tephra (T-PKV-WMR-D, Appendix D) in the Randsburg Wash Member ~300 m higher in section (Fig. 3.2). This accounts for, at minimum, ~0.1 My QTpr1 depositional period prior to T-PKV-WMR-D eruption, and is consistent with the ~0.3 My span and ~300 m depositional thickness between T-PKV-WMR-D and T-PKV-WMR-C ash beds.

QTpe2 – Gypsiferous sandstone, siltstone and claystone unit

This distal alluvial facies makes up the top of the Eagle Crags Member and consists of gypsiferous sandstone, siltstone and claystone. Pebbles occur in some sandstone beds and are mafic and intermediate volcanic clasts belonging to the Eagle Crags uplands (Sabin, 1994; Monastero et al., 1997) to the southeast. This unit (QTpe2; Fig. 3.2) occurs along and

stratigraphically below the southern exposure of the Randsburg Wash Member (QTpr1, see below), but locally is interfingered with it. The contact between QTpe2 and QTpr1, as defined by the last occurrence of Eagle Crags pebbles and sand, is gradational both upward in section and laterally to the west.

Because of the fine-grained, poorly cemented and evaporitic nature of the deposit, QTpe2 is more easily erodible than QTpe1 and is a slope former north of Christmas Canyon gate. Along Slate Road, QTpe2 weathers similarly to QTpr1, but is of a slightly darker color and less hummocky.

The composite exposed thickness of QTpe1 and QTpe2 varies significantly between Christmas Canyon gate and Slate Road (Figs. 3.2, and 3.4a and b) and is discussed further in the interpretations below. Presumed growth strata in the hanging wall of the Marine Gate fault creates additional variability north-south along the A-A' cross section (Fig. 3.4a). A minimum thickness of 1150-1300 m is estimated in the hangingwall of the north strand of the Marine Gate fault based on cross section construction. At Slate Road along the B-B' cross section (Fig. 3.4b), up to 200 m of Eagle Crags Member rocks are exposed along the GF. True thicknesses cannot be established at either location as the base is not exposed.

Randsburg Wash Member

The Randsburg Wash member is the next higher member of the PKFm. To the west of Slate Road and along the Randsburg Wash-Searles Valley spillway, these rocks are predominately white to light-tan sandstone, siltstone, claystone and evaporite. East of Slate Road, these rocks grade laterally into coarser lithofacies with distinct provenance from the

surrounding mountain ranges. The age of exposed Randsburg Wash Member is ~3.7-3.1 Ma as all units composing this member are stratigraphically equivalent.

QTpr1 – White siltstone, claystone and evaporite unit

This is a sequence of light-colored and finely laminated gypsiferous sandstone, siltstone and claystone (QTpr1; Figs. 3.2, and 3.6c,d,e and g). The true thickness of this deposit is difficult to measure due to abundant folding and faulting of the section, but there is at least ~700-750 m of section exposed near Slate Road (Fig. 3.4b). These rocks are relatively well indurated, but silt- and clay-rich beds are generally poorly exposed and commonly have a weathered, popcorn-like surface texture. Karstification is common at ravine bottoms owing to runoff dissolving salt deposits and other soluble constituents. Sandstone beds may locally contain a few pebbles with a Slate Range provenance. Numerous ash layers are exposed throughout the section, but many are altered to yellowish clays. These ash beds make excellent strain markers and provide an opportunity to partially reconstruct stratigraphic sections of this strongly deformed unit. Two tephrochronologic samples from this member correlate with ~3.3 to 3.6 Ma tephras (see discussion below, Appendix D). We estimate a ~3.7-3.1 Ma age for this unit.

QTpr2 – Mixed Eagle Crags & Slate Range sandstone and siltstone unit

This is a poorly sorted and graded, fine-grained sandstone and siltstone unit interbedded with coarse-grained arkosic sandstone and pebble conglomerate. This unit, labeled QTpr2 on Figure 3.2, grades laterally into, and is age equivalent to QTpr1 to the west. QTpr2 is interpreted to be a lacustrine margin-distal alluvial fan deposit. This unit crops out just south of, and

stratigraphically below QTpr3 at the eastern pinch-out of QTpr1. Poor field exposures of these highly folded and steeply dipping strata adjacent to the GF complicate unit thickness determinations. A ~50-80 m thick estimate, assuming the ~120-m-wide outcrop dips to the south ~25-40º, is tenable. QTpr2 is dissimilar to other distal alluvial fan facies of the PKFm in that provenance appears to be both Slate Range and Eagle Crags. The clasts consist of ~80% Slate Range lithologies and 20% Eagle Crags mixed volcanic rock types. Incorporation of both north- and south-derived sediments suggests that QTpr2 represents the axial topographic low of PKV during this stage of deposition.

QTpr3 – Slate Range sandstone and siltstone unit

This is a poorly sorted and poorly graded fine-grained sandstone and siltstone interbedded with coarse-grained arkosic sandstone and pebble conglomerate (QTpr3; Figure 3.2). The clasts have a Slate Range provenance and is interpreted it to be a distal alluvial fan on the eastern margin of the QTpr1 playa-lacustrine basin. Unit thickness is ~100-150 m. Because QTpr3 is age equivalent to, and grades laterally into QTpr1, it is included in the Randsburg Wash Member.

QTpr4 – Slate Range rockfall unit

This unit (QTpr4) is a deposit of mostly pink-weathering coarse granite with ~ 5% dark greenish-black metamorphic rock. QTpr4 occurs as a layer 1 to 5 m thick within the playa-lacustrine facies (QTpr1) and Slate Range sandstone and siltstone (QTpr3) (Fig. 3.6e). The heavily fractured nature of the clasts and the presence of scaly sediments at its base suggest a

rockfall transport mechanism out into the lacustrine part of the basin from a source in the Slate Range. The clasts types correlate with Jurassic rocks along the southwestern flank of the Slate Range, or it may correlate to coarse alaskitic granite that intruded Jurassic volcanic rocks along the southeast flank of the Slate Range. Because QTpr4 is interbedded with other Randsburg Wash Member units, we include it in this member. The age of the rockfall is likely close to 3.1 Ma as it sits stratigraphically near the top of QTpr1 where tephra sample T-PKV-WMR-C (see below) was collected.

Slate Range Member

The Slate Range Member forms the top of the PKFm and is composed of coarse sandstone and conglomerate (Units QTps1, QTps2 and QTps4), and a siltstone and claystone deposit (Unit QTps2). It corps out to the east of the Randsburg Wash-Searles Valley spillway and is predominantly sourced from the Slate Range to the north. The age of this member spans ~3.1-0.3 Ma based on bracketing between dated older members and younger flat-lying sediments. These units are described below.

QTps1 – Conglomerate, sandstone and siltstone unit

QTps1 is a well-bedded siltstone, sandstone and pebble conglomerate unit sourced from the southern Slate Range (Fig. 3.6f). The lower portions of this unit are siltstone and sandstone. The upper half of this unit is conglomerate with clasts of meta-rhyolite, white granite, light-colored gneiss or mylonite, red granite, and bluish-green gneiss. Unit thicknesses varies greatly east-west, but is as least 200 m thick along the C-C' cross section line (Fig. 3.4c).

Bedding thicknesses range from 2-10 cm at the bottom to up to 0.5 m at the top. Normal grading patterns and lack of cut-and-fill channels suggest sheet-flood deposition on a low-relief fan surface. The bottom of QTps1 sits conformably on the white playa-lacustrine sequence (QTpr1) and bedding attitudes gradually decrease up-section. Fanning of dips here is probably both a function of syn-tectonic deposition, and an increased mechanical strength of these thick clastic sediments compared to the playa-lacustrine unit below. QTps1 pinches out to the west where QTps2 and QTps4 sit locally unconformably on QTpr1, but thickens dramatically to the east before grading laterally into an orange siltstone and claystone (QTps3) (Fig. 3.2). QTps1 is more resistant to erosion than underlying playa-lacustrine and distal alluvial deposits, and forms a noticeable break in slope with the playa-lacustrine section. This unit is generally moderate red to orange in color, indicative of arid alluvial deposition. QTps1 is interpreted to be a distal to medial arid alluvial fan deposit derived from the southern Slate Range. QTps1 forms the base of the Slate Range Member of the PKFm and is no older than 3.1 Ma and as young as 1.2 Ma.

QTps2 – Hematite- and manganese oxide-stained Slate Range conglomerate unit

QTps2 is a 20 to 30-m-thick conglomeritic unit of meta-igneous and granitic clasts stratigraphically below QTps4 (Fig. 3.6g and i). QTps2 beds generally dip to the north and northeast ~40-20º that fan upward to be conformable with QTps4. QTps2 has a conformable base with QTps1, but has a scoured base on top of QTpr1 playa-lacustrine sediments. The clasts are commonly angular and locally resemble breccia. QTps2 is very well indurated and commonly crops out as cliffs and overhangs. Conglomerate is mostly matrix-supported, but

clast-supported locally. Matrix is a coarse sandy arkose. Bedding is thick to massive (>20 cm), poorly sorted and imbricated, flat sheet-flood deposits with locally interbedded debris flows that are unsorted. This unit has distinctive dark red to purple hematite and manganese-oxide staining. In places, thick concretions of hematite and manganese-oxide completely incase the clasts and cements the sandy matrix. A similar red staining occurs in the southwestern Slate Range basement rock along the Marine Gate fault. This staining occurs across several contacts of meta-plutonic bodies, and the top of the hematite stain is roughly horizontal. Hematite and manganese-oxide staining is interpreted to post-date QTps2 deposition, as all clasts and matrix within this unit are stained. However, staining terminates during subsequent QTps4 deposition as stained clasts are rare and the matrix is unaffected. QTps2 is interpreted to be a syn-tectonic conglomerate derived from the adjacent southwest Slate Range face. We speculate that the hematite and manganese-oxide staining may be a byproduct of dehydration of QTpr1 evaporites into anhydrites following shallow burial beneath Slate Range Member deposits, and that the Marine Gate fault acted as a conduit for fluid flow. This unit is estimated to be no older than ~2.5 Ma, its base sits on top of ~150-m-thick section of QTps1, that in turn rests on a ~3.3 Ma tephra T-PKV-WMR-C. We speculate that its minimum age is ~2-1.5 Ma because these sediments project beneath the 1.2-0.6 Ma QTps3 playa-lacustrine unit to the east.

QTps3 – Brown gypsiferous siltstone and claystone unit

Claystone, siltstone and sandstone comprise QTps3 of the Slate Range Member. A distinctive brown hue defines the lower portion of this unit (Fig. 3.6h). The upper section locally contains a sand-matrix-supported pebble conglomerate consisting of meta-rhyolite, red granite,

light-gray granite, slate, schist from the Slate Range, and also vesicular basalt, plagioclase-rich basalt, gray dacite or andesite and red plagioclase-rich basaltic andesite from Eagle Crags. These upper beds are interpreted to be lag deposits on top of playa surfaces within QTps3. QTps3 weathers and erodes easily, similar to QTpr1, and forms large rounded mounds with white ash beds giving a sense of bedding orientation across a typically poorly exposed surface. Coarser-grained facies are more resistant to erosion and thus forms steeper slopes and protective caps over siltstone and claystone beds. To the east, the top of QTps3 locally has a slight angular unconformity with unit QTps4. QTps3 is estimated to be ~175 m thick (Fig. 3.4), but, because the base is not exposed, this is a minimum estimate. Two tephrochronology samples from this member correlate with ~1.2-0.64 Ma tephras (see discussion below, Appendix D) and suggest a 1.2-0.6 Ma age for the deposit.

QTps4 – Slate Range conglomerate unit

Unit QTps4 is a thick and aerially extensive exposure of Slate Range Member coarse conglomerate at the top of the PKFm. Its thickness varies across the study area due to facies transitions, but is probably in excess of 300 m between cross-section lines B-B' and C-C' (Figs. 3.2, and 4b and c). Other alluvial units adjacent to the Slate Range are identical in form, but are late Pleistocene or younger and are in angular discordance with QTps4 (e.g., units that are yellow colored in figure 3.2). QTps4 deposits are less deformed than older PKFm units, and have generally low dips between 0º and 10º to the north to northeast, making this unit back-tilted toward its source. Bedding is parallel and indicates a sheet-flooding alluvial fan environment. Beds range in thickness from 10 cm to greater than 1 meter. Sorting and grading of clasts are poor. Clast size ranges from pebbles to boulders greater than 1 m in diameter. Clast

composition consists of granite, quartz monzodiorite, gneiss, schist, slate and meta-rhyolite, and closely matches the rocks present along the south flank of the Slate Range with no evidence of lateral separation. The deposit has an overall gray color due to chlorite-bearing clasts derived from the Jurassic igneous and metavolcanic rocks. Otherwise, the light orange-red matrix color suggests an arid alluvial setting with oxidation of near-surface sediments (Fig. 3.6i). A Slate Range source is also supported by paleoflow indicators indicating flow from the north. Locally, this deposit may show a different clast composition than the modern washes and neighboring Slate Range bedrock, because presumably, some of the bedrock source area presently exposed was covered during QTps4 deposition. An example is the lack of maroon hematite- and manganese-stained clasts in close proximity to the stained Slate Range bedrock exposures. QTps4 is well indurated and is a hill-former. Hillside steepness increases over QTps1, but is not commonly a cliff-former like QTps2. This unit is mostly a sand-matrix-supported to locally clast-supported fanglomerate. Age is highly diachronous from east to west as facies merge laterally with QTps1 and QTps3. A maximum age of ~2.5 Ma is estimated along Slate Road. To the east, QTps4 deposition initiates shortly after 1.2 Ma and 0.6 Ma north of tephra samples "T-PKV-WMR-B" and "T-PKV-WMR-A", respectively. A minimum age for QTps4 is subjectively estimated at ~0.3 Ma as these sediments are still tectonically tilted nor do they share genetic relations to the mid to late Pleistocene Christmas Canyon Formation (discussed below) west of the Randsburg Wash-Searles Valley spillway.

QTpe3(?) – Pilot Knob Formation(?) south of Garlock fault

A 100-300-m-thick Late Pliocene, metasedimentary clast-rich alluvial deposit crops out south of the GF near Christmas Canyon gate (Fig. 3.2). Clast provenance in this unit (QTpe3(?))

is similar to that in the Eagle Crags Member of the PKfm. These beds were previously included within the Christmas Canyon Formation by Smith (1964) and were separated out as older units by Smith (2009). QTpe3(?) is also deformed a similar amount to the Eagle Crags Member and Randsburg Wash Member of the PKFm, as evidenced by the generally steep NW and SE dips. It comprises beds of siltstone and fine arkosic sandstone with lenses of pebble sandstone and pebble conglomerate. This unit only occurs south of the GF in the southwestern corner of the map area. The clasts are a mixture of basalt, intermediate volcanic rocks, hornblende diorite, L-S tectonite and metasedimentary rocks including quartzite. This clast assemblage matches the rocks along the south side of the PKV where a set of north-south striking metasedimentary rocks (Carr et al., 1992) is overlain by the Eagle Crags volcanic rocks (Sabin, 1994; Monastero et al., 1997). A tephrochronology sample from QTpe3(?) correlates with a 3.14 Ma tuff (T-PKV-WMR-E, Appendix D). Thus, unit QTpe3(?) is time correlative with the top of the Randsburg Wash Member - bottom of the Slate Range Member of the PKFm, but was presumably far away when deposited.

Mid to Late Pleistocene Sedimentary Units

We use the following convention to identify the two units of the exposed Christmas Canyon Formation in northwestern PKV. We note that our unit labeling system differs from Smith (2009). Herein, a capitalized "Q" indicates the age of the rocks as Quaternary and the lowercase "c" identifies it with the Christmas Canyon Formation. A lowercase “l” and “f” associates it with lacustrine and fanglomerate facies, respectively. These units were previously interpreted by Smith (2009) as Searles Valley Formation and Christmas Canyon Formation, respectively.

Qcl is a flat-lying to sub-horizontal, light-green to bluish lacustrine siltstone and claystone that crops out along the Randsburg Wash - Searles Valley spillway. Unit thicknesses in the study area are ~10-15 m. Its notable feature is its sharp angular unconformity with underlying PKFm units QTpe1 and QTpe2 (Fig. 3.6b). Qcl weathers easily and forms low-relief rounded hills that are commonly veneered by cobbles and boulders shed off neighboring Qcf deposits. Planar hilltops are mantled with Qcf clasts and indicate a wave-cut platform from high stands of a late Pleistocene Searles Lake. Locally, the base of Qcl is a 20-50-cm-thick, well bedded and well sorted, fine white silt spring deposit or reworked ash. Samples were collected and analyzed, but no datable material was recovered. Smith (2009) mapped this deposit as "sag" and "sa" members of his Searles Valley Formation Unit A. Smith (2009) assigned an age range of 150-32 ka for this deposit based on U-series dating of salts and ^{14}C dating of organic carbon in the center of the basin. Because Qcl appears to be uplifed relative to Searles Valley, yet is still flat-lying, we here suggest a minimum age of 150 ka. A preferred range of 150-300 ka is suggested. No absolute age control is available, however. A maximum age estimate is established from the minimum age estimate for QTps4 adjacent to the Slate Range because this latter deposit is tilted, whereas Qcl is not.

Qcf is a ~30-m-thick, flat-lying, poorly bedded layer of alluvium capping Qcl. Qcf consists of rounded plutonic and metamorphic rocks from Slate Range, and mixed volcanic rocks from Eagle Crags. Vesicular basalt cobbles and boulders are common on the surface. Well-rounded quartzite clasts are also found on the surface, although their source is not known. Rounded and mixed nature of clasts suggests a lake-modified alluvial fan deposit. Numerous late Pleistocene shorelines are cut into the north, west and eastern faces of this deposit. Qcf probably formed at a lower elevation with respect to Searles Valley, and has since been uplifted

adjacent to the Marine Gate fault. Evidence for this uplift includes increasing riser heights and incision magnitudes along the active Randsburg Wash - Searles Valley spillway with proximity to the Marine Gate fault. Smith (2009) interpreted these sediments as a course gravel upper facies of the Christmas Canyon Formation (ccg). We note that Qcf depositionally overlies Qcl, and thus must be younger than ca. 150 ka. We suggest a minimum age of 50 ka, with a preferred age of 100-150 ka. No volcanic ashes or datable fossils were recovered from Qcf, but soil development characteristics suggest abandonment of deposition and surface stabilization at ~50 ka or older. But since we do not have a detailed soil profile description on these deposits, our age correlation is tentative.

Tephrochronologic Data

Five volcanic, distal ash-fall samples (T-PKV-WMR-A to T-PKV-WMR-E) were collected from PKV playa-lacustrine sediments (Fig. 3.2; Appendix D) and submitted to the U.S.G.S. Tephrochronology Lab in Denver, CO for geochemical determination of major and minor oxide abundances, and for comparison with dated tephra deposits of western North America. An ion microprobe was used to determine the concentrations of 9 oxides (SiO_2, Al_2O_3, FeO, MgO, MnO, CaO, TiO_2, Na_2O and K_2O) to generate a geochemical fingerprint of the tephra. Statistical correlations were used to determine the closest match among a geochemical database of ~5,900 dated volcanic ashes. In the absence of large phenocrysts suitable for conventional dating techniques, this method has proven to be quite robust (Sarna-Wojcicki, 2000).

Sample T-PKV-WMR-A was collected from near the top of playa-lacustrine unit QTps3 of the PKFm at -117.093º W and 35.587º N (Fig. 3.2). This sample correlates well to the 0.64

Ma Lava Creek B ash from the Yellowstone National Park area in Wyoming. This sample has a ≥95 statistical correlation (SC), both with and without alkalis, to Lava Creek B ash. A second plausible correlation is to the 2.1 Ma Huckleberry Ridge ash (0.96 SC without alkalis). Glass shards from T-PKV-WMR-A are moderately to well hydrated (93.8% total wt.). This degree of hydration is typical for older volcanic glass samples. However, because sample T-PKV-WMR-A sits stratigraphically higher than T-PKV-WMR-B (discussed below), the Lava Creek B ash correlation is preferred.

Sample T-PKV-WMR-B was collected from near the middle of the exposed playa-lacustrine unit QTps3 of the PKFm at -117.130º W and 35.582º N. It is most similar to the ~1.13-0.87 Ma Upper Tuffs of Glass Mountain and the ~0.76 Ma Bishop Tuff (Appendix D). The eruptive source for both of these tuffs is the Long Valley Caldera to the north of the study area in Owens Valley, CA. We use a ~1.13 Ma age for Upper Tuffs of Glass Mountain to date deposition in this part of the QTps2 basin.

Sample T-PKV-WMR-C was collected from the top of playa-lacustrine unit QTpr1 of the PKFm along Slate Road at -117.225º W and 35.569º N. It has a similar geochemistry to the 3.28 Ma Tuff of Mesquite Springs and the 3.35 Ma Tuff of Zabriskie Wash. The Tuff of Mesquite Springs has a slightly higher SC value than the Tuff of Zabriskie Wash (Appendix D). The eruptive source for the Tuff of Mesquite is in northern Death Valley. This ash establishes the cessation of Randsburg Wash member lacustrine deposition in the Slate Road area.

Sample T-PKV-WMR-D was collected from the middle of playa-lacustrine unit QTpr1 of the PKFm at -117.231º W and 35.563º N. This sample correlates well to the >3.58 Ma Tuff of Artists Drive of the lower Nomlaki group, and the 3.27 Ma Nomlaki Tuff. Sample T-PKV-WMR-D sits stratigraphically lower in the Randsburg Wash Member, and thus is older than T-

PKV-WMR-C. Additionally, the Tuff of Artist Drive has a slightly higher SC value. We suggest that this tuff better represents the age of the PKFm here. The eruptive sources for the Tuff of Artist Drive and the Nomlaki Tuff is in the southern Cascades of California (Knott et al., 2008).

Sample T-PKV-WMR-E was collected from a possible correlative playa-lacustrine unit QTpe3(?) at -117.346º W and 35.523º N. It is most similar to a 3.14 Ma Coso eruptive center tephra using alkali and non-alkali oxides. A second, slighly weaker correlation using non-alkali oxides is to the 2.9 Ma Mt. Jackson (Nevada) tuffs and the 2.89-2.58 Ma lower tuffs of the Badlands. Note (in Appendix D) that the calcium oxide concentrations in the Mt. Jackson and Badlands samples are somewhat lower than that of T-PKV-WMR-E. Titanium oxide, in particular, is much higher in the lower Badlands samples. Conversely, the calcium concentrations for the Coso tephra matches are closer. This further supports the premise than the age of T-PKV-WMR-E is closer to 3.14 Ma.

INTERPRETATIONS

Marine Gate Fault

Several lines of evidence suggest that a significant fault cuts east-west across the northern Quail Mountains and northern PKV, and the southern Slate Range and southern Searles Valley, including: (1) fanning of dips and thickening of pre-2.5 Ma PKFm strata to the north (Fig. 3.4); (2) fault juxtaposition of QTpr1 lacustrine rocks against the southwest Slate Range; (3) lack of Slate Range clasts in exposed pre-3.1 Ma PKFm strata, except for locally in QTpr2, QTpr3 and QTpr4 to the east; (4) zone of intense deformation in PKFm along the Randsburg Wash-Searles Valley spillway where the Marine Gate fault projects; and (5) linear pattern of late-Quaternary

fault scarps and broadly uplifted sediments across the aforementioned area. The Marine Gate fault is interpreted to bifurcate near the Randsburg Wash-Searles Valley spillway into a dominant northern strand and a subordinate southern strand that acts as a relay fault (Figs. 3.1 and 3.2). The northern strand projects westward into the southwest arm (e.g., Teagle Wash, Fig. 3.1) of Searles Valley and likely transfers slip back onto the GF. The southern strand terminates on the GF at Christmas Canyon gate and appears to influence modern deformation there (e.g.., uplift of the Christmas Canyon anticline of Smith [1991]). Further discussion of the Marine Gate fault follows below.

Searles Valley Fault

Smith and others (1968) mapped two northwest-striking, southwest-dipping normal faults cutting across the southwest corner of the Slate Range. They suggested a Quaternary age based on field relations showing faulted Christmas Canyon Formation (herein reinterpreted as the QTpr1 of the Randsburg Wash Member and QTps1 of the Slate Range Member of the PKFm) and Quaternary gravels (herein reinterpreted as QTps4 of the Slate Range Member of the PKFm). One fault was shown terminating on the Marine Gate fault, and the second cutting across it before bending to the southeast and terminating on the GF east of Slate Road. Our mapping reinterprets these relationships and indicates that the second fault does not cut across the Marine Gate fault, but are separate faults of different ages that conspicuously line up. The north-northwest-striking reverse fault south of the GF is not synchronous with or genetically related to the older northwest-striking normal fault in the Slate Range.

The presence of active fault scarps near the apex of an alluvial fan at 35º 35' 0" N and 117º 15' 22" N and 822 m a.s.l. (Fig. 3.2), well above the highstand shoreline of Searles Lake,

demonstrates that the Searles Valley fault presently cuts this far south along the western Slate Range front. This is significant as it implies that the Searles Valley fault is kinematically and structurally linked to the Marine Gate fault. That the modern Searles Valley fault terminates, and presumably transfers slip onto the Marine Gate fault today, suggests that the same kinematic and structural interaction occurred during the past ~5 Ma. An active Searles Valley fault terminating against the Marine Gate fault would allow open for depositional communication between Searles Valley and PKV, as will be shown below.

Pilot Knob Formation Depositional Environments

The Eagle Crags, Randsburg Wash and Slate Range Members of the PKFm record the complex interactions between the GF, Marine Gate fault, Searles Valley fault and ECSZ during Pliocene and Pleistocene time. Although paleoflow indicators are rare in many of the fanglomerates in PKV, the unique rock types exposed north and south of PKV makes interpreting sediment source direction straightforward. This in turn allows for a rough reconstruction of the evolution of paleogeography and paleotopography of PKV through time (Fig. 3.7).

The three members of the PKFm can be further subdivided into a five-component depositional model (Fig. 3.5) that helps explain the late-Miocene/Pliocene to late Pleistocene development of PKV. The first depositional stage is loosely bracketed between ~5-3.7 Ma, during which time Eagle Crags material was deposited north of the GF. A second stage occurs between 3.7 - 3.1 Ma and involves significant playa-lacustrine deposition along and west of Slate Road. A third stage involving a southward progradation Slate Range fanglomerate occurs between 3.1 - 1.2 Ma. Sediments deposited before 2.5 Ma generally have steeper dips and are

interpreted to thicken to the north against the Marine Gate fault (Fig. 3.4). The fourth stage is a diachronous 2.5 - 0.3 Ma coarse Slate Range fanglomerate (QTps4) that disconformably overlies QTpr1, laterally grades into a finer fanglomerate and sandstone (QTps1), and grades sharply upward from QTps3 (Figs. 3.2 and 3.5). A 1.2 - 0.6 Ma fifth stage of playa-lacustrine deposition occurs in eastern PKV near Charlie Airfield. These lithofacies are discussed below with respect to their relevance to understanding the physiographic and structural development of PKV since the late Miocene.

Eagle Crags Member – northward progradation of Eagle Crags alluvium

The presence of Eagle Crags material indicates a downslope direction to the north from a high-standing Eagle Crags-Pilot Knob. Areas along and west of Slate Road sloped down towards the modern Searles Lake area (Fig. 3.2). The 903-m-deep KM-3 borehole in Searles Valley revealed a 230-m-thick section of coarse alluvial material deposited on plutonic basement rock (Smith et al., 1983). The report noted that the source of the dacite clasts are unknown and are not derived from the Argus or Slate Range. We suggest that late Miocene to middle Pliocene alluvial fans being shed off the Eagle Crags-Pilot Knob massif may have been the source of these enigmatic dacite clasts. Palinspastic reconstructions of PKV using a 6-7 mm/yr slip rate on the GF (Table 3.1) restores Searles Valley with central PKV and north-northeastern Eagle Crags volcanic field (Fig. 3.7c-e) between 4 and 2 Ma. The presence of an active Marine Gate fault with sinistral-oblique-normal slip, combined with an active Searles Valley fault, would allow alluvial sedimentation northward into Searles Valley from the high-standing Eagle Crags volcanic field.

Randsburg Wash Member – low-relief basin floor, slight southward shift in PKV paleo-low

The Randsburg Wash Member is made up of dominantly marginal playa-lacustrine to playa-lacustrine sands, silts and clays, with numerous evaporite deposits throughout (e.g., QTpr1. Fig. 3.2). It is predicted that fine-grained clastic sediments are derived from both the Slate Range and Eagle Crags volcanic field, but also from the Searles Valley fluvial-pluvial input. The massive evaporite deposits are likely from upstream dissolved salts and ions sourced between Searles Valley and Owens Valley (e.g., Jannik et al., 1991). QTpr1 grades laterally to the east into QTpr2 and QTpr3, which contain subordinate amounts of mixed Eagle Crags and Slate Range rocks, and Slate Range clasts, respectively. These units are interpreted as the eastern margin of the Randsburg Wash Member playa-lacustrine basin (Fig. 3.2).

A small rockfall deposit (QTpr4) that is in stratigraphic position similar to the ~3.3 Ma "T-PKV-WMR-C" tephra (Fig. 3.2, Appendix D) bears a Slate Range clast assemblage and is interbedded in QTpr1 and QTpr3. Its occurrence is important and suggests that (1) the near presence of the Slate Range north of QTpr4 and (2) that significant relief existed between the valley floor and the southern Slate Range at ~3.3 Ma. Randsburg Wash member playa-lacustrine sediments west of Slate Road (~3 km west of QTpr4), however, do not contain Slate Range rocks. These rocks west of Slate Road are now faulted against the Slate Range via the Marine Gate fault. We interpret this to indicate 1-3 km of sinistral slip on the Marine Gate fault between 3.1-2.5 Ma, but prefer a ~1.5 km estimate (Table 3.1, Fig. 3.2).

In terms of stratigraphic relationships and spatial proximity, the Randsburg Wash Member playa-lacustrine rocks appear to compare well to the Unit I lacustrine sediments described by Smith and others (1983) in the KM-3 borehole in central Searles Valley. Liddicoat

and others (1980) and Smith and others (1983) suggested lacustrine deposition began ~3.18 Ma in Searles Valley and continued intermittently through the middle Holocene, culminating in 693 m of section. All of this sits on top of 222 m of older alluvium sourced from the Argus Range and possibly the Eagle Crags volcanic field, as indicated by the presence of enigmatic dacitic clasts.

To explain the relationship between deposition of the Randsburg Wash Member and the alluvial-lacustrine rocks at the bottom of Searles Valley, we suggest the following hypothesis. If, for example, Unit I lacustrine depositional ages in Searles Valley (e.g., Smith and others [1983]) are underestimated by ~1-0.5 Ma, then these sediments become synchronous with the ~3.7-3.1 Ma Randsburg Wash member. This would allow the alluvial fanglomerate at the bottom of the KM-3 borehole to better correlate with the Eagle Crags Member unit QTpe1 that underlies the Randsburg Wash Member. Liddicoat and others (1980) use of a presumed Bishop Tuff ash to calibrate their magnetic reversal history would then be in error. They attributed the presence of numerous ash layers between 169-179 m to the ~0.7 Ma Bishop Tuff, but provided no geochemical or chronologic data identifying it as Bishop Tuff. However, because we lack any evidence to prove that this ash is not of the Bishop Tuff, we reject the above hypothesis. Instead, our preferred view is that large-scale shedding of sediments off the Slate Range and into PKV, starting ~3.1 Ma, raises base level in Searles Valley, resulting in the creation of a long-lived Searles Lake and associated lacustrine deposition therein. Additionally, increased shortening after ~2.5 Ma in northern PKV along the Marine Gate fault and GF would further restrict outflow from Searles Valley, and result in significant lacustrine deposition.

Slate Range Member playa-lacustrine lithofacies – low-relief basin floor, possible obstruction to Panamint Valley drainage

A stratigraphically higher playa-lacustrine deposit (unit QTps3) within the Slate Range Member grades upsection and laterally to the west from QTps1 in the eastern PKV study area. QTps3 appears to be a middle Pleistocene depositional center in eastern PKV between 1.2-0.6 Ma (Appendix D). It is inferred here to be an older version of the modern Charlie Airfield playa deposit just east of the study area. Because QTps3 sedimentation is synchronous with Slate Range conglomerate and sandstone to the west, it is included in the Slate Range Member.

Although there were no growth structures or fanning of dips in adjacent QTp3, the upward grading into a low-relief lacustrine basin from a south-sloping Slate Range fanglomerate may indicate two possibilities. The first involves a downstream damming of the fluvial outlet into southern Panamint Valley via N-S contraction between the Quail Mountains and Slate Range, or shortening adjacent to the GF creating the QTps3 depocenter. A second idea is that a small, fault-controlled topographic barrier existed to the north that protected eastern PKV from coarse sediments shed off the Slate Range. We favor the first hypothesis on the basis that no such sedimentary or fault structures (i.e., onlapping alluvial beds, buried fault-cored anticlines, etc.) were observed north of the QTps3 outcrops. It is more likely that playa-lacustrine silt, clay and evaporites were deposited contemporaneously with coarser Slate Range fanglomerates to the west due to sudden changes in baselevel, such as the blocking of the drainage into Panamint Valley.

Slate Range Member conglomeratic lithofacies – southward migration of paleo-low, uplift of Slate Range and/or increased N-S shortening across GF

Units QTps1, QTps2 and QTps4 of the Slate Range Member share a common sedimentologic provenance in the Slate Range. Beginning at ~3.1 Ma, the Slate Range starts shedding significant amounts of alluvium southward across the GF east of the Randsburg Wash-Searles Valley spillway. The Slate Range Member is more than 500 m thick north of Robbers Mountain between the B-B' and C-C' cross sections based on average dips and outcrop exposure. However, the true thickness cannot be determined from outcrop patterns because the base of this sedimentary package is not exposed.

A multi-colored, meta-rhyolite unit in the southeastern Slate Range provides a unique provenance identifier in units QTps1 and QTps4. In figure 3.2, a white-and-black line marks the westward extent of this clast type present in the Slate Range fanglomerate units. As the fans decrease in age upsection, the westward extent of the meta-rhyolite clasts decreases until it aligns closely with its bedrock contact. This relation suggests no sinistral slip adjacent to the Slate Range via the Marine Gate fault after 2.5 Ma. Instead, this clast distribution through the Slate Range fanglomerate suggests deposition in a bajada-type setting where alluvial sedimentation from other parts of the Slate Range occasionally restricts the lateral spread of meta-rhyolite clasts.

The diachroneity exhibited within the interbedding of QTps4 with other facies of the PKFm is a function of the limited lateral continuity of the coarse alluvial fan. West of Slate Road it rests disconformably on lacustrine sediments (QTpr1) of the Randsburg Wash Member, without first grading upward into a distal fanglomerate (e.g., QTps1). East of Slate Road, the QTps4 basal contact cuts upsection near the C-C’ cross-section line as the deposit grades

laterally into unit QTps1. In the far eastern section of the study area, QTps4 grades sharply up from a lacustrine-distal fanglomerate facies at the top of QTps3. This contact then turns into a disconformable relationship east of tephra sample location "T-PKV-WMR-B" (Fig. 3.2).

Provenance & Facies Evolution – Changing Strain & Fault Kinematics In PKV

A three-stage tectonic model is evoked to explain the three PKFm members discussed above. Stage 1 is a pre-3.1 Ma transtensional phase in northern PKV with a moderate paleo-low developed between the GF and Slate Range. Stage 2 is a 3.1-1.2 Ma transitional period of predominately sinistral slip on the GF with waning sinistral-oblique-normal slip on the Marine Gate fault through ~2.5 Ma; ~2.5-1.2 Ma may involve minimal N-S contraction and uplift in northern PKV. A post-1.2 Ma stage 3 is characterized by significant contraction and uplift of sediments north of the GF, as well as some contraction and uplift of the southern Slate Range. During this stage, the Marine Gate fault is reactivated as an en echelon series of reverse faults that primarily uplift sediments adjacent to the Slate Range, but also thrust Slate Range rocks on top of QTps4 of the PKFm. During all three stages, east-west-directed extensional faulting occurs along the western margin of the southern Slate Range on the Searles Valley fault.

During deposition of the Eagle Crags Member (~5-3.7 Ma) and early periods of the Randsburg Wash Member (3.7-3.1 Ma), northern PKV may have resembled an asymmetric pull-apart basin bounded by an active Marine Gate fault and the GF. Our post-5 Ma tectonic reconstructions suggest ~7.5 km of sinistral offset between 5-2.5 Ma (Fig. 3.7). It is likely that the Marine Gate fault was active prior to 5 Ma (e.g., Andrew, 2007), but we only interpret its post-5 Ma history in this report.

The pre-2.5 Ma Marine Gate fault was an active sinistral-oblique complement to the GF and cut adjacent to the southern Slate Range face. It allowed a paleo-low depocenter north of the present GF to form, as evidenced by the progradation of Eagle Crags sediments into northern PKV (Figs. 3.2, 3.5 and 3.7). West of Slate Road, playa-lacustrine silts, clays and evaporites as young as 3.1 Ma are exposed less than 1 km from the southwest Slate Range front. To the west of Randsburg Wash-Searles Valley spillway, ~5-3.7 Ma Eagle Crags-derived sediments are exposed as far north as the southern Slate Range front and project across one strand of the poorly exposed Marine Gate fault. These Eagle Crags sediments probably project to the center of Searles Lake and intermingle with the coarse alluvial deposits described by Smith and others (1983) in the KM-3 dill core. We speculate that an active Searles Valley fault lowered baselevel north of the Marine Gate fault in Searles Valley during this time, which aided the northward transport of Eagle Crags material into Searles Valley.

The presence of playa-lacustrine sediments close to and juxtaposed against the southwestern corner of the Slate Range indicates active subsidence of the valley floor adjacent to the Slate Range through 3.1 Ma followed by waning sinistral slip on the Marine Gate fault until ~2.5 Ma. It also requires the occurrence of significant sinistral displacement on the Marine Gate fault to juxtapose these fine-grained sediments against a range front with ~700 m of relief. Immediately west of Slate Road, the westward pinchout of QTps1, combined with QTps2 and QTps4 disconformably overlying QTpr1, suggests 1-3 km of sinistral displacement between ~3.1-2.5 Ma (Fig. 3.2). Along and east of Slate Road, the upward coarsening of the Slate Range Member from the playa-lacustrine units of the Randsburg Wash Member is both a response of (1) decreasing subsidence of the valley floor adjacent to the Slate Range and (2) continued slip on the Marine Gate fault bringing the Slate Range closer to the QTpr1 playa-lacustrine basin.

The cessation of sinistral slip on the Marine Gate fault by ~2.5 Ma is supported by the occurrence of meta-rhyolite clasts within units QTps1 and QTps4 of the Slate Range Member of the PKFm (black-and-white dashed line in figure 3.2). There is no discernable lateral offset of this clast-bearing fanglomerate from its source in the southeastern Slate Range.

A second tectonic stage (3.1-1.2 Ma) is characterized by arid alluvial fan deposition of QTps1 and QTps4 derived from the Slate Range. We consider 3.1 Ma as an approximate start to the middle stage because the end of playa-lacustrine deposition appears to indicate the cessation of a significant topographic subsidence north of the GF around this time. This compares well to a 3.4 Ma development of the ECSZ along the Panamint Valley-Owens Valley-Barstow corridor estimated by Gan and others (2003) from back-calculating vorticity in the regional strain field and the total rotations of the GF segments. We view it likely that the ECSZ rotates the GF and Marine Gate fault, causing the latter structure to no longer be ideally oriented for sinistral slip (Fig. 3.7).

Additionally, north-south shortening should commence as dextral shear on faults of the ECSZ, especially the Panamint Valley fault, become increasingly diffuse near the GF and cause off-fault deformation. Limited basin inversion coupled with moderate northeast tilting of the sediments occurs during this time. North-south shortening is inferred to gradually increase after ~2.5 Ma as no sharp angular discordances were observed in the QTps1 and QTps4 strata. However, the progressive fanning of dips upsection indicates either (1) syn-tectonic sedimentation during low to moderate shortening rates, or (2) increasing mechanical strengths and shallower structural levels of the coarser Slate Range fanglomerates perhaps hindered tilting and folding. In this second idea, shortening is confined primarily to the mechanically weaker evaporitic and playa-lacustrine units QTpr1 and QTps3 (Fig. 3.4). In support of this speculative

conclusion, the Eagle Crags Member is similarly tilted as the Randsburg Wash Member, but is not as strongly folded and faulted on the local outcrop scale as the QTpr1 playa-lacustrine sediments are. QTps3 also shows tight and isoclinal folding that is not commonly present in the older QTps1 unit. In both examples, the younger, QTps3 playa-lacustrine units are more strongly deformed on the meso-scale, suggesting the possibility that strain is being localized in the rheologically weaker playa-lacustrine layers.

Tectonic stage 3 (~1.2 Ma-present) represents the ongoing rapid basin inversion in northern PKV. However, in spite of strong uplift and tilting in western- and central-northern PKV, relatively low and flat topography was maintained east of tephra sample "T-PKV-WMR-B" (Fig. 3.2) until ~0.6 Ma, as evidenced by eastward thickening of QTps3 playa-lacustrine sediments. In central-northern PKV, deposition of QTps4 coarse conglomerate through 0.3 Ma signifies a moderately sloping alluvial fan occupying much of the area north and south of the GF here. These sediments are back-tilted to the northeast by as much as 25º at the bottom of the section but generally dip 5-15º elsewhere. This decrease in stratal tilts indicates both decreasing age, and thus shorter periods of strain accumulation, and an increase in mechanical competence in relation to the older, finer-grained PKFm members. The lack of Slate Range Member lithofacies of the PKFm near the Randsburg Wash-Searles Valley spillway suggests significant uplift and erosion of these younger, stratigraphically higher sedimentary sections. The only Slate Range-derived material west of the spillway crops out in mid to late Pleistocene Christmas Canyon Formation (discussed below).

An alternative to the afore-described model, incorporating ~7.5 km of sinistral slip on the Marine Gate fault since ~5 Ma, is one that suggests more significant uplift and shortening at the southern boundary of the Slate Range. Where QTpr1 lacustrine sediments are juxtaposed against

Slate Range basement rocks via reverse faults, several hundreds of meters of throw is required. At this time there is insufficient evidence to suggest such uplift magnitudes are present in the southern Slate Range after 3.1 Ma. A more tenable model thus invokes significant strike-slip offset on the Marine Gate fault prior to post-2.5 Ma reverse faulting along the southern Slate Range front.

The existence of a sinistral-oblique-normal Marine Gate fault between ~5-2.5 Ma would be expected to contribute to the greater NE-dip magnitudes among these sedimentary rocks. However, significant erosion of post-3.7 Ma sediments west of the Randsburg Wash-Searles Valley spillway, and the absence of definitive angular unconformaties between the three PKFm Members to the east prevent us from placing strong brackets on possible basin subsidence that would be expected. It may be that subsidence of northern PKV was minimal on the Marine Gate fault. But we do note that bedding dips are significantly steeper along the spillway where the Marine Gate fault crosses it (Fig. 3.2).

Provenance & Facies Assemblages Of Exposed Christmas Canyon Formation

As described above, an additional package of sub-horizontal to flat-lying sediments crop out in northwestern PKV and southern Searles Valley. Smith (1964, 2009) first noted these sediments and proposed the Christmas Canyon Formation and the Searles Valley Formation to include sediments between 1-0.3 Ma and sediments younger than 150 ka, respectively. However, we here reinterpret the ages and formation associations of these sediments based on field relations, but note that we do not have absolute age control. Outcrop relations show that both Qcl and Qcf (Fig. 3.2) compose the Christmas Canyon Formation north of the GF. Further, Qsw, Qsh and Qst are the only Searles Valley Formation sediments exposed in the study area.

The oldest Christmas Canyon Formation section exposed here is Qcl, a 150-300 ka sub-horizontal, light-green to bluish lacustrine siltstone and claystone west of Randsburg Wash-Searles Valley spillway. Its sharp angular disconformity with underlying PKFm indicates (Fig. 3.6b) a significant hiatus due to uplift and erosion preceding Qcl deposition (Fig. 3.5). This area of southern Searles Valley probably sat lower in elevation with respect to the modern lake bed than it does today due do differential uplift along the Marine Gate fault. Conversely, the spillway into PKV was not as deeply incised as it currently is across the GF to the south. This lower relative elevation would allow for moderate lacustrine deposition during a highstand period. Sub-horizontal bedding of the Ocl suggests minimal tectonic disturbance, although broad uplift of several tens of meters following Qcf deposition is suggested below.

Deposited disconformably on top of Qcl is a younger, 50-150 ka Qcf. Qcf is a flat-lying, poorly bedded package of alluvium and colluvium. There is no discernable angular discordance along its basal contact with Qcl, but there is a scour surface locally. We support the interpretation of Smith (2009) that Qcf is a northward-prograding alluvial fan complex into Searles Valley during a low-stand event. However the entrainment of Slate Range clasts and the locally rounded clast morphology suggests fluvial-pluvial reworking and amalgamation with fans mantling the Slate Range. Deep incision of the Randsburg Wash-Searles Valley spillway to the east, and an appreciable topographic slope to the north, west and south, suggest several tens of meters of broad uplift along the northern strand of the buried Marine Gate fault. Small reverse scarps are present locally and support this conclusion.

Tephrochronologic Data – Implications For Distinguishing The Pilot Knob Formation From Christmas Canyon Formation

A significant revision to the late Cenozoic stratigraphy is proposed in this paper. Based on field relations, provenance data and tephrochronologic data, the tilted and deformed sediments older than 0.3 Ma north of the GF cannot belong to the Christmas Canyon Formation as previously interpreted by Smith (1964, 2009) and Smith and others (1968). Tephra sample T-PKV-WMR-E (Appendix D) dates sediments that formerly interpreted to be Christmas Canyon Formation at 2.9-3.2 Ma and suggests that these are more likely PKFm deposits. Recent mapping by Rittase (unpublished data) in the northeast Lava Mountains re-interpreted the Christmas Canyon Formation to be two distinct alluvial deposits; a late Miocene, El Paso Mountains fanglomerate (Tf-el), and a Pliocene, distal Eagle Crags alluvial deposit (QTpe3(?), (Fig 3.2). We note that Members 4 and 5 of the PKFm are partially time correlative to QTpe3(?) south of the GF.

SUMMARY & CONCLUSIONS

Depositional and provenance patterns, combined with deformation patterns, offer critical clues to basin architecture and the tectonic development of a basin. PKV is ideally situated along the central GF to record the evolving tectonic environment along the southwestern US plate boundary from east-west extension to NW-directed dextral shear and concomitant north-south shortening.

The study area consists of four fault blocks, from north to south: (1) southern Slate Range cored by Mesozoic metamorphic rocks, (2) Searles Valley underlain by the west-dipping Searles Valley fault, (3) uplifted and northerly tilted Pliocene to Holocene sediments between the Marine

Gate fault and GF, and (4) buried (sub-horizontal?) late Neogene sediments and the Eagle Crags volcanic field south of the GF in PKV. The newly recognized PKFm is key to understanding the geometric and kinematic evolution of the faults bounding these four blocks. Evidence for an evolving strain field includes three lithostratigraphic members within the PKFm: (1) Eagle Crags Member - a basal, distal alluvial fan deposit with Eagle Crags-derived volcanic clasts that grades upward into a playa-lacustrine-margin deposit; (2) Randsburg Wash Member - a medial, playa-lacustrine facies with evaporites, siltstones and claystones that grades laterally to the east to sandstone; and (3) Slate Range Member - an upper, sandstone and conglomerate facies with an interbedded playa-lacustrine deposit to the east. During PKFm deposition, the topographic low within the central and western PKV migrated progressively southward from its former position adjacent to the Marine Gate fault and continuous with Searles Valley. A short-lived topographic low existed in the eastern PKV study area between 1.2-0.6 Ma before being uplifted and tilted.

The presence of Eagle Crags clasts in northern and western PKV indicates a continuous paleo-low north of the present GF through ~3.7 Ma. An overlapping and interfingering 3.7-3.1 Ma lacustrine Randsburg Wash Member indicates a decrease in slope and slight southward shift in the valley's depocenter, and/or, a downstream blockage in drainage, resulting in a pluvial setting. Finally, southward progradation of coarse Slate Range fanglomerates at ~2.5 Ma indicates a further southward shift in PKV's depocenter. East-west variations and interfingering with different members of the PKFm suggests that these members are diachronous.

A three-stage tectonic model invoking a second sinistral-oblique-normal strand of the GF (e.g., Marine Gate fault) is invoked to best explain the present structural and depositional configuration here. An initial pre-3.1 Ma tectonic period of significant slip on the Marine Gate fault resulted in a significant paleo-low north of the GF that was filled with Eagle Crags clasts

sourced from the south. These sediments likely made it north into the adjoining Searles Valley where the KM-3 borehole recorded the presence of dacitic clasts in pre-3.18 Ma alluvial sediments (Smith et al., 1983). Restoring slip on the GF and Marine Gate fault would place Searles Valley adjacent to PKV at this time. A subsequent 3.1-1.2 Ma stage of increasing north-south shortening related to development of the ECSZ, and in particular the Panamint Valley fault, results in a southward progradation of Slate Range sediments across the GF. The Marine Gate appears to accommodate up to 7.5 km of sinistral slip by 2.5 Ma, of which, ~1.5 km occurs between 3.1-2.5 Ma. The lack of offset of a distinct meta-rhyolite in post-2.5 Ma sediments indicates the cessation of sinistral slip on the Marine Gate fault. A final post-1.2 Ma tectonic stage is characterized by rapid uplift and shortening north of the GF and reactivation of the Marine Gate fault as an en echelon series of reverse faults. Additional reverse faults place Slate Range basement rocks on top of the 2.5-0.3 Ma QTps4 unit of the PKFm.

TABLES

TABLE 3.1 - PILOT KNOB VALLEY PALINSPASTIC RECONSTRUCTION

Time *(Ma)*	Garlock Fault *(km, sinistral)*	Marine Gate Fault *(km, sinistral)*	Panamint Valley Fault *(km, dextral)*	Searles Valley Fault *(km, East-West)*
0 – 1 Ma	7	0	2.5	0.3
1 – 2 Ma	7	0	2.5	0.5
2 – 3 Ma	6	1.5	2	1.5
3 – 4 Ma	6	3	0.5	1.5
4 – 5 Ma	6	3	0	1.5
0 – 5 Ma	32	7.5	7.5	4.8

FIGURES

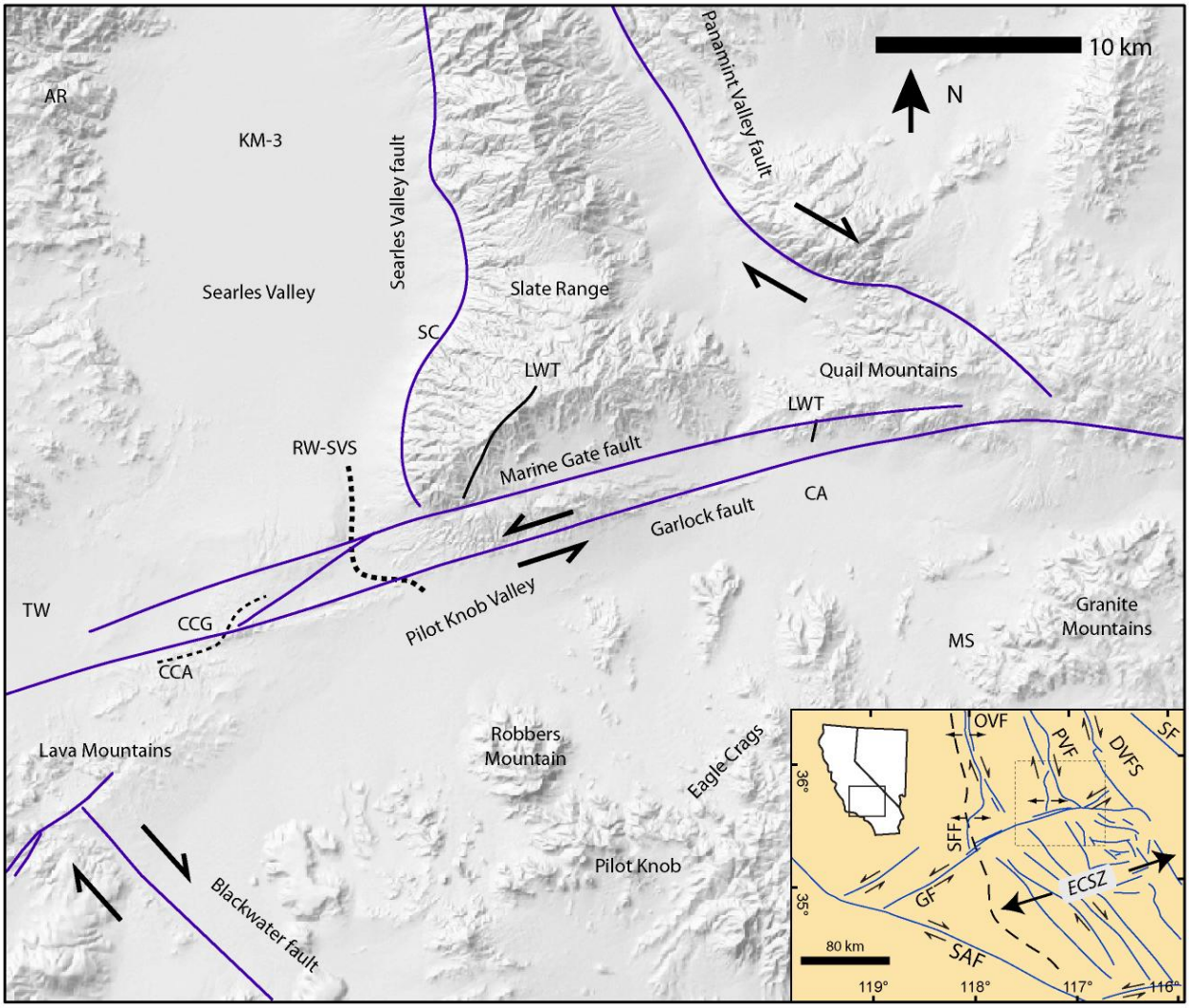
10 km
N
AR
KM-3
Searles Valley fault
Panamint Valley fault
Searles Valley
Slate Range
SC
LWT
Quail Mountains
LWT
RW-SVS
Marine Gate fault
CA
Garlock fault
TW
CCG
CCA
Pilot Knob Valley
Granite Mountains
MS
Lava Mountains
Robbers Mountain
Eagle Crags
Pilot Knob
Blackwater fault
OVF
PVF
DVFS
SF
SFF
GF
ECSZ
SAF
80 km
36°
35°
119°
118°
117°
116°

Figure 3.1 – Shaded-relief Quaternary fault map of Pilot Knob Valley study area with inset stylized neotectonic map of southern California (lower right). Dashed box in inset map indicates coverage of gray-scale shaded-relief map. Inset California-Nevada map shows the location of stylized neotectonic map with a solid box. Arrows indicate sense of strike-slip and dip-slip motion. Heavy dashed line on inset map locates the Eastern California shear zone (ECSZ). AR, Argus Range; CA, Charlie Airfield; CCA, Christmas Canyon anticline ; CCG, Christmas Canyon gate; DVFS; Death Valley fault system; GF, Garlock fault; KM-3, KM-3 borehole; LWT, Layton Well thrust; MS, Myrick Spring; OVF, Owens Valley fault; PVF, Panamint Valley fault; RW-SVS, Randsburg Wash-Searles Valley spillway; SAF, San Andreas fault; SC, South Canyon; SF, Stateline fault; SFF, Sierra frontal fault; TW, Teagle Wash.

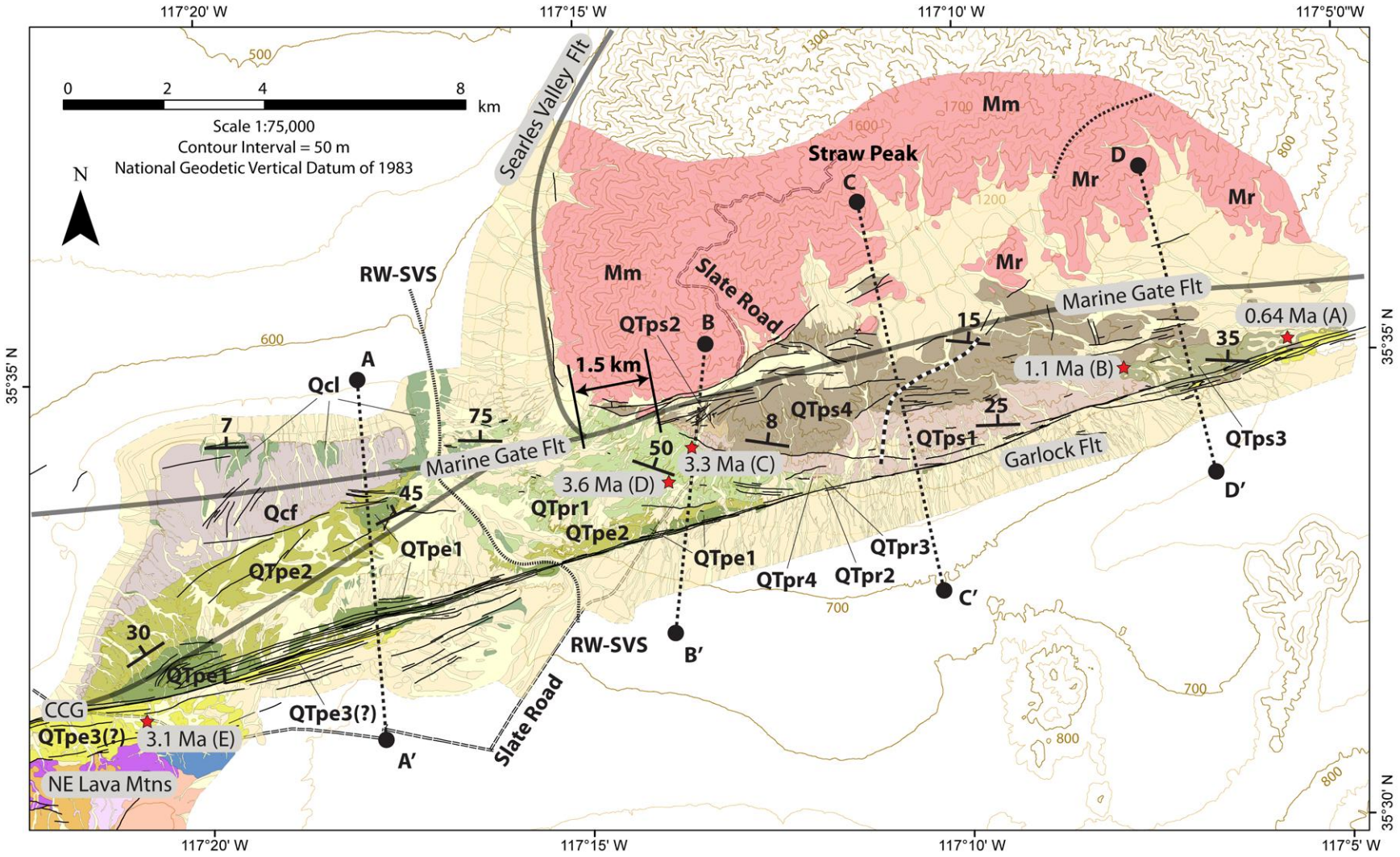
117°20' W
117°15' W
117°10' W
117°5'0"W
35°35' N
35°30' N
0 2 4 8 km
Scale 1:75,000
Contour Interval = 50 m
National Geodetic Vertical Datum of 1983
N
Searles Valley Flt
Straw Peak
Mm
Mr
Slate Road
RW-SVS
Marine Gate Flt
Garlock Flt
QTps2
QTps4
QTps1
QTps3
Qcl
Qcf
QTpe1
QTpe2
QTpe3(?)
QTpr1
QTpr2
QTpr3
QTpr4
CCG
NE Lava Mtns
0.64 Ma (A)
1.1 Ma (B)
3.3 Ma (C)
3.6 Ma (D)
3.1 Ma (E)
1.5 km
A
A′
B
B′
C
C′
D
D′
7
75
45
30
50
8
15
35
25
500
600
700
800
1200
1300
1600
1700

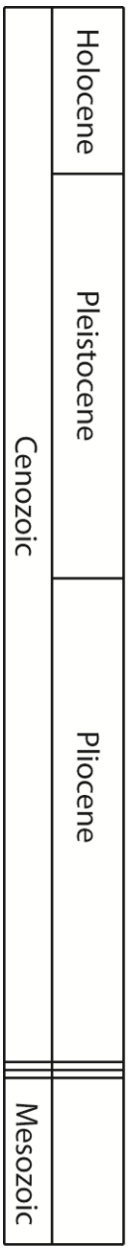

	Undifferentiated Late Pleistocene - Holocene alluvium
Qcf	Christmas Canyon Fm - Coarse alluvium & colluvium
Qcl	Christmas Canyon Fm - mudstone, siltstone & evaporite
QTps4	PKFm - Slate Range Member - coarse conglomerate & sandstone
QTps3	PKFm - Slate Range Member - brown mudstone, siltstone & evaporite
QTps2	PKFm - Slate Range Member - coarse conglomerate with hematite & mangnese-oxide staining
QTps1	PKFm - Slate Range Member - pebble conglomerate & sandstone
QTpr4	PKFm - Randsburg Wash Member - rockfall deposit
QTpr3	PKFm - Randsburg Wash Member - pebble conglomerate, sandstone & siltstone
QTpr2	PKFm - Randsburg Wash Member - pebble conglomerate, sandstone & siltstone
QTpr1	PKFm - Randsburg Wash Member - white siltstone, mudstone & evaporite
QTpe2	PKFm - Eagle Crags Member - gypsiferous sandstone, siltstone & mudstone
QTpe3(?)	Possible PKFm correlative unit - sandstone, siltstone & mudstone
QTpe1	PK Fm - Eagle Crags Member - pebble conglomerate & sandstone
Mm	Undifferentiated Mesozoic Meta-Igneous & -sedimentary rocks of Slate Range (Mr = meta-rhyolite unit in SE Slate Range)

Figure 3.2 – Simplified geologic map of Pilot Knob Valley study area. For simplicity, modern streams and sediments younger than ~100 Ka have been shaded light yellow and yellow, respectively. Red stars denote 5 tephra samples "T-PKV-WMR-A" to "T-PKV-WMR-E" described in the text and Appendix D. Dashed white-and-black line denotes western extent of meta-rhyolite clasts in the Pilot Knob Formation. "M" denotes locations where meta-rhyolite crops out in the Slate Range. Heavy dashed lines A-A' to D-D' show locations for structural cross-sections in figure 3.4. Light dashed lines locate Slate Road and Randsburg Wash-Searles Valley spillway. Heavy transparent lines locate inferred faults. CAF, Charlie Airfield; CCG, Christmas Canyon gate; RW-SVS, Randsburg Wash-Searles Valley spillway.

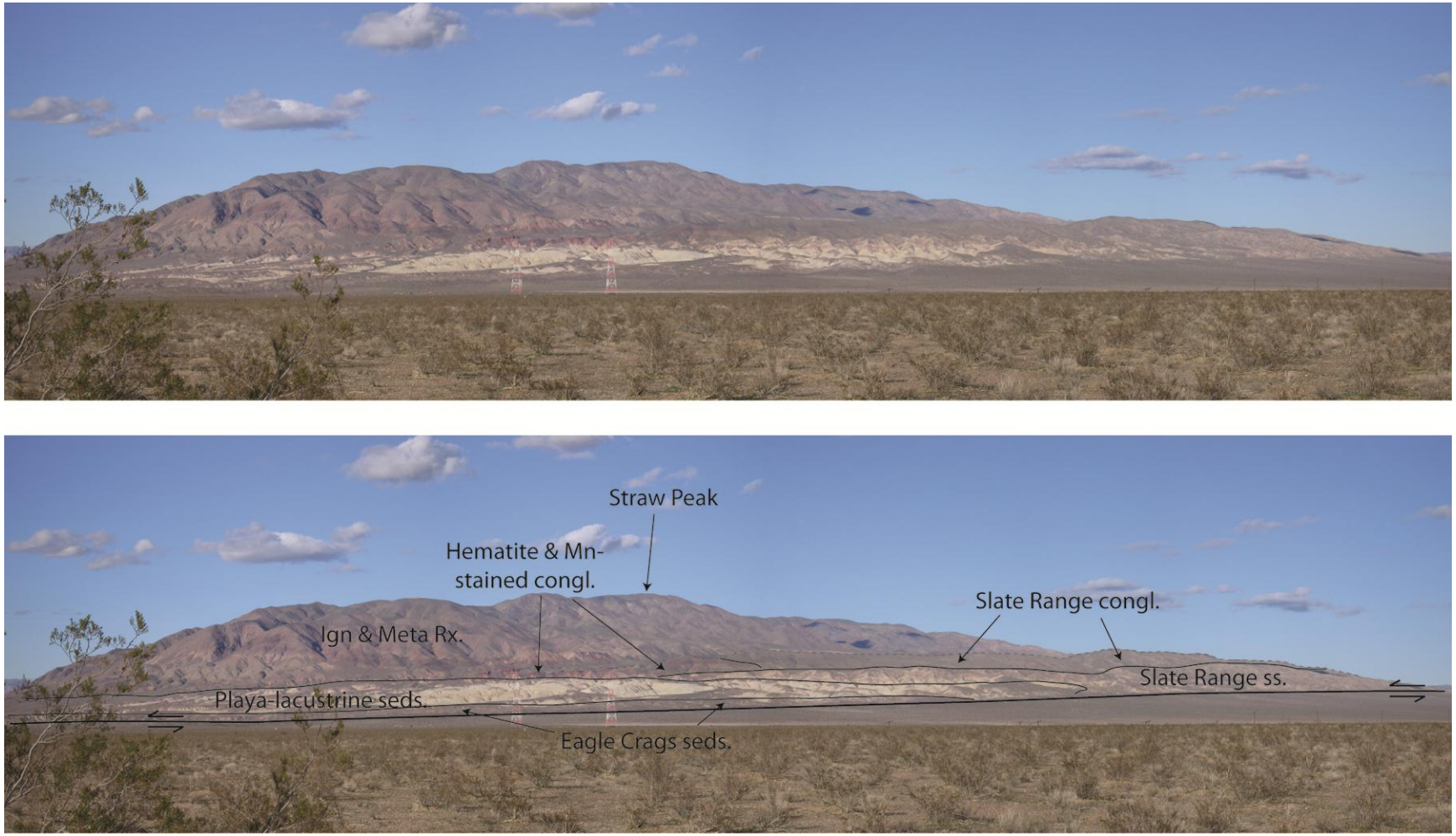
Straw Peak
Hematite & Mn-
stained congl.
Ign & Meta Rx.
Slate Range congl.
Slate Range ss.
Playa-lacustrine seds.
Eagle Crags seds.

Figure 3.3 – Annotated field photograph showing uplifted late-Cenozoic sediments in northern Pilot Knob Valley. View is looking northeast. Heavy-weight line marks the Garlock fault and arrows indicate slip direction. Medium-weight lines separate sedimentologic and lithologic facies as labeled. Thin dashed line marks top of conglomerate hilltop in front of Slate Range.

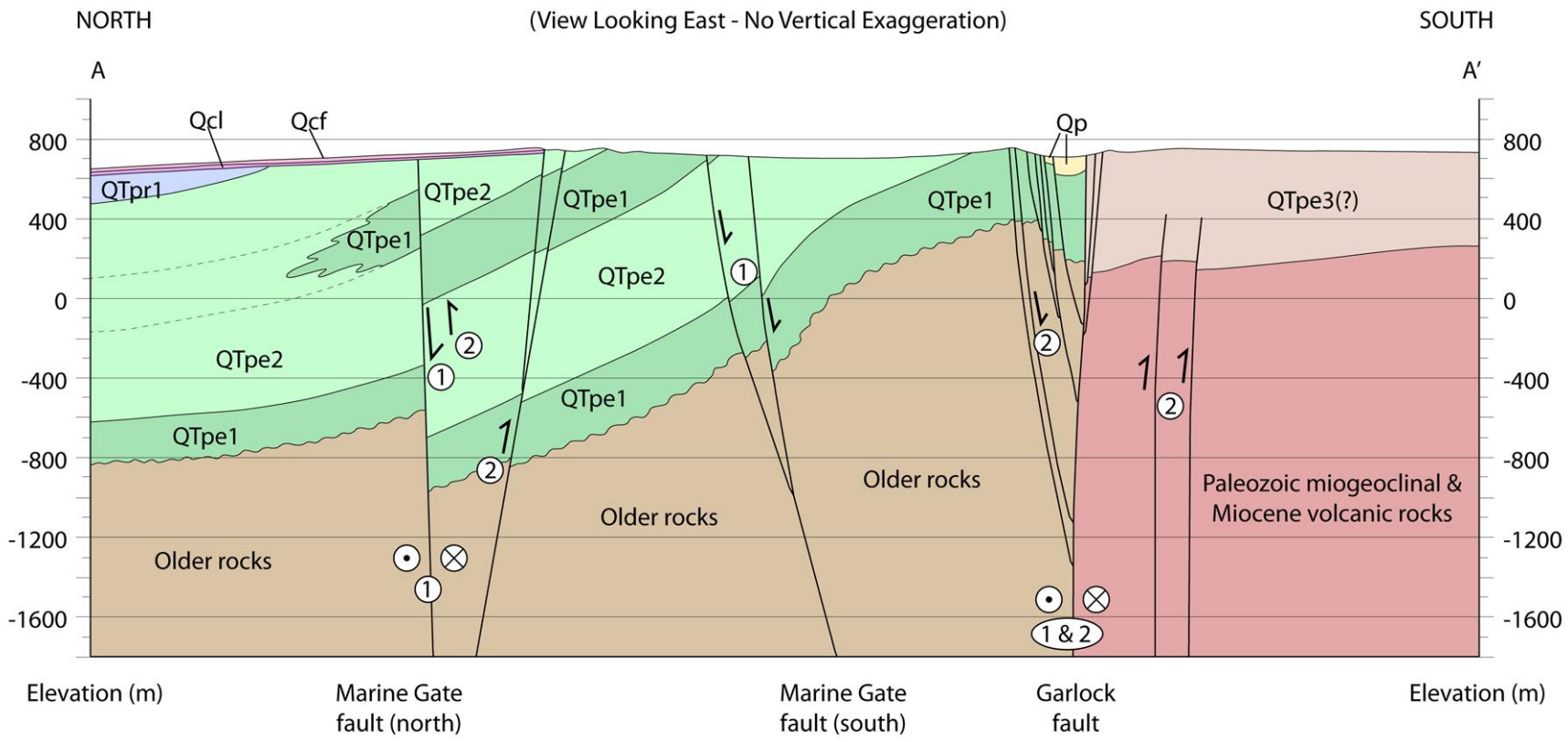
NORTH
(View Looking East - No Vertical Exaggeration)
SOUTH
A
A'
Qcl
Qcf
Qp
QTpr1
QTpe2
QTpe1
QTpe3(?)
Older rocks
Paleozoic miogeoclinal &
Miocene volcanic rocks
1 & 2
800
400
0
-400
-800
-1200
-1600
Elevation (m)
Marine Gate
fault (north)
Marine Gate
fault (south)
Garlock
fault

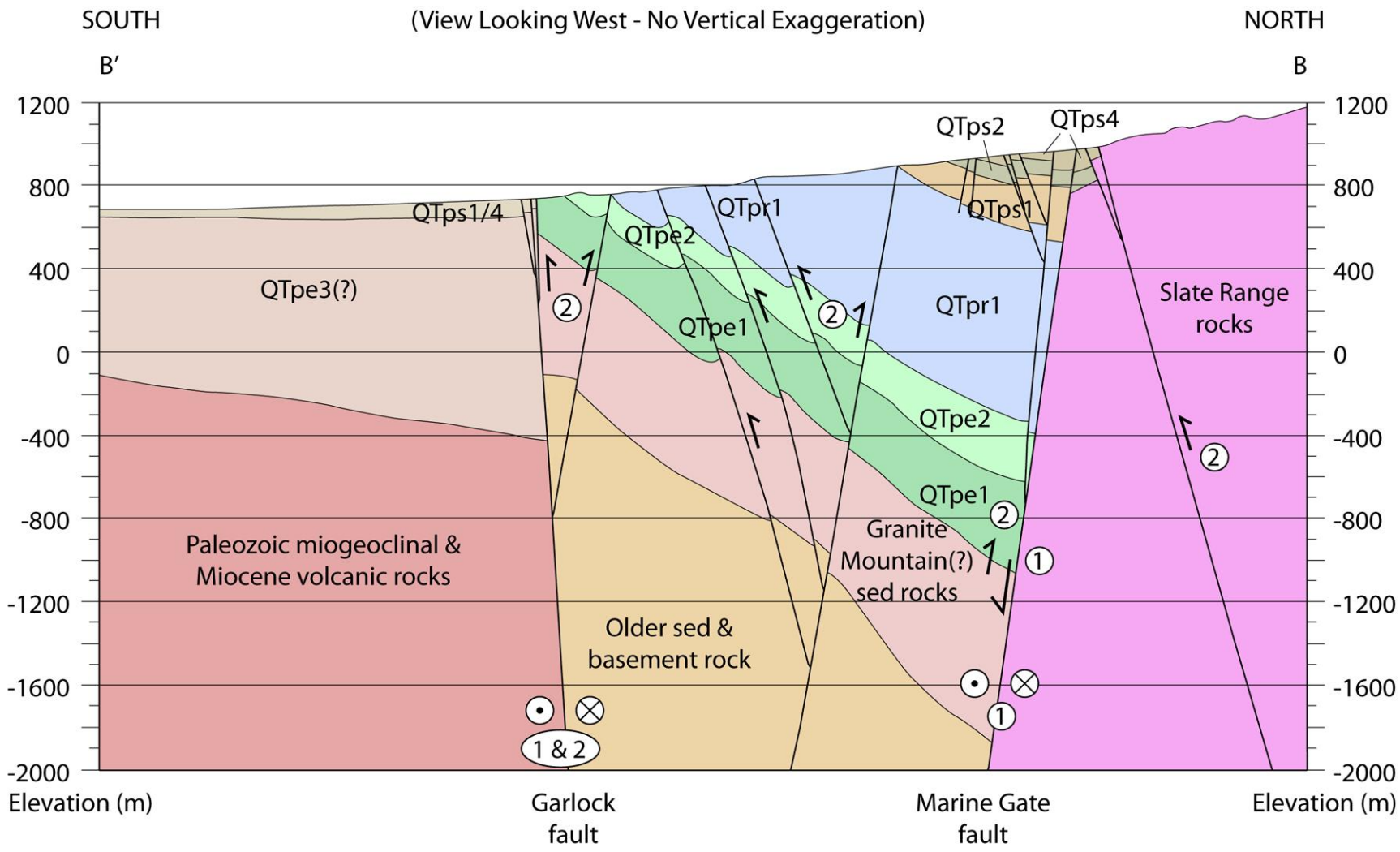
SOUTH
(View Looking West - No Vertical Exaggeration)
NORTH
B'
B
1200
800
400
0
-400
-800
-1200
-1600
-2000
Elevation (m)
QTps1/4
QTpe3(?)
QTpe2
QTpr1
QTps2
QTps4
QTps1
QTpe1
Slate Range rocks
Paleozoic miogeoclinal & Miocene volcanic rocks
Older sed & basement rock
Granite Mountain(?) sed rocks
1 & 2
Garlock fault
Marine Gate fault

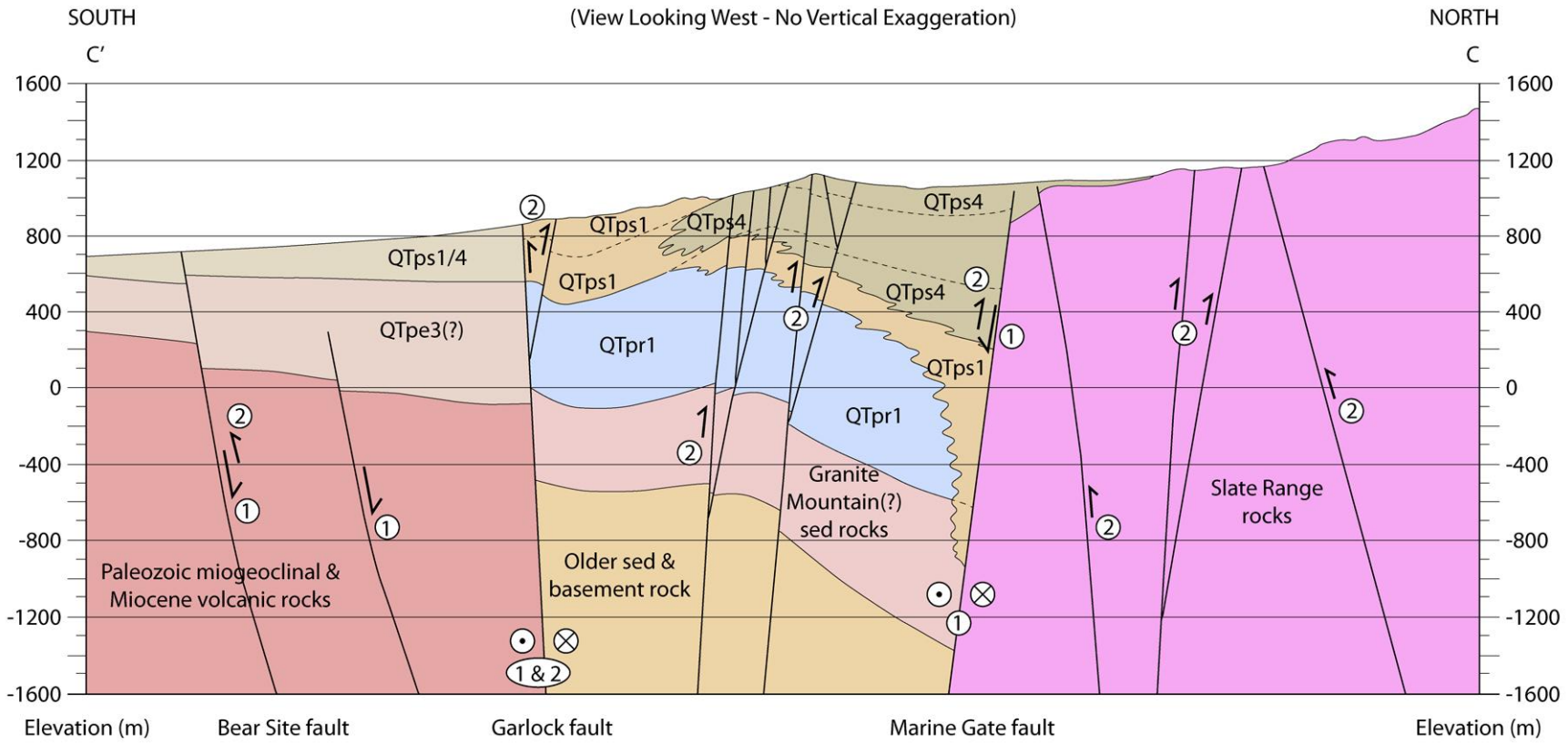
SOUTH
(View Looking West - No Vertical Exaggeration)
NORTH
C′
C
1600
1200
800
400
0
-400
-800
-1200
-1600
QTps1/4
QTps1
QTps4
QTpe3(?)
QTpr1
Paleozoic miogeoclinal &
Miocene volcanic rocks
Older sed &
basement rock
Granite
Mountain(?)
sed rocks
Slate Range
rocks
1 & 2
Elevation (m)
Bear Site fault
Garlock fault
Marine Gate fault
Elevation (m)

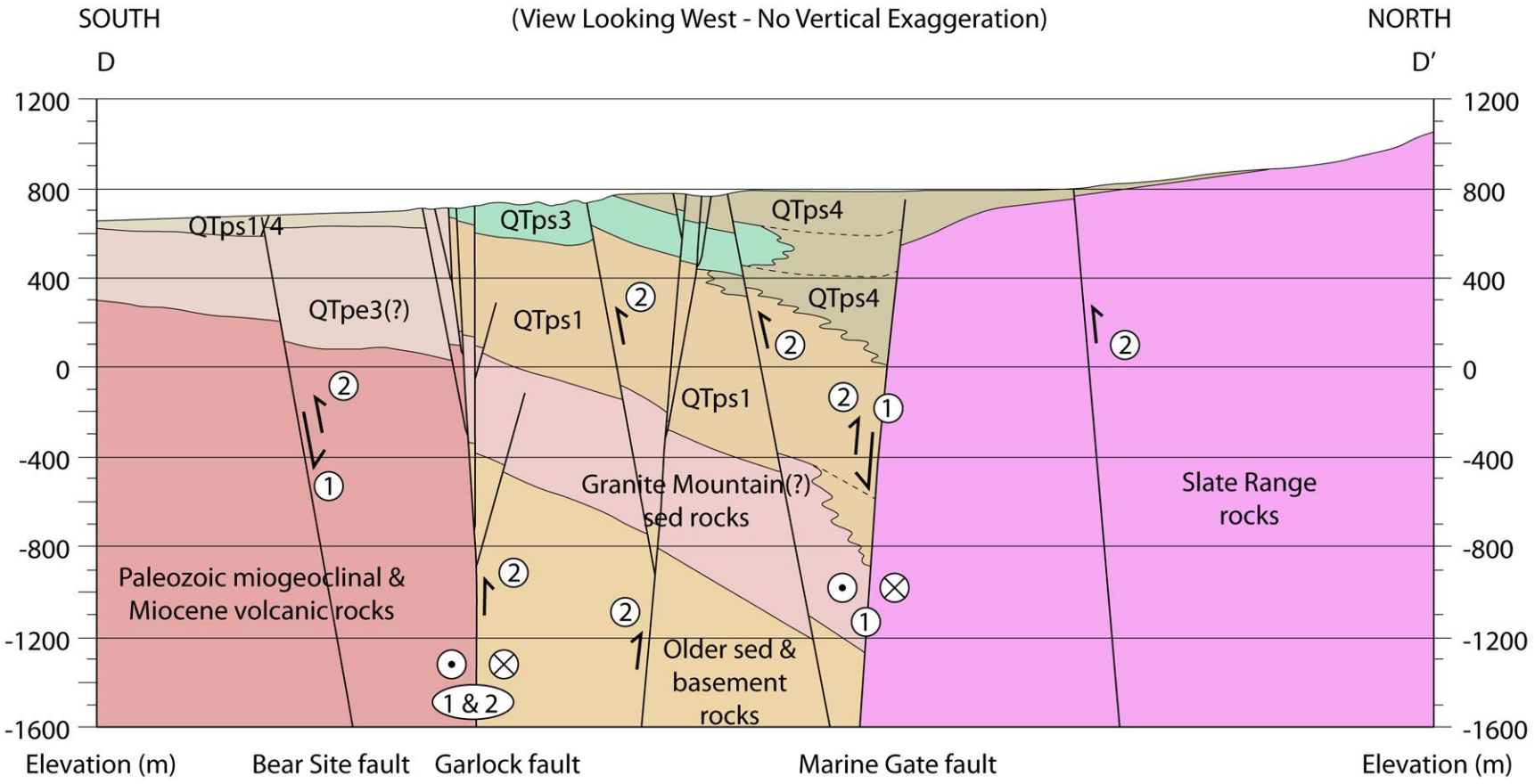
SOUTH
(View Looking West - No Vertical Exaggeration)
NORTH
D
D'
1200
800
400
0
-400
-800
-1200
-1600
QTps1/4
QTps3
QTps4
QTps4
QTpe3(?)
QTps1
QTps1
Granite Mountain(?)
sed rocks
Slate Range
rocks
Paleozoic miogeoclinal &
Miocene volcanic rocks
Older sed &
basement
rocks
1 & 2
Elevation (m)
Bear Site fault
Garlock fault
Marine Gate fault
Elevation (m)

Figure 3.4 – Structural and stratigraphic cross sections through A-A', B-B', C-C' and D-D' lines on figure 3.2. White circles with "1" and "2" inside indicate pre-2.5 Ma and post-2.5 Ma activity. Arrows indicate relative sense of block displacement.

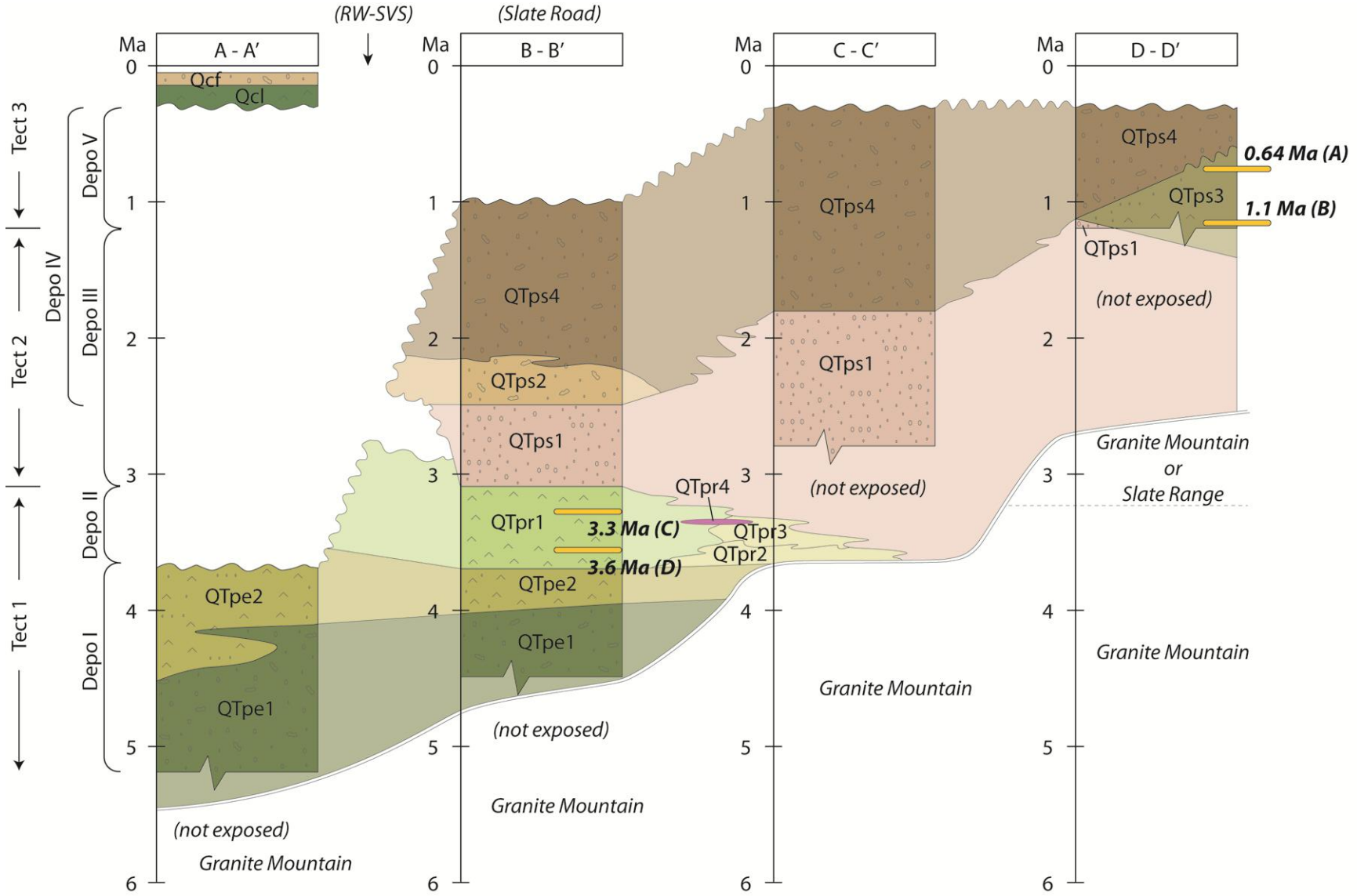
(RW-SVS)
(Slate Road)
A - A'
B - B'
C - C'
D - D'
Ma
0
1
2
3
4
5
6
Tect 3
Tect 2
Tect 1
Depo V
Depo IV
Depo III
Depo II
Depo I
Qcf
Qcl
QTps4
QTps3
QTps2
QTps1
QTpr4
QTpr3
QTpr2
QTpr1
QTpe2
QTpe1
0.64 Ma (A)
1.1 Ma (B)
3.3 Ma (C)
3.6 Ma (D)
(not exposed)
Granite Mountain
Granite Mountain
or
Slate Range

Figure 3.5 – Generalized stratigraphic columns for the four structural cross-sections located on figure 3.2. Only late-Cenozoic sediments are depicted. See figure 3.2 for explanation of unit labels. Four tephrochronology samples (T-PKV-WMR-A, T-PKV-WMR-B, T-PKV-WMR-C and T-PKV-WMR-D) are plotted with yellow-orange rectangles in columns B-B' and D-D'. RW-SVS, Randsburg Wash-Searles Valley spillway; CCG, Christmas Canyon gate.

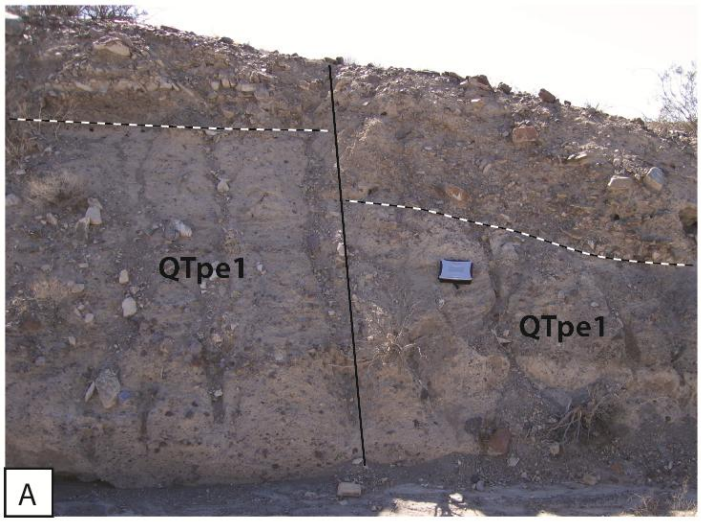
QTpe1
QTpe1
A

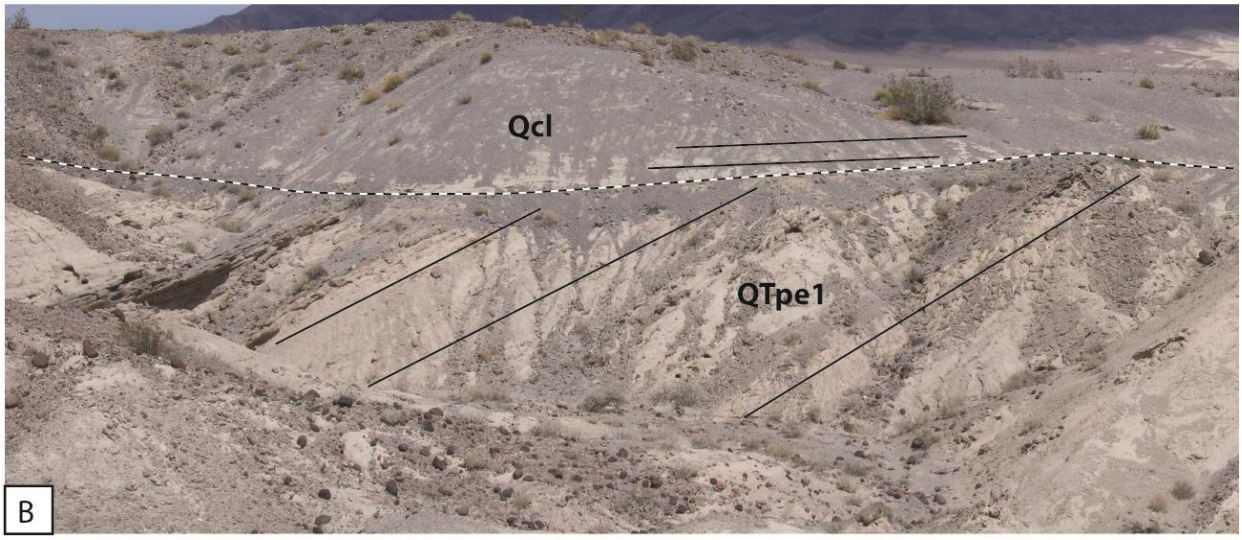
Qcl
QTpe1
B


QTpr1
C


QTpr1
D

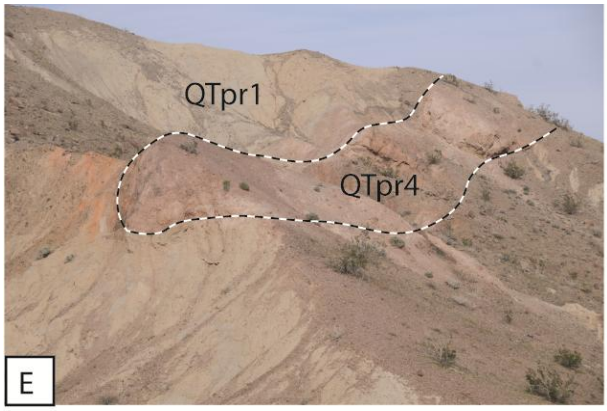
QTpr1
QTpr4
E


QTps1
F

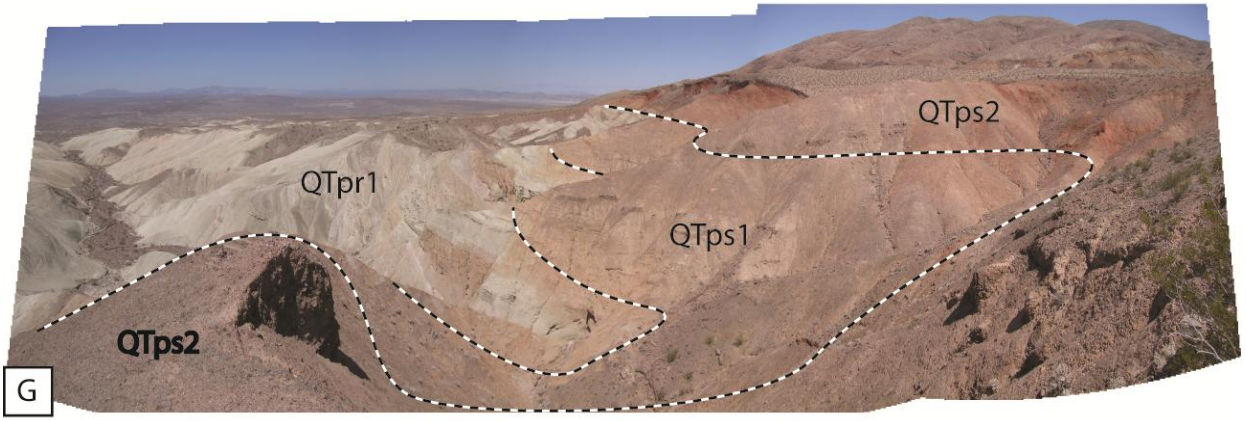
QTps2
QTpr1
QTps1
QTps2
G


QTps3
H

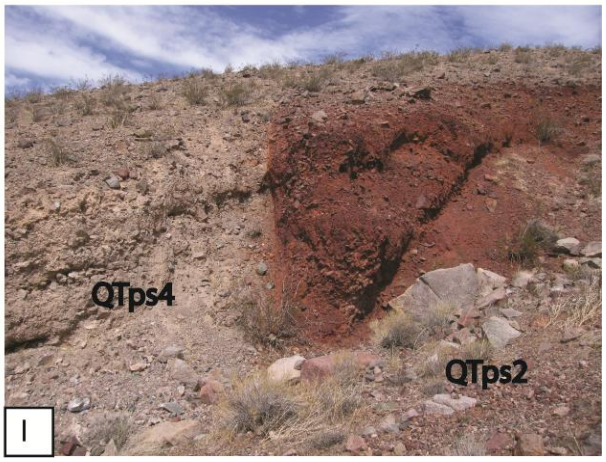
QTps4
QTps2
I

Figure 3.6 – Annotated field photographs showing key sedimentologic and litho-facies of the Pilot Knob Formation. (A) Lower distal Eagle Crags conglomerate and sandstone (QTpe1). (B) Lower distal Eagle Crags conglomerate and sandstone (QTpe1) dipping ~45° N is capped unconformably by sub-horizontal Christmas Canyon Formation lacustrine sediments (Qcl). Photo was taken ~2 km west of Randsburg Wash-Searles Valley spillway along the A-A' cross-section line. View is looking north. (C) Close-up of folded white playa-lacustrine siltstone, claystone and evaporite beds (QTpr1). Photo was taken along the B-B' cross-section line. Outcrop rapidly weathers to popcorn-like surface on left. (D) White QTpr1 playa-lacustrine outcrops ~1 km west of "T-PKV-WMR-D" tephra sample. (E) Red granite and black meta-sedimentary rockfall deposit (QTpr4) within QTpr1. (F) Lower distal Slate Range conglomerate and sandstone (QTps1) ~1 km east of B-B' cross-section line. (G) Panoramic view looking west. White QTpr1 coarsens upsection into distal Slate Range sandstone and conglomerate (QTps1), and hematite- and manganese-oxide-stained proximal Slate Range conglomerate (QTps2). (H) Eastward view of younger playa-lacustrine sediments (QTps3) near Charlie Airfield. White layers are altered ash beds. (I) Upper proximal Slate Range conglomerate (QTps4, left) faulted against a hematite- and manganese-oxide-stained lower Slate Range conglomerate (QTps2, right).

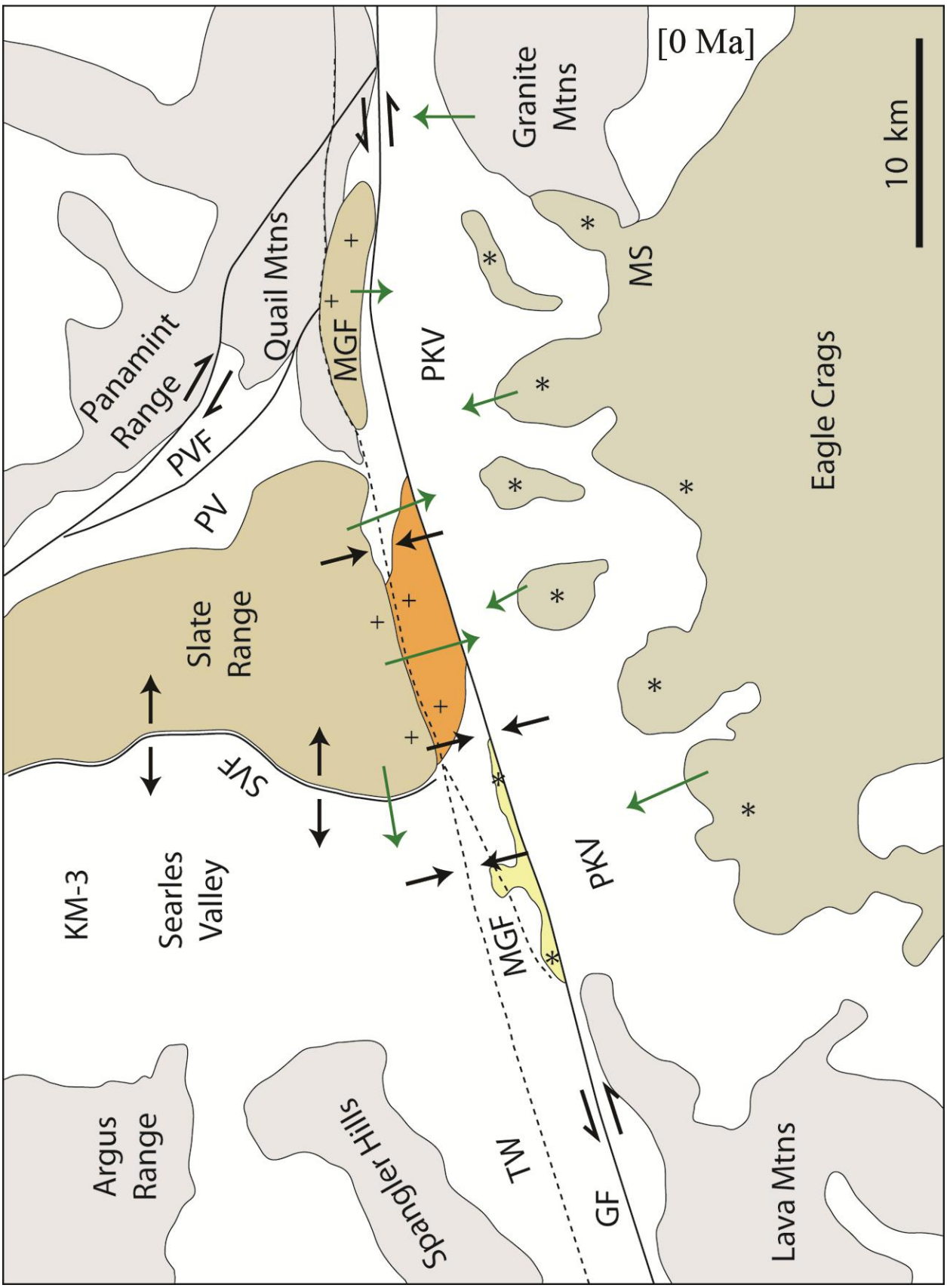
[0 Ma]
10 km
Granite Mtns
Quail Mtns
Panamint Range
PVF
PV
MGF
PKV
MS
Eagle Crags
Slate Range
SVF
KM-3
Searles Valley
MGF
PKV
TW
GF
Argus Range
Spangler Hills
Lava Mtns

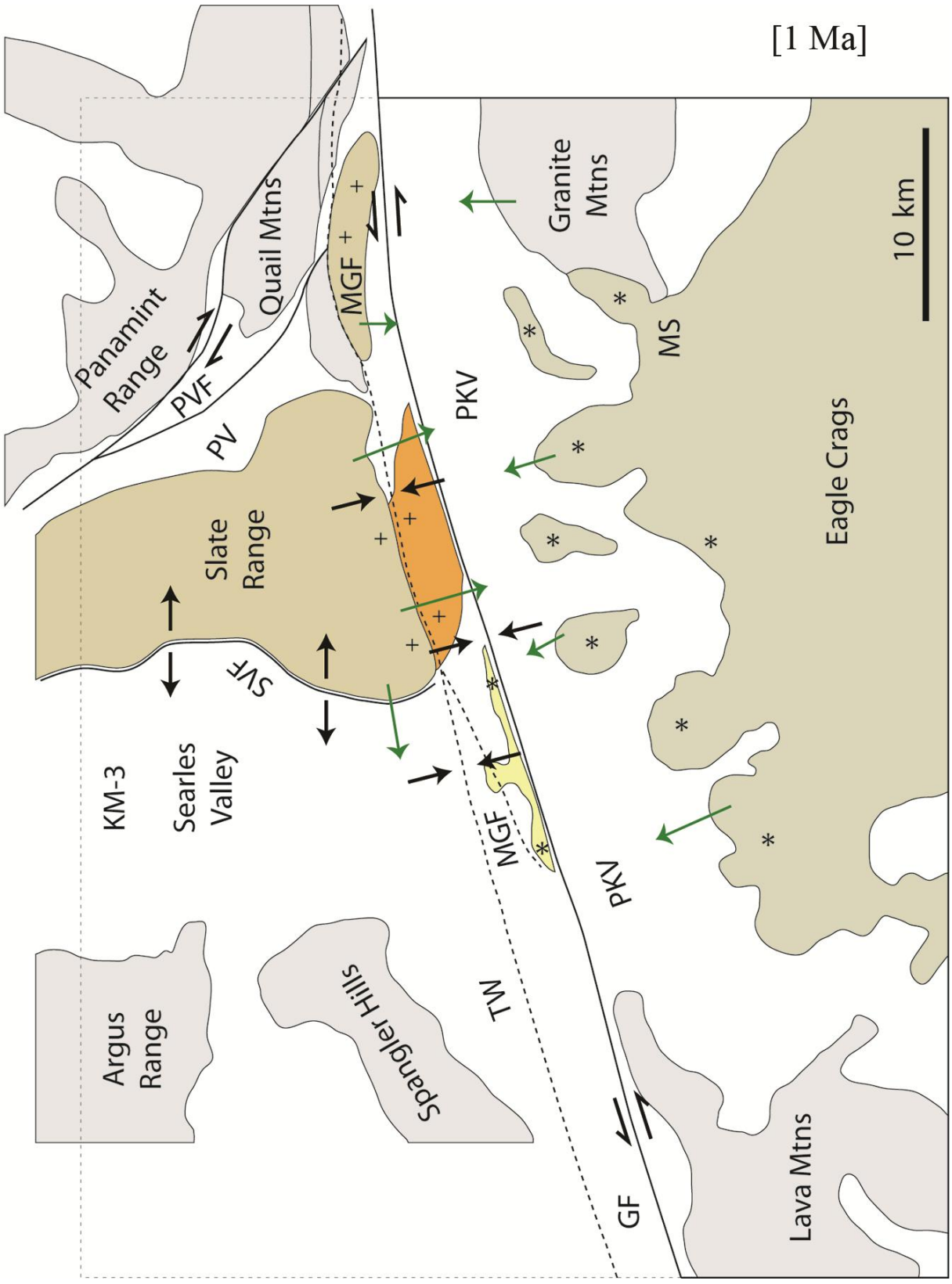
[1 Ma]
Panamint Range
PVF
Quail Mtns
MGF
Granite Mtns
10 km
PV
PKV
MS
Slate Range
Eagle Crags
SVF
KM-3
Searles Valley
MGF
PKV
Argus Range
Spangler Hills
TW
GF
Lava Mtns

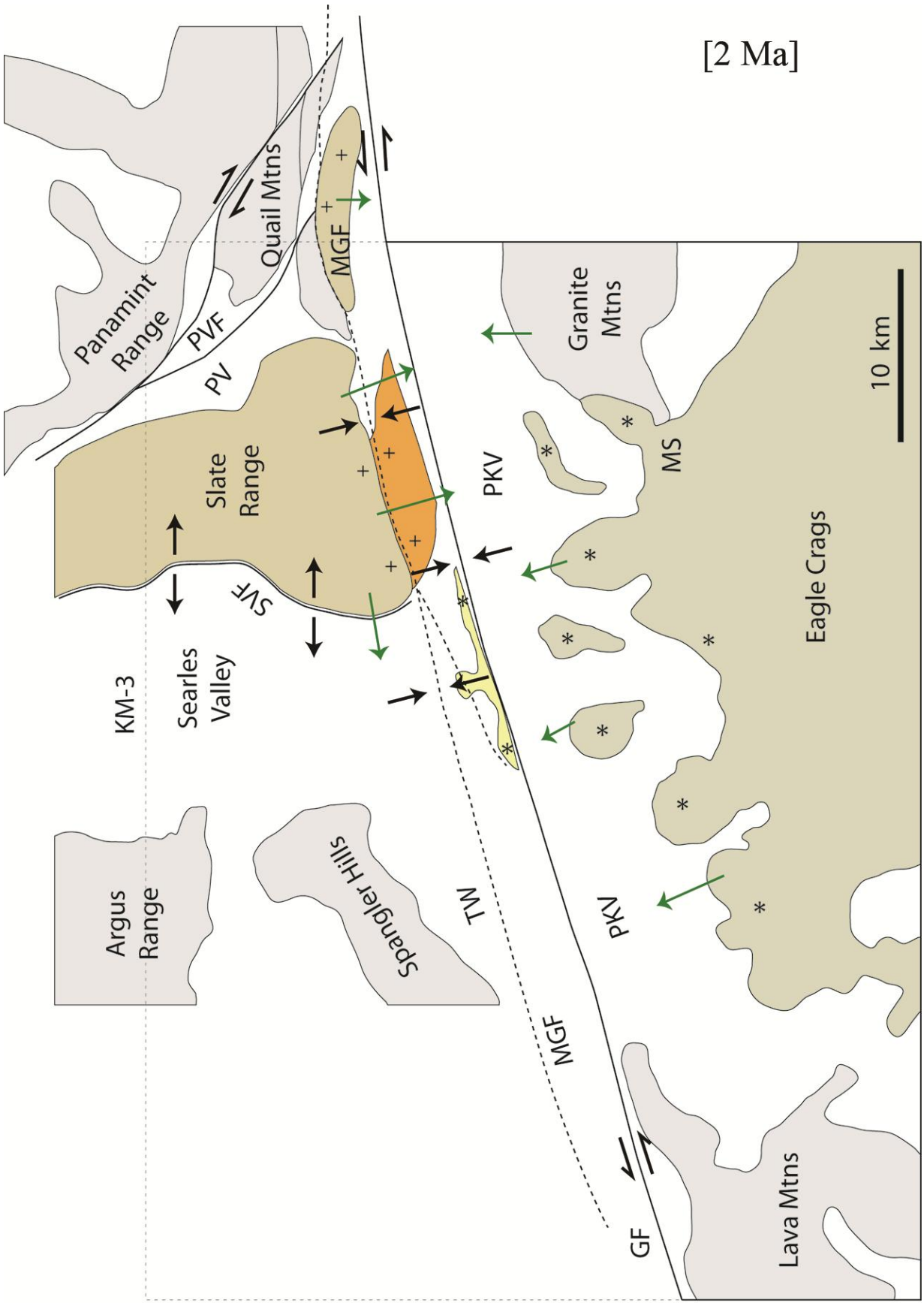
[2 Ma]
Panamint Range
PVF
PV
Quail Mtns
MGF
Granite Mtns
10 km
Slate Range
SVF
PKV
MS
Eagle Crags
KM-3
Searles Valley
Argus Range
Spangler Hills
TW
PKV
MGF
GF
Lava Mtns

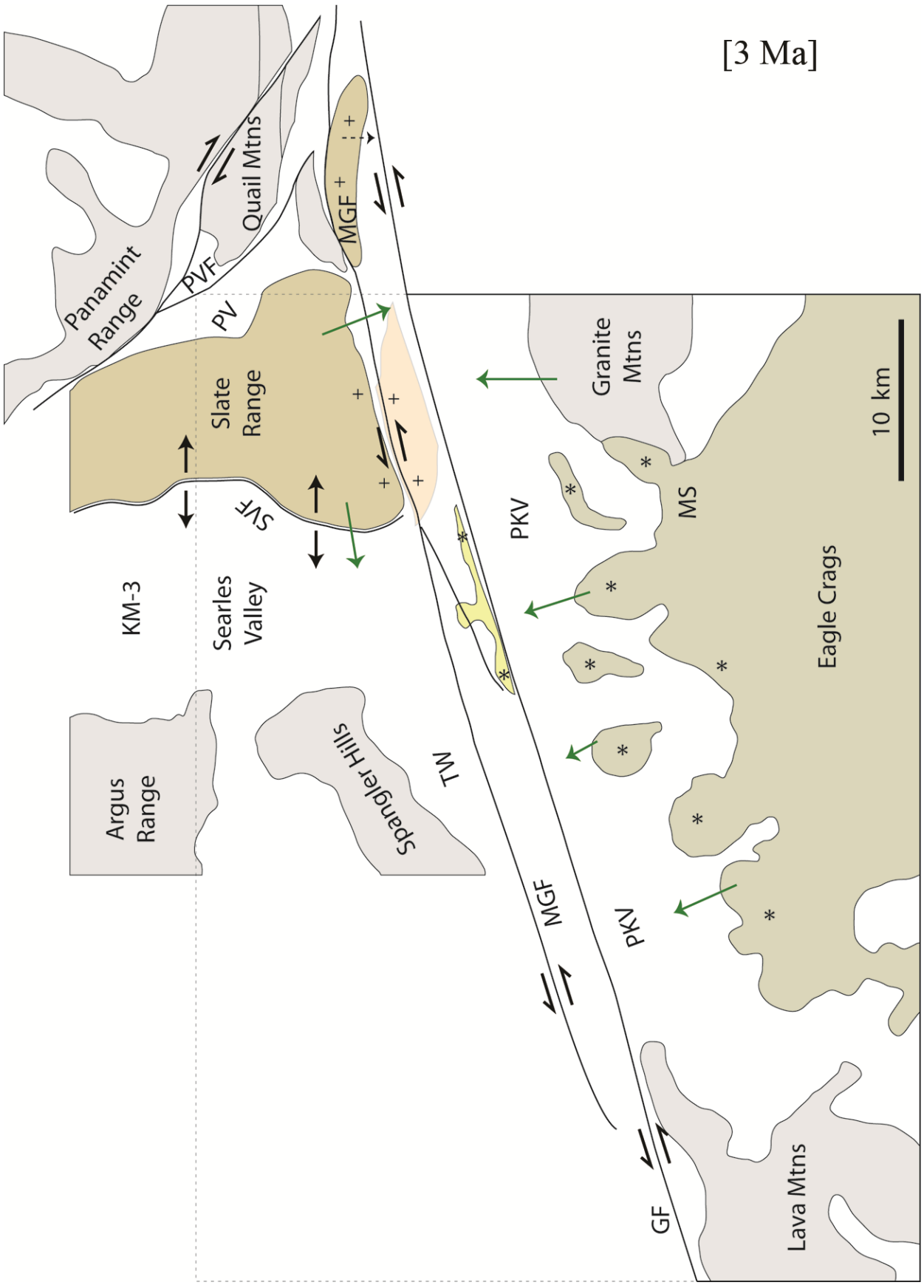
[3 Ma]
Panamint Range
PVF
Quail Mtns
MGF
PV
Slate Range
SVF
KM-3
Searles Valley
Argus Range
Spangler Hills
TW
MGF
PKV
PKV
Granite Mtns
MS
Eagle Crags
10 km
GF
Lava Mtns

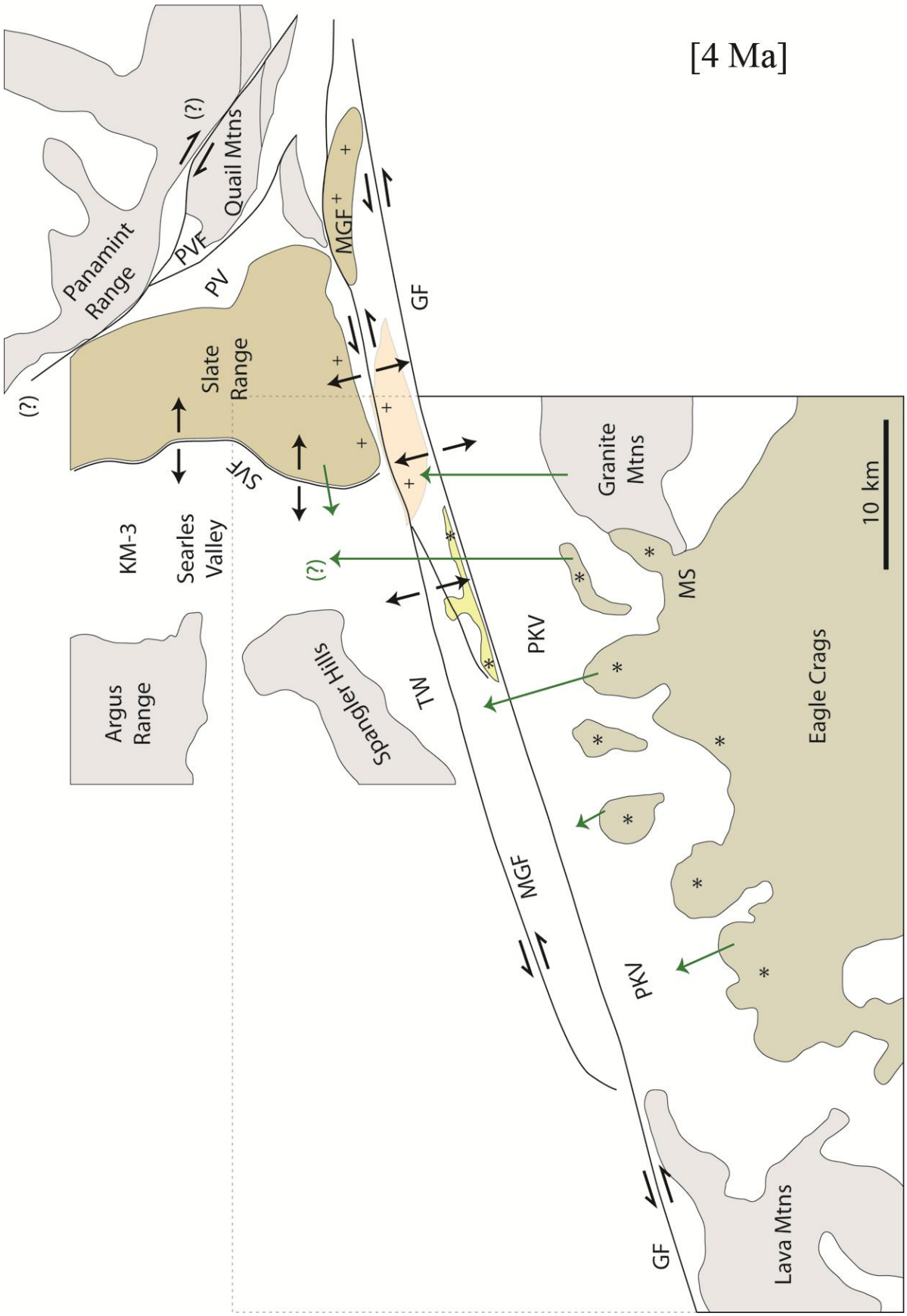
[4 Ma]
Panamint Range
(?)
Quail Mtns
PVF
PV
MGF
GF
Slate Range
SVF
KM-3
Searles Valley
Granite Mtns
10 km
(?)
MS
PKV
Argus Range
Spangler Hills
TW
Eagle Crags
MGF
PKV
GF
Lava Mtns

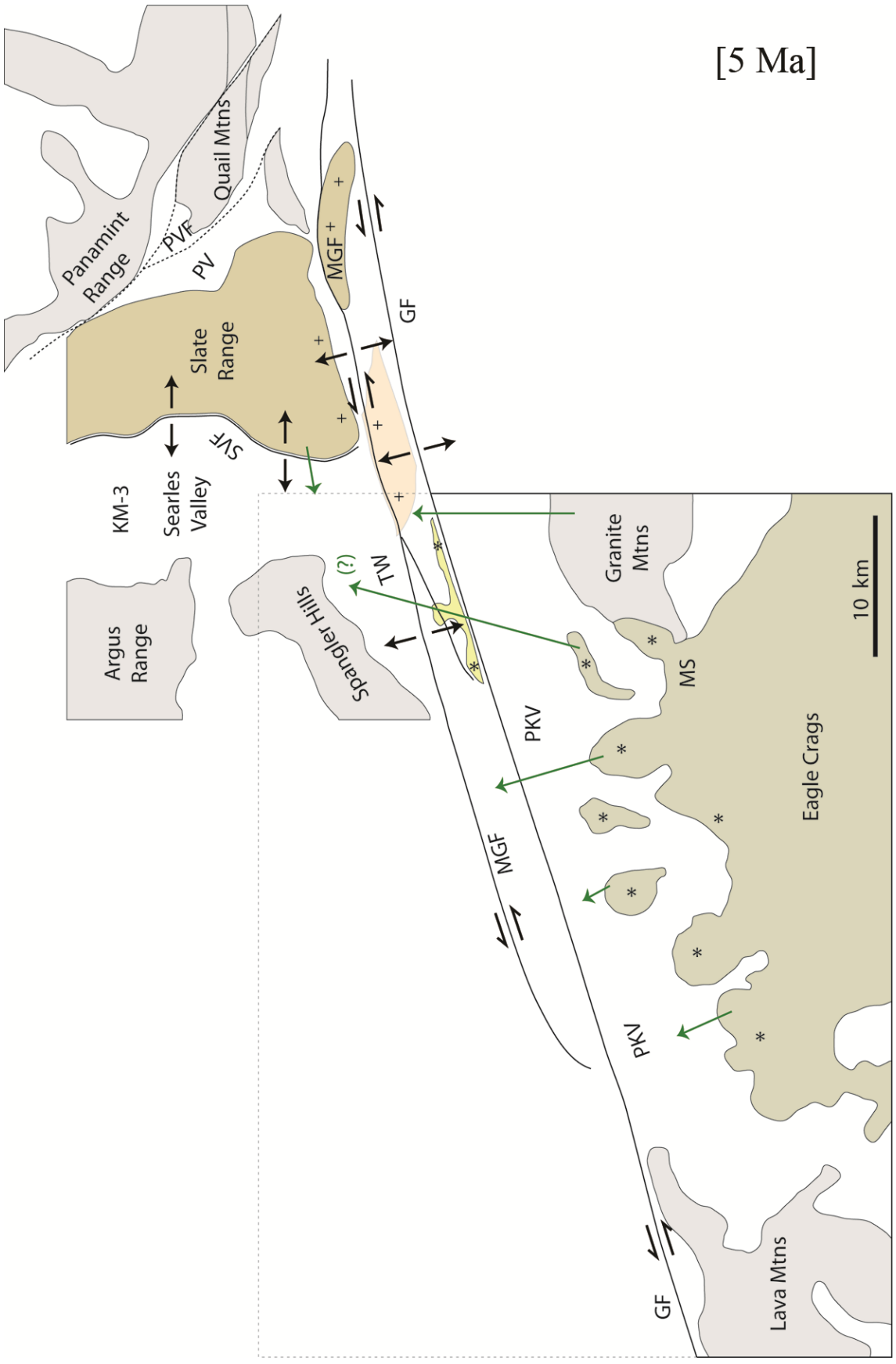
[5 Ma]
Panamint Range
Quail Mtns
PVF
PV
Slate Range
SVF
KM-3
Searles Valley
Argus Range
Spangler Hills
(?)
TW
MGF
GF
Granite Mtns
MS
PKV
Eagle Crags
10 km
Lava Mtns

Figure 3.7 – (5 Ma to present) Palinspastic reconstruction of Pilot Knob Formation and immediate region. Solid black lines show active faults. Dashed black lines are inactive strike-slip faults. Black arrows indicate relative sense of displacement across fault lines. Green arrows indicate sediment transport vectors with arrow heads suggesting depocenters. "+" and "*" signs indicate provenance links between bedrock and basin deposits. Orange polygon containing "+" symbols locates the spatial extent of Slate Range Member outcrops through time (lightly shaded prior to deposition). Yellow polygon represents Eagle Crags Member rocks. SKM-3, KM-3 borehole location; MGF, Marine Gate fault; PKV, Pilot Knob Valley; PV, Panamint Valley; PVF, Panamint Valley fault; SVF, Searles Valley fault; TW, Teagle Wash.

REFERENCES CITED

Andrew, J.E., 2007, Western Quail Mountains Geologic Map: Geological Society of America Maps and Charts, scale 1:12,000, doi: 10.1130/2007.DMCH005.

Bennett, R.A., Wernicke, B.P., Niemi, N.A., Friederich, A.M., and Davis, J.L., 2003, Contemporary strain rates in the northern Basin and Range province from GPS data: Tectonics, v. 22, p. 3-1-3-31.

Bourne, S.J., England, P.C., and Parsons, B., 1998, The motion of crustal blocks driven by flow of the lower lithosphere and implications for slip rates of continental strike-slip faults: Nature, v. 391, p. 655-659, doi: 10.1038/35556.

Carr, M.D., Harris, A.G., Poole, F.G., and Fleck, R.J., 1992, Stratigraphy and structure of Paleozoic outer continental-margin rocks in Pilot Knob Valley, north-central Mojave desert, California: U.S. Geological Survey Bulletin, v. 2015, 33 p.

Clark, M.M., 1973, Map showing recently active breaks along the Garlock and associated faults, California: U.S. Geological Survey Miscellaneous Geologic Investigations Map I-741, scale 1:24,000, 3 sheets.

Davis, G.A., and Burchfiel, B.C., 1973, Garlock fault: An intracontinental transform structure, southern California: Geological Society of America Bulletin, v. 84, p. 1407-1422.

DeMets, C., and Dixon, T.H., 1999, New kinematic models for Pacific-North American motion from 3 Ma to present, I: evidence for steady motion and biases in the NUVEL-1A model: Geophysical Research Letters, v. 26, p. 1921-1924.

Didericksen, B., 2005, Middle Miocene to recent faulting and exhumation of the central Slate Range, Eastern California shear zone [MS Thesis]: Lawrence, University of Kansas, 104 p.

Didericksen, B.D., Stockli, D.F., Walker, J.D., and Andrew, J.E., (in prep), Middle Miocene to recent exhumation of the Slate Range, eastern California, and implications for the timing of extension and transition to transtension.

Dixon, T.H., Robaudo, S., Lee, J., and Reheis, M.C., 1995, Constraints on present-day Basin and Range deformation from space geodesy: Tectonics, v. 14, p. 755-772.

Dixon, T.H., Miller, M., Farina, F., Wang, H., Johnson, D., 2000, Present-day motion of the Sierr Nevada block and some tectonic implications for the Basin and Range Province, North America Cordillera: Tectonics, v. 19, p. 1-24.

Dokka, R.F., and Travis, C.J., 1990, Late Cenozoic strike-slip faulting in the Mojave Desert, California: Tectonics, v. 9, p. 311-340.

Dunne, G.C., and Walker, J.D., 2004, Structure and evolution of the East Sierran thrust system, east central California: Tectonics, v. 23, 23 pp., doi: 10.1029/2002TC001478.

Helms, J.G., McGill, S.F., and Rockwell, T.K., 2003, Calibrated, late Quaternary age indices using clast rubification and soil development on alluvial surfaces in Pilot Knob Valley, Mojave Desert, southeastern California: Quatern. Res., v. 60, p. 377-393, doi: 10.1016/j.yqres.2003.08.002.

Gan, W., Svarc, J.L., Savage, J.C., and Prescott, W.H., 2000, Strain accumulation across the Eastern California shear zone at latitude 36°30'N: Journal of Geophysical Research, v. 105, p. 16,229-16,236.

Gan, W., Zhang, P., Shen, Z., Prescott, W.H., and Svarc, J.L., 2003, Initiation of deformation of the Eastern California shear zone: constraints from Garlock fault geometry and GPS observations: Geophysical Research Letters, v. 30, 1496, 4 pp., doi: 10.1029/2003GL017090.

Glazner, A.F., and Loomis, D.P., 1984, Effect of subduction of the mendocino fracture zone on tertiary sedimentation in southern California: Sedimentary Geology, v. 38, p. 287-303.

Guest, B., Pavlis, T.L., Golding, H., and Serpa, L., 2003, Chasing the Garlock: A study of tectonic response to vertical axis rotation: Geology, v. 31, p. 553-556.

Jannik, N.O., Phillips, F.M., Smith, G.I., and Elmore, D., 1991, A 36Cl chronology of lacustrine sedimentation in the Pleistocene Owens River system: Geological Society of America

Bulletin, v. 103, p. 1146-1159, doi: 10.1130/0016-7606(1991)103<1146:ACCOLS> 2.3.CO;2.

Knott, J.R., Machette, M.N., Klinger, R.E., Sarna-Wojcicki, A.M., Liddicoat, J.C., Tinsley, J.C., III, David, B.T., and Ebbs, V.M., 2008, *in* Reheis, M.C. et al., eds., Late Cenozoic drainage history of the southwestern Great Basin and lower Colorado River region: Geologic and biotic perspectives: Geological Society of America Special Paper 439, p. 1-26, doi: 10.1130/2008.2439(01).

Liddicoat, J.C., Opdyke, N.D., and Smith, G.I., 1980, Paleomagnetic polarity in a 930-m core from Searles Valley, California: Nature, v. 286, p. 22-25, doi: 10.1038/286022a0.

McClusky, S.C., Bjornstad, S.C., Hager, B.H., King, R.W., Meade, B.J., Miller, M.M., Monastero, F.C. and Souter, B.J., 2001, Present day kinematics of the Eastern California shear zone from a geodetically constrained block model: Geophysical Research Letters, v. 28, p. 3,369-3,372.

McGill, S.F. and Sieh, K.E., 1991, Surficial offsets on the central and eastern Garlock fault associated with prehistoric earthquakes: Journal of Geophysical Research, v. 96, p. 21,597-21,621.

McGill, S.F. and Sieh, K.E., 1993, Holocene slip rate of the central Garlock fault in southeastern Searles Valley, California: Journal of Geophysical Research, v. 98, p. 14,217-14,231.

McGill, S.F., Wells, S.G., Fortner, S.K., Kuzma, H.A., McGill, J.D., 2009, Slip rate of the western Garlock fault, at Clark Wash, near Lone Tree canyon, Mojave desert, California: Geological Society of America Bulletin, v. 121, p. 536-554, doi: 10.1130/B26123.1.

McQuarrie, N., and Wernicke, B.P., 2005, An annimated tectonic reconstruction of southwestern North America since 36 Ma: Geosphere, v. 1, p. 147-172, doi: 10.1130/GES00016.1.

Miller, M.M., Johnson, D.J., Dixon, T.H., and Dokka, R.K., 2001, Refined kinematics of the Eastern California shear zone from GPS observations, 1993-1998: Journal of Geophysical Research, v. 106, p. 2,245-2,263.

Monastero, F.C., Sabin, A.E., and Walker, J.D., 1997, Evidence for post-early Miocene initiation movement on the Garlock fault from offset of the Cudahy Camp Formation, east-central California: Geology, v. 25, p. 247-250.

Numelin, T., Kirby, E., Walker, J.D., and Didericksen, B., 2007, Late Pleistocene slip on a low-angle normal fault, Searles Valley, California: Geosphere, v. 3, p. 163-176.

Oskin, M., and Stock, J., 2003a, Marine incursion synchronous with plate-boundary localization in the Gulf of California, Geology: v. 31, p. 23-26, doi: 10.1130/0091-7613(2003) 031<0023:MISWPB>2.0.CO;2.

Oskin, M., and Stock, J., 2003b, Pacific-North America plate motion and opening of the Upper Delfin basin, northern Gulf of California, Mexico: Geological Society of America Bulletin, v. 115, p. 1173-1190, doi: 10.1130/B25154.1.

Roy, M., and Royden, L.H., 2000a, Crustal rheology and faulting at strike-slip plate boundaries; 1, an analytic model: Journal of Geophysical Research, v. 105, p. 5583-5597, doi: 10.1029/1999JB900339.

Roy, M., and Royden, L.H., 2000b, Crustal rheology and faulting at strike-slip plate boundaries; 2, effects of lower crustal flow: Journal of Geophysical Research, v. 105, p. 5589-5613.

Sabin, A.E., 1994, Geology of the Eagle Crags volcanic field, northern Mojave desert, China Lake Naval Air Weapons Station, California [Ph.D. Thesis], Golden, Colorado School of Mines, 209 p.

Sarna-Wojcicki, A., 2000, Tephrochronology, *in* Noller, J.S., Sowers, J.M., and Lettis, W.R., eds., Quaternary Geochronology Methods and Applications: AGU Reference Shelf 4, American Geophysical Union, Washington, DC.

Savage, J.C., 2000, Viscoelastic-coupling model for the earthquake cycle driven from below: Journal of Geophysical Research, v. 105, p. 25,525-25,532, doi: 10.1029/2000JB900276.

Savage, J.C., Gan, W., and Svarc, J.L., 2001, Strain accumulation and rotation in the Eastern California shear zone, Journal of Geophysical Research, v. 106, p. 21,995-22,007, doi:

Savage, J.C., Lisowsky, M., and Prescott, W.H., 1990, An apparent shear zone trending north-northwest across the Mojave Desert into Owens Valley, eastern California: Geophysical Research Letters, v. 12, p. 2,113-2,116.

Smith, G.I., 1964, Geology and volcanic petrology of the Lava Mountains, San Bernardino County, California: U.S. Geologic Survey Professional Paper 457, 97 p.

Smith, G.I., Troxel, B.W., Gray, C.H., Jr., and Von, H.R., 1968, Geologic reconnaissance of the Slate Range, San Bernardino and Inyo counties, California: Special Report - California Division of Mines and Geology, v., 96, p. 1-33.

Smith, G.I., and Church, J.P., 1980, Twentieth-century crustal deformation in the Garlock fault-Slate Range area, southeastern California: Geological Society of America Bulletin, v. 91, p. 524-534.

Smith, G.I., Barczak, V.J., Moulton, G.F., and Liddicoat, J.C., 1983, Core KM-3, a surface-to-bedrock record of the late Cenozoic sedimentation in Searles Valley, California: U.S. Geological Survey Professional Paper 1256, 24 p.

Smith, G.I., 1991, Anomalous folds associated with the east-central part of the Garlock fault, southeast California: Geological Society of America, v. 103, p. 615-624.

Smith, G.I., 2009, Late Cenozoic geology and lacustrine history of Searles Valley, Inyo and San Bernardino counties, California: U.S. Geological Survey Professional Paper 1727, 115 p.

Snow, J.K., and Wernicke, B., 2000, Cenozoic tectonism in the Central Basin and Range: magnitude, rate, and distribution of upper crustal strain: American Journal of Science, v. 300, p.659-719.

Walker, J.D., Kirby, E., and Andrew, J.E., 2005, Strain transfer and partitioning between Panamint Valley, Searles Valley, and Ash Hill fault zones, California: Geosphere, v. 1, p. 111-118, doi: 10.1130/GES00014.1.

Wernicke, B., and Snow, J.K., 1998, Cenozoic tectonism in the Central Basin and Range: motion of the Sierran-Great Valley block: International Geology Review, v. 40, p. 403-410.

CHAPTER 4

QUATERNARY NORTH-SOUTH SHORTENING ACROSS THE GARLOCK FAULT IN PILOT KNOB VALLEY, CALIFORNIA

William M. Rittase [1]

J. Douglas Walker [1]

Eric Kirby [2]

Eric McDonald [3]

John Gosse [4]

AJ Herrs [1]

[1] University of Kansas

[2] Pennsylvania State University

[3] Desert Research Institute, University of Nevada Reno

[4] Dalhousie University

ABSTRACT

This paper describes the interaction of the sinistral Garlock Fault (GF) with the dextral transtensional Eastern California shear zone. These fault systems are orthogonal and thus strain must transfer between the systems in a complex manner. New mapping, Earthscope™ airborne and ground-based LiDAR, and chronology of Quaternary deposits exposed along the GF, including (1) three ^{10}Be terrestrial cosmogenic nuclide (TCN) depth profiles and (2) one soil description, place bounds on the vertical components of recent deformation.

Here we focus on two incised terrace treads adjacent to the GF and one adjacent to the southern Slate Range, which are displaced vertically relative to local base-level. A $40.4^{+17.8}_{-10.0}$ ka ^{10}Be TCN profile age for a 16-m-high terrace tread adjacent to the GF (site PKV-1) suggests a differential incision (uplift) rate of 0.40 ± 0.13 mm/yr. A $55.2^{+13.3}_{-11.0}$ ka ^{10}Be TCN profile age from a 12.5-m-high tread located 4.5 km west on the GF (site PKV-5) suggests a differential incision (uplift) rate of 0.23 ± 0.05 mm/yr. A 25.5-m-high terrace adjacent to the southern Slate Range (site PKV-3) was dated using a soil profile development index (PDI) technique. A soil PDI age estimate of ~162 ka brackets the maximum age of uplift, and suggests a minimum uplift rate of ~0.16 mm/yr here. Using these ages and assuming dips on the GF between 90° and 80° to the north, resultant shortening magnitudes of 0-2.2 m and 0-2.8 m at sites PKV-5 and PKV-1, respectively, and 0-0.04±0.01 mm/yr at PKV-5 and 0-0.07±0.02 mm/yr at PKV-1 are estimated. At PKV-3, we estimate the dip of the newly recognized Marine Gate fault to be 70-80° to the south, resulting in 4.4-8.7 m of N-S shortening, suggesting a 0.03-0.05 mm/yr shortening rate. The shortening rate estimated at PKV-1 corresponds to 2-4% of Panamint Valley fault slip rate. Shortening at PKV-1 and PKV-3 can be summed to partially integrate 0.08-0.12 mm/yr shortening between the GF and Slate Range, or approximately 3-7% of Panamint Valley fault

slip rate. The presence of numerous active reverse faults between PKV-1 and PKV-3 suggests that this is a minimum estimate.

We attribute the localized uplift in northern Pilot Knob Valley to strain accommodation primarily between the Panamint Valley fault and GF, and to a lesser extent, between the Paradise fault zone of the Mojave Desert and the GF. Localized slip along the Panamint Valley fault dies out southward toward the intersection with the GF. Shortening along the southern end of the Slate Range and associated vertical motions, plus clockwise rotation of the GF, provide a plausible mechanism to maintain strain compatibility in the region over the short term (10^{3-4} yr).

INTRODUCTION

Pilot Knob Valley (PKV) forms an arcuate 45 km by 6 km east-west elongated depression between the Slate Range to the north and Eagle Crags to the south (Fig. 4.1). The modern strand of the central Garlock fault (GF) cuts ENE-WSW across the northern third of the valley and demarks the locus of active uplift between it and the Slate Range. Additionally, the southern Slate Range front appears to accommodate some active tectonic shortening and uplift, as north-dipping strands of the newly recognized Marine Gate fault place Mesozoic Slate Range basement rock on top of Pleistocene conglomerates. This active strain provides the opportunity to study important kinematic interactions among the GF, Eastern California shear zone (ECSZ), Marine Gate fault and existing structures nearby. Because of its proximity to the Panamint Valley fault to the east and Paradise fault zone to the south, PKV is ideally located for understanding modern tectonic relations between the GF and ECSZ.

PKV lies entirely within the Naval Weapons Air Station at China Lake, where public access is restricted. Thus, detailed interpretation of the late Cenozoic geology of the valley has

not been made. Mapping of the Lava Mountains to the west, Searles Valley to the northwest, and Slate Range to the north by G.I. Smith (1964, 2009) and Smith and others (1968), respectively, covered our study area at a reconnaissance level only; no modern geochronological dating of rocks and sediments was presented in these studies. Clark (1973) surveyed Holocene ground ruptures and displacement along the GF through the study area. McGill (1991, 1993) mapped late Pleistocene and Holocene offsets along the GF through PKV in much greater detail. Helms and others (2003) investigated clast rubification as a potential Mojave Desert soil geochronometer. However, no comprehensive neotectonic study existed for the northern PKV prior to this study.

This paper aims to, (1) characterize the style and magnitude of uplift in northern PKV, and (2) present a model for strain compatibility between the GF, ECSZ, Marine Gate fault and numerous reverse fault structures. Herein, we identify the surficial geology and geomorphology of northern PKV and quantify incision and uplift rates through both quantitative geochronological dating techniques (e.g., ^{10}Be cosmogenic dating) and qualitative soil development dating techniques.

TECTONIC SETTING

This section discusses the basic geologic setting of PKV as well as major structural features in the area that influence the late Quaternary N-S shortening here. PKV has a base level at ~660 m. To the north lies the 1,700-m-high Slate Range. Smith and others (1968), Dunne and Walker (2004) and J. Andrew (2010, unpublished data) identified Paleozoic and Mesozoic igneous and metasedimentary rocks that were contractionally deformed and displaced along the East Sierran thrust system during late Jurassic time. The Slate Range was uplifted in the

Pliocene time via footwall unroofing along the west-dipping Searles Valley fault (Didericksen, 2005; Numelin et al., 2007; Didericksen et al., *in prep*; Rittase, unpublished data). Active slip on the fault is indicated by high-angle strands that cut Pleistocene Searles Lake shorelines and sole into the detachment along the western Slate Range front (Numelin et al., 2007).

Post-Miocene Garlock Fault Evolution

Development of the ECSZ is shown to have warped the trend of the central and eastern GF segments up to 20º and 50°, respectively, since ~5 Ma (Dokka and Travis, 1990; Gan et al., 2003 and Guest et al., 2003; Fig. 4.1). This change in fault orientation profoundly altered the nature of the GF, including how it still slips and its tectonic role within the North America-Pacific plate boundary. Single-stage models (e.g., Davis and Burchfiel, 1973; Guest et al., 2003; McGill et al., 2009) attempting to explain pre-ECSZ GF activity do not account for post-ECSZ activity, and vice versa. A pre-ECSZ GF accommodates large magnitude E-W extension to the north during the Miocene (Wernicke and Snow, 1998; Snow and Wernicke, 2000; McQuarrie and Wernicke, 2005). Development of the ECSZ reorients the regional stress field in eastern California and drives significant N-S contraction across the central and eastern portions of the GF. Thus, a syn-ECSZ sinistral GF is controlled by the same sigma-1 stress direction that drives dextral faults of the ECSZ to the north and south of it (Savage et al., 2001).

Eastern California Shear Zone Development

Between 6-3 Ma, a significant portion of the dextral shear between the Pacific and North America plates jumped inboard of the San Andreas fault system in southern California

(Wernicke and Snow, 1998; Snow and Wernicke, 2000; McQuarrie and Wernicke, 2005). A precondition for this inboard migration of dextral shear is the opening of the Gulf of California around 6 Ma (Oskin and Stock, 2003a and b) and subsequent formation of the modern San Andreas fault system south of ~35° N (Fig 4.1). Today, approximately 10-14 mm/yr of geodetically observed dextral simple shear oriented ~N23°W passes through a diffuse zone between the Sierra Nevada-western Mojave Desert and Spring Mountains-Providence Mountains (Dokka and Travis, 1990; Savage et al., 1990; Dixon et al., 1995; DeMets and Dixon, 1999; Dixon et al., 2000; Gan et al., 2000; McClusky et al., 2001; Miller et al., 2001; Bennett et al., 2003; Gan et al., 2003). The rheological structure of the lithosphere across this corridor south and north of the GF is debated (e.g., Bourne et al., 1998; Roy and Royden, 2000a, 2000b; Savage, 2000), but is important to the strain localization processes ongoing in the ECSZ.

The structural and kinematic characteristics of the ECSZ differ greatly north and south of the GF. Large-scale strain transfer and partitioning are more established among ECSZ faults north of the GF (e.g., Oldow, 1992; Reheis and Dixon, 1996; Oldow et al., 2001; Walker et al., 2005; Wesnousky 2005; Lee et al., 2006; Le et al., 2007; Andrew and Walker, 2009; Ganev et al., 2010). The three principal faults that accommodate most of the dextral shear north of the GF, include, from west to east: (1) Owens Valley-Airport Lake fault system, (2) Panamint Valley-Hunter Mountain fault system and (3) Death Valley fault system (Fig. 4.1). A fourth ECSZ fault, the Stateline fault, is located farther east along the California-Nevada state border and accommodates a minor portion of modern strain (Guest et al., 2007). The orientations of these fault systems between the GF and Mina deflection are oblique to the transport direction of the Sierra Nevada block with respect to the Colorado Plateau, resulting in an overall transtensional strain north of the GF (Oldow, 1992; Wesnousky, 2005; Lee et al., 2006).

South of the GF, the ECSZ has two established zones with unique structural and kinematic styles (Garfunkel, 1974; Miller and Yount, 2002). The northeastern Mojave block is characterized by E-W-striking faults that accommodate sinistral slip and large clockwise block rotations (Schermer et al., 1996; Savage et al., 2004). The western and southern Mojave block is cut by northwest-striking dextral faults that are roughly parallel to shear direction (Gan et al., 2003). Because of their parallelism to shear direction, these established principal faults were thought to show less strain transfer and partitioning between faults (Miller et al., 2007). However, the 28 June 1992 Landers (M_w 7.3) and 16 October 1999 Hector Mine (M_w 7.1) earthquakes revealed previously unknown kinematic linkages between the established faults (e.g., Nur et al., 1993; Miller and Yount, 2002).

Panamint Valley fault

The Panamint Valley fault is one of three principal faults of the ECSZ that lie directly north of the GF (Fig. 4.1). A piercing line, formed by the high-angle intrusive contact between the Hunter Mountain batholith and Paleozoic passive-margin rocks, is overlain by Pliocene basalt and is dextrally offset 8-10 km on the Hunter Mountain fault (Burchfield et al., 1987), which links with the Panamint Valley fault. From this, Burchfield and others (1987) suggested a 2-3 mm/yr slip rate for the northern Panamint Valley fault and Hunter Mountain fault. Oswald and Wesnousky (2002) measured late Pleistocene and Holocene offsets along the Hunter Mountain fault and suggested a 3.3-4 mm/yr slip rate during this interval. The Panamint Valley fault does not demonstrably cut the GF, but rather appears to mostly terminate slip north of the GF ~20-25 km east of the study area. Portions of the Panamint Valley fault also display strain partitioning during the late Cenozoic, including the most recent earthquake ground ruptures, with

adjacent fault strands accommodating simultaneous dip-slip and strike-slip motions (Hodges et al., 1987; Zhang et al., 1990; Walker et al., 2005).

Paradise fault zone-Goldstone Lake fault

Miller and others (2007) documented a newly recognized fault zone striking north-northwest across the northern Mojave Desert. Comprising several discontinuous fault scarps of late Pleistocene to early Holocene age, they termed this semi-linear array of faults the Paradise fault zone. It separates the northeastern block of the Mojave Desert province from the western Mojave Desert province. The northern Paradise fault zone interacts with the Goldstone Lake fault before continuing north-northwestward towards Eagle Crags and eastern PKV (Miller et al., 2007; their Figure 2). They interpreted this fault as evidence for an evolving strain field whereby newer, cross-block faults with north-northwesterly strikes are feeding dextral slip across the northern Mojave Desert block towards the GF. Miller and others (2007) suggested that slip on the Paradise fault zone is partially responsible for warping the GF. For brevity in the following discussions, we will refer to the Paradise fault zone and Goldstone lake fault as the Paradise fault zone.

Marine Gate fault

High-angle Quaternary faults were first mapped at a reconnaissance level along the southern flank of the Slate Range by Smith and others (1968), but were not discussed. They were portrayed as an east-west-oriented en echelon set of faults that project towards the GF near the Quail Mountains to the east. Rittase (*Chapter 3 – This study*) documented evidence for an

older strand of the GF in this area that sinistrally offsets strata within the Pilot Knob formation (PKFm) as young as ~2.5 Ma, and named it the Marine Gate fault. An ~18-20 km offset the Layton Well thrust in the Slate Range from a similar thrust in the Quail Mountains to the east brackets total sinistral slip on the Marine Gate fault (Andrew, 2007). By ~1.2 Ma, this fault was reactivated as an en echelon set of reverse faults that stretches from north of Christmas Canyon gate to Charlie Airfield (Fig. 4.1) and cuts adjacent to the southern Slate Range front (Rittase, *Chapter 3 – This study*).

METHODS

TCN Sampling Technique & Preparation

To ensure that the highest-quality and most useful *in situ* terrestrial cosmogenic nuclide (TCN) samples were obtained in this study, the criteria listed in Table 4.1 were accessed prior to actual sampling. It is critical that a sample site be located on a stable geomorphic surface within a clear geologic context. At each of the three TCN sites reported in this study, pits were hand excavated to a sufficient depth (>150 cm) to observe soil characteristics and be able to sample sufficiently below the surface mixing zone and still capture the primary ^{10}Be production zone (e.g., Gosse and Phillips, 2001). Basic soil characteristics were described, such as presence of Av, Bt and Bk, and C horizons, as well as the presence or absence of disconformities and buried soils. Describing the subsurface soil geomorphology is useful to ascertain whether the deposit was deposited at one time or in several stages.

At each site, 1-3 cm sized quartz-rich surface clasts were collected, followed by 5 depth samples of sandy material. Following the surface clast sample, the next three sample intervals were generally located within the uppermost meter in order to capture the spallation production

relationship to depth (e.g., Gosse and Phillips, 2001). Approximately 2 kg of sediment material was collected from each surface and depth level. Following sampling, soil density measurements were made by excavating softball-sized pits at different horizons, lining them with thin plastic bags, and measuring the volume of water required to fill each hole. Bagged soil from each pit was then weighed on a digital balance shortly thereafter to prevent drying and modification of soil density.

Samples were washed and sieved at the University of Kansas (KU) Terrestrial Cosmogenic Nuclide Isotope Laboratory. Sediment fractions between 500-250 um were retained for quartz separation. Quartz separation and chemical conversion to Be-oxide for AMS analysis was performed at KU and at Purdue University (PRIME lab). AMS analysis of Be-oxide occurred at PRIME lab.

Matlab™ Modeling Of ^{10}Be TCN Data

All ^{10}Be TCN data from the three sample sites in this study were modeled using the "10Be_profile_simulator_V1.1" program (Hidy et al., 2010), a Matlab™-based Monte Carlo simulator. For each data set, 100,000 iterations were run to find the best-fitting age to the ^{10}Be concentration versus depth curve. Site-specific geologic information was required for each profile (i.e., ^{10}Be inheritance and the potential for erosion or aggradation), to find the most probable depositional age estimate. Curves of production vs. depth were fitted to a 1σ or 2σ tolerance for all samples. In some situations where lab or analytical error skews individual depth samples away from a theoretical production curve (see specific discussion below), profile data are re-modeled without these samples. Additionally, surface clasts may have lower ^{10}Be concentration values than the next depth sample owing to surface erosion. Stacked soils may

result in inverted concentration versus depth profiles whereby a buried soil has accumulated more daughter product than the younger deposit on top. These situations necessitate careful treatment of the modeled profile data.

ALLUVIAL SURFACE DESCRIPTIONS

Alluvial surfaces described in this study span ages of 0 – 200 ka and are divided into nine units, Qa to Qa9 in order of increasing age (see Table 4.2 for descriptions and depositional ages), based on quantitative age data, qualitative morphological characteristics and stratigraphic position. TCN and soil pits were excavated into Qa6, Qa7 and Qa9 surfaces for this study and are discussed below.

PILOT KNOB VALLEY DATA

PKV-5 – Near Slate Road & Adjacent To GF

PKV-5 is located at 35º 33' 23" N, 117º 14' 01" W on a Qa7 terrace in western PKV approximately 310 m north of the GF and adjacent to Slate Road (Figs. 4.2 and 4.3). The surface is a strath terrace comprised of 1-2 m of coarse Slate Range-derived alluvium deposited discomformably on late Miocene-Pliocene sediments of the Pilot Knob Formation (PKFm) (Table 4.2). Here, a 175-cm-deep pit was hand excavated to examine soil characteristics and sample sediment for ^{10}Be TCN and OSL dating. A well-developed 7-10 cm thick A_v-horizon is at the surface. Below, a B_{tk} soil with stage I and III carbonate morphology (e.g., following soil nomenclature of Gile et al., 1981), extended down to ~60 cm depth. A B_{wky} soil extends ~60-80 cm depth and is characterized by gypsum and $CaCO_3$ nodules in a light tan sandy matrix. A B_{wk} soil extends ~80-130 cm depth, followed by a C_y soil beyond ~130 cm depth.

A12.5-m-deep stream incision into the Qa7 terrace provides a minimum uplift proxy as the stream probably not has equilibrated to baselevel in PKV. Evidence for this is significant stream incision downstream of GF, which appears to indicate uplift on the south side. Because corresponding Qa7 surfaces were not present on the south side of the GF, precise vertical separation could not be established. For uplift rate estimations, this minimum incision is used.

TCN-PKV-5 produced a model mean age of $55.2^{+13.3}_{-11.0}$ ka 2σ (Table 4.3; Fig. 4.3). The top five samples were used to calculate the ^{10}Be concentration versus depth curve. A sixth sample at 149 cm depth had a higher ^{10}Be concentration and was not modeled. It may be that a second soil horizon exists between 105 cm and 149 cm, allowing for an inverted concentration trend at depth. For the top 5 samples modeled, erosion values were allowed to vary between -15 cm (deposition) to 40 cm. Modeled ages approach ~60 ka for higher erosion totals and decrease toward ~50 ka for negative erosion. From the model mean age, a stream incision rate of 0.23 ± 0.05 mm/yr is determined. Because incision must occur after the surface forms and stabilizes to a point where a predictive TCN depth production curve can be measured, these incision rates are a minimum.

PKV-1 – North Of & Adjacent To GF

PKV-1 is located at 35º 34' 01" N, 117º 11' 09" W, and is 460 m north of the GF on a Qa6 terrace tread (Figs. 4.2 and 4.4). The surface formed on a 2-5-m-thick strath terrace composed of coarse Slate Range-derived alluvium deposited disconformably on Pliocene sediments of the PKFm. A generalized description of a Qa6 surface is listed in Table 4.2.

A 195-cm-deep pit was hand excavated at PKV-1 into the Qa6 tread for ^{10}Be TCN dating (Fig. 4.4). Here, the A_v horizon was 6-8 cm thick. Below the A_v soil, a B_{tk} soil, with stage I and

III carbonate morphology (e.g., Gile et al., 1981), extended down to ~51 cm depth. A B_{wky} soil extends ~51-80 cm depth and is characterized by gypsum and $CaCO_3$ nodules in a light tan sandy matrix. A B_{wk} soil extends ~80-160 cm depth, followed by a C_y soil beyond ~160 cm depth.

A 16-m-deep stream incision to the west provides a minimum uplift proxy, as this stream is also not equilibrated to modern base level. It is clear that this stream is presently incising on both sides of the GF, indicating uplift on each side. Corresponding Qa6 surfaces are not found on the south side of the GF, and thus this incision magnitude is used to proxy relative uplift magnitude.

TCN-PKV-1 produced a model mean age of $40.4^{+17.8}_{-10.0}$ ka 2σ (Table 4.3; Fig. 4.4). Because the surface clasts here had a lower ^{10}Be concentration than the second sample at 18 cm depth, the bottom five samples were used to calculate the ^{10}Be concentration versus depth curve. Although the surface exposure age at PKV-1 models younger than that of PKV-5, TCN-PKV-1 displays almost twice the ^{10}Be concentration at comparable depths than does TCN-PKV-5. Erosion parameters for TCN-PKV-1 at PKV-1 were allowed to vary between -15 cm and 40 cm. Modeled ages approach ~50 ka for the highest erosion values and ~30 ka for the lowest erosion values. From the model mean age, a corresponding stream incision rate of 0.40 ± 0.13 mm/yr is determined.

PKV-3 – Marine Gate Fault

PKV-3 is located at 35º 34' 55" N, 117º 12' 22" W on a Qa9 surface near the southern Slate Range (Figs. 4.2 and 4.5; Table **4.**2). It encompasses the hanging wall of a south-dipping reverse fault that is interpreted to be an en echelon strand of a reactivated Marine Gate fault (Rittase, *Chapter 3 – This study*). A 207-cm-deep pit was hand excavated into the terrace tread

for soil development characterization and sampled for ^{10}Be TCN dating. The sedimentologic and pedologic makeup of the site is complex. Soil and sediment morphology suggests that the soil may have formed from three different parent materials. The youngest is comprised of locally derived hillslope colluvium (0-72 cm depth) with in situ playa silts intermixing at the top (0-35 cm). A debris-flow deposit makes up the middle unit (72-134 cm), and sits disconformably on top of an older alluvial deposit (134-207+ cm). PKV 3 trench is the location of CLK-4 in the Mojave soil database of McDonald and Kirby (unpublished data). CLK-4 soil is well developed with a general Av-Btky-Byk-BCk-Ck horizon sequence. Soil depth exceeds 200 cm. The B horizon is well developed with common to many cutans coating gravel and ped faces with few to many irregular small masses of gypsum and stage I to III carbonate morphology (e.g., Gile et al., 1981).

The complex soils pattern is further reflected in the ^{10}Be TCN profile data. An inversion in ^{10}Be concentration at ~40 cm depth required the six profile samples be modeled as two separate profiles (Fig. 4.5). The top two samples from the playa-colluvium deposit yielded a $175.7^{+46.8}_{-53.5}$ ka mean age 2σ. The bottom four samples from the debris flow and older alluvial deposit produced a $353.5^{+146.4}_{-107.7}$ ka mean age 2σ.

A detailed soil description was generated to calculate its PDI value using rubification, texture, dry consistence and cutans. A soil PDI value of 83.7 was determined for PKV-3. This correlates to a ~162 ka age estimate extrapolated from a Mojave-wide soil chronofunction (McDonald and Kirby, unpublished data) using soil PDI's from dated surfaces and deposits spanning 10^3-10^5 yr.

The Qa9 surface developed at PKV-3 sits 25.5 m higher than an active playa surface on the footwall block to the north, although true vertical separation of the tread is likely greater than

as its corresponding surface is presumably buried beneath the active playa. Using the soil PDI age estimate, which is more reliable in this instance, and 25.5 m of uplift, a minimum uplift rate of ~0.16 mm/yr is estimated (Table 4.3). The ^{10}BeTCN model age estimate for the uppermost two samples suggest a $\mathbf{0.15^{+0.06}_{-0.04}}$ mm/yr uplift rate.

INTERPRETATIONS

Spatial Variations In Late Pleistocene-Present Incision & Uplift

The close spatial proximity (4.5 km) between Sites A and B allows for the detailed assessment of variation in incision rates, and thus tectonic uplift rates, along strike of the GF in PKV. A 0.23 ± 0.05 mm/yr incision rate at PKV-5 is about half the 0.40 ± 0.13 mm/yr incision rate estimated at PKV-1. We suggest that this marked decrease in incision rates may reflect a similar decrease in tectonic uplift rates towards the west within the study area. Although these values slightly overlap at a 95% confidence interval, the tectonic geomorphology corroborates the idea of along-strike uplift rate variability. To the west at PKV-5, the surrounding Qa7 terraces are less incised than are younger surfaces near PKV-1. Additionally, the average elevations of the uplifted PKFm sediments, on which the two terrace treads sit, are higher at PKV-1 than at PKV-5. This demonstrates significant along-strike variation in tectonic uplift rates over short distances.

Three hypotheses may help to explain the difference in incision-uplift rates between the two sites. The first is that a slight asperity on the GF exists in the subsurface between Sites A and B. A second possibility is that uncertainty in the TCN model ages misreports the terraces' true ages. This could be a function of differing ^{10}Be inheritances of the sand grains analyzed and/or the possibilities of complex erosional-depositional histories of the two surfaces. A third is

that proximity to the Panamint Valley fault and Paradise fault zone, coupled with the presence of the Slate Range in conjunction with the Marine Gate fault affects uplift. Our preferred interpretation is that a combination of both a small asperity on the GF near PKV-1, and proximity to the Panamint Valley fault and Paradise fault zone and the Slate Range to enhance N-S contraction and uplift locally.

The first hypothesis is tenable as the surface trace of the GF immediately south and east of PKV-1 bends slightly to the south (Fig. 4.2). Approximately 2 km east and west of PKV-1, the GF is multi-stranded, but south of PKV-1 it focuses slip on one primary strand with several 1-5 m stepovers and small Riedel shear bands. This suggests the potential for an asperity at depth, whereby the northern block passes through a zone of greater constriction to the northwest were the GF bends northward again. To the northeast of PKV-1, the presence of numerous active fault scarps on the hillside suggests rapid uplift here, as well. A broad anticline folding PKFm strata is conspicuously located just north of where the GF bows southward and is structural evidence for a potential asperity on the GF. However, the coarser facies of the PKFm here lends itself to longer preservation of geomorphic formations compared to the more easily erodible lacustrine rocks cropping out around PKV-5, and the differing mechanical strengths between coarse clastic sediments and lacustrine rocks probably affects the structural makeup of both sites.

It is possible, too, that the modeled TCN exposure ages are inaccurate. Differing ^{10}Be inheritances of the sand grains analyzed and/or the possibilities of complex erosional-depositional histories of the two alluvial surfaces could affect their model ages. At PKV-1, where ^{10}Be concentration is significantly higher at all depths compared to PKV-5, TCN-PKV-1 is still ~20% younger than TCN-PKV-5. However, because the slope of the concentration versus

depth curve is significantly steeper for TCN-PKV-5 than for TCN-PKV-1, the former is likely to be older as indicated. This is because the spallogenic production of ^{10}Be isotopes will steepen this concentration versus depth curve through time. We note that the modeled erosion rate estimates are similar between Sites A and B, meaning that post-depositonal influences are similar, but that inheritance values are approximately seven times higher at PKV-1 than they are at PKV-5. The significantly higher inheritance may indicate slower erosion rates in PKV-1's catchment basin to the north of the Marine Gate fault, or the incorporation of uplifted PKFm sediments along and south of the Marine Gate fault that could have elevated ^{10}Be inheritance.

A third hypothesis is that proximity to the intersecting Panamint Valley fault and Paradise fault zone-Goldstone Lake fault, and the presence of the Slate Range and Marine Gate fault to the north influences N-S shortening and uplift magnitude (Figs. 4.1 and 4.6). Although modeling the 4-D parameters of strain accommodation related to the termination of a dextral fault (e.g., Panamint Valley fault) against a sinistral fault (e.g., GF) is beyond the scope of this paper, it can be assumed that locations along GF that are closer to the Panamint Valley fault and Paradise fault zone will experience greater shortening. In this model, where fault slip is focused on the fault plane along much of its strike, the greatest rotational field and simple shear gradient is projected out from both termini. In this setting, locations along the GF should experience greater shortening and uplift towards the east. This is somewhat reflected in the topography of PKFm sediments. The modern elevation of Charlie Airfield playa, where there is no substantial Slate Range massif to the north, is lower than uplifted PKFm in the study area to the west. This supports the notion that the Slate Range block may act as a mechanical backstop or a plow, resulting in uplifting of sediments along a south-dipping reverse fault.

We assert, however, that a higher rate of N-S shortening and uplift at PKV-1 is a combination of the first and third ideas. It is probable that an asperity on the GF combined with proximity to the Panamint Valley fault and Paradise fault zone, and the Slate Range acting as a backstop to the north, drives the higher uplift rate. This would also explain the presence of the highest-standing PKFm rocks north-northeast of PKV-1.

Finally, a 0.16 mm/yr estimated uplift rate at PKV-3 next to the Slate Range characterizes the shortening on a south-dipping strand of the Marine Gate fault. Its calculated rate is difficult to compare to the two sites along the GF for several reasons. First, there is no similar baselevel (e.g., stream channel) that exists between it and PKV-5 and PKV-1 to compare incision and/or uplift magnitudes too. Ideally, relative riser heights between terrace treads and the active stream channel would predict spatial trends in uplift magnitudes, but this is not possible at PKV-3. Second, the condition that surface stabilization and soil development must precede uplift at PKV-3 means that the age of the tread surface will overestimate the initiation of uplift. Thus, we suggest that the uplift and N-S shortening rates estimated for PKV-3 are minimum and that the true rate is much higher.

Total PKFm Uplift

Figure 4.7 shows the amount of relief that exists between the highest-standing PKFm sediments and the adjacent PKV floor at ~660 m. Here (Fig. 4.2), unit QTps4, an early Pleistocene, coarse fanglomerate of the Pilot Knob Formation (Rittase, *Chapter 3 – This study*), crops out at 1125 m and is backtilted to the north between 10-20º. This backtilting is important as it negates possible depositional relief that may have existed between the Slate Range and the modern PKV floor. Because this ~465 m of relief is entirely tectonic, and not depositional, it can

stand as a proxy for strain resulting in N-S shortening. Although the lack of datable ash beds within the highest-standing PKFm QTps4 fanglomerate precludes the precise bracketing of this uplift, tephra layers within the underlying QTpr1 unit and the interbedded QTps2 unit brackets the maximum age of uplift between 3.1-1.2 Ma. We suggest that modern relief generation post-dates 1.2 Ma (Rittase 2012, *Chapter 3 – This study*). In spite of difficulties in establishing when the present relief initiated, it is still possible to quantify the amount of shortening required to produce this uplift. As done before, if we assume that uplift between the GF and Slate Range is facilitated by reverse faults with dips of 70° to 90°, then we can suggest that shortening magnitudes vary from 160 m to 0 m, respectively. These north-south shortening estimates are considered a minimum because (1) an unknown amount of QTps4 section has been eroded from the 1125-m-high hilltop, and (2) the presence of an anticline-syncline fold train (Fig. 4.8b) deforming PKFm sediments to the south.

North-South Shortening Accommodation Rates

Although we lack appropriate geophysical and/or borehole data to constrain dip on many of the faults within the study areas, clues such as sinuosity of the fault's trace are insightful. Because the GF cuts across topography in much of the study area with essentially no sinuosity, we can be certain that its dip is vertical. Ranges of dip on other faults were verified by conducting several 3-point structural problems throughout the study area. Reverse faults adjacent to the Slate Range also likely have high dips, based on their fault-trace patterns. Their slightly higher sinuosity allows for a slightly larger variation in dips, however.

Here we estimate N-S shortening magnitudes based on estimates of fault-plane dip at the three sites. The dip slip component of motion on the GF is responsible for uplift of PKV-5 and

PKV-1. If the GF's dip ranges between 90° and 80°, then possible N-S shortening magnitudes lie between 0 and 2.2 m- for PKV-5, and between 0 and 2.8 m at PKV-1, respectively. If the reverse faults responsible for uplift at PKV-3 dip between 80-70° to the north, then N-S shortening ranges between 4.4 and 8.7 m, respectively (Table 4.3).

Because the terrace ages are known for each of the three sites, a range of N-S shortening rates can be estimated. At PKV-5, where a dry wash is incised 12.5 m into the Qa7 terrace, an incision rate of 0.23 ± 0.05 mm/yr was estimated. If the GF dips 80° to 90º here, then a N-S shortening rate of 0.04 ± 0.01 mm/yr to 0 mm/yr N-S is implied, respectively. At PKV-1, with 16 m of incision in a neighboring dry wash, the N-S shortening rate of 0.07 ± 0.02 mm/yr to 0 mm/yr is estimated for an 80° to 90° GF, respectively. Shortening rates on a 70° to 80° fault plane at PKV-3 with 25.5 m of uplift range between 0.05 mm/yr and 0.03 mm/yr, respectively (Table 4.3).

Because PKV-1 and PKV-3 lie north-south of each other on different hanging walls, their shortening rates can be integrated to 0.08-0.14 mm/yr. The presence of numerous active reverse faults between these two sites, plus a north-dipping reverse fault that juxtaposes Slate Range bedrock on top of Quaternary gravels to the north of PKV-3, indicate that actual shortening in northern PKV is higher than the sum of PKV-1 and PKV-3. Along the Slate Road B-B' cross-section, at least eight faults, and possibly nine, are mapped cutting late Quaternary sediments (Fig. 4.2). Approximately seven young fault scarps exist northeast of PKV-1 between it and the highest-standing PKFm rocks. For these additional faults, hillslope steepness and lack of datable surfaces precludes our ability to quantify slip rates on these faults.

Strain Patterns & Kinematic Relationships Among Regional Faults

One of the biggest tectonic mysteries surrounding the GF is how ECSZ strain is transmitted across the fault and how this strain compatibility in the upper crust is maintained over time. The presence of N-S shortening in PKV is attributed to decreased slip on the southern Panamint Valley fault to the ENE and the Paradise fault zone to the SE. A total of 2-3 mm/yr slip on the Panamint Valley fault apparently decreases to zero, or near zero, as this fault does not cut the GF. This decreased slip is taken up via dextral warping of the GF and off-fault accommodation with increasing proximity to the Panamint Valley fault-Paradise fault zone intersection (Fig. 4.6). A ~30° kink and a broad northward bulge in the trace of the GF here is linked to this decreased slip on the Panamint Valley fault (Fig. 4.1).

We suggest that N-S shortening in northern PKV accommodates a low percentage of NW-directed dextral simple shear. Table 4.3 lists the estimated shortening rates based on terrace ages, incision and/or uplift magnitudes, and estimated fault dips. PKV-1 appears to suggest the highest N-S shortening rate assuming an 80° dipping GF plane. Here, its estimated shortening rate is approximately 2-4% of the Panamint Valley fault's slip rate. If the shortening rate estimated at PKV-3 is added to that at PKV-1, ~3% to 7% of the Panamint Valley fault slip, can be accommodated in northern PKV. Many of the active faults between the GF and Slate Range are not suitable for slip-rate calculations, and thus the true integrated shortening in this area is higher than 3-7%. Given the density of faults, it is possible for shortening in northern PKV to accommodate up to 25%, or more, of Panamint Valley fault slip. However, the remainder of slip must either warp the GF or shorten other crustal blocks outside the study area. It is likely, that in the near term ($\leq 10^5$ yr), the combined dextral shear on the Panamint Valley fault and Paradise fault zone will cut and/or over-rotate the GF in eastern PKV.

Currently, an additional component of strain compatibility in PKV is maintained via E-W extension on the Searles Valley fault to the north along the western front of the Slate Range (Fig. 4.6). Walker and others (2005) (their Figure 1) suggested that E-W extension in Searles Valley is balanced by dextral and dextral-normal-oblique on the Ash Hill and Panamint Valley faults, respectively. We suggest herein that this kinematic link between the Panamint Valley fault and Searles Valley fault extends south of the Manly Pass fault along the Searles Valley fault (e.g., Walker et al., 2005) to the Marine Gate fault. This strain-partitioning pattern results from NW-directed simple shear across primarily north- to NNW-striking faults of the ECSZ north of the GF. Along and south of the Marine Gate fault, and southward to the GF, strain is partitioned into local N-S shortening. South of the GF, the ECSZ faults change strike and are parallel to the shear direction. Thus, minimal strain partitioning is observed there.

Together, this allows for a single principal stress field to drive the ECSZ both north and south of the GF, as well as sinistral motion on the GF. The ~075º-trending central GF within the study area is oriented 45° from the ~030º σ_1 orientation defined by Monastero and others (2002) for Indian Wells Valley and 55º from the ~020º σ_1 orientation defined by Hardebeck and Hauksson (1999). N-S shortening in northern PKV is certainly compatible with this principal stress field, as are dextral shear across the three ECSZ faults near PKV and E-W extension on the Searles Valley fault to the north of PKV (Fig. 4.6).

SUMMARY & CONCLUSIONS

North-south shortening and associated uplift in northern PKV is an important tectonic response to the interaction between the sinistral GF and dextral simple shear of the ECSZ across it. New mapping and ages of Quaternary deposits exposed along the GF place bounds on the

vertical components of recent deformation. These new constraints on differential vertical motions and inferred shortening provide insight into the nature of strain transfer between these active orthogonal strike-slip fault systems.

Total relief between the highest uplifted sediments and the modern PKV floor is ~465 m. Because these sediments are backtilted to the north 10-20º, any potential primary depositional relief in PKV is negated. Although the lack of geophysical and borehole data prevent the precise determination of fault dips and structures, cross-sections and reasonable estimates of fault dips can allow for the total shortening between the GF and Slate Range to be calculated. Collectively, if the faults controlling this uplift dip 70° to 90°, then N-S shortening magnitudes of 160-0 m, between the GF and Slate Range is expected. Because there is no tighter age control for when this relief began than ~1.2 Ma, an accurate PKV-integrated shortening rate cannot be established.

However, three individual locations within the study area do allow for uplift and N-S shortening estimations. Two terrace treads (Sites PKV-5 and PKV-1), which lie adjacent to the GF, and another tread (PKV-3), which is adjacent to the southern Slate Range, are displaced vertically relative to local base-level. Uplift of the two terraces adjacent to the GF is inferred from modern stream channel incisions. A $40.4^{+17.8}_{-10.0}$ ka ^{10}Be TCN profile age for a 16-m-high terrace tread adjacent to the GF suggests a differential incision (uplift) rate of 0.40 ± 0.13 mm/yr at PKV-1. A $55.2^{+13.3}_{-11.0}$ ka ^{10}Be TCN profile age from a 12.5-m-high tread located 4.5 km west on the GF suggests a differential incision (uplift) rate of 0.23 ± 0.05 mm/yr at PKV-5. PKV-3 is a 25.5-m-high terrace adjacent to the southern Slate Range and was dated via TCN, OSL and soil PDI. Acquiring reliable TCN and OSL data were problematic here. The upper two ^{10}Be TCN samples produced a poorly constrained $175.7^{+46.8}_{-53.5}$ ka model age. This would predict a $0.15^{+0.06}_{-0.04}$ mm/yr uplift rate. Two OSL samples collected from 36-42 cm and ~116 cm depths

produced inconclusive age estimates. A soil PDI age estimate of ~162 ka supports the TCN age estimate and helps bracket the maximum age of uplift, and suggests a minimum uplift rate of ~0.16 mm/yr here.

With estimates of fault dip at each of the three sites, N-S shortening magnitudes and rates can be established. We suggest that the GF at Sites PKV-5 and PKV-1 dips between 90° and 80° to the north, resulting in shortening magnitudes of 0-2.2 m and 0-2.8 m at Sites PKV-5 and PKV-1, respectively, and shortening rates of 0.04±0.01 mm/yr at PKV-5 and 0.07±0.02 mm/yr at PKV-1. For PKV-3, we estimate the dip of the Marine Gate fault to be 70-80° to the south, resulting in 4.4-8.7 m of N-S shortening, suggesting a 0.03-0.05 mm/yr shortening rate. Because Sites PKV-5 and PKV-1 are located 4.5 km apart along the GF, we suggest that a combination of a slight asperity on the GF, proximity eastward toward intersecting strands of the ECSZ and the presence of the Slate Range to the north, enhance uplift magnitudes.

The shortening rate estimated for PKV-1 corresponds to 2-4% of Panamint Valley fault slip rate. Because Sites B and C lie north and south of each other on separate tectonic structures, shortening at these sites can be summed to partially integrate shortening between the GF and Slate Range. The presence of numerous active reverse faults between Sites B and C, and other reverse faults north of PKV-3 along the Slate Range front, suggests that this is a minimum estimate. Total shortening of 0.08-0.12 mm/yr between the GF and Slate Range constitutes, at minimum, 3-7% of Panamint Valley slip rate.

Other mechanisms such as tectonic block rotation must be evoked to maintain kinematic compatibility between the GF, Marine Gate fault, Searles Valley fault and the ECSZ. If the GF can be treated as a material line (e.g., Dokka and Travis, 1990; Gan et al., 2003), then its ~30º deflection around the intersection with the Panamint Valley fault is a testament to the amount of

diffuse strain imparted on the GF. We suggest that the maximum percentage of the Panamint Valley fault's 2-3 mm/yr slip rate that can be accommodated by N-S shortening in PKV is ~25%. This would suggest that current strain compatibility cannot be maintained much longer and that the Panamint Valley fault and Paradise fault zone-Goldstone Lake fault may soon cut or over-rotate the GF in eastern PKV.

TABLES

TABLE 4.1 - ^{10}BE TCN SITE SELECTION CRITERIA

Pre-excavation:

- Useful for dating strain marker / clear geomorphic context
- Not significantly eroded or buried
- Stable surface (no petrocalcite fragments on surface, good uniform pavement, few overturned clasts)
- Away from terrace's edges or beveled surfaces
- Potential locations for duplicate pits
- No major source of eolian sand nearby, or likely in the past

Post-excavation:

- Quartz-rich lithologies present throughout profile
- Straightforward soil, one soil profile
- Clearly definable mixing zone & thick fluvial beds

TABLE 4.2 - PILOT KNOB VALLEY LATE QUATERNARY SURFACE DESCRIPTIONS

Unit	Age (ka)	Description
Qa / Qa2	0 – 0.6	Active wash and abandoned alluvial sediments younger than last surface rupture of the GF.
Qa3	0.6 – 5	Alluvial deposits with incipient pavement development and desert varnish. Clast bottoms are weakly rubified. Bar and swale morphology well preserved but slightly eroded. Av-horizons less than 3 cm between bars. Weak Bt-horizon with no discernable rubification. Stage I petrocalcic development.
Qa4	5 - 15	Alluvial surface with moderate desert pavement development with subdued bar and swale morphology. Moderate varnish and rubification on granitic and metamorphic clasts. 3-5 cm Av-horizon developed under pavement. Lightly rubified B-horizon with stage I-II petrocalcic development. Surface may be locally incised by up to a meter.
Qa5	15 - 35	Alluvial surfaces older than latest Searles Lake highstand. Well-developed desert pavement surfaces with clasts touching, strong varnish and rubification on clasts, and sparse vegetation with widely spaced creosotes. A 5+ cm Av-horizon and 20-30 cm thick rubified Bt-horizon beneath surface. Stage II-III petrocalcic development. Surface is commonly incised up to several meters.
Qa6	30 - 50	Well-developed desert pavement with strong varnish and rubification of clasts, and sparse vegetation. A 6-8 cm thick Av-horizon and 20-30 cm thick Bt-horizon beneath surface with stage III petrocalcic development. Surface is incised as much as 10+ meters and is only exposed north of the GF.
Qa7	45 - 65	Surfaces are smooth and display very strong desert pavement development with strong varnish and rubification of clasts. Locally, surfaces are beveled and younger-looking due to erosion and stripping of surface. Here, rubified clasts are commonly overturned with orange side up and stage III and IV petrocalcic clasts are exposed on the surface. Stream incision is commonly 10+ meters. Av-horizon is 7-10 cm thick and sits on top of a 60+ cm thick B_{tk}, B_{wky} and B_{wk} soil. Only exposed north of GF.
Qa8	60 - 100	Older, more deeply incised alluvial surface north of the GF. Similar to Qa7, but topographically higher and cut by numerous reverse faults sub-parallel to the GF. Surface disturbance creates appearance of a younger surface. Possible secondary soil formation. Surface was not excavated and thus no detailed soil description exists for this study.

Qa9	100 +	Oldest alluvial surface within the study area and is located along the Marine Gate fault and southern Slate Range. A minimum relief of 20+ meters between it and Qa/Qa2 surfaces. Qa9 surface is beveled and stripped locally, but also contains areas of well-developed pavement with strong varnish and rubification of clasts. Underlying soil is strongly rubified to beyond 1 meter depth. Petrocalcic horizon development is at least stage III.

TABLE 4.3 - DATA FOR PILOT KNOB VALLEY INCISION-UPLIFT SITES PKV-5, PKV-1 & PKV-3

	Terrace Label	2σ Age (ka)	Method	Incision-Uplift (m)	Incision-Uplift Rate (mm/yr)	Fault Dip (°)	N-S Shortening (m)	N-S Shortening Rate (mm/yr)
Site PKV-5	Qa7	$55.2^{+13.3}_{-11.0}$	^{10}Be TCN	12.5	0.23 ± 0.05	80°	2.2	0.04 ± 0.01
						90°	0	0
Site PKV-1	Qa6	$40.4^{+17.8}_{-10.0}$	^{10}Be TCN	16	0.40 ± 0.13	80°	2.8	0.07 ± 0.02
						90°	0	0
Site PKV-3	Qa9	~162	Soil PDI	25.5	~0.16	70°	8.7	~0.05
						80°	4.4	~0.03

FIGURES

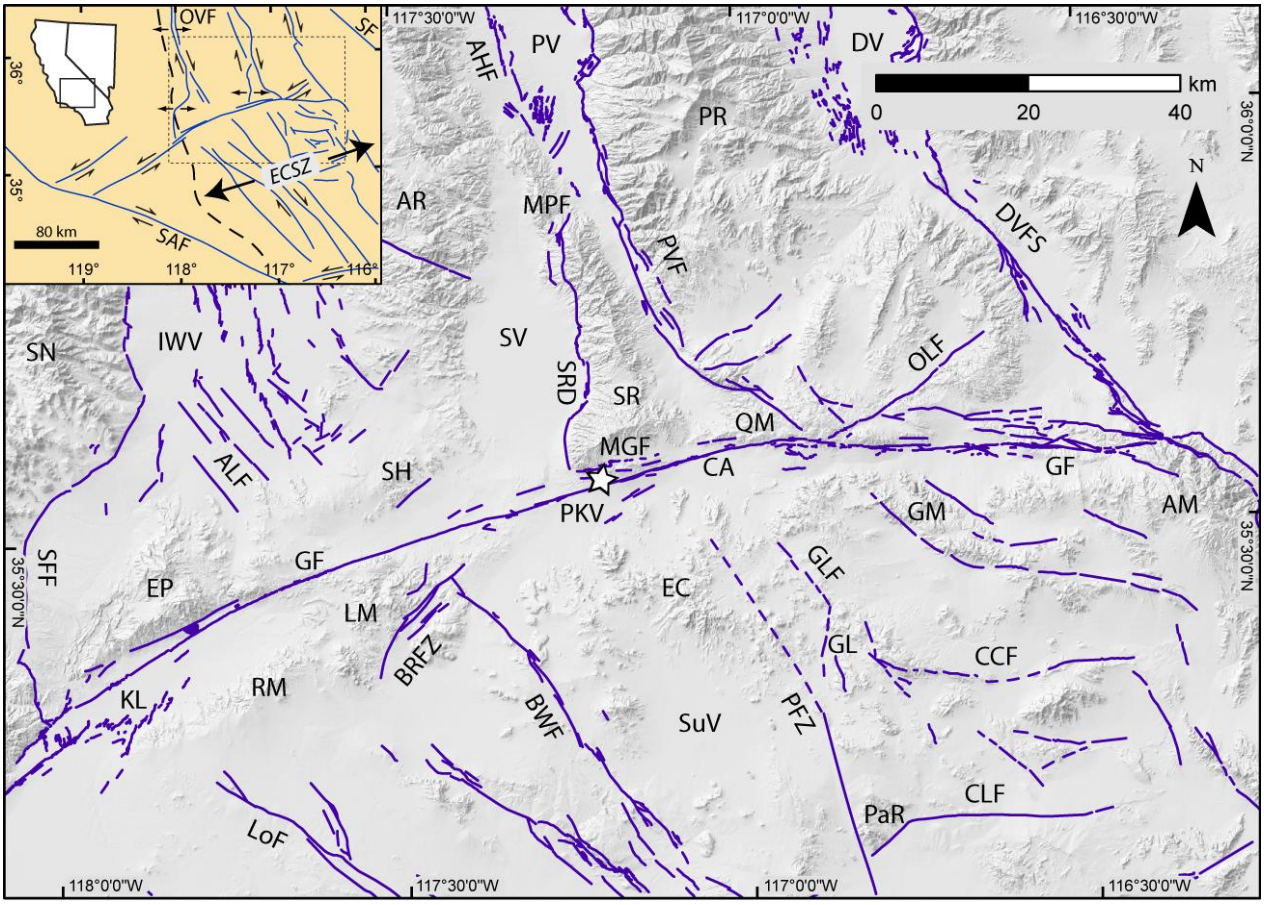
OVF
SF
ECSZ
SAF
80 km
36°
35°
119°
118°
117°
116°
117°30'0"W
117°0'0"W
116°30'0"W
36°0'0"N
35°30'0"N
118°0'0"W
AHF
PV
DV
PR
km
0
20
40
N
AR
MPF
PVF
DVFS
SN
IWV
SV
SRD
SR
OLF
QM
MGF
CA
GF
ALF
SH
PKV
GM
AM
SFF
EP
GF
LM
EC
GLF
GL
CCF
BRFZ
KL
RM
BWF
SuV
PFZ
CLF
PaR
LoF

Figure 4.1 – Shaded-relief Quaternary fault map of southern California with inset stylized fault map (upper left). Dashed box in inset map indicates coverage of gray-scale shaded-relief map. Inset California-Nevada map shows the location of stylized fault map with a solid box. Arrows indicate sense of strike-slip and dip-slip motion. Heavy dashed line on inset map locates the Eastern California shear zone (ECSZ). White star on shaded-relief map shows location of study area. A ~17° change in strike is observed between the central and eastern Garlock fault (GF), west and east of the Quail Mountains (QM), respectively. The slight north-ward "bulge" in the trace of the GF south of the QM shows rotation of the GF up to 30° locally. AHF, Ash Hill fault; ALF, Airport Lake fault; AM, Avawatz Mountains; AR, Argus Range; BRFZ, Browns Ranch fault zone; BWF, Blackwater fault; CA, Charlie Airfield; CLF, Coyote Lake fault; CCF, Coyote Canyon fault; CR, Coso Range; DV, Death Valley; DVFS; Death Valley fault system; EC, Eagle Crags; EP, El Paso Mountains; GL, Goldstone Lake; GLF, Goldstone Lake fault; GM, Granite Mountains; IWV, Indian Wells Valley; KL, Koehn Lake; LM, Lava Mountains; LoF, Lockhart fault; MGF, Marine Gate fault; MPF, Manly Pass fault; OLF, Owl Lake fault; OV, Owens Valley; OVF, Owens Valley fault; PFZ, Paradise fault zone; PKV, Pilot Knob Valley; PaR, Paradise Range; PR, Panamint Range; PV, Panamint Valley; RM, Rand Mountains; SAF, San Andreas fault; SF, Stateline fault; SFF, Sierra frontal fault; SH, Spangler Hills; SN, Sierra Nevada; SR, Slate Range; SRD, Slate Range detachment; SuV, Superior Valley; and SV, Searles Valley.

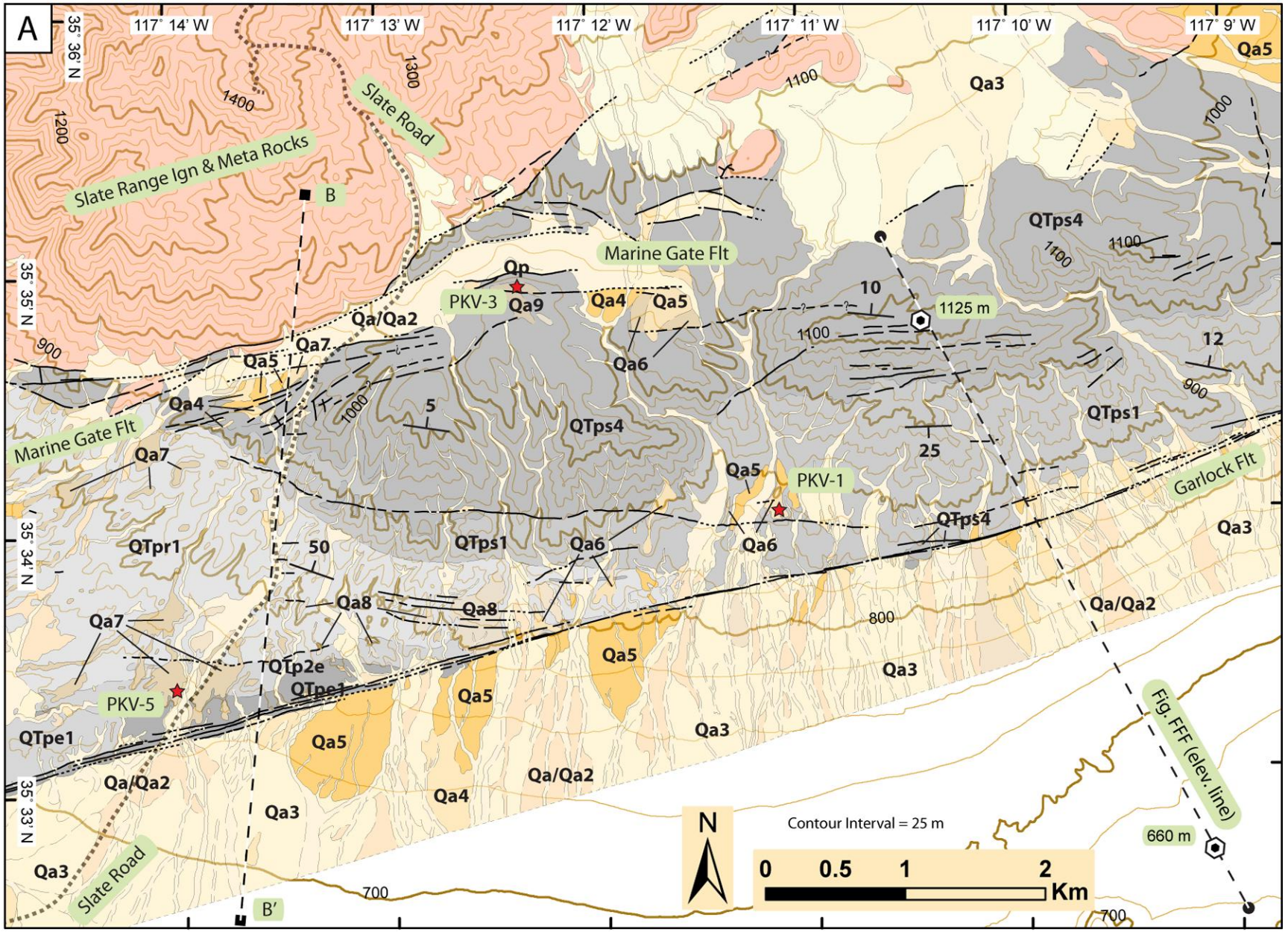
A
B
B′
117° 14' W
117° 13' W
117° 12' W
117° 11' W
117° 10' W
117° 9' W
35° 36' N
35° 35' N
35° 34' N
35° 33' N
Slate Range Ign & Meta Rocks
Slate Road
Marine Gate Flt
Garlock Flt
PKV-1
PKV-3
PKV-5
Qp
Qa9
Qa/Qa2
Qa7
Qa5
Qa4
Qa6
Qa3
QTps4
QTps1
QTpr1
QTp2e
QTpe1
Qa8
1125 m
660 m
Fig. FFF (elev. line)
Contour Interval = 25 m
N
0 0.5 1 2
Km

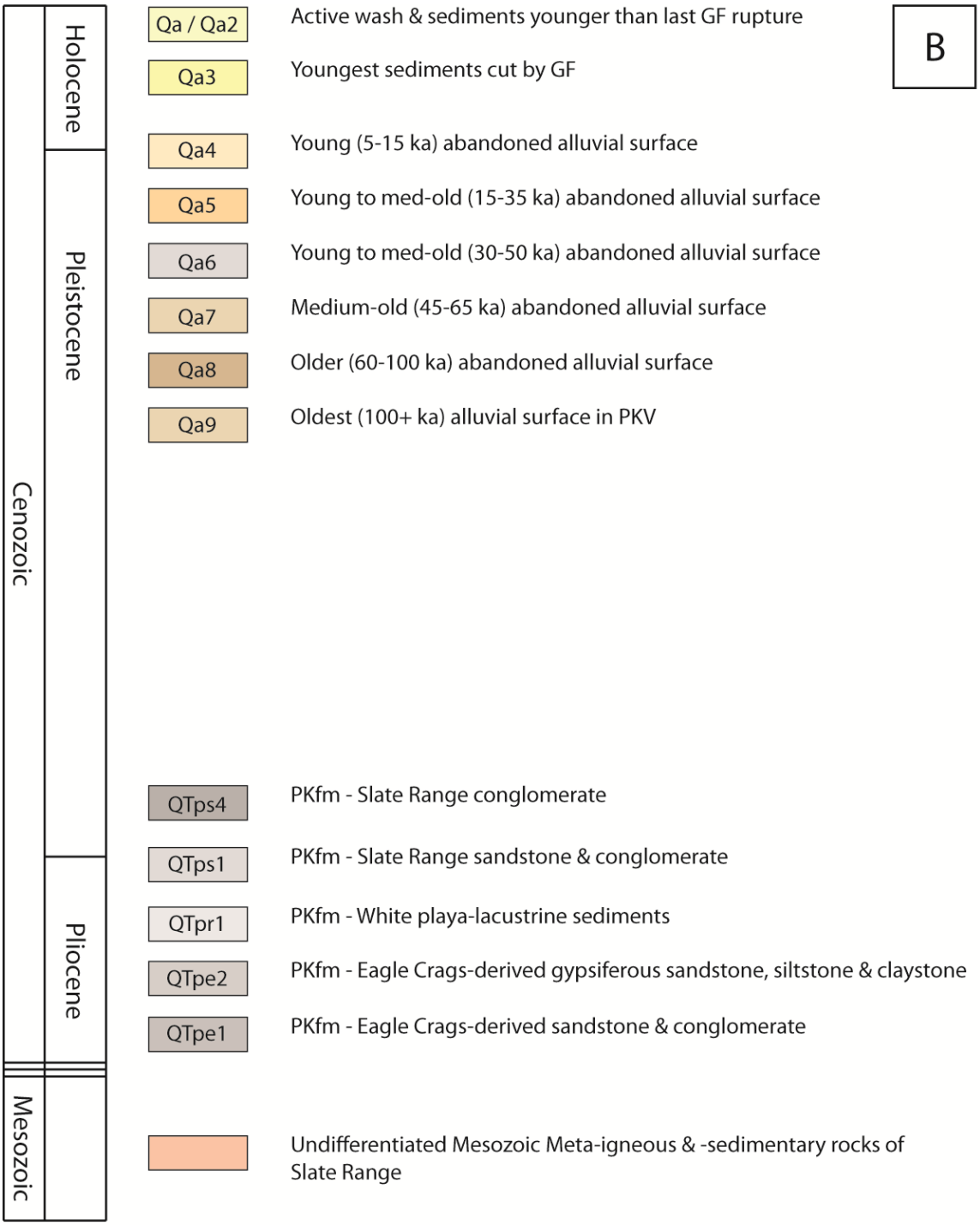
Cenozoic
Holocene
Pleistocene
Pliocene
Mesozoic
Qa / Qa2
Active wash & sediments younger than last GF rupture
Qa3
Youngest sediments cut by GF
B
Qa4
Young (5-15 ka) abandoned alluvial surface
Qa5
Young to med-old (15-35 ka) abandoned alluvial surface
Qa6
Young to med-old (30-50 ka) abandoned alluvial surface
Qa7
Medium-old (45-65 ka) abandoned alluvial surface
Qa8
Older (60-100 ka) abandoned alluvial surface
Qa9
Oldest (100+ ka) alluvial surface in PKV
QTps4
PKfm - Slate Range conglomerate
QTps1
PKfm - Slate Range sandstone & conglomerate
QTpr1
PKfm - White playa-lacustrine sediments
QTpe2
PKfm - Eagle Crags-derived gypsiferous sandstone, siltstone & claystone
QTpe1
PKfm - Eagle Crags-derived sandstone & conglomerate
Undifferentiated Mesozoic Meta-igneous & -sedimentary rocks of Slate Range

Figure 4.2 – (A) Simplified geologic map of Pilot Knob Valley study area. For simplicity, Pilot Knob Formation (PKFm) sediments older than ~300 Ka have been shaded gray. "PKV-5", "PKV-1" and "PKV-3" are locations of uplift sites in Pilot Knob Valley that have been dated via ^{10}Be TCN and/or soil PDI extrapolation. Corresponding data are described in table 4.3 and in the text. White-and-black line with square bookends show location of B-B' structural cross section in figure 4.8. White-and-black line with circular bookends show location of elevation transect in figure 4.7. (B) Stratigraphic key for PKFm sediments and late Quaternary terrace units.

Figure 4.3 - Site PKV-5 = TCN-PKV-5 data

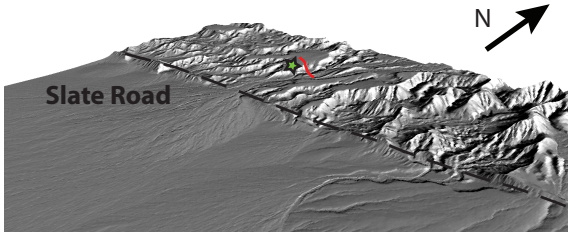

(A) Vertically exaggerated shaded-relief map of incised terrace treads and sediments north of the Garlock fault (dashed black line). View is looking northwest. Red line denotes elevational transect shown to the right. Green star locates ^{10}Be TCN-PKV-5 site.

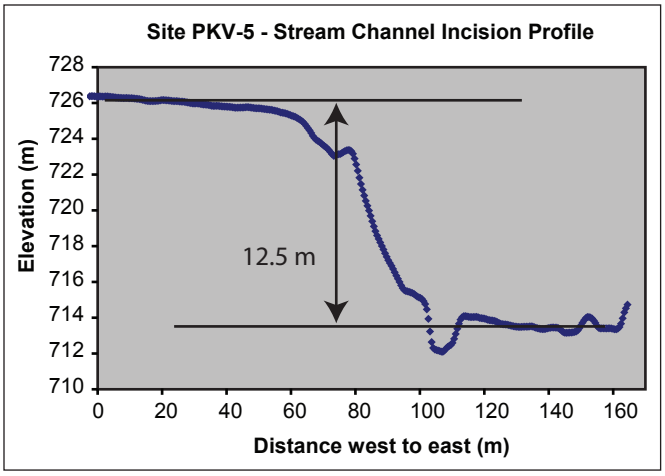

(B) Elevational transect across an incised terrace tread immediately north of the Garlock fault adjacent to Slate Road. Vertical separation is 12.5 meters.

Sample (#)	Depth (cm)	Thickness (cm)	Conc. (atoms * g^{-1})	Error (atoms * g^{-1})
1	0.1	2	472,112	0.0271
2	24	5	372,695	0.0308
3	45	6	288,268	0.0306
4	70	6	220,500	0.0473
5	105	7	158,683	0.0356
6	149	7	169,028	0.0402

(C) ^{10}Be TCN concentration plot with depth for TCN-PKV-5. Horizontal and vertical error bars indicate AMS uncertainty and sampling interval, respectively. Sample depths and thicknesses, concentration, and AMS error are listed in the table above.

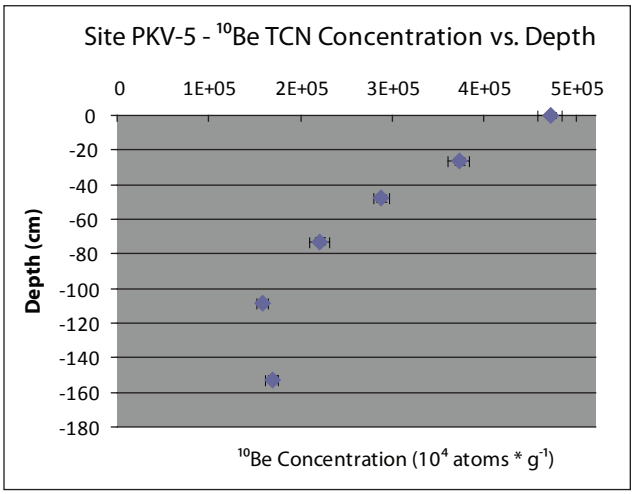

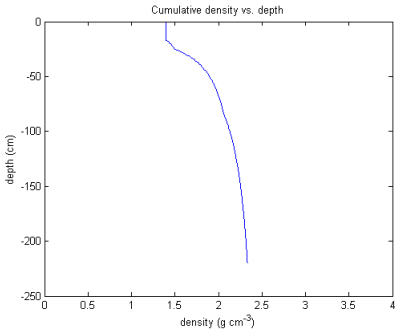

Depth (cm)	Density (g * cm^{-3})	Error (g * cm^{-3})
0	1.4	0.2
18	1.7	0.2
26	2.3	0.2
57	2.3	0.2
85	2.5	0.2

(D) Soil density profile graph and table. PKV-5 was excavated to ~175 cm depth.

(E) -- Figure 4.3 - TCN-PKV-5 (top 5)

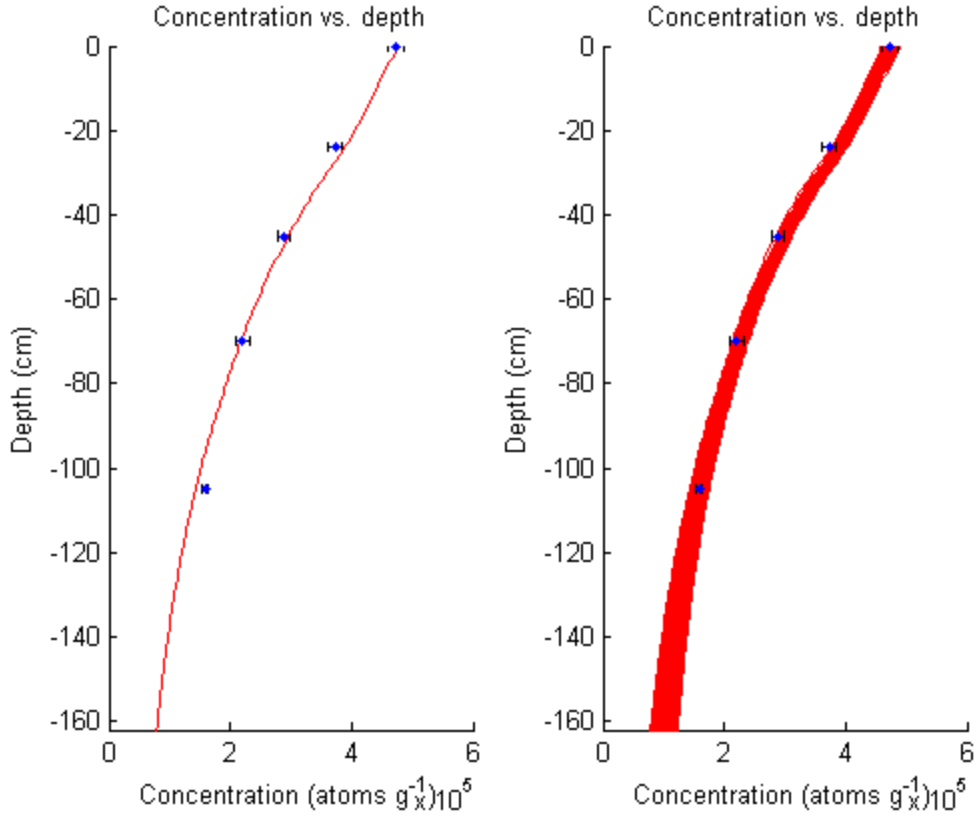

(F)

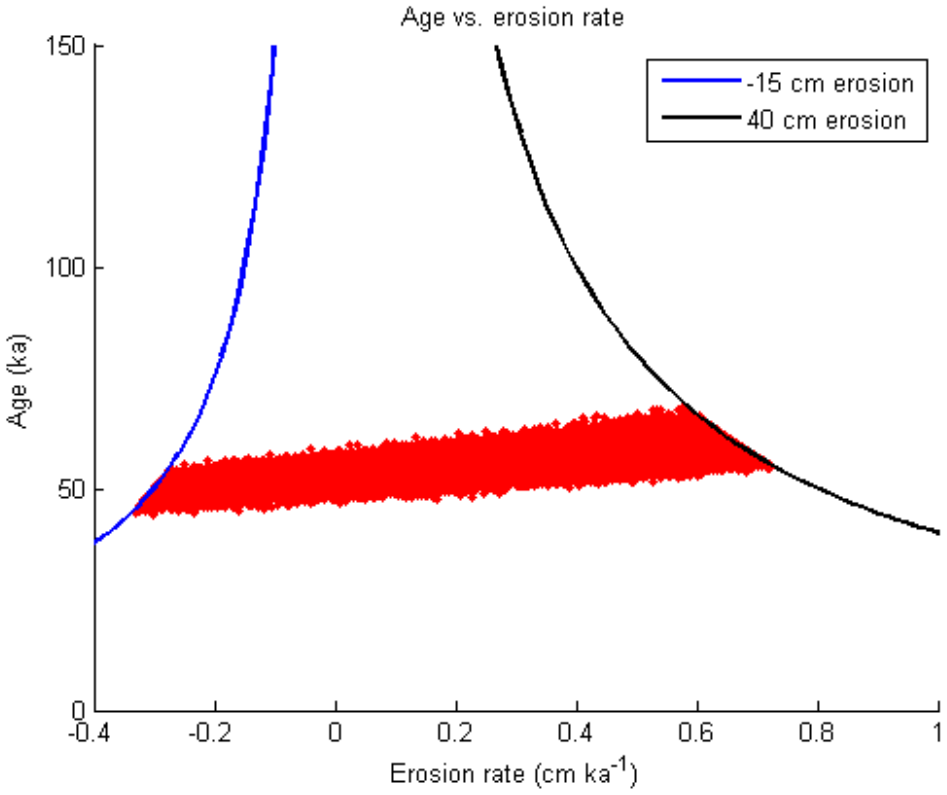

(G)

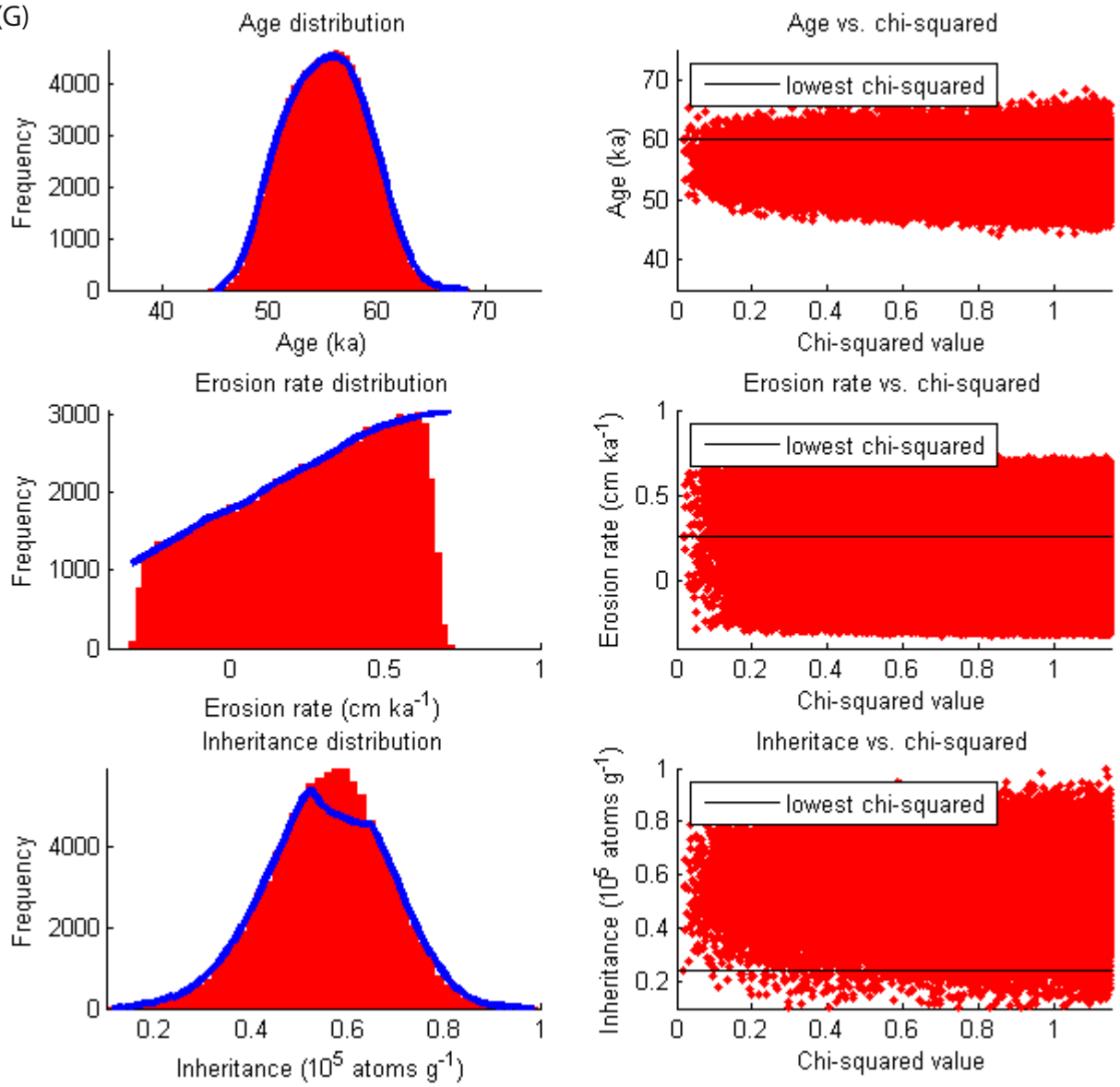
Age distribution
Frequency
Age (ka)
Age vs. chi-squared
lowest chi-squared
Age (ka)
Chi-squared value
Erosion rate distribution
Frequency
Erosion rate (cm ka-1)
Erosion rate vs. chi-squared
lowest chi-squared
Erosion rate (cm ka-1)
Chi-squared value
Inheritance distribution
Frequency
Inheritance (10^5 atoms g-1)
Inheritace vs. chi-squared
lowest chi-squared
Inheritance (10^5 atoms g-1)
Chi-squared value

(H) -- Figure 4.3 - TCN-PKV-5 (top 5 samples)

Site PKV-5 -- TCN-PKV-5 INFO

Latitude: 35.555˚
Longitude: -117.221˚
Elevation: 755 m
Be site production rate: 7.92738 atoms * yr^{-1} g^{-1}
Be half-life: 1.387 Ma

Monte Carlo Simulator:
age: 35,000 min // 75,000 max
erosion rate: -0.4 to 1 cm * ka^{-1}
total erosion: -15 to 40 cm
inheritance: 10,000 to 100,000 atoms * $gram^{-1}$
neutrons: 160 mean value // 5 std

Matlab model output:
N = 100,000 runs @ 1 sigma
43,470,862 iterations required
Simulation took 3,406.8 seconds

	age (ka)	inht. (10^4 atoms * g^{-1})	erosion rate (cm * ka^{-1})
mean	55.2	5.57	0.25
median	55.3	5.61	0.29
mode	55.6	5.60	0.61
lowest χ^2	60.0	2.42	0.26
maximum	68.5	9.97	0.72
minimum	44.2	1.01	-0.33

Preferred Age = 55.2 +13.3 / -11.0 ka

(I)

Resultant incision rate from "top 5" samples' age estimate
Incision rate: 0.23 ± 0.05 mm * yr^{-1}

Figure 4.3 – (A – D) ^{10}Be TCN data for top 5 profile samples of TCN-PKV-5. (E) ^{10}Be TCN concentration vs. depth profile of Site PKV-5 uplift along the GF in north-central Pilot Knob Valley. (F) Age variance as a function of erosion rates. (G) Age, erosion rate and inheritance distribution plots. (H) Matlab™ modeling input parameters and statistics. Maximum and minimum values represent the 95% confidence interval (2s). (I) Incision rate estimate is calculated by dividing incision magnitude by mean age and maximum and minimum ages.

Figure 4.4 - Site PKV-1 = TCN-PKV-1 data

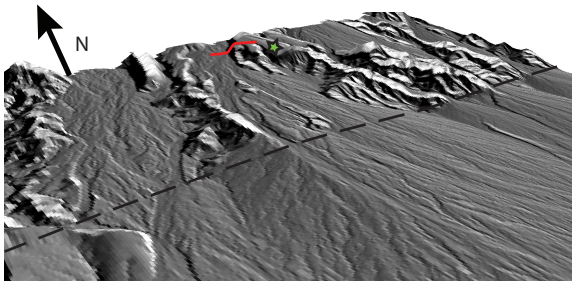

(A) Vertically exaggerated shaded-relief map of incised terrace treads and sediments north of the Garlock fault (dashed black line). View is looking northeast. Red line denotes elevational transect shown to the right. Green star locates ^{10}Be TCN-PKV-1 site.

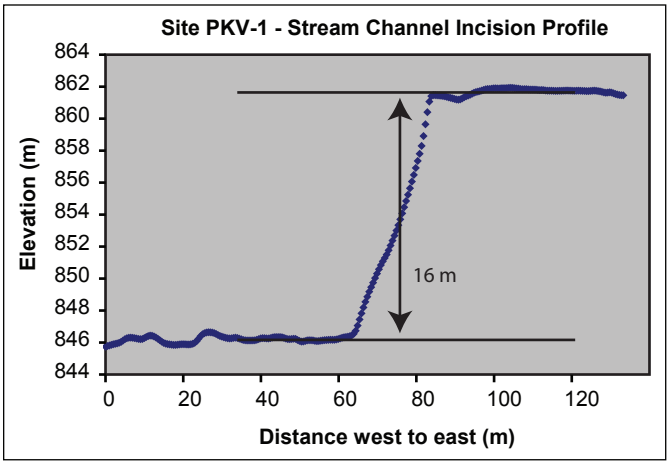

(B) Elevational transect across an incised terrace tread immediately north of the Garlock fault. Vertical separation is 16 meters.

Sample (#)	Depth (cm)	Thickness (cm)	Conc. (atoms * g^{-1})	Error (atoms * g^{-1})
1	0.1	2	584,192	0.0195
2	18	5	659,732	0.0171
3	31	5	598,741	0.0171
4	56	6	537,287	0.0408
5	99	5	484,084	0.0423
6	164	6	389,904	0.0426

(C) ^{10}Be TCN concentration plot with depth for TCN-PKV-1. Horizontal and vertical error bars indicate AMS uncertainty and sampling interval, respectively. Sample depths and thicknesses, concentration, and AMS error are listed in the table above.

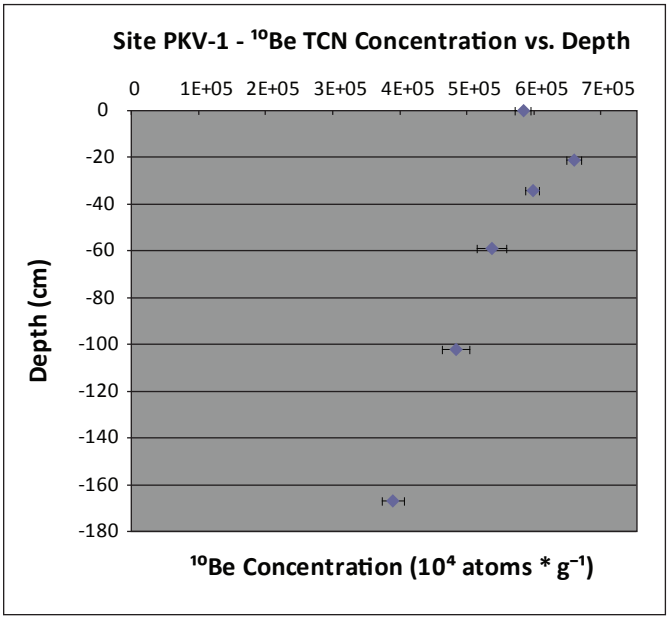

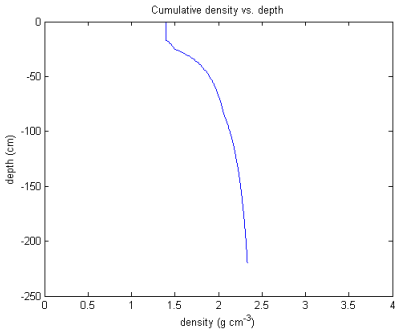

Depth (cm)	Density (g * cm^{-3})	Error (g * cm^{-3})
0	1.4	0.2
18	1.7	0.2
26	2.3	0.2
57	2.3	0.2
85	2.5	0.2

(D) Soil density profile graph and table. PKV-1 was extracted to ~195 cm depth.

(E) -- Figure 4.4 - TCN-PKV-1 (bottom 5 samples)

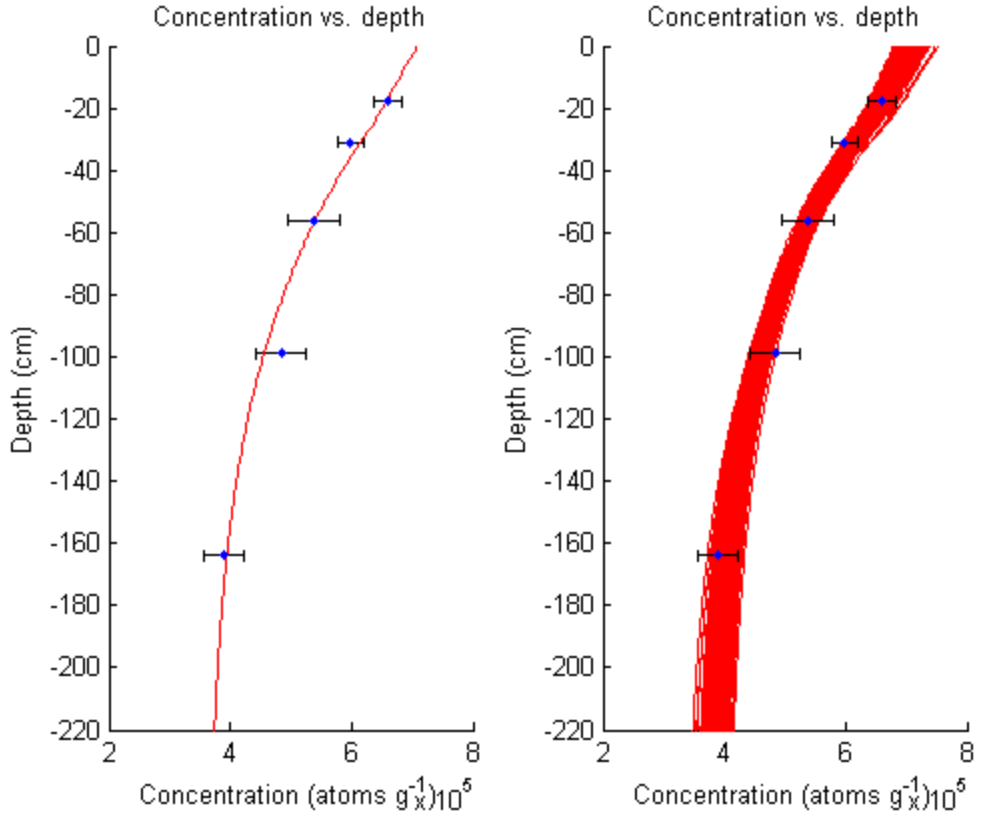

(F)

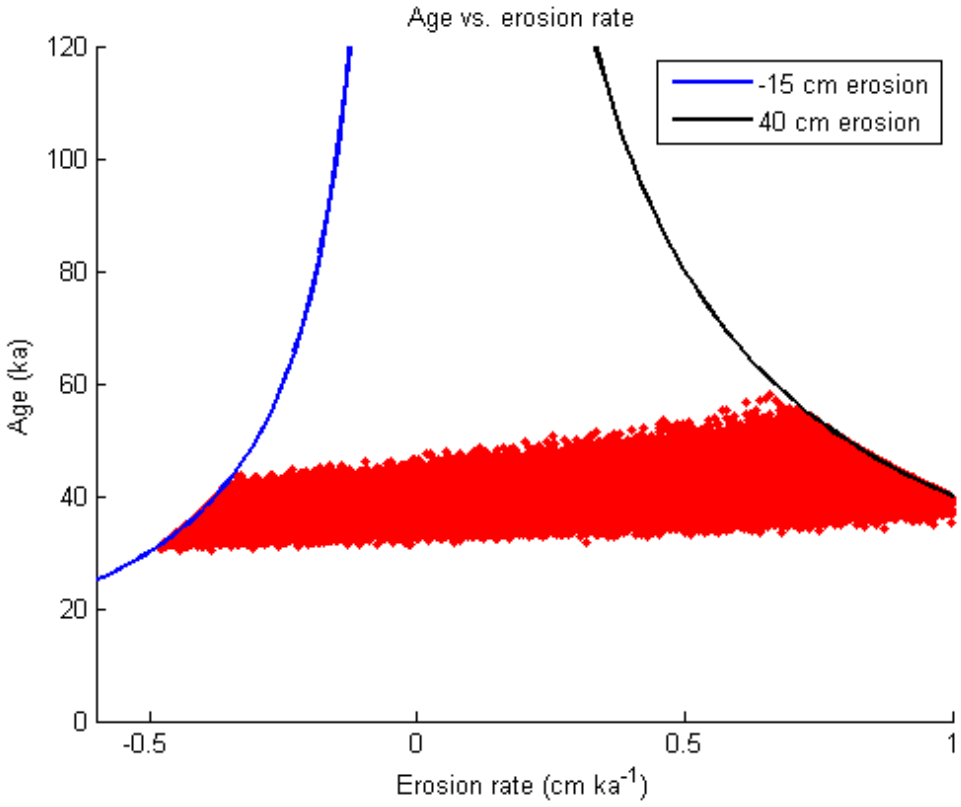

(G)

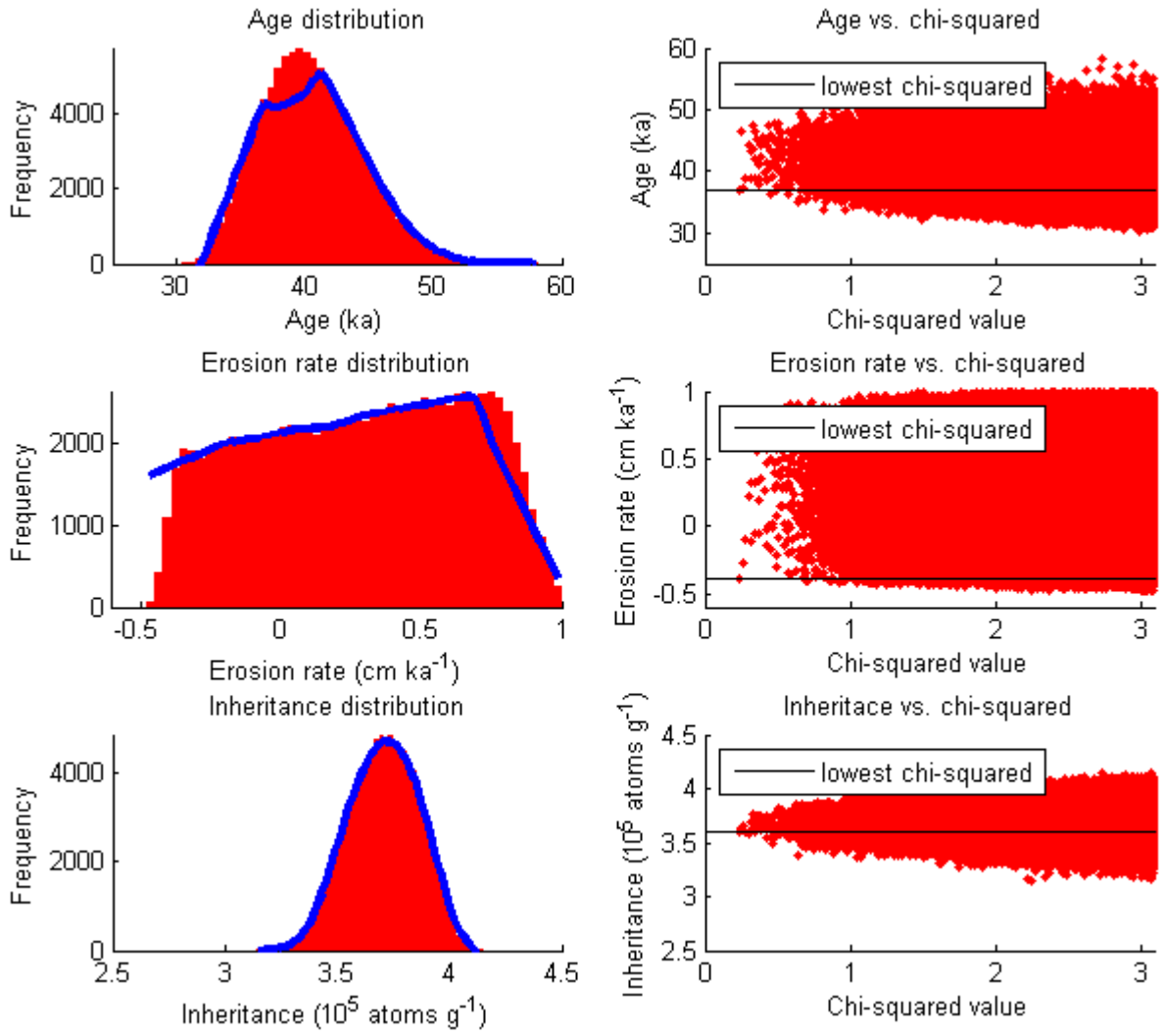
Age distribution
Frequency
Age (ka)
Age vs. chi-squared
lowest chi-squared
Age (ka)
Chi-squared value
Erosion rate distribution
Frequency
Erosion rate (cm ka-1)
Erosion rate vs. chi-squared
lowest chi-squared
Erosion rate (cm ka-1)
Chi-squared value
Inheritance distribution
Frequency
Inheritance (10^5 atoms g-1)
Inheritace vs. chi-squared
lowest chi-squared
Inheritance (10^5 atoms g-1)
Chi-squared value

(H) -- Figure 4.4 - TCN-PKV-1 (bottom 5 samples)

Site PKV-1 -- TCN-PKV-1 INFO

Latitude: 35.555˚
Longitude: -117.221˚
Elevation: 895 m
Be site production rate: 8.83323 atoms * yr^{-1} g^{-1}
Be half-life: 1.387 Ma

Monte Carlo Simulator:
age: 25,000 min // 60,000 max
erosion rate: -0.6 to 1 cm * ka^{-1}
total erosion: -15 to 40 cm
inheritance: 25,000 to 45,000 atoms * $gram^{-1}$
neutrons: 160 mean value // 5 std

Matlab model output:
N = 100,000 runs @ 2 sigma
6,165,165 iterations required
Simulation took 1,060.4 seconds

	age (ka)	inht. (10^4 atoms * g^{-1})	erosion rate (cm * ka^{-1})
mean	40.4	37.07	0.28
median	40.1	37.11	0.30
mode	40.2	37.29	0.52
lowest χ^2	36.9	36.06	-0.39
maximum	58.2	41.52	1.00
minimum	30.4	31.39	-0.48

Preferred age = 40.4 +17.8 / -10.0 ka

(I)

Resultant incision rate from bottom 5 samples' age estimate
Incision rate: 0.40 ± 0.13 mm * yr^{-1}

Figure 4.4 – (A – D) ^{10}Be TCN data for bottom 5 profile samples of TCN-PKV-1. (E) ^{10}Be TCN concentration vs. depth profile of Site PKV-1 uplift along the GF in north-central Pilot Knob Valley. (F) Age variance as a function of erosion rates. (G) Age, erosion rate and inheritance distribution plots. (H) Matlab™ modeling input parameters and statistics. Maximum and minimum values represent the 95% confi-dence interval (2s). (I) Incision rate estimate is calculated by dividing incision magnitude by mean age and maximum and minimum ages.

Figure 4.5 - Site PKV-3 = TCN-PKV-3 and CLK-4 soil data

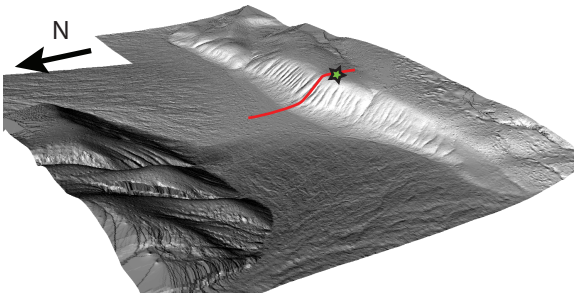

(A) Vertically exaggerated shaded-relief map of antithetic reverse faults adjacent to the southern Slate Range. View is looking southeast. Red line denotes elevational transect shown to the right. Green star locates ^{10}Be TCN-PKV-3 and CLK-4 soil PDI site. LiDAR resolution is ~0.05 m.

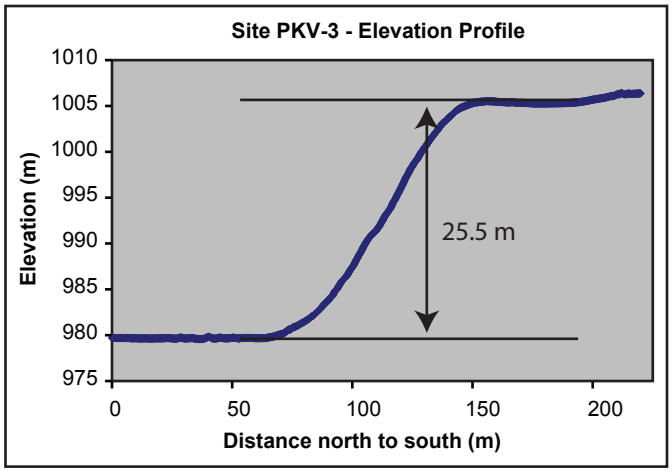

(B) Elevational transect across south-dipping reverse fault adjacent to the southern Slate Range. Vertical separation is 25.5 meters.

Sample (#)	Depth (cm)	Thickness (cm)	Conc. (atoms * g^{-1})	Error (atoms * g^{-1})
1	0.1	2	1,762,592	0.0152
2	28	5	1,334,628	0.0438
3	45	4	2,223,065	0.0459
4	67	3	1,732,326	0.0151
5	117	7	1,040,486	0.0392
6	158	7	744,594	0.0317

(C) ^{10}Be TCN concentration plot with depth for TCN-PKV-3. Horizontal and vertical error bars indicate AMS uncertainty and sampling interval, respectively. Sample depths and thicknesses, concentration, and AMS error are listed in the table above.

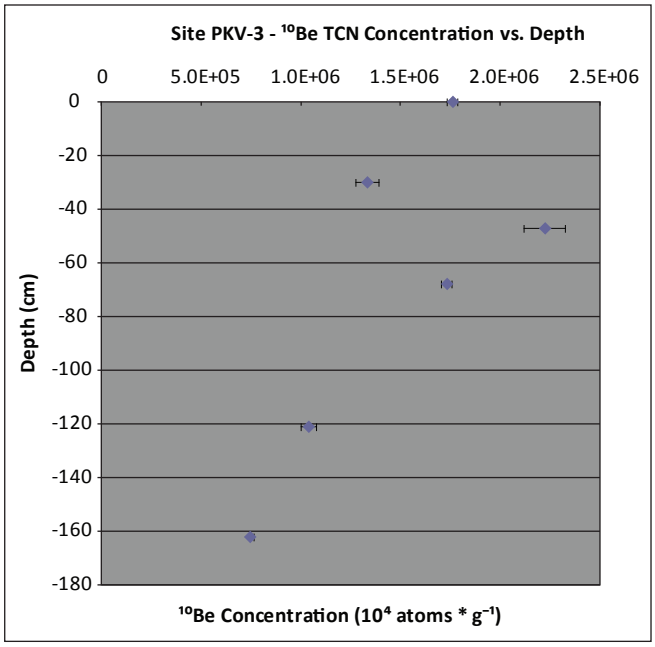

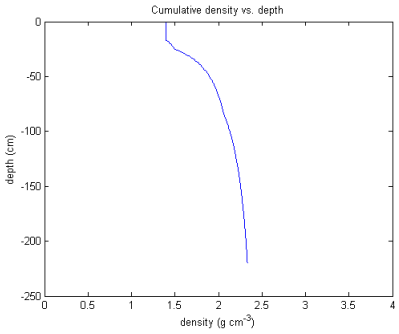

Depth (cm)	Density (g * cm^{-3})	Error (g * cm^{-3})
0	1.4	0.2
18	1.7	0.2
26	2.3	0.2
57	2.3	0.2
85	2.5	0.2

(D) Soil density profile graph and table. PKV-3 was excavated to ~207 cm depth.

(E) -- Figure 4.5 - TCN-PKV-3 (top 2 samples)

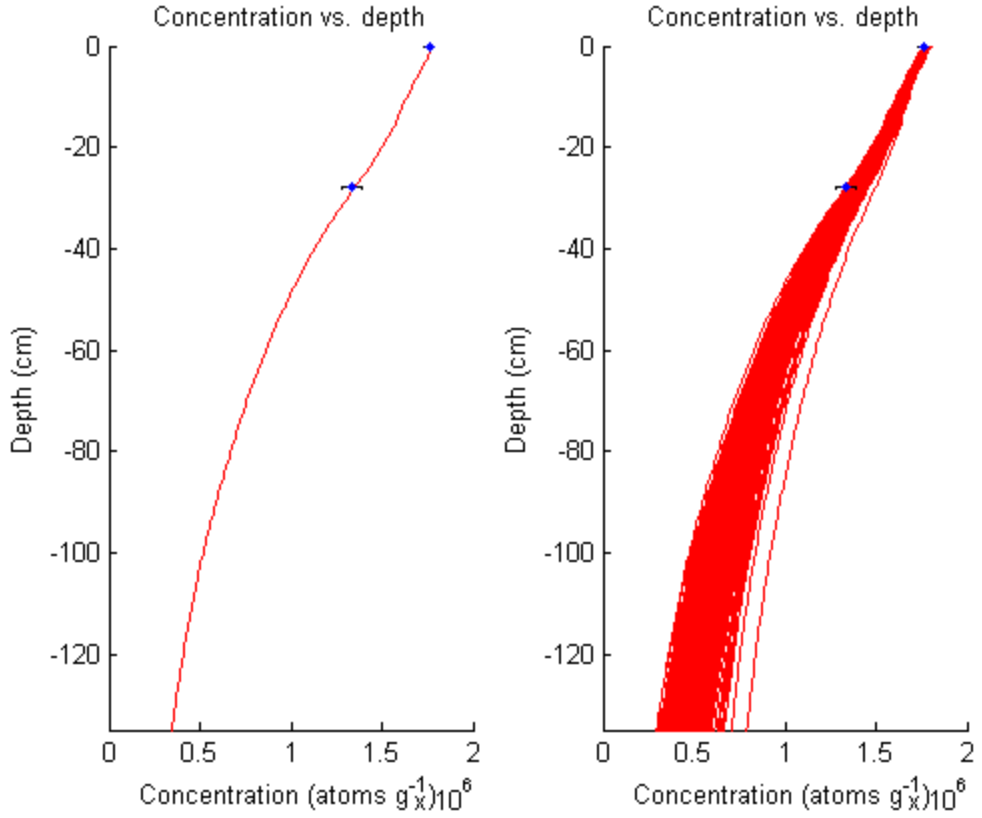

(F)

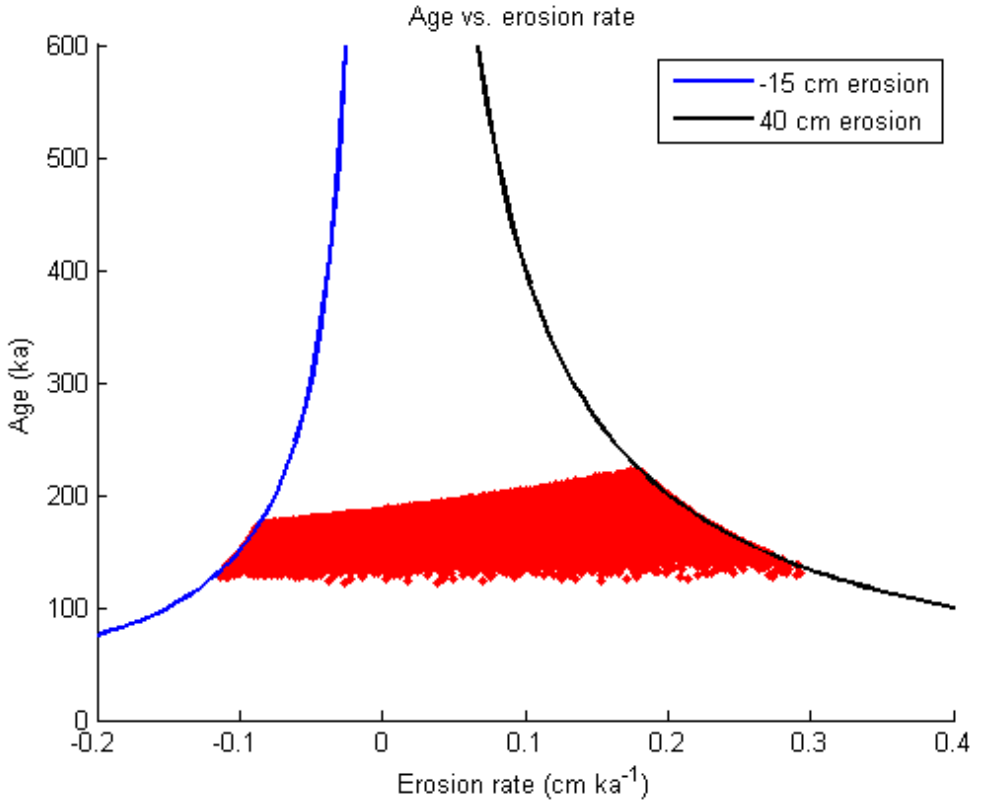

(G)

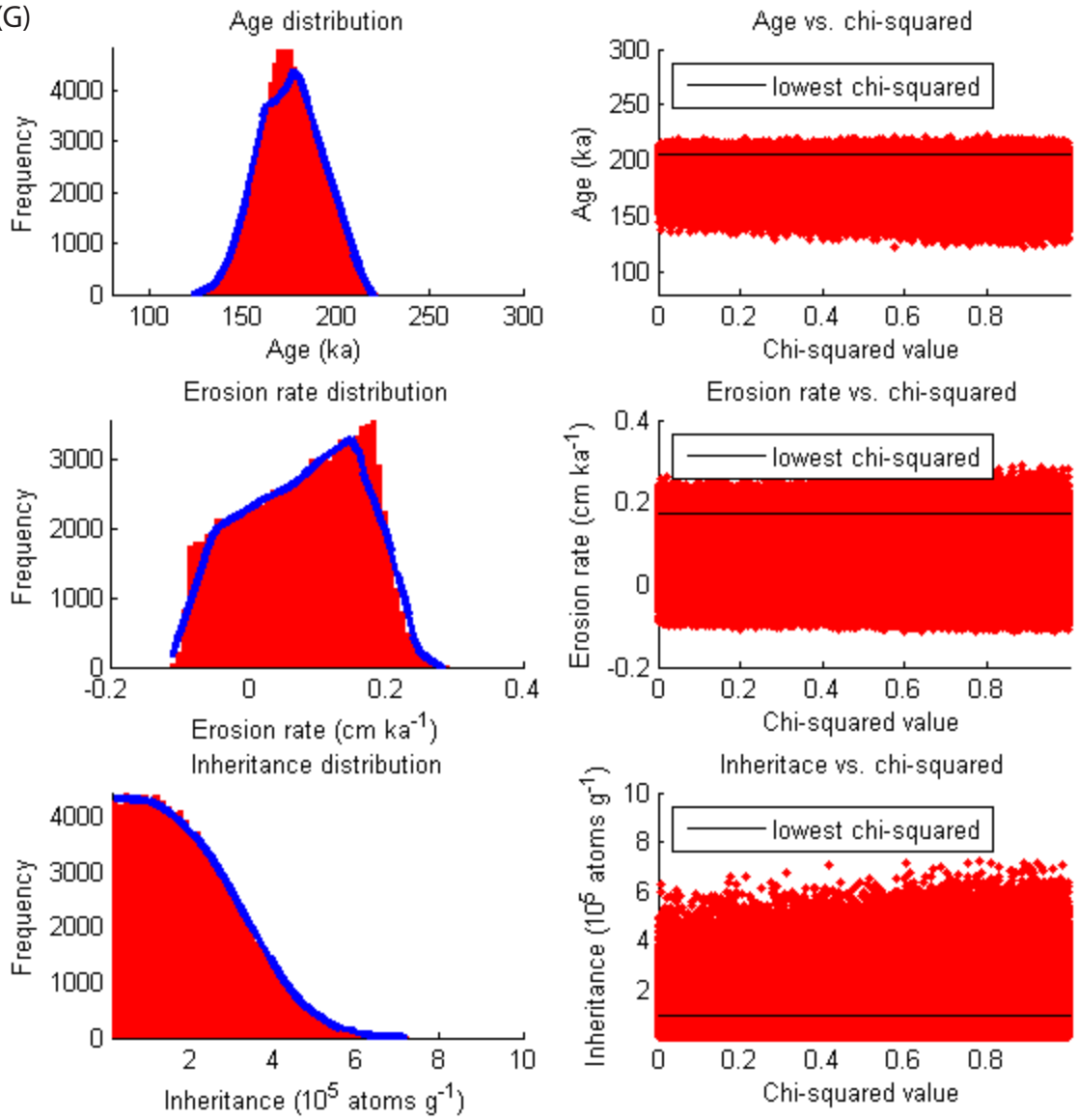
Age distribution
Frequency
Age (ka)
Age vs. chi-squared
lowest chi-squared
Age (ka)
Chi-squared value
Erosion rate distribution
Frequency
Erosion rate (cm ka-1)
Erosion rate vs. chi-squared
lowest chi-squared
Erosion rate (cm ka-1)
Chi-squared value
Inheritance distribution
Frequency
Inheritance (10^5 atoms g-1)
Inheritace vs. chi-squared
lowest chi-squared
Inheritance (10^5 atoms g-1)
Chi-squared value

(H) -- Figure 4.5 - TCN-PKV-3 (top 2 samples)

Site PKV-3 -- TCN-PKV-3 INFO

Latitude: 35.555˚
Longitude: -117.221˚
Elevation: 1,035 m
Be site production rate: 9.82786 atoms * yr^{-1} g^{-1}
Be half-life: 1.387 Ma

Monte Carlo Simulator:
age: 80,000 min // 300,000 max
erosion rate: -0.2 to 0.4 cm * ka^{-1}
total erosion: -15 to 40 cm
inheritance: 10,000 to 100,000 atoms * $gram^{-1}$
neutrons: 160 mean value // 5 std

Matlab model output:
N = 100,000 runs @ 1 sigma
17,544,782 iterations required
Simulation took 1,167.9 seconds

	age (ka)	inht. (10^4 atoms * g^{-1})	erosion rate (cm * ka^{-1})
mean	175.7	19.50	0.08
median	175.0	17.70	0.09
mode	173.7	17.52	0.18
lowest χ^2	205.5	9.67	0.17
maximum	222.5	72.46	0.29
minimum	122.2	1.00	-0.11

Preferred age = 175.7 +46.8 / -53.5 ka

(I)

Resultant uplift rate from top 2 samples' ^{10}Be TCN age estimate:
0.15 + 0.06 / - 0.04 mm * yr^{-1}

(J) -- Figure 4.5 - CLK-4

Site PKV-3 -- Soil PDI INFO

Soil PDI = 83.7 (Rubification, Texture, Dry Consistence and Cutans) --> 162 ka

CLK-4 soil is well developed with a general Av-Btky-Byk-BCk-Ck horizon sequence. Soil depth exceeds 200 cm, and the B horizon is well developed with common cutans coating gravel and ped faces with few to many irregular small masses of gypsum. Stage I to III carbonate morphology (e.g., Giles et al., 1981) is present. Soil and sediment morphology suggest that the soil may have formed in 3 different parent materials:
(1) A locally derived hillslope colluvium (0-72 cm) with in-situ playa deposits at top (0-35 cm).
(2) A debris flow deposit (72-134 cm).
(3) An older alluvial deposit (134-207+ cm).

The CLK-4 soil PDI age estimate was extrapolated from a Mojave-wide soil chronofuction (McDonald & Kirby, unpublished data) developed using multiple soil PDI values from dated surfaces and deposits spanning 1 - 100,000+ ka.

(K)

Resultant uplift rate from soil PDI age estimate:
0.16 mm * yr^{-1}

Figure 4.5 – (A – D) ^{10}Be TCN data for top 2 profile samples of TCN-PKV-3. (E) ^{10}Be TCN concentration vs. depth profile of Site PKV-3 uplift adjacent to the southern Slate Range front in north-central Pilot Knob Valley. (F) Age variance as a function of erosion rates. (G) Age, erosion rate and inheritance distribution plots. (H) Matlab™ modeling input parameters and statistics. Maximum and minimum values represent the 95% confidence interval (2s). (I) Uplift rate estimate is calculated by dividing incision magnitude by mean age and maximum and minimum ages. (J) Soil PDI information and age estimate. (K) Uplift rate estimate resulting from the soil PDI age estimate.

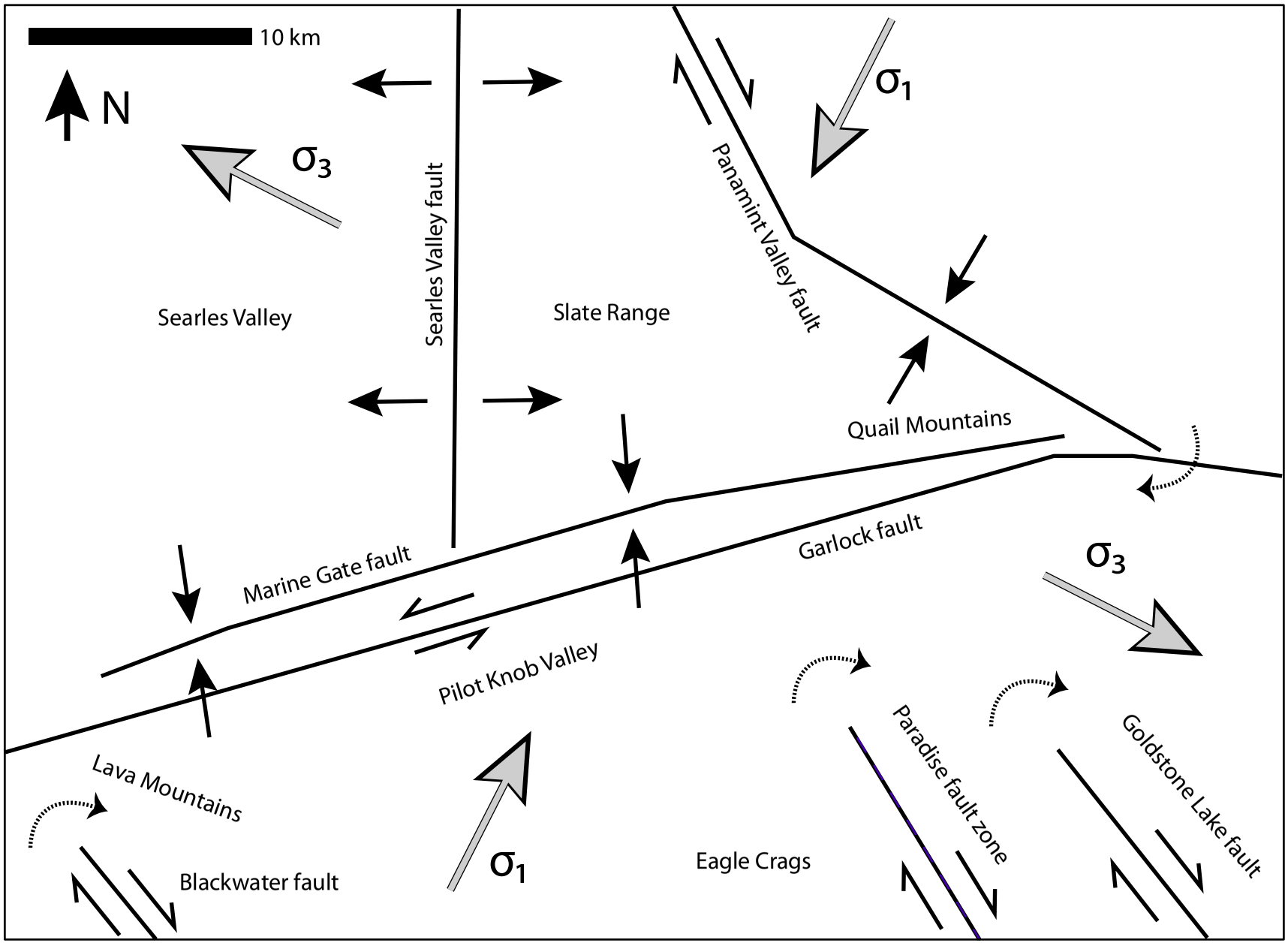
10 km
N
σ3
σ1
Searles Valley fault
Panamint Valley fault
Searles Valley
Slate Range
Quail Mountains
Marine Gate fault
Garlock fault
σ3
Pilot Knob Valley
Lava Mountains
Blackwater fault
σ1
Eagle Crags
Paradise fault zone
Goldstone Lake fault

Figure 4.6 – Stylized fault block model of Pilot Knob Valley and vicinity. Four major types of faults are shown: (1) a sinistral Garlock fault; (2) a contractional Marine Gate fault; (3) an extensional Searles Valley fault; and (4) a dextral Panamint Valley fault, Paradise fault zone-Goldstone Lake fault and Blackwater fault of the Eastern California shear zone. Solid black arrows show block motions across fault zones. Large black-and-white arrows indicate principal stress directions of $\sigma 1$ and $\sigma 3$. Principal stress directions are from Monastero and others (2002) with $\sigma 1$ oriented N27E and $\sigma 3$ oriented N63W. North-south shortening along the Marine Gate fault is a consequence of clockwise crustal warping around the termination of the Panamint Valley fault and the Paradise fault zone-Goldstone Lake fault to the east against the Garlock fault. Reduced slip on these intersecting faults requires increased contractional strain in eastern Pilot Knob Valley.

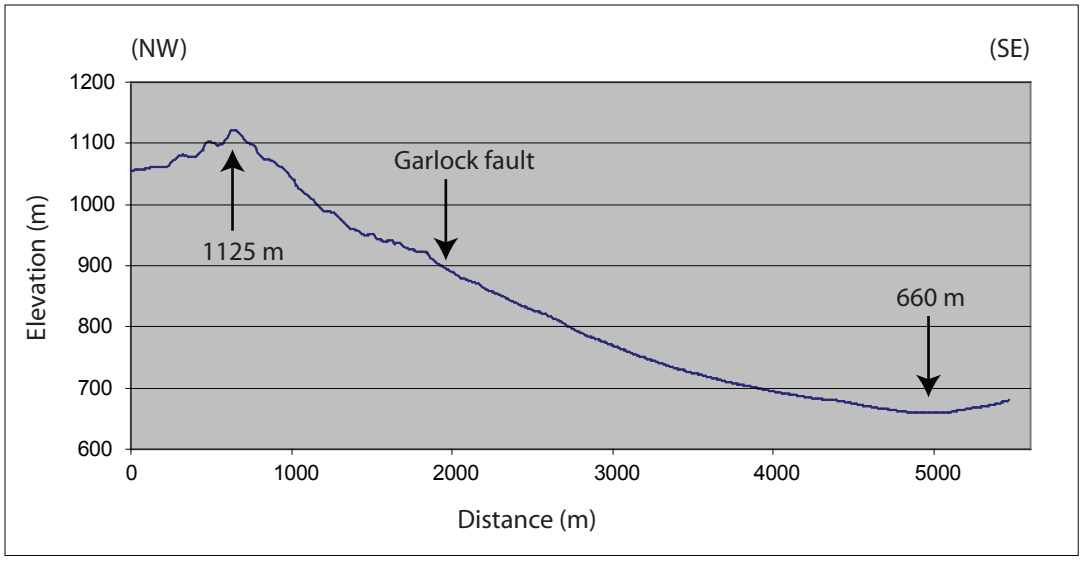
(NW)
(SE)
1200
1100
1000
900
800
700
600
Elevation (m)
Garlock fault
1125 m
660 m
0
1000
2000
3000
4000
5000
Distance (m)

Figure 4.7 – Northwest to southeast elevation transect across uplifted Pilot Knob Formation strata from crest to valley floor in northern Pilot Knob Valley. See figure 4.2 for location of transect.

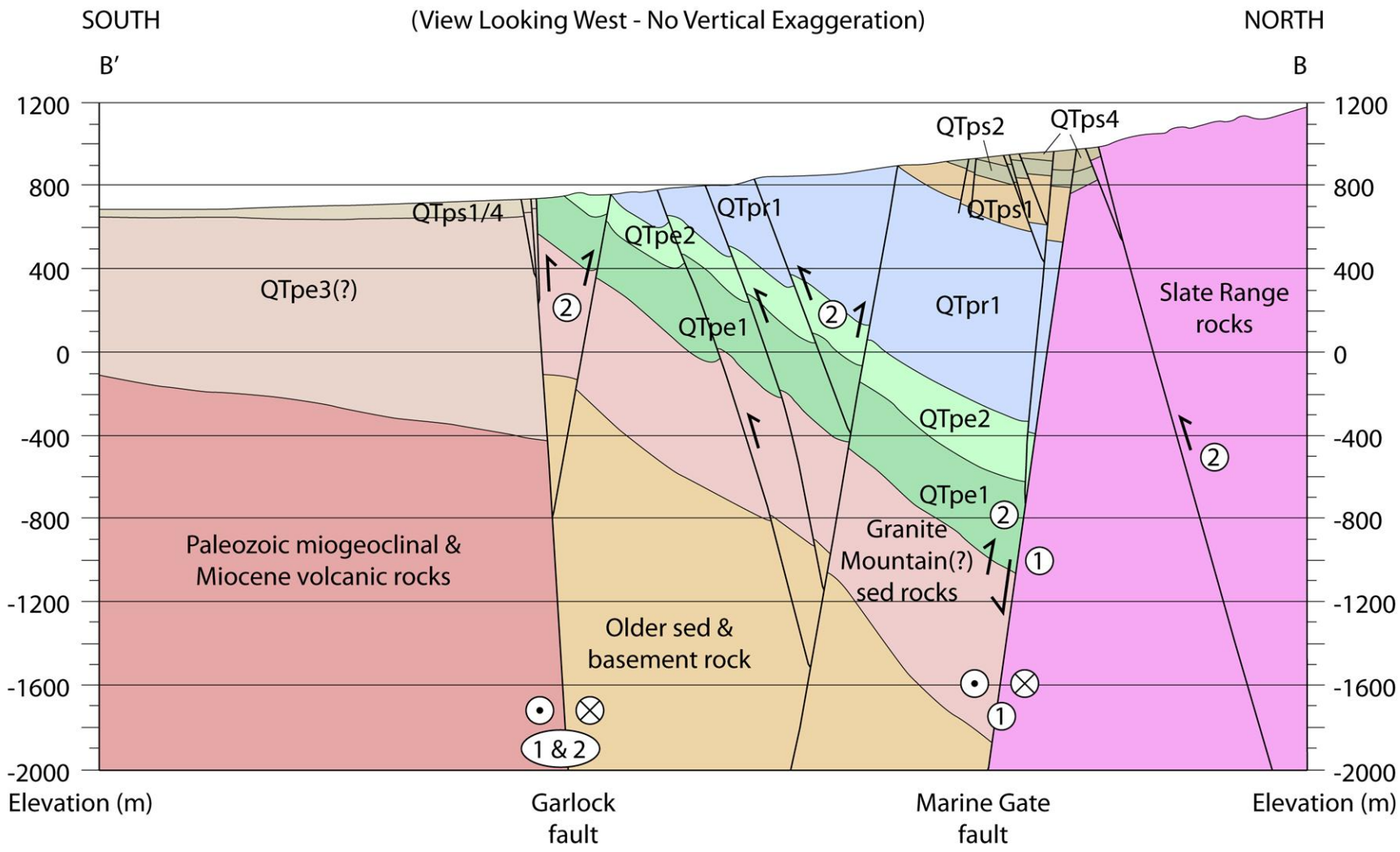
SOUTH
(View Looking West - No Vertical Exaggeration)
NORTH
B'
B
1200
800
400
0
-400
-800
-1200
-1600
-2000
Elevation (m)
QTps2
QTps4
QTps1/4
QTps1
QTpr1
QTpe2
QTpe3(?)
QTpe1
Slate Range rocks
Paleozoic miogeoclinal & Miocene volcanic rocks
Granite Mountain(?) sed rocks
Older sed & basement rock
1 & 2
Garlock fault
Marine Gate fault

Figure 4.8 – Structural cross section along B-B’ line in northern Pilot Knob Valley. See figure 4.2 for map location and unit explanations.

REFERENCES CITED

Andrew, J.E., 2007, Western Quail Mountains Geologic Map: Geological Society of America Maps and Charts, scale 1:12,000, doi: 10.1130/2007.DMCH005.

Andrew, J.E., and Walker, J.D., 2009, Reconstructing late Cenozoic deformation in central Panamint Valley, California: Evolution of slip partitioning in the Walker Lane: Geosphere, v. 5, p. 172-198, doi: 10.1130/GES00178.1

Bennett, R.A., Wernicke, B.P., Niemi, N.A., Friederich, A.M., and Davis, J.L., 2003, Contemporary strain rates in the northern Basin and Range province from GPS data: Tectonics, v. 22, p. 3-1-3-31.

Bourne, S.J., England, P.C., and Parsons, B., 1998, The motion of crustal blocks driven by flow of the lower lithosphere and implications for slip rates of continental strike-slip faults: Nature, v. 391, p. 655-659, doi: 10.1038/35556.

Burchfiel, B.C., Hodges, K.V., and Royden, L.H., 1987, Geology of Panamint Valley-Saline Valley pull-apart system, California; palinspastic evidence for low-angle geometry of a Neogene range-bounding fault: Journal of Geophysical Research, v. 92, p. 10,422-10,426, doi: 10.1029/JB092iB10p10422.

Clark, M.M., 1973, Map showing recently active breaks along the Garlock and associated faults, California: U.S. Geological Survey Miscellaneous Geologic Investigations Map I-741, scale 1:24,000, 3 sheets.

Davis, G.A., and Burchfiel, B.C., 1973, Garlock fault: An intracontinental transform structure, southern California: Geological Society of America Bulletin, v. 84, p. 1407-1422.

DeMets, C., and Dixon, T.H., 1999, New kinematic models for Pacific-North American motion from 3 Ma to present, I: evidence for steady motion and biases in the NUVEL-1A model: Geophysical Research Letters, v. 26, p. 1921-1924.

Didericksen, B., 2005, Middle Miocene to recent faulting and exhumation of the central Slate Range, Eastern California shear zone [MS Thesis]: Lawrence, University of Kansas, 104 p.

Didericksen, B.D., Stockli, D.F., Walker, J.D., and Andrew, J.E., (in prep), Middle Miocene to recent exhumation of the Slate Range, eastern California, and implications for the timing of extension and transition to transtension.

Dixon, T.H., Robaudo, S., Lee, J., and Reheis, M.C., 1995, Constraints on present-day Basin and Range deformation from space geodesy: Tectonics, v. 14, p. 755-772.

Dixon, T.H., Miller, M., Farina, F., Wang, H., Johnson, D., 2000, Present-day motion of the Sierr Nevada block and some tectonic implications for the Basin and Range Province, North America Cordillera: Tectonics, v. 19, p. 1-24.

Dokka, R.F., and Travis, C.J., 1990, Late Cenozoic strike-slip faulting in the Mojave Desert, California: Tectonics, v. 9, p. 311-340.

Dunne, G.C., and Walker, J.D., 2004, Structure and evolution of the East Sierran thrust system, east central California: Tectonics, v. 23, 23 pp., doi: 10.1029/2002TC001478.

Gan, W., Svarc, J.L., Savage, J.C., and Prescott, W.H., 2000, Strain accumulation across the Eastern California shear zone at latitude 36°30'N: Journal of Geophysical Research, v. 105, p. 16,229-16,236.

Gan, W., Zhang, P., Shen, Z., Prescott, W.H., and Svarc, J.L., 2003, Initiation of deformation of the Eastern California shear zone: constraints from Garlock fault geometry and GPS observations: Geophysical Research Letters, v. 30, 1496, 4 pp., doi: 10.1029/2003GL017090.

Ganev, P.N., Dolan, J.F., Frankel, K.L., and Finkel, R.C., 2010, Rates of extension along the Fish Lake Valley fault and transtensional deformation in the Eastern California shear zone-Walker Lane belt: Lithosphere, v. 2, p. 33-49, doi: 10.1130/L51.1.

Garfunkel, Z., 1974, Model for the late Cenozoic tectonic history of the Mojave Desert, California, and for its relation to adjacent regions: Geological Society of America Bulletin, v. 85, p. 1,931-1,944.

Gile, L.H., Hawley, J.W., and Grossman, R.B., 1981, Soils and geomorphology in the Basin and Range area of southern New Mexico - guidebook to the Desert Project: New Mexico Bureau of Mines and Mineral Resources Memoir 39, 222 pp.

Gosse, J.C., and Phillips, F.M., 2001, Terrestrial in situ cosmogenic nuclides: theory and application: Quaternary Sciences Reviews, v. 20, p. 1475-1560, doi: 10.1016/S0277-3791(00)00171-2.

Guest, B., Pavlis, T.L., Golding, H., and Serpa, L., 2003, Chasing the Garlock: A study of tectonic response to vertical axis rotation: Geology, v. 31, p. 553-556.

Guest, B., Niemi, N., and Wernicke, B., 2007, Stateline fault system: A new component of the Miocene-Quaternary Eastern California shear zone: Geological Society of America Bulletin, v. 119, p. 1,337-1,346, doi: 10.1130B26138.

Le, K., Lee, J., Owen, L.A., and Finkel, R., 2007, Late Quaternary slip rates along the Sierra Nevada frontal fault zone, California: Slip partitioning across the western margin of the Eastern California shear zone-Basin and Range province: Geological Society of America Bulletin, v. 119, p. 240-256, doi: 10.1130/B25960.1.

Lee, J., Stockli, D., Schroeder, J., Tincher, C., Bradley, D., Owen, L., Gosse, J., Finkel, R., and Garwood., J., 2006, Fault slip transfer in the Eastern California shear zone-Walker Lane Belt:

Geological Society of America Penrose Conference Field Trip Guide (Kinematics and Geodynamics of Intraplate Dextral Shear in Eastern California and Western Nevada, Mammoth Lakes, California, 21-26 April 2005), 26 p., doi: 10.1130/2006.FSTTTE.PFG.

Hardebeck, J.L., and Hauksson, E., 1999, Roles of fluids in faulting inferred from stress field signatures: Science, v. 285, p. 236-239.

Helms, J.G., McGill, S.F., and Rockwell, T.K., 2003, Calibrated, late Quaternary age indices using clast rubification and soil development on alluvial surfaces in Pilot Knob Valley, Mojave Desert, southeastern California: Quatern. Res., v. 60, p. 377-393, doi: 10.1016/j.yqres.2003.08.002.

Hidy, A.J., Gosse, J.C., Pederson, J.L., Mattern, J.P., and Finkel, R.C., 2010, A geologically constrained Monte Carlo approach to modeling exposure ages from profiles of cosmogenic nuclides: An example from Lees Ferry, Arizona: Geochemistry Geophysics Geosystems, v. 11, 18 pp., doi: 10.1029/2010GC003084.

Hodges, K.V., Walker, J.D., and Wernicke, B.P., 1987, Footwall structural evolution of the Tucki Mountain detachment system, Death Valley region, southeastern California, *in* Coward, M.P., et al., eds., Continental extensional tectonics: Geological Society of London Special Publication 28, p. 393-408.

McClusky, S.C., Bjornstad, S.C., Hager, B.H., King, R.W., Meade, B.J., Miller, M.M., Monastero, F.C. and Souter, B.J., 2001, Present day kinematics of the Eastern California shear zone from a geodetically constrained block model: Geophysical Research Letters, v. 28, p. 3,369-3,372.

McGill, S.F. and Sieh, K.E., 1991, Surficial offsets on the central and eastern Garlock fault associated with prehistoric earthquakes: Journal of Geophysical Research, v. 96, p. 21,597-21,621.

McGill, S.F. and Sieh, K.E., 1993, Holocene slip rate of the central Garlock fault in southeastern Searles Valley, California: Journal of Geophysical Research, v. 98, p. 14,217-14,231.

McGill, S.F., Wells, S.G., Fortner, S.K., Kuzma, H.A., McGill, J.D., 2009, Slip rate of the western Garlock fault, at Clark Wash, near Lone Tree canyon, Mojave desert, California: Geological Society of America Bulletin, v. 121, p. 536-554, doi: 10.1130/B26123.1.

McQuarrie, N., and Wernicke, B.P., 2005, An annimated tectonic reconstruction of southwestern North America since 36 Ma: Geosphere, v. 1, p. 147-172, doi: 10.1130/GES00016.1.

Miller, D.M., and Yount, J.L., 2002, Late Cenozoic tectonic evolution of the north-central Mojave Desert inferred from fault history and physiographic evolution of the Fort Irwin area, California, *in* Glazner, A.F., Walker, J.D., and Bartley, J.M., eds., Geologic evolution of the Mojave Desert and southwestern Basin and Range: Boulder, Colorado, Geological Society of America Memoir 195, p. 173-197.

Miller, M.M., Johnson, D.J., Dixon, T.H., and Dokka, R.K., 2001, Refined kinematics of the Eastern California shear zone from GPS observations, 1993-1998: Journal of Geophysical Research, v. 106, p. 2,245-2,263.

Miller, D.M., Dudash, S.L., Green, H.G., Lidke, D.J., Amoroso, L., Phelps, G.A., and Schmidt, K.M., 2007, A new Quaternary view of northern Mojave Desert tectonics suggests changing fault patterns during the late Pleistocene, *in* Miller, D.M., and Valin, Z.C., ed., Geomorphology and tectonics at the intersection of Silurian and Death Valleys, southern California – 2005 Guidebook, Pacific Cell Friends of the Pleistocene, 17 pp.

Monastero, F.C., Walker, J.D., Katzenstein, A.M., and Sabin, A.E., 2002, Neogene evolution of the Indian Wells Valley, east-central California, *in* Glazner, A.F., Walker, J.D., and Bartley, J.M., eds., Geologic evolution of the Mojave Desert and southwestern Basin and Range: Boulder, Colorado, Geological Society of America Memoir 195, p. 199-228.

Numelin, T., Kirby, E., Walker, J.D., and Didericksen, B., 2007, Late Pleistocene slip on a low-angle normal fault, Searles Valley, California: Geosphere, v. 3, p. 163-176, doi: 10.1130/GES00052.1.

Nur, A., Ron, H. and Beroza, G.C., 1993, The nature of the Landers-Mojave earthquake line: Science, v. 261, p. 201-203, doi: 10.1126/science.261.5118.201.

Oldow, J.S., 1992, Late Cenozoic displacement partitioning in the northwestern Great Basin, in Craig, S.D., ed., Walker Lane symposium; structure, tectonics & mineralization of the Walker Lane: Reno, Nevada, Geological Society of Nevada, p. 17-52.

Oldow, J.S., Aiken, C.L.V., Hare, J.L., Ferguson, J.F., and Hardyman, R.F., 2001, Active displacement transfer and differential block motion within the central Walker Lane, western Great Basin: Geology, v. 29, p. 19-22, doi:

Oskin, M., and Stock, J., 2003a, Marine incursion synchronous with plate-boundary localization in the Gulf of California, Geology: v. 31, p. 23-26, doi: 10.1130/0091-7613(2003) 031<0023:MISWPB>2.0.CO;2.

Oskin, M., and Stock, J., 2003b, Pacific-North America plate motion and opening of the Upper Delfin basin, northern Gulf of California, Mexico: Geological Society of America Bulletin, v. 115, p. 1173-1190, doi: 10.1130/B25154.1.

Oswald, J.A., and Wesnousky, S.G., 2002, Neotectonics and Quaternary geology of the Hunter Mountain fault zone and Saline Valley region, southeastern California: Geomorphology, v. 42, p. 255-278, doi: 10.1016/S0169-555X(01)00089-7.

Reheis, M.C., and Dixon, T.H., 1996, Kinematics of the eastern California shear zone; evidence for slip transfer from Owens and Saline Valley fault zones to Fish Lake Valley fault zone : Geology, v. 24, p. 339-342, doi: 10.1130/0091-7613(1996)024<0339:KOTECS>2.3CO;2.

Roy, M., and Royden, L.H., 2000a, Crustal rheology and faulting at strike-slip plate boundaries; 1, an analytic model: Journal of Geophysical Research, v. 105, p. 5583-5597, doi: 10.1029/1999JB900339.

Roy, M., and Royden, L.H., 2000b, Crustal rheology and faulting at strike-slip plate boundaries; 2, effects of lower crustal flow: Journal of Geophysical Research, v. 105, p. 5589-5613.

Savage, J.C., 2000, Viscoelastic-coupling model for the earthquake cycle driven from below: Journal of Geophysical Research, v. 105, p. 25,525-25,532, doi: 10.1029/2000JB900276.

Savage, J.C., Gan, W., and Svarc, J.L., 2001, Strain accumulation and rotation in the Eastern California shear zone: Journal of Geophysical Research, v. 106, p. 21,995-22,007.

Savage, J.C., Lisowsky, M., and Prescott, W.H., 1990, An apparent shear zone trending north-northwest across the Mojave Desert into Owens Valley, eastern California: Geophysical Research Letters, v. 12, p. 2,113-2,116.

Savage, J.C., Svarc, J.L., and Prescott, W.H., 2004, Interseismic strain and rotation rates in the northeast Mojave domain, eastern California: Journal of Geophysical Research, v. 109, 13 pp., doi: 10.1029/2003JB002705.

Schermer, E.R., Luyendyk, B.P., and Cisowski, S., 1996, Late Cenozoic structure and tectonics of the northern Mojave Desert: Tectonics, v. 15, p. 905-932.

Smith, G.I., 1964, Geology and volcanic petrology of the Lava Mountains, San Bernardino County, California: U.S. Geologic Survey Professional Paper 457, 97 p.

Smith, G.I., Troxel, B.W., Gray, C.H., Jr., and Von, H.R., 1968, Geologic reconnaissance of the Slate Range, San Bernardino and Inyo counties, California: Special Report - California Division of Mines and Geology, v., 96, p. 1-33.

Smith, G.I., 2009, Late Cenozoic geology and lacustrine history of Searles Valley, Inyo and San Bernardino counties, California: U.S. Geological Survey Professional Paper 1727, 115 p.

Snow, J.K., and Wernicke, B., 2000, Cenozoic tectonism in the Central Basin and Range: magnitude, rate, and distribution of upper crustal strain: American Journal of Science, v. 300, p.659-719.

Walker, J.D., Kirby, E., and Andrew, J.E., 2005, Strain transfer and partitioning between Panamint Valley, Searles Valley, and Ash Hill fault zones, California: Geosphere, v. 1, p. 111-118, doi: 10.1130/GES00014.1.

Wernicke, B., and Snow, J.K., 1998, Cenozoic tectonism in the Central Basin and Range: motion of the Sierran-Great Valley block: International Geology Review, v. 40, p. 403-410.

Wesnousky, S.G., 2005, Active faulting in the Walker Lane: Tectonics, v. 24, 35 pp., doi: 10.1029/2004TC001645

Zhang, P., Ellis, M., Slemmons, D.B., and Mao, F., 1990, Right-lateral displacements and the Holocene slip rate associated with prehistoric earthquakes along the southern Panamint Valley fault zone; implications for southern Basin and Range tectonics and coastal California deformation: Journal of Geophysical Research, v., 95, p. 4,857-4,872, doi: 10.1029/JB095iB04p04857.

APPENDICES

Appendix A - TCN-PKV-2 INFO

Elevation: 792 m
Latitude / Longitude: 35º 33' 50" N, -117º 12' 09" W
^{10}Be production rate (at site): 8.1592 atoms/gram*year
^{10}Be half-life: 1.387 Ma
Topographic Shielding: None

Sample Site Characteristics:

TCN-PKV-2 was sampled from a vertical stream bank incised into an alluvial fan with a Qa5 tread surface developed on top. The northern extent of the Qa5 fan is truncated by the Garlock fault. Potential corresponding deposits on the northern side of the Garlock fault are not preserved. Surface and deposit materials are quartz-rich and are derived from the Slate Range to the north. The Qa5 surface here suggests minimal erosional disturbance (i.e., well-developed pavement with no overturned clasts, well-developed Av horizon, and no petracalcite clasts at the surface).

Eric McDonald performed a detailed soil description here to serve as a soil profile development index (PDI) site to develop a Mojave-wide soil chronofunction. Labeled "CLK-3" in the chronofunction, his PDI age estimate (see data repository item # 2) was ~31.9 ka.. Carbonate morphologic stage (e.g., Gile et al., 1981) II-III is observed.

Table 1. Soil Horizon Data for "CLK-3" (i.e., TCN-PKV-2) Site

Soil Horizon	Depth (cm)	Bulk Density of Peds ($g\ cm^{-3}$)	Error ($g\ cm^{-3}$)
Av	0	1.74	0.2
Btk	4	1.89	0.2
Bty_1	10	1.89	0.2
Bty_2	22	1.89	0.2
Bky_1	25	1.89	0.2
Bky_2	54	1.89	0.2
Bky_3	68	1.89	0.2
Bky_4	85	1.89	0.2
Bcky	108	1.89	0.2

Horizon nomenclature: k (pedogenic carbonate), t (translocated clay and silt), w (incipient color or structure development), y (pedogenic gypsum).

**Gile, L.H., Hawley, J.W., and Grossman, R.B., 1981, Soils and geomorphology in the Basin and Range area of southern New Mexico - guidebook to the Desert Project: New Mexico Bureau of Mines and Mineral Resources Memoir 39, 222 pp.*

Sampling Techniques & Lab Procedures:

Approximately 1.5 kg of surface clasts 1-3 cm in diameter were collected. Approximately 1-2 kg of sand and silt samples were also collected at 5 different depth intervals (Table 1). Soil density measurements (Table 2) were made by excavating softball-sized pits at different horizons, lining them with thin plastic bags, and measuring the volume of water required to fill each hole. Bagged soil from each pit was then weighed on a digital balance shortly thereafter to prevent drying and modification of soil density. Surface clasts were crushed and sieved at the University of Kansas. Depth profile samples were washed, dried and sieved at the University of Kansas. Sieve fractions between 250-500 μm were initially collected and weighed. For each depth sample, additional mass was needed prior to acid treatment, so sieve fractions up to 2,000 μm were re-crushed and sieved to 250-500 μm, to facilitate mineral separation procedures. This re-crushed and re-sieved sediment was then combined with the initial 250-500 μm fraction before proceeding with further chemical separation procedures at the PRIME laboratory at Purdue University and the University of Kansas. AMS analysis of all samples was performed at PRIME laboratory.

Terrestrial Cosmogenic Nuclide Production Theory:
(Please refer to Gosse and Phillips (2001) for a detailed explanation of processes and theory.)

Gosse, J.C., and Phillips, F.M., 2001, Terrestrial in situ cosmogenic nuclides: theory and application: Quaternary Sciences Reviews, v. 20, p. 1475-1560, doi: 10.1016/S0277-3791(00)00171-2.

TCN-PKV-2 AMS & Soil Density Data:

Table 2. Summary of sample data from the Qa5 terrace in Pilot Knob Valley

Sample ID	Depth to top of sample (cm)	Thickness (cm)	Grain Size Range (μm)	Dissolved Mass (g)	Carrier Mass* (g)	Corrected $^{10}Be/^{9}Be$	^{10}Be Concentration (atoms g^{-1})	1σ AMS Error (%)	1σ Total Measured Error (%)
TCN-PKV-2,1	0	1-3	10000-30000	40.030	0.298	5.195E-13	249424	2.9	2.92
TCN-PKV-2,2	14	3	250-2000	40.101	0.316	4.653E-13	236252	3.3	3.38
TCN-PKV-2,3	36	3	250-2000	40.299	0.295	4.245E-13	199568	3.6	3.68
TCN-PKV-2,4	65	4	250-2000	40.043	0.301	2.784E-13	132926	4.7	4.82
TCN-PKV-2,5	100	4	250-2500	80.700	0.300	5.124E-13	122835	3.5	3.62
TCN-PKV-2,6	175	4	250-2000	61.632	0.313	2.096E-13	66985	4.5	4.77

*Be-carrier solution:
Concentration: 995 ppm
Density: 1.013 g ml^{-1}

Table 3. Soil Density Profile Data

Sample #	Depth (cm)	Density (g cm^{-3})
1	0	1.4
2	18	1.7
3	26	2.3
4	57	2.3
5	85	2.5

Modeling Results:
All ^{10}Be cosmogenic nuclide age modeling herein was performed using Hidy and others (2010) Matlab™-based Monte Carlo "10Be_profile_simulator_V1.2".

**Hidy, A.J., Gosse, J.C., Pederson, J.L., Mattern, J.P., and Finkel, R.C., 2010, A geologically constrained Monte Carlo approach to modeling exposure ages from profiles of cosmogenic nuclides: An example from Lees Ferry, Arizona: Geochemistry Geophysics Geosystems, v. 11, 18 pp., doi: 10.1029/2010GC003084.*

Table 4. Statistics for age modeling of all 6 TCN-PKV-2 profile samples.
(N = 100,000 analyses at 3σ fit)

	Age (ka)	Inheritance (10^4 atoms g^{-1})	Erosion rate (cm ka^{-1})
Mean	25.8	5.07	0.27
Median	25.7	5.09	0.26
Mode	25.4	5.19	-0.23
Lowest χ^2	25.7	4.52	-0.05
Maximum	31.9	6.51	1.00
Minimum	21.6	3.12	-0.40

[Monte Carlo Simulation Parameters]
Age: 18,000 minimum // 35,000 maximum
Erosion Rate: -0.4 cm * ka^{-1} minimum // 1 cm * ka^{-1} maximum
Total Erosion: -15 cm minimum // 50 cm maximum
Inheritance: 30,000 atoms * $gram^{-1}$ // 70,000 atoms * $gram^{-1}$
Neutrons: 160 mean value // 5 standard deviation

Mean exposure age $(\mathrm{X}) = 25.8^{+6.1}_{-4.2} ka$ with 95% (2σ) confidence interval

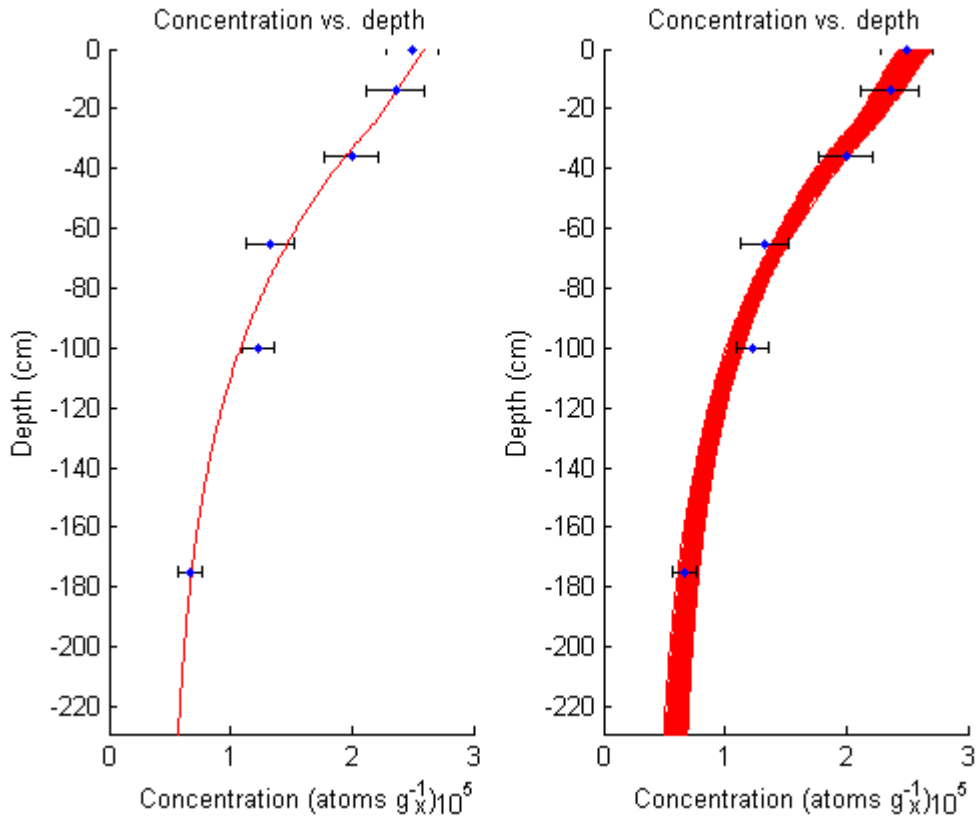

Figure 1. ^{10}Be concentration versus depth plots illustrating the (right) 2σ profile solution spaces and (left) best fit model for all 6 TCN-PKV-2 profile samples.

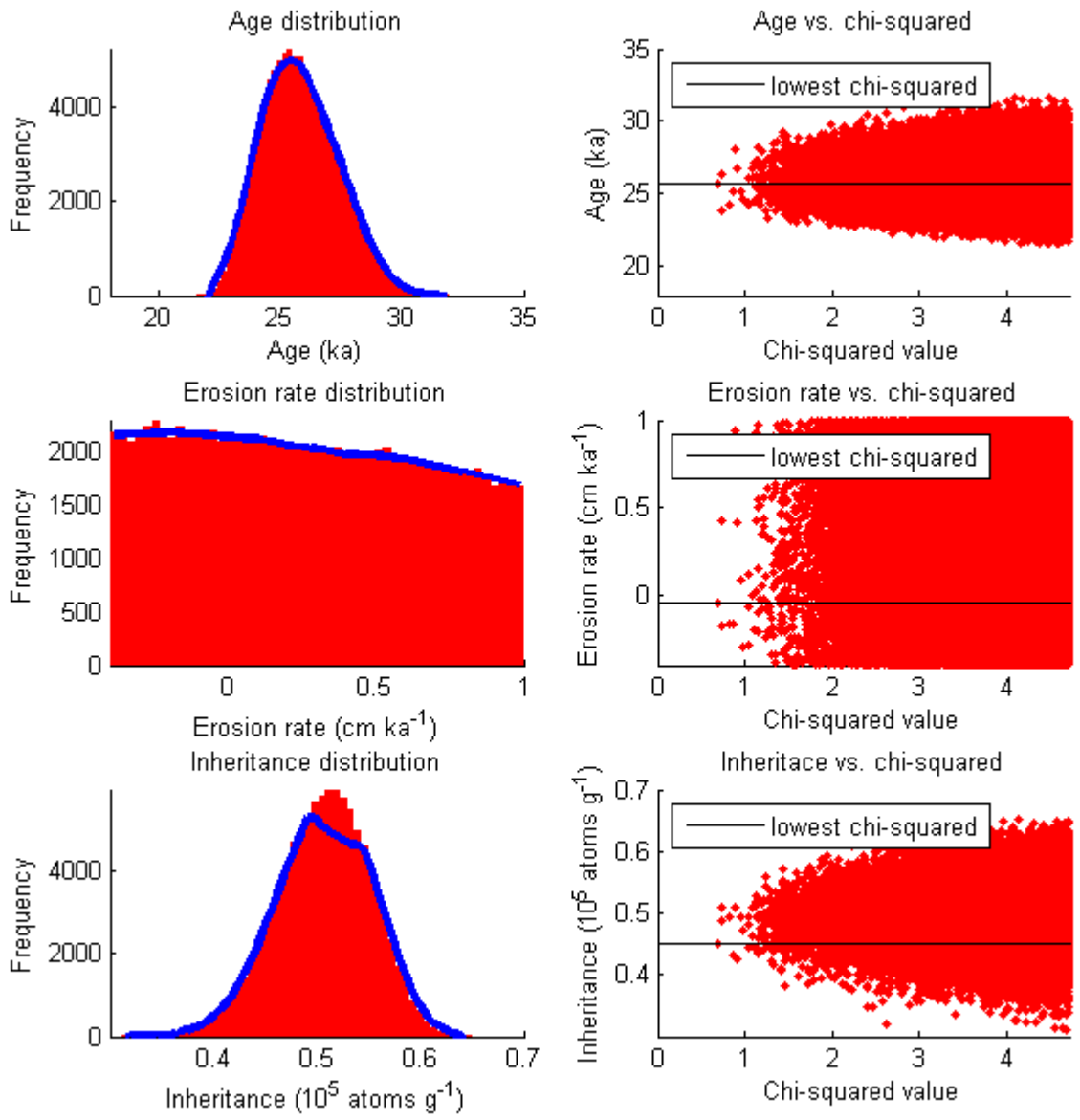

Figure 2. Results for the 2σ age, inheritance and erosion rate solution spaces for all 6 TCN-PKV-2 profile samples. Solid black lines (right plot) indicate the lowest chi-squared value.

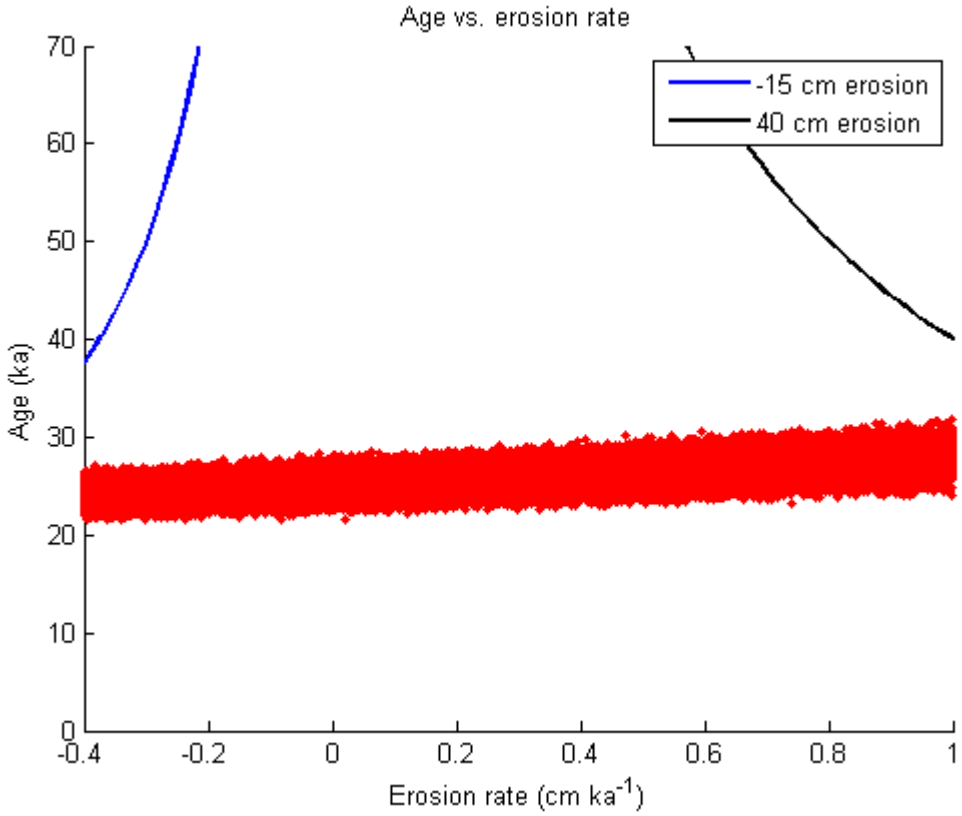

Figure 3. Age versus erosion plot for all 6 TCN-PKV-2 profile samples, with constraints of 15 cm deposition (blue line) and 40 cm erosion (black line).

Table 5. Statistics for age modeling of TCN-PKV-2 profile samples 2, 3, 4 and 6.
(N = 100,000 analyses at 1σ fit)

	Age (ka)	Inheritance (10^4 atoms g^{-1})	Erosion rate (cm ka^{-1})
Mean	28.5	4.60	0.65
Median	28.5	4.62	0.72
Mode	28.5	4.64	1.13
Lowest χ^2	29.4	4.63	1.22
Maximum	36.1	5.75	1.44
Minimum	23.3	2.61	-0.40

[Monte Carlo Simulation Parameters]
Age: 18,000 minimum // 38,000 maximum
Erosion Rate: -0.4 cm * ka^{-1} minimum // 1.7 cm * ka^{-1} maximum
Total Erosion: -15 cm minimum // 40 cm maximum
Inheritance: 25,000 atoms * $gram^{-1}$ // 65,000 atoms * $gram^{-1}$
Neutrons: 160 mean value // 5 standard deviation

Mean exposure age $(\mathrm{X}) = 28.5^{+7.6}_{-5.2} ka$ with 95% (2σ) confidence interval

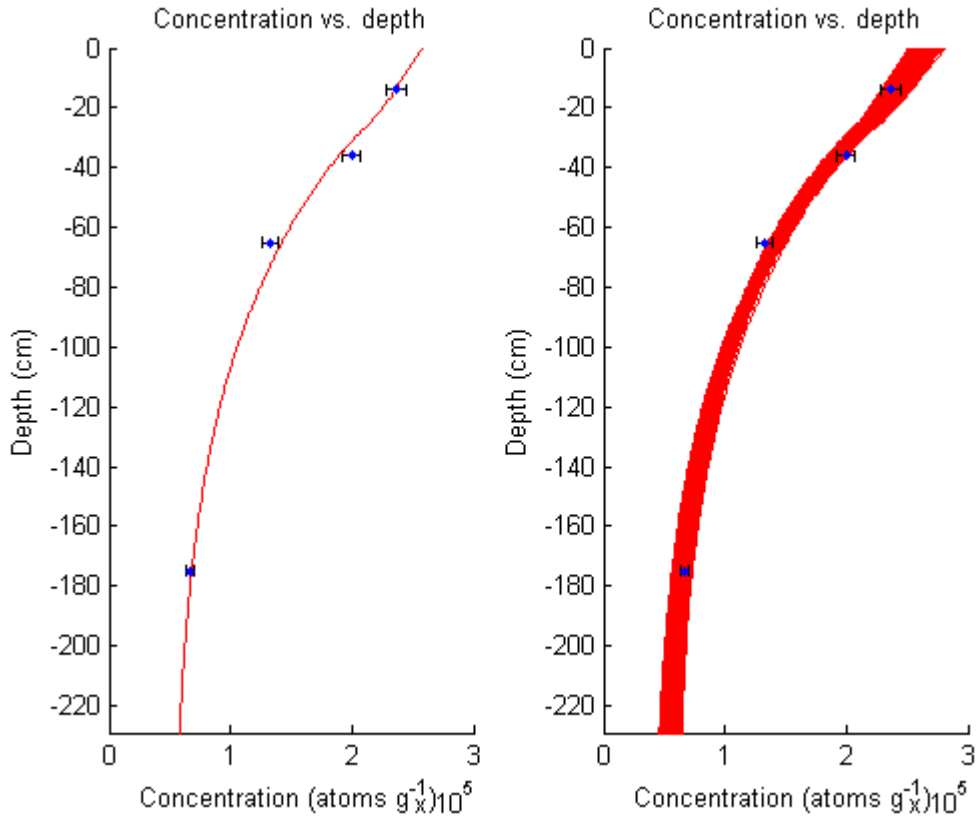

Figure 4. ^{10}Be concentration versus depth plots illustrating the (right) 2σ profile solution spaces and (left) best fit model for all TCN-PKV-2 profile samples 2, 3, 4 and 6.

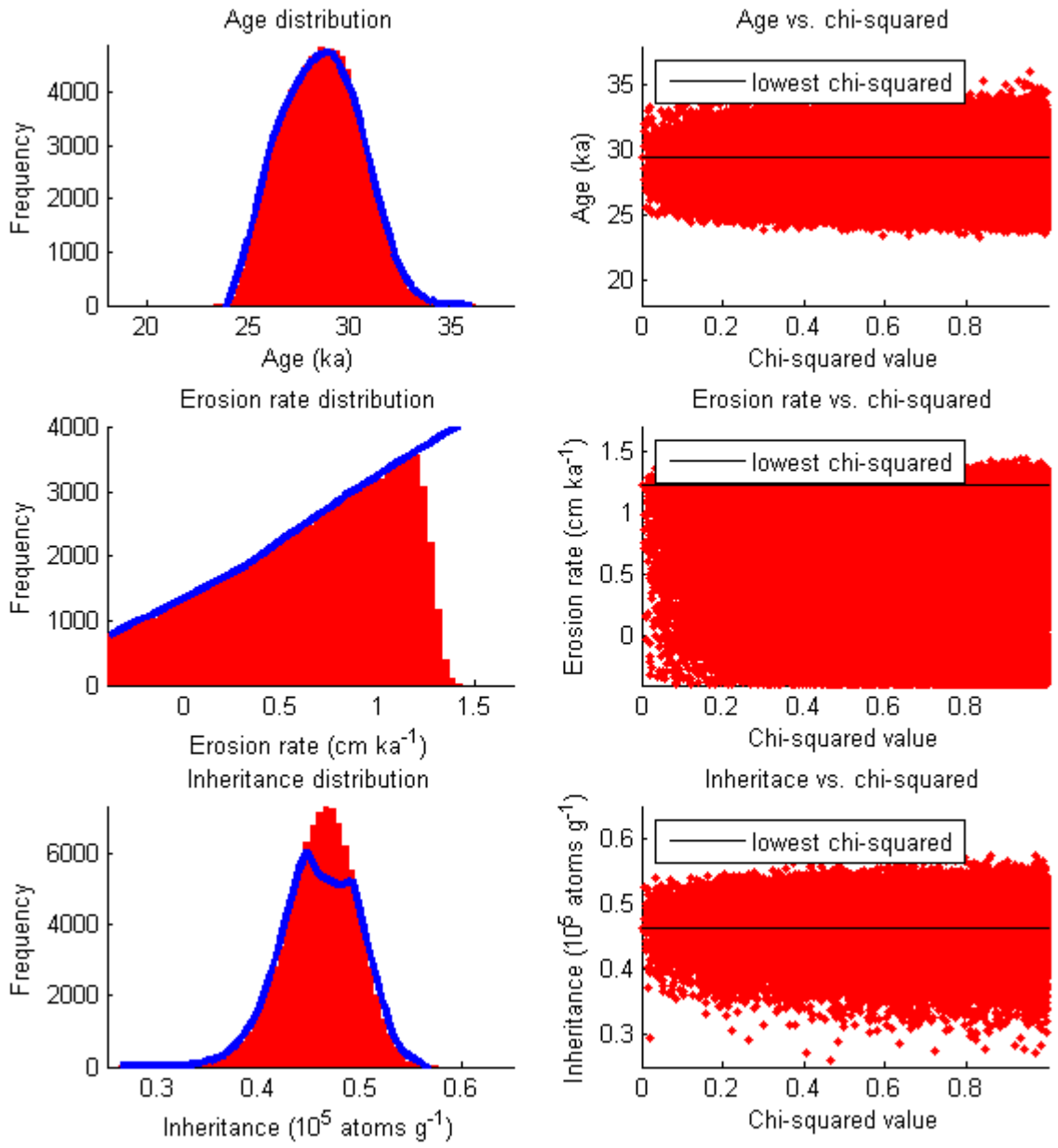

Figure. 5. Results for the 2σ age, inheritance and erosion rate solution spaces for TCN-PKV-2 profile samples 2, 3, 4 and 6. Solid black lines (right plot) indicate the lowest chi-squared value.

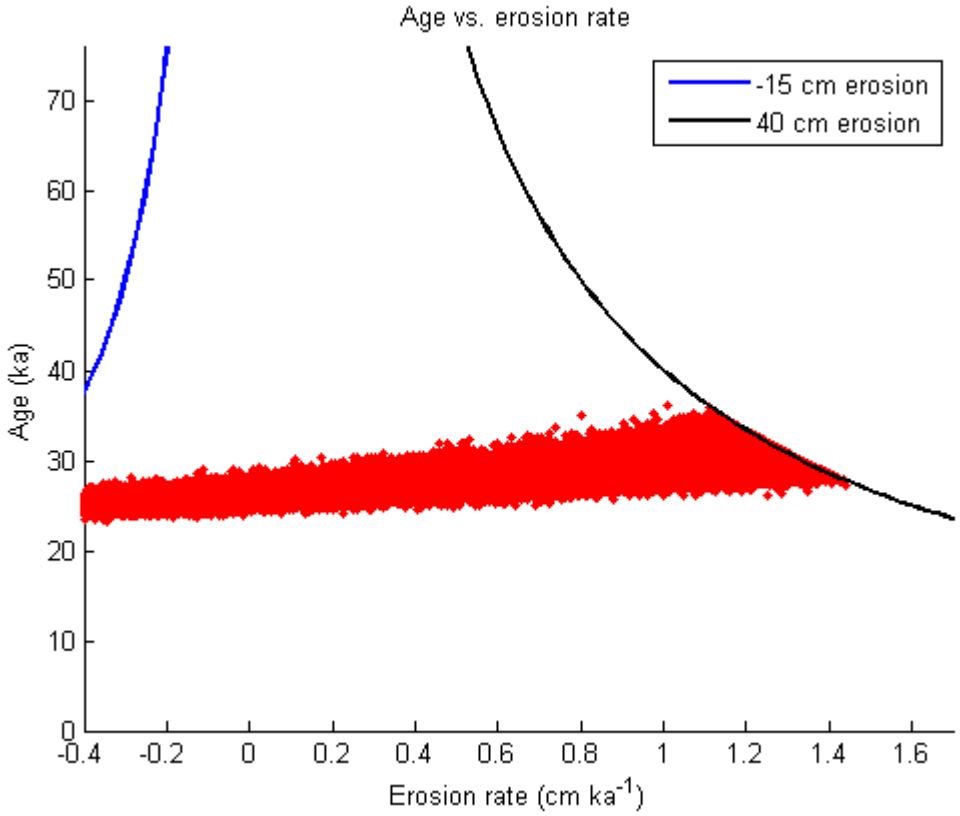

Figure 6. Age versus erosion plot for TCN-PKV-2 profile samples 2, 3, 4 and 6, with constraints of 15 cm deposition (blue line) and 40 cm erosion (black line).

Interpretations of Model Results:

Model results from the 6 depth profile samples are in good agreement with what would be expected from one depositional history followed by stabilization of the surface. This is additionally supported by Eric McDonald's soil analysis (see Table 1). Figure 1 shows a general asymptotic decrease in ^{10}Be concentration with depth, although some scatter exists among the deepest 3 samples (>60 cm).

Individual sample uncertainties vary between 2.92% and 4.82% (see Table 2) of total ^{10}Be concentration.

Because of the shatter among the deepest 3 samples, TCN-PKV-2 was modeled twice. The first model incorporates all 6 surface and depth profile samples (Figures 1-3). The second model uses samples 2, 3, 4 and 6 (Figures 4-7). Results of modeling TCN-PKV-2 will all 6 samples are shown in Table 4, and a mean surface exposure age of $(\mathrm{X}) = 25.8^{+6.1}_{-4.2} ka$ at 95% (2σ) confidence interval is estimated. When the surface sample and sample 5 are excluded, the profile plot better resembles a theoretical production curve. The modeled age from using samples 2, 3, 4 and 6 is $(\mathrm{X}) = 28.5^{+7.6}_{-5.2} ka$ with a 95% (2σ) confidence interval. Because these data better fit an expected TCN depth-concentration relationship, and because of the stronger soil development consistent with ca. 30 ka soils in the Mojave Desert, the older $28.5^{+7.6}_{-5.2} ka$ age is preferred.

The "^{10}Be_profile_simulator_V1.2" profile modeling of the TCN-PKV-2 data has several assumptions that affect the resultant age interpretations. First, erosion is bracketed between values that are based upon a "users" a priori judgments. Amounts of erosion and/or deposition must be estimated

based on field relations at the site and related geomorphological processes. A second assumption of the model is that the entire sampled profile represents one deposition event with no significant time gaps from bottom to top. A third assumption is that ^{10}Be inheritance is the same throughout the profile for a given sediment grain size. A fourth assumption of the model is that ^{10}Be production rates are time invariant (or at least their fluctuations are known and quantifiable), meaning that the age calculation assumes equal production since deposition of the deposit and stabilization of it's surface.

Appendix B: Common soil characteristics for soils along the Garlock fault (this study) and soils on dated alluvial deposits.

Site	General Horizon Sequence[1]	Carbonate Stage[2]	Pavement Development	PDI value[3]	Age (ka)	Reference
Soils Formed on Late Holocene Alluvial Deposits						
CLK-1	Av-Bwk-Bky-Cky	I	weak	3.1	3.5-4.2	This study
CLK-2	Av-Bwk-Bky-Cky	I	weak	3.6	3.5-4.2	This study
MM	Avk-Bwk-Ck-Cky	I	weak	2.5	3.2-2.9	Bacon et al (2009)
PM Qf6	Avk-Bwk-Ck-C	I	weak	4.2	3.5-4.2	McDonald et al (2003)
CWG-2	A-C-Ab1-Ckb1-Ab2-Ckb2-Cb2	I-	weak	2.2	2.5	McGill (2009). Soil formed in deposit Hya
SIL-1	Av-Bwk-Ck-C	I	weak	1.8	2.9-3.6	Mahan et al (2010) site M999VJ-991
Soils Formed on Pre-Late Holocene Alluvial Deposits						
CWG-1	A-AB-Bwk-CBk	I-II	Weak-moderate	7.9	8.1	McGill (2009). Soil formed in deposit H1b
PM Qf5	Avk-Bwk-Btk-Ck-C	II	Moderate-strong	12.1	8.4-14.1	McDonald et al (2003)
CLK-3	Av-Btk-Bty-Bky-CBky-Cky	II-III	strong	44.4	31.9	This study

1: Horizon nomenclature: k (pedogenic carbonate), t (translocated clay and silt), w (incipient color or structure development), y (pedogenic gypsum).

2: Carbonate morphologic stage (Gile et al., 1981).

3: Profile Development Index (PDI) value based on 10 profile properties of color lightening, melinization, rubification, carbonate stage, structure, argillans, consistence (dry, moist), texture using technique of Taylor and Harden (1983).

Appendix C - for sample OSL-PKV-2

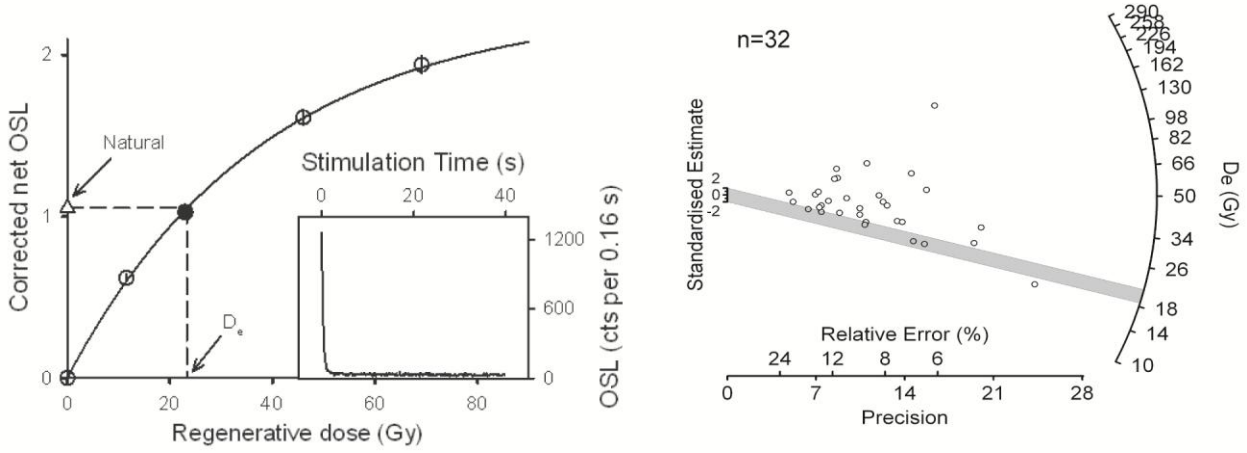

Figure S1 for sample OSL-PKV-2. OSL data (left) and radial plot (right). OSL data show dose response and natural decay (inset); filled circles are recycled points. Shaded area on radial plot indicates 2-sigma band centered on calculated D_e.

Table S1 for sample OSL-PKV-2. OSL dating summary data

D_e[1]	^{234}Th [2]	^{226}Ra [3]	^{228}Ra [4]	^{40}K	$W_{in\text{-}situ}$	Cosmic[5]	Total dose-rate	OSL age
(Gy)	(Bq.kg^{-1})	(Bq.kg^{-1})	(Bq.kg^{-1})	(Bq.kg^{-1})	(%)	(mGya^{-1})	(mGya^{-1})	(ka)
19.81±1.55	43.8±14.2	32.4±1.49	45.8±1.97	1092.5±5.46	0.68	0.21	5.11±0.25	3.88±0.36

1. Calculated using Minimum Age Model
2. Average of ^{234}Th at 63 and 93 keV
3. Average of ^{226}Ra at 186 keV and 6 further gammas in decay series
4. Average of ^{228}Ra and 5 further gammas in decay series
5. Uncertainty 10%

Optically Stimulated Luminescence Dating of sample OSL-PKV-2

Preparation and Instrumentation

Optically Stimulated Luminescence (OSL) dating was performed at the Kansas State University luminescence laboratories on fine-grained quartz (125-175 μm). Dating procedures were carried out under low-intensity red safe-lighting. About 5 cm of sediment was removed from each end of the sampling cylinder to exclude the possibility of analyzing sediment that had been exposed to daylight during sampling. Standard preparation steps (e.g. Spencer & Robinson, 2008) included dry sieving, 10% HCl and 30% H_2O_2 pre-treatments to remove carbonates and organic matter, respectively, separation of heavy minerals (<2.70 gcm^{-3}) with lithium metatungstate (LMT) heavy liquid, and treating with 48% HF for 40 min to dissolve feldspar minerals and etch the surface of quartz grains to minimise luminescence due to ionization from external alpha particles. Monolayers (~3 mm circles; ~240 grains) of quartz grains were dispensed onto ~10 mm diameter stainless steel discs using silicone oil and a spray template. OSL measurements were carried out using a Risø TL/OSL-DA-20 reader (Bøtter-Jensen et al., 2003), with optical stimulation of quartz provided by an array of blue light (470±30 nm) diodes, optical stimulation of feldspar with infrared (880Δ80 nm) diodes, a calibrated $^{90}Sr/^{90}Y$ beta source (~0.16 Gys^{-1}) to administer laboratory radiation doses, and a heating stage for thermal stabilization. All luminescence signals were detected in the ultraviolet (peak transmission ~340 nm) using 7.5 mm of Hoya U-340 filter with an EMI 9235QB photomultiplier tube.

Equivalent dose (D_e) measurement procedures

Determination of the equivalent dose (D_e) was carried out using a single-aliquot regenerative-dose (SAR) protocol (Murray & Wintle, 2000, 2003; Wintle & Murray, 2006). Continuous power or *continuous wave* OSL (CW-OSL) was conducted in all measurements. Similar to other recent studies, post-infrared optically stimulated luminescence (post-IR OSL) was used to measure the luminescence from the quartz grains (Lukas et al., 2007; Morrocco et al., 2007; Spencer & Robinson, 2008). This procedure removes charge sensitive to infrared stimulation, commonly associated with remnant feldspatic minerals, before measuring OSL from the quartz grains. The post-IR OSL measurement comprised 40 s infrared stimulated luminescence (IRSL) at ~117.9 $mWcm^{-2}$ (22 Vishay TSFF5200 IR led's at 90% power) at a sample temperature of 50°C, followed by 40 s OSL at ~38.7 $mWcm^{-2}$ (28 Nichia NSPB500S blue led's at 90% power) at a sample temperature of 125°C.

For all measurements the net OSL signal was defined as the initial 0.8 s integral with subtraction of the final 8 s integral. Test dose administered for sensitivity correction was ~31 Gy (equivalent to between ~12-185% of D_e). The D_e value was estimated by interpolation of the natural OSL with a saturating exponential curve fitted to regenerative OSL data (Fig. S1). Uncertainty in D_e was estimated by combining error from counting statistics for the natural OSL, curve fitting, and instrumental systematic uncertainty (Duller, 2007). Preheat plateaux (Wintle & Murray, 2006) and dose recovery (Murray & Wintle, 2003; Roberts et al., 1999; Wallinga et al., 2000) with preheat variation (Spencer & Robinson, 2008) tests were used to determine appropriate preheat and cutheat thermal treatments. Dose recovery and D_e results were only accepted if the following test thresholds were met: measured-to-given ratios and recycling ratios between 0.9-1.1; recuperation <5% of the natural level (Murray & Wintle, 2000, 2003). A hot bleach

measurement of 40 s OSL at 280°C was incorporated at the end of each SAR cycle (Murray & Wintle, 2003).

The dose-distribution from replicated D_e measurements was assessed using a radial plot (Fig. S1) (Galbraith, 1990) and estimate of over-dispersion (σ_b; Galbraith et al., 2005), together with geomorphological and sedimentological details from the sampling site. On the basis of this assessment either the Minimum Age Model or Central Age Model (Galbraith et al., 1999) was chosen to calculate final D_e.

Assessment of dose-rate

Environmental dose-rate applied during age calculation was based on U, Th and K measurement using high-resolution gamma spectrometry. These data were converted to annual dose-rate using conversion factors from Adamiec & Aitken (1998). Calculated beta dose was corrected using attenuation factors for grain size and HF etching (e.g. Spencer & Owen, 2004). Attenuation of dose-rate via moisture conditions over the burial time of the samples was calculated by using present day field moisture content with a maximum absolute error of 5% to allow for past changes. The dose-rate from the ionizing cosmic ray component was calculated following Prescott & Hutton (1994).

Dating results and discussion

Initial OSL measurements generally indicated low specific luminescence sensitivity in natural signals and poor sensitivity to laboratory dose. Initial decay of natural luminescence signal varied in rapidity and, although linearly modulated OSL (LM-OSL) measurements were not

made, significant variation in the proportion of fast to medium and slow components in CW-OSL is evident from aliquot-to-aliquot. These observations are consistent with a proximal and geologically young source, and lack of recycling from earlier sedimentary deposits. To ensure adequate test dose signals for all aliquots measured, test dose used in SAR measurements of dose recovery and D_e was ~31 Gy. For a particular sequence of preheat and cutheat treatments dose recovery data were generally inconsistent from aliquot-to-aliquot. However, measured-to-given ratios were closest to unity for lower preheat treatments at 220°C or 240°C for 10 s, with best overall data with preheat at 220°C for 10 s and cutheat at 160°C. This combination of heat treatments was used to generate D_e data. The D_e distribution obtained from 32 aliquots shows a large spread with over-dispersion of ~61% (Fig. S1). The sample was collected from a silt lens in an arid alluvial fan; an asymmetric distribution is not unexpected given the debris flow depositional mechanism. Partial bleaching is a reasonable explanation for the asymmetry shown in Figure S1 and the Minimum Age Model was used to calculate the weighted mean D_e. Measured data, calculated dose-rate and OSL age are shown in Table S1. The OSL age quoted is in ka before AD 2011. For direct comparison with radiocarbon ages in ka BP, OSL ages should be adjusted to AD 1950 by subtracting 0.061 ka.

Acknowledgements

Art Lucas, Lucas-Newman Science & Technologies, is thanked for high-resolution gamma spectrometry measurements. Matt Rankin and Jennifer Boswell, both K-State, are thanked for assistance with OSL sample preparation and Sébastien Huot, UQAM Montreal, for use of his Minimum Age Model spreadsheet.

References

Adamiec, G., & Aitken, M. (1998). Dose-rate conversion factors: update. Ancient TL 16, 37-50.

Bøtter-Jensen, L., Andersen, C. E., Duller, G. A. T., & Murray, A. S. (2003). Developments in radiation, stimulation and observation facilities in luminescence measurements. Radiation Measurements 37, 535-541.

Duller, G. A. T. (2007). Assessing the error on equivalent dose estimates derived from single aliquot regenerative dose measurements. Ancient TL 25, 15-24.

Galbraith, R. F. (1990). The radial plot: Graphical assessment of spread in ages. Nuclear Tracks and Radiation Measurements 17 (3), 197-206.

Galbraith, R. F., Roberts, R. G., Laslett, G. M., Yoshida, H., & Olley, J. M. (1999). Optical dating of single and multiple grains of quartz from Jinmium rock shelter, northern Australia: part I, experimental design and statistical models. Archaeometry 41(2), 339-364.

Galbraith, R. F., Roberts, R. G., & Yoshida, H. (2005). Error variation in OSL palaeodose estimates from single aliquots of quartz: a factorial experiment. Radiation Measurements 39, 289-307.

Lukas, S., Spencer, J. Q. G., Robinson, R. A. J., & Benn, D. I. (2007). Problems associated with luminescence dating of Late Quaternary glacial sediments in the NW Scottish Highlands. Quaternary Geochronology 2, 243-248.

Morrocco, S. M., Ballantyne, C. K., Spencer, J. Q. G., & Robinson, R. A. J. (2007). Age and significance of aeolian sediment reworking on high plateaux in the Scottish Highlands. The Holocene 17, 349-360.

Murray, A. S., & Wintle, A. G. (2000). Luminescence dating of quartz using an improved single-aliquot regenerative-dose protocol. Radiation Measurements 32, 57-73.

Murray, A. S., & Wintle, A. G. (2003). The single-aliquot regenerative-dose protocol: potential for improvements in reliability. Radiation Measurements 37, 377-381.

Prescott, J. R., & Hutton, J. T. (1994). Cosmic ray contributions to dose rates for luminescence and ESR dating: large depths and long-term time variations. Radiation Measurements 23, 497-500.

Roberts, R. G., Galbraith, R. F., Olley, J. M., Yoshida, H., & Laslett, G. M. (1999). Optical dating of single and multiple grains of quartz from Jinmium rock shelter, northern Australia: Part II, Results and implications. Archaeometry 41, 365-395.

Spencer, J. Q. G., & Robinson, R. A. J. (2008). Dating intramontane alluvial deposits from NW Argentina using luminescence techniques: problems and potential. Geomorphology 93, 144-156.

Wallinga, J., Murray, A. S., & Duller, G. A. T. (2000). Underestimation of equivalent dose in single-aliquot optical dating of feldspars caused by preheating. Radiation Measurements 32, 691–695.

Wintle, A. G., & Murray, A. S. (2006). A review of quartz optically stimulated luminescence characteristics and their relevance in single-aliquot regeneration dating protocols. Radiation Measurements 41, 369-391.

Appendix D

E-mail from Elmira Wan to Willy Rittase

HI Willy,

Finally! Here is the USGS Tephrochronology Project Laboratory report on T-PKV-WMR-A through E, and T-SWSV-WMR-F, your six volcanic ash samples from along the Garlock Fault in San Bernardino County, southern California.

Using EMA, we probed for nine major and minor oxides (SiO2 Al2O3, FeO, MgO, MnO, CaO, TiO2, Na2O, K2O). The raw data were then recalculated to a 100% fluid-free basis. Next, similarity coefficient analyses were performed on the chemical data, and the normalized values compared to geochemical "fingerprints" (currently ~5,900) in our geochemical reference database. The raw and normalized chemical data, comparative chemical data, and lists of chemical correlatives are in the attached MS-Excel and Word files. In the Word recomputed data file, the closest matches have been highlighted and annotated. For a complete tephrochronologic interpretation, independent age control, stratigraphic positions, field and petrographic characteristics, and mineralogy were also considered. Holly Olson did the sample processing and lab descriptions, Dave Wahl performed the microprobe and computer analyses, and I evaluated and interpreted all of our data.

T-PKV-WMR-A: correlates well (≥ 0.95 SC, with and w/o alkalis) with multiple Lava Creek B (0.639 ± 0.002 Ma, Ar/Ar, sanidine) samples collected from the northernmost California to the north-central Gulf of Mexico. The best match (~0.95-0.973, SC) is to HL-NH06-T4 a sample from the Noble Hills area of Death Valley (collector: Heather Lackey, SFSU). Other relevant correlations are to distal Lava Creek ash deposits in Inyo County, the Lake Tecopa section in Death Valley, Balcom Canyon, Ventura Basin, and Manix Basin in southern California, among other sites. (See MS-Word file: rec T-PKV-WMR-A T582-1.doc; yellow highlighted samples) The eruptive source area for the Lava Creek ash is in the Yellowstone National Park area of Wyoming.

Equally good correlations (0.96 SC, w/o alkalis, gray highlighted samples) are to Huckleberry Ridge ash bed (2.063±0.007 Ma) deposits in southern California (TECO-30G, TECO-12B1, MANIX-6, collector: Andrei Sarna-Wojcicki, USGS, Emeritus) to northern California (SM-ASH-36, coll.: S. Morrison; FALOR-2, Coll. G. Carver, Humboldt State U.), and DSDP-36-4-6, a Deep Sea Drilling Project Site 36, located offshore of approximately the California and Oregon border in an abyssal plain between Gorda Ridge and the Mendocino Fracture Zone.

The raw microprobe data (Excel file) show that the analyzed glass shards in T-PKV-WMR-A are moderately to well-hydrated (93.8 % total wt.). This degree of hydration is typical for older volcanic glass samples. In addition, the Ca *vs*. Fe scatter plot shows a chemical fingerprint which displays a trending upwards patterns that is also typical of older and depleted tephra.

T-PKV-WMR-B: Is highly similar to the Upper tuffs of Glass Mountain (~1.13 to ~0.87 Ma) and Bishop tuff (~0.76 Ma). The eruptive source for both of these ash beds is Long Valley Caldera, California. With, and without alkalis, the closest chemical correlations are to CP-WHD-1, a sample from the White Hills of the Coso Range (coll.: C. Pluhar, UCSC), and WMFZ-05-09-JL, -08-JL, and -06A-JL from the White Mountain Fault Zone (WMFZ; coll.: Jeffrey Lee, Central Washington Univ.) The calcium concentrations are generally lower in the WMFZ tephra though. Other distal correlatives are JB-WAD-3, from Gardella Canyon, Wadsworth, NV (coll.: J. Bell, UNR), and JG-CH-T124a and JG-CH-T124-b from the Confidence Hills area of Death Valley, CA (submitted by J. Caskey, SFSU).

In your last e-mail you said you were more comfortable with the older age call for T-PKV-WMR-B (and T-

PKV-WMR-A). I suggest that to better constrain the age of these samples, other stratigraphic constraints and/or the paleomagnetostratigraphy should be re-examined. Note:

1) The Bishop ash is the largest eruption from the Glass Mountain (GM) – Long Valley caldera source, so not only is this ash bed the stratigraphically highest of this chemical type, it is usually the thickest and coarsest, compared to underlying Glass Mountain tephra layers. Your description of this sample as fine-grained suggests that it may be derived from GM ash beds. The moderate to high degree of hydration (94.1%, total wt.) also suggests this may be an older tephra. Lastly, if this sample is contained within a single sedimentary package of thin layers, then it is probably the Glass Mountain ash, unless unconformities are present.

2) The presence of the Huckleberry Ridge ash bed, a short stratigraphic distance below T-PKV-WMR-B would argue for it being derived from the Glass Mountain tephra set. The lower Glass Mountain ash beds do not get older than ~1.96 Ma.

3) Check p-mag data to locate the Bruhnes Matuyama boundary. The Bishop ash is normally magnetized and lies near the base of the Brunhes, a short stratigraphic distance above the Matuyama/Brunhes transition. Glass Mountain tephra layers, close below the Bishop, are mostly reversed. Some were probably erupted during the Jaramillo subchron, but we've never been able to document that. The older Glass Mountain tephra layers are reversed down to the Olduvai subchron, and a few have been identified below the Olduvai.

T-PKV-WMR-C: = Tuff of Mesquite Springs (3.28 Ma) or the Tuff of Zabriskie Wash (3.35 Ma) The chemistry of the Mesquite Springs tephra is very similar to that of the upper Glass Mountain tephra layers. However, the manganese oxide concentration is much higher compared to Glass Mountain tephra. With, and without alkalis, there are multiple correlations to Mesquite Springs and Zabriskie Wash tephra localities in Death Valley (JRK-DV-XX samples, Collected by Jeff Knott, CSUF, and JT-NOVA-1 , J. Tinsley, USGS, Menlo Park), Fish Lake Valley (M. Reheis, USGS, Denver), Afton subbasin, Mojave area (D. Miller, USGS), etc.

T-PKV-WMR-D: chemically correlates to the tuff of Artists Drive (>3.58 Ma, *aka* lower Nomlaki group, yellow highlighted samples) and the Nomlaki Tuff (3.27 Ma) gray-highlighted samples (see Excel file; rec T-PKV-WMR-D T582-4.xls). Best correlation (~0.91 - 0.976 SC, w/& w/o alkalis) is to JRK-DV-104, Jeff Knott's (CSUF) tuff of Artists Drive sample from Artist's Drive, Death Valley, CA. Without alkalis, JT-BPT-1 is the best Nomlaki tuff match. JT-BPT-1 is from Black Tail Point, Death Valley, CA. John Tinsley (USGS) was the investigator. Note that the calcium values are slightly higher for the Nomlaki samples vs. T-PKV-WMR-D.

T-PKV-WMR-E: (3.14 ±0.15 Ma – >2.58 Ma). With and without alkalis, T-PKV-WMR-E is most similar to MNM-DV-10-FC, MNM-DV-6-FC, MNM-DV-9-FC, which are tephra from Furnace Creek, Death Valley, CA. Mike Machette (USGS, retired) was the investigator and collector. MNM-DV-10, -9, and -6 form a set that could be the same bed or a part of the same eruptive sequence. In turn, T-PKV-WMR-E and the MNM-DV- set of samples are generically similar to 9-85-2A (~0.94 – 0.97 SC), a K-Ar dated, Coso eruptive center tephra (3.14 ±0.15 Ma, K-Ar, weighted avg.). Note that 9-85-2A contains a slightly higher calcium level relative to T-PKV-WMR-E.

The Coso volcanic field produced silicic fall- and flow- units (Bacon and others, 1981, 1982), but these were not of very great volume and areal extent. However, the east side of Death Valley is only ~100-120 km due east of this field, so there is a good possibility that the MNM-DV layers and your sample were derived from the Coso field.

In addition to the above correlations, T-PKV-WMR-E without alkalis is also generically similar to 1) EL-4-F, which correlates to 2.9 Ma tuffs on Mt. Jackson (Nevada), and underlies distal equivalents to the Tuff of Blind Springs (2.22-2.13 Ma) in Death Valley. Marith Reheis (USGS, Denver) collaborated with us on

EL-4-FL, and the late Pliocene tuff of Mt Jackson sample; and 2) JRK-DV-217, which is the lower tuffs of the Badlands (<2.89->2.58 Ma, p-mag, correl). Jeff Knott (CSUF) collected this tephra from the Willow Wash section south of Fish Lake Valley, in east-central CA.

Note that the calcium oxide concentrations in the above two correlatives are somewhat lower than that of T-PKV-WMR-E. Titanium oxide in particular, is much higher in the lower Badlands tuff sample. Conversely, the calcium concentrations for the Coso tephra matches are closer. This further supports the premise that the age of T-PKV-WMR-E is closer to 3.14 Ma.

T-SWSV-WMR-F: Discontinued – sample contains <1% devitrified shards. Per your request, this sample will be returned to you for storage at the University of Kansas.

I hope that the tephrochronologic results provide a good framework for your investigation. If you have any questions about the data, identifications, or age calls, please don't hesitate to contact me. Again, my contact info follows below.

Cheers,

Elmira

Elmira Wan
Tephrochronology Project
U.S. Geological Survey
345 Middlefield Road, MS 975
Menlo Park, CA 94025
Direct: 1(650) 329-4964
Tephra Lab: 1(650) 329-4939
Fax: 1(650) 329-4936
Email: ewan@usgs.gov

APPENDIX D - TABLE A. TEPHROCHRONOLOGIC CORRELATIONS FOR SAMPLE T-PKV-WMR-A

Listing of 37 closest matches for COMP. NO. 5879 for elements: **Na, Al, Si, K , Ca, Ti, Fe**

	C.No	Sample Number	An. Date	SiO2	Al2O3	Fe2O3	MgO	MnO	CaO	TiO2	Na2O	K2O	Total,R	Sim. Co	Sample Location
1	5879	T-PKV-WMR-A T582-1	2/16/11	77.95	12.79	1.65	0.03	0.05	0.57	0.14	2.72	4.10	100.00	1.0000	
2	5636	HL-NH-T10 T563-1	9/25/08	77.74	12.55	1.74	0.03	0.03	0.56	0.12	2.70	4.53	100.00	0.9520	Noble Hills, Death Valley
3	5458	HL-NH06-T4 T538-9	4/13/06	77.33	12.48	1.63	0.03	0.04	0.56	0.13	2.93	4.87	100.00	0.9481	Noble Hills, Death Valley
4	2437	DPB-6 T210-3	8/13/90	77.49	12.85	1.60	0.11	0.03	0.66	0.15	3.09	4.02	100.00	0.9453	
5	5637	HL-983-SDV108 T563-2	9/25/08	77.86	12.58	1.65	0.03	0.04	0.54	0.11	2.66	4.54	100.01	0.9424	Southern Death Valley, CA
6	5639	JC-108-LT30 T563-4	9/25/08	77.53	12.55	1.75	0.03	0.04	0.56	0.12	2.65	4.78	100.01	0.9415	Shoshone, and Tecopa Basin
7	392	TECO-30G, T17-14		76.75	12.66	1.72	0.03	0.03	0.55	0.13	2.78	5.36	100.01	0.9387	Lake Tecopa
8	5068	DPB-6_(2) T210-3	4/23/03	77.21	13.30	1.60	0.11	0.02	0.69	0.16	2.87	4.04	100.00	0.9366	
9	5824	JEO 5/11/06-1(1) T577-1 (pop1)	10/7/09	77.24	12.92	1.78	0.07	0.06	0.60	0.18	2.79	4.36	100.00	0.9358	
10	4660	MRM00-22 T444-6	11/3/00	77.10	13.14	1.77	0.08	0.02	0.62	0.17	2.93	4.17	100.00	0.9356	
11	5640	JC-108-LT37 T563-5	9/25/08	77.71	12.58	1.63	0.03	0.03	0.54	0.11	2.66	4.72	100.01	0.9354	Tecopa Basin
12	5638	JC-108-LT10 T563-3	9/25/08	77.74	12.57	1.62	0.03	0.04	0.54	0.11	2.66	4.69	100.00	0.9353	Shoshone, and Tecopa Basin
13	5645	JC-LT4-T1 T563-10	9/25/08	77.54	12.57	1.64	0.02	0.03	0.54	0.11	2.79	4.76	100.00	0.9344	Shoshone, CA
14	5735	JS-5-3-08-5 T572-5	6/4/09	77.00	13.04	1.48	0.07	0.04	0.53	0.13	2.93	4.78	100.00	0.9300	
15	5155	DPB-16 T211-7(2)	9/2/03	77.54	12.34	1.75	0.05	0.03	0.56	0.18	2.83	4.72	100.00	0.9275	
16	2447	DPB-16 T211-7	8/14/90	77.59	12.52	1.70	0.07	0.03	0.58	0.20	2.95	4.36	100.00	0.9271	
17	1445	126-2040 T116-1	1/27/85	77.08	12.30	1.75	0.02	0.05	0.56	0.13	3.33	4.77	99.99	0.9258	
18	5740	M08-164 T572-10(pop1)	6/4/09	77.34	12.83	1.74	0.02	0.05	0.58	0.10	3.10	4.24	100.00	0.9255	
19	5436	MRM 16-05Bpop2 T533-1	12/19/05	75.62	13.47	1.65	0.06	0.03	0.55	0.14	3.94	4.54	100.00	0.9254	
20	1456	126-2040 (AVG 3) T116-1	1/28/85	76.96	12.28	1.80	0.02	0.05	0.57	0.13	3.33	4.85	99.99	0.9221	
21	2073	CDH-D87-O T172-4	9/28/88	76.78	12.37	1.58	0.01	0.03	0.54	0.14	3.60	4.96	100.01	0.9199	
22	2221	FPUP-1 T184-4	2/28/89	76.57	12.72	1.65	0.02	0.05	0.47	0.14	3.36	5.01	99.99	0.9185	
23	2465	T89-5/6/9 #1 T215-7	9/25/90	76.88	12.16	1.67	0.03	0.04	0.56	0.13	3.49	5.05	100.01	0.9182	
24	5490	SL-MM06-91 T542-6 (pop2)	9/19/06	76.96	12.29	1.73	0.02	0.04	0.54	0.13	3.29	5.00	100.00	0.9178	
25	212	MANIX-6, T7-10		76.15	12.98	1.63	0.03	0.03	0.61	0.13	4.07	4.37	100.00	0.9171	
26	2222	FBP2-1 T184-5	2/28/89	76.64	12.65	1.66	0.03	0.05	0.47	0.14	3.35	5.02	100.01	0.9171	
27	3846	758-207C T355-8	1/97	75.76	13.12	1.61	0.07	0.02	0.54	0.14	3.68	5.07	100.01	0.9168	
28	253	P5-23, T23-1		76.69	12.27	1.71	0.02	0.04	0.57	0.13	3.72	4.84	99.99	0.9164	
29	857	LM-13		76.61	12.72	1.62	0.03	0.03	0.55	0.12	3.41	4.91	100.00	0.9163	
30	3485	MANIX-2B T318-4 (redo)	5/6/95	76.45	12.68	1.76	0.02	0.04	0.61	0.13	4.23	4.09	100.01	0.9162	
31	3837	HW692-12 T354-9	1/97	76.37	13.11	1.76	0.09	0.03	0.58	0.16	3.92	3.97	99.99	0.9161	
32	746	HC-8		76.97	12.33	1.64	0.02	0.03	0.58	0.12	3.51	4.81	100.01	0.9161	
33	5609	JRK-DV-237 T558-8	2/29/08	75.74	13.07	1.67	0.09	0.02	0.60	0.15	3.30	5.37	100.01	0.9156	
34	863	LM-20		76.42	12.54	1.70	0.03	0.03	0.51	0.14	3.41	5.22	100.00	0.9156	
35	4339	EL-92-LT T397-1	10/21/98	76.89	12.31	1.66	0.02	0.03	0.56	0.12	3.30	5.12	100.01	0.9154	
36	5276	MRM01-04A T515-6	8/24/04	75.80	13.13	1.73	0.08	0.03	0.62	0.16	2.74	5.71	100.00	0.9151	
37	747	HC-8		76.87	12.33	1.64	0.02	0.03	0.58	0.12	3.41	5.01	100.01	0.9143	

Listing of 37 closest matches for COMP. NO. 5879 for elements: **Al, Si, Ca, Ti, Fe**

	C.No	Sample Number	An. Date	SiO2	Al2O3	Fe2O3	MgO	MnO	CaO	TiO2	Na2O	K2O	Total,R	Sim. Co	Sample Location
1	5879	T-PKV-WMR-A T582-1	2/16/11	77.95	12.79	1.65	0.03	0.05	0.57	0.14	2.72	4.10	100.00	1.0000	
2	5436	MRM 16-05Bpop2 T533-1	12/19/05	75.62	13.47	1.65	0.06	0.03	0.55	0.14	3.94	4.54	100.00	0.9769	
3	3846	758-207C T355-8	1/97	75.76	13.12	1.61	0.07	0.02	0.54	0.14	3.68	5.07	100.01	0.9740	
4	5458	HL-NH06-T4 T538-9	4/13/06	77.33	12.48	1.63	0.03	0.04	0.56	0.13	2.93	4.87	100.00	0.9733	Noble Hills, Death Valley
5	2073	CDH-D87-O T172-4	9/28/88	76.78	12.37	1.58	0.01	0.03	0.54	0.14	3.60	4.96	100.01	0.9714	Espanola Basin NM
6	253	P5-23, T23-1		76.69	12.27	1.71	0.02	0.04	0.57	0.13	3.72	4.84	99.99	0.9673	
7	2465	T89-5/6/9 #1 T215-7	9/25/90	76.88	12.16	1.67	0.03	0.04	0.56	0.13	3.49	5.05	100.01	0.9672	Inyo County, CA
8	392	TECO-30G, T17-14		76.75	12.66	1.72	0.03	0.03	0.55	0.13	2.78	5.36	100.01	0.9654	Lake Tecopa, Death Valley, CA
9	863	LM-20		76.42	12.54	1.70	0.03	0.03	0.51	0.14	3.41	5.22	100.00	0.9652	
10	378	TECO-12B1, T47-6		76.30	12.36	1.75	0.03	0.05	0.61	0.14	3.46	5.29	99.99	0.9645	Lake Tecopa, CA
11	5609	JRK-DV-237 T558-8	2/29/08	75.74	13.07	1.67	0.09	0.02	0.60	0.15	3.30	5.37	100.01	0.9643	
12	212	MANIX-6, T7-10		76.15	12.98	1.63	0.03	0.03	0.61	0.13	4.07	4.37	100.00	0.9626	Manix Basin, CA
13	4816	AFPL2_(44.4'-44.9') T471-2	10/18/01	76.45	12.39	1.60	0.03	0.03	0.55	0.13	3.28	5.54	100.00	0.9625	
14	5503	K06CO-3 T543-2	12/4/06	76.52	12.38	1.68	0.03	0.04	0.54	0.13	3.60	5.06	99.98	0.9615	Kelso Gulch to Gunnison R, CO
15	5558	D1764		76.45	12.39	1.68	0.12	0.04	0.54	0.13	3.48	5.18	100.01	0.9615	
16	1541	CHV-5 T124-14	5/5/86	78.49	12.45	1.65	0.03	0.02	0.56	0.12	3.96	2.73	100.01	0.9612	northern Gulf of Mexico
17	390	TECO-30E, T17-12		76.14	12.58	1.60	0.02	0.04	0.54	0.13	3.51	5.44	100.00	0.9612	Lake Tecopa, CA
18	1445	126-2040 T116-1	1/27/85	77.08	12.30	1.75	0.02	0.05	0.56	0.13	3.33	4.77	99.99	0.9609	
19	93	DSDP-36-4-6, T47-3		76.33	12.46	1.73	0.03	0.06	0.59	0.13	3.61	5.05	99.99	0.9604	DSDP Site 36, Core 4-6, CA
20	2221	FPUP-1 T184-4	2/28/89	76.57	12.72	1.65	0.02	0.05	0.47	0.14	3.36	5.01	99.99	0.9603	
21	599	SM-ASH-36, T56-9	07/01/83	76.39	12.59	1.61	0.02	0.03	0.57	0.12	3.67	5.00	100.00	0.9595	Carlotta Fm, Humboldt, CA
22	102	FALOR-2, T41-7		76.24	12.53	1.72	0.02	0.04	0.60	0.13	3.66	5.06	100.00	0.9591	Falor Fm, Humboldt CA
23	4044	96TT131 T371-3	10/97	76.26	12.10	1.79	0.03	0.03	0.54	0.14	2.33	6.76	99.98	0.9587	McDermott Caldera? NV
24	1456	126-2040 (AVG 3) T116-1	1/28/85	76.96	12.28	1.80	0.02	0.05	0.57	0.13	3.33	4.85	99.99	0.9585	
25	2222	FBP2-1 T184-5	2/28/89	76.64	12.65	1.66	0.03	0.05	0.47	0.14	3.35	5.02	100.01	0.9582	
26	3483	MANIX-3A T318-5 (redo)	4/11/95	76.19	12.73	1.73	0.02	0.04	0.61	0.13	3.93	4.63	100.01	0.9579	Manix Basin, Mojave, CA
27	296	PICO-157(1), T47-7		76.61	12.25	1.73	0.03	0.04	0.59	0.13	3.72	4.89	99.99	0.9578	Pico Fm., Ventura Basin, CA
28	1932	DW-SPB-R-1 T163-2	5/14/88	75.17	13.56	1.51	0.07	0.03	0.59	0.14	4.17	4.76	100.00	0.9578	
29	389	TECO-30D, T17-11		75.95	12.76	1.64	0.02	0.03	0.55	0.12	3.44	5.49	100.00	0.9576	Lake Tecopa, Death Valley, CA
30	746	HC-8		76.97	12.33	1.64	0.02	0.03	0.58	0.12	3.51	4.81	100.01	0.9571	Pershing Cty NV
31	747	HC-8		76.87	12.33	1.64	0.02	0.03	0.58	0.12	3.41	5.01	100.01	0.9568	Pershing Cty NV
32	4339	EL-92-LT T397-1	10/21/98	76.89	12.31	1.66	0.02	0.03	0.56	0.12	3.30	5.12	100.01	0.9565	Lone Tree
33	857	LM-13		76.61	12.72	1.62	0.03	0.03	0.55	0.12	3.41	4.91	100.00	0.9562	Pershing Cty, NV
34	5295	MRM 16-04 T520-3	12/21/04	76.61	13.59	1.53	0.07	0.03	0.53	0.14	2.23	5.28	100.01	0.9562	
35	2542	PU-14 T225-1	4/22/19	75.80	12.88	1.67	0.09	0.02	0.60	0.16	3.89	4.88	99.99	0.9557	
36	5490	SL-MM06-91 T542-6 (pop2)	9/19/06	76.96	12.29	1.73	0.02	0.04	0.54	0.13	3.29	5.00	100.00	0.9556	San Luis, CO
37	5274	CDH-D56-11B T515-4	8/24/04	76.63	12.43	1.65	0.03	0.04	0.55	0.12	3.58	4.97	100.00	0.9554	Espanola Basin, NM

Yellow highlighted samples correlate to Lava Creek B (0.639 ± 0.002 Ma)
Gray highlighted samples correlate to Huckleberry Ridge ash bed (2.063 ± 0.007 Ma)

APPENDIX D - TABLE B. TEPHROCHRONOLOGIC CORRELATIONS FOR SAMPLE T-PKV-WMR-B

Listing of 37 closest matches for COMP. NO. 5880 for elements: **Na, Al, Si, K , Ca, Ti, Fe**

	C.No	Sample Number	An. Date	SiO2	Al2O3	Fe2O3	MgO	MnO	CaO	TiO2	Na2O	K2O	Total,R	Sim. Co	Sample Location
1	5880	T-PKV-WMR-B T582-2	2/16/11	77.97	13.24	0.71	0.05	0.05	0.55	0.06	2.71	4.66	100.00	1.0000	
2	5363	CP-WHD-1 T526-2	05/31/20	77.81	12.89	0.68	0.04	0.05	0.54	0.06	2.95	4.97	99.99	0.9668	White Hills, Cosos Range, CA
3	5394	WMFZ05-09-JL T529-8	8/9/05	78.17	12.94	0.72	0.04	0.06	0.56	0.06	3.08	4.37	100.00	0.9658	White Mtn Fault Zone, CA
4	5456	HL-NH06-T2 T538-7	4/13/06	77.92	13.09	0.73	0.04	0.09	0.48	0.06	3.01	4.58	100.00	0.9595	
5	5393	WMFZ05-08-JL T529-7	8/9/05	78.40	12.74	0.73	0.03	0.04	0.44	0.06	2.73	4.84	100.01	0.9550	White Mtn Fault Zone, CA
6	5005	JB-WAD-3 T493-8	3/17/02	77.32	12.95	0.70	0.04	0.06	0.54	0.06	3.40	4.92	99.99	0.9545	Gardella Cyn, Wadsworth, NV
7	5580	M07-101a T548-1	5/29/07	78.23	13.42	0.75	0.04	0.08	0.46	0.06	2.76	4.18	99.98	0.9493	
8	5831	JG-CH-T124b T578-3	2/10/01	77.11	12.96	0.71	0.03	0.04	0.54	0.06	3.59	4.97	100.01	0.9489	Death Valley, Confidence Hills
9	5392	WMFZ05-06A-JL T529-6	8/9/05	78.08	12.85	0.72	0.03	0.07	0.44	0.06	3.15	4.61	100.01	0.9435	White Mtn Fault Zone, CA
10	5644	JC-CH-T1 T563-9	9/25/08	78.15	12.92	0.82	0.04	0.04	0.43	0.06	2.80	4.73	99.99	0.9392	
11	5157	MOD-9 T30-5(2)	9/2/03	78.31	12.82	0.67	0.03	0.06	0.48	0.07	2.90	4.66	100.00	0.9389	
12	3740	FLV-SP-8B T347-2	11/96	76.94	13.23	0.72	0.04	0.09	0.48	0.06	3.75	4.69	100.00	0.9373	
13	3742	FLV-SP-8C MINOR T347-3	11/96	76.89	13.12	0.73	0.04	0.08	0.49	0.06	3.16	5.45	100.02	0.9362	
14	4646	JRK-DV-207 T442-9	8/3/00	77.13	13.08	0.76	0.04	0.08	0.48	0.06	3.03	5.34	100.00	0.9359	
15	5642	JC-108-CH104 T563-7	9/25/08	78.43	12.92	0.76	0.05	0.04	0.45	0.07	2.74	4.55	100.01	0.9350	
16	5701	EW043008-B T568-10	1/8/09	77.25	13.04	0.70	0.03	0.06	0.47	0.06	3.72	4.67	100.00	0.9346	
17	381	TECO-26, T18-11		77.61	12.73	0.72	0.03	0.03	0.48	0.06	3.70	4.63	99.99	0.9345	
18	5830	JG-CH-T124a T578-2	2/10/201	77.13	12.92	0.67	0.04	0.06	0.52	0.06	3.72	4.88	100.00	0.9339	Death Valley, Confidence Hills
19	3526	TPSS-346 T326-4	7/6/95	77.02	13.05	0.65	0.03	0.06	0.58	0.06	3.49	5.05	99.99	0.9338	
20	5147	DPB-11 T211-2(2)	9/2/03	78.03	12.89	0.66	0.09	0.06	0.54	0.08	2.99	4.64	99.98	0.9338	
21	2659	LOVW-14 T238-7	10/16/91	77.05	12.68	0.81	0.05	0.06	0.58	0.06	2.75	5.98	100.02	0.9336	
22	5285	BTD-DV-01 T519-9	8/24/04	77.15	12.92	0.71	0.04	0.08	0.47	0.06	3.22	5.35	100.00	0.9332	
23	3194	Y72-11-1P (1150-1160)majT302	3/25/94	77.20	12.81	0.74	0.04	0.05	0.58	0.06	3.60	5.11	100.19	0.9329	
24	103	FRIANT-1, T18-5		77.54	12.73	0.73	0.03	0.03	0.48	0.06	3.56	4.83	99.99	0.9325	
25	3212	FRIANT 11A T302-14	3/25/94	77.03	12.85	0.74	0.03	0.02	0.52	0.06	3.88	4.87	100.00	0.9312	
26	1930	SC-45B T163-5	5/14/88	77.23	12.81	0.73	0.05	0.08	0.49	0.06	3.56	4.98	99.99	0.9312	
27	104	FRIANT-2, T18-6		77.53	12.86	0.68	0.03	0.03	0.47	0.06	3.40	4.94	100.00	0.9312	
28	3100	DLS-413L T284-3	11/4/93	77.06	12.95	0.72	0.04	0.08	0.47	0.06	3.15	5.48	100.01	0.9311	
29	2417	PR-137 T199-3	5/24/90	77.16	12.39	0.85	0.04	0.06	0.55	0.06	2.72	6.17	100.00	0.9303	
30	265	PICO-5(2), T20-5		77.24	12.73	0.71	0.03	0.03	0.49	0.06	3.56	5.15	100.00	0.9299	
31	5765	MRR-BSL86-91cmT575-8(pop2)	8/4/09	78.18	13.21	0.77	0.02	0.05	0.53	0.07	3.06	4.11	100.00	0.9294	
32	2516	FLV-161-CS T221-6	3/8/91	77.48	12.80	0.71	0.03	0.06	0.45	0.06	3.45	4.96	100.00	0.9291	
33	4219	RKDVW-5-Tt T387-9	5/29/98	77.30	12.73	0.72	0.04	0.09	0.48	0.06	3.73	4.84	99.99	0.9287	
34	5833	JG-CH-T127a T578-5	2/10/201	77.41	12.84	0.71	0.03	0.07	0.45	0.06	3.60	4.82	99.99	0.9286	
35	4650	JRK-DV-203_POP1 T443-3	9/25/00	77.33	12.90	0.73	0.04	0.04	0.46	0.06	3.41	5.02	99.99	0.9283	
36	5564	M07-101b T548-2	5/29/07	78.35	13.47	0.74	0.04	0.08	0.46	0.07	2.73	4.07	100.01	0.9282	
37	1842	FLV-19-WW T146-7	8/25/87	77.31	13.24	0.72	0.04	0.08	0.48	0.06	3.76	4.31	100.00	0.9280	

Listing of 37 closest matches for COMP. NO. 5880 for elements: **Al, Si, Ca, Ti, Fe**

	C.No	Sample Number	An. Date	SiO2	Al2O3	Fe2O3	MgO	MnO	CaO	TiO2	Na2O	K2O	Total,R	Sim. Co	Sample Location
1	5880	T-PKV-WMR-B T582-2	2/16/11	77.97	13.24	0.71	0.05	0.05	0.55	0.06	2.71	4.66	100.00	1.0000	
2	5831	JG-CH-T124b T578-3	2/10/201	77.11	12.96	0.71	0.03	0.04	0.54	0.06	3.59	4.97	100.01	0.9899	Death Valley, Confidence Hills
3	5394	WMFZ05-09-JL T529-8	8/9/05	78.17	12.94	0.72	0.04	0.06	0.56	0.06	3.08	4.37	100.00	0.9886	White Mtn Fault Zone
4	5005	JB-WAD-3 T493-8	3-17-02	77.32	12.95	0.70	0.04	0.06	0.54	0.06	3.40	4.92	99.99	0.9875	Gardella Cyn, Wadsworth, NV
5	5363	CP-WHD-1 T526-2	05/31/20	77.81	12.89	0.68	0.04	0.05	0.54	0.06	2.95	4.97	99.99	0.9822	White Hills, Coso Range
6	3194	Y72-11-1P(1150-1160)majT302	3/25/94	77.20	12.81	0.74	0.04	0.05	0.58	0.06	3.60	5.11	100.19	0.9731	
7	3212	FRIANT 11A T302-14	3/25/94	77.03	12.85	0.74	0.03	0.02	0.52	0.06	3.88	4.87	100.00	0.9727	Bishop ash
8	5830	JG-CH-T124a T578-2	2/10/201	77.13	12.92	0.67	0.04	0.06	0.52	0.06	3.72	4.88	100.00	0.9708	Death Valley, Confidence Hills
9	1842	FLV-19-WW T146-7	8/25/87	77.31	13.24	0.72	0.04	0.08	0.48	0.06	3.76	4.31	100.00	0.9701	
10	3740	FLV-SP-8B T347-2	11/96	76.94	13.23	0.72	0.04	0.09	0.48	0.06	3.75	4.69	100.00	0.9690	
11	265	PICO-5(2), T20-5		77.24	12.73	0.71	0.03	0.03	0.49	0.06	3.56	5.15	100.00	0.9686	
12	3742	FLV-SP-8C MINOR T347-3	11/96	76.89	13.12	0.73	0.04	0.08	0.49	0.06	3.16	5.45	100.02	0.9681	
13	3526	TPSS-346 T326-4	7/6/95	77.02	13.05	0.65	0.03	0.06	0.58	0.06	3.49	5.05	99.99	0.9674	
14	3209	FRIANT 2A T302-11	3/25/94	77.11	12.77	0.73	0.03	0.04	0.50	0.06	3.32	5.56	100.12	0.9670	
15	5456	HL-NH06-T2 T538-7	4/13/06	77.92	13.09	0.73	0.04	0.09	0.48	0.06	3.01	4.58	100.00	0.9667	
16	4218	RKSC-3-Tt T387-6	5-29-98	76.99	12.82	0.71	0.03	0.09	0.48	0.06	3.70	5.13	100.01	0.9657	
17	5459	JC-NH06-T1 T538-5	4/13/06	78.76	13.19	0.75	0.04	0.08	0.49	0.06	3.24	3.40	100.01	0.9648	
18	1930	SC-45B T163-5	5/14/88	77.23	12.81	0.73	0.05	0.08	0.49	0.06	3.56	4.98	99.99	0.9643	
19	5285	BTD-DV-01 T519-9	8/24/04	77.15	12.92	0.71	0.04	0.08	0.47	0.06	3.22	5.35	100.00	0.9640	
20	5701	EW043008-B T568-10	1/8/09	77.25	13.04	0.70	0.03	0.06	0.47	0.06	3.72	4.67	100.00	0.9632	
21	381	TECO-26, T18-11		77.61	12.73	0.72	0.03	0.03	0.48	0.06	3.70	4.63	99.99	0.9631	
22	4219	RKDVW-5-Tt T387-9	5-29-98	77.30	12.73	0.72	0.04	0.09	0.48	0.06	3.73	4.84	99.99	0.9623	
23	3280	PH-2 T307-8	8/1/94	75.86	13.77	0.72	0.03	0.09	0.49	0.06	4.25	4.71	99.98	0.9623	
24	4034	ORT-1 POP2 T369-10	9/97	77.30	12.91	0.72	0.01	0.04	0.47	0.06	3.91	4.58	100.00	0.9614	
25	3100	DLS-413L T284-3	11/4/93	77.06	12.95	0.72	0.04	0.08	0.47	0.06	3.15	5.48	100.01	0.9614	
26	3814	JRK-DV-SIX SP T352-5	12/96	76.99	12.83	0.74	0.04	0.07	0.49	0.06	3.28	5.50	100.00	0.9614	
27	3208	FRIANT 1A T302-10	3/25/94	76.96	12.81	0.74	0.03	0.02	0.49	0.06	3.34	5.54	99.99	0.9610	
28	1825	FLV-2-CS T145-5	8/24/87	77.61	12.81	0.72	0.05	0.09	0.47	0.06	3.73	4.47	100.01	0.9607	
29	103	FRIANT-1, T18-5		77.54	12.73	0.73	0.03	0.03	0.48	0.06	3.56	4.83	99.99	0.9603	
30	4968	SAM_5-012102 T490-1	10-26-02	77.66	13.13	0.77	0.04	0.09	0.49	0.06	3.82	3.95	100.01	0.9601	
31	2051	CAES#2 1683.5 T171-7	9/5/88	79.67	12.63	0.73	0.01	0.08	0.49	0.06	4.19	2.14	100.00	0.9592	
32	3627	EL-35A-MS T335-6	3/96	77.37	12.59	0.63	0.05	0.05	0.53	0.06	2.25	6.37	99.90	0.9588	
33	3516	JRK-DV-40 T325-6	7/6/95	77.07	13.19	0.76	0.04	0.09	0.48	0.06	4.54	3.77	100.00	0.9583	
34	239	OAK RUN-2, T27-6		76.04	14.25	0.64	0.13	0.09	0.54	0.06	4.43	3.82	100.00	0.9575	
35	3272	PH-1 T307-7	8/1/94	75.16	14.28	0.66	0.04	0.11	0.53	0.06	4.57	4.58	99.99	0.9569	
36	3519	JRK-DV-41 REV T325-7	7/6/95	77.21	13.23	0.77	0.04	0.07	0.48	0.06	4.58	3.56	100.00	0.9569	
37	4646	JRK-DV-207 T442-9	8-3-00	77.13	13.08	0.76	0.04	0.08	0.48	0.06	3.03	5.34	100.00	0.9568	

Yellow highlighted samples correlate to Tuffs of Glass Mountain, Long Valley Caldera, California (~1.13 - ~0.87 Ma)
Gray highlighted samples correlate to Bishop Ash, Long Valley Caldera, California (~0.76 Ma)

APPENDIX D - TABLE C. TEPHROCHRONOLOGIC CORRELATIONS FOR SAMPLE T-PKV-WMR-C

Listing of 37 closest matches for COMP. NO. 5881 for elements: **Na, Al, Si, K , Ca, Mn**

	C.No	Sample Number	An. Date	SiO2	Al2O3	Fe2O3	MgO	MnO	CaO	TiO2	Na2O	K2O	Total,R	Sim. Co	Sample Location
1	5881	T-PKV-WMR-C T582-3	2/16/11	78.56	13.43	0.73	0.05	0.08	0.48	0.07	2.02	4.59	100.01	1.0000	
2	5611	EB-ASH-WA2(3) T561-3	4/28/08	78.80	13.22	0.68	0.06	0.07	0.46	0.08	1.96	4.65	99.98	0.9620	
3	1880	FLV-38-WW T147-12	9/30/87	79.16	12.71	0.54	0.05	0.08	0.42	0.10	2.15	4.79	100.00	0.9519	
4	5610	EB-ASH-WA1 T561-2	4/28/08	78.34	13.48	0.77	0.06	0.06	0.50	0.10	2.06	4.63	100.00	0.9459	
5	5365	NA-51A T526-7	05/31/20	78.55	13.10	0.52	0.09	0.07	0.53	0.09	2.23	4.83	100.01	0.9354	
6	5580	M07-101a T548-1	5/29/07	78.23	13.42	0.75	0.04	0.08	0.46	0.06	2.76	4.18	99.98	0.9327	Mesquite Springs
7	5564	M07-101b T548-2	5/29/07	78.35	13.47	0.74	0.04	0.08	0.46	0.07	2.73	4.07	100.01	0.9299	Mesquite Springs
8	5366	NA-30C T526-8	05/31/20	78.46	13.08	0.54	0.09	0.07	0.55	0.09	2.18	4.93	99.99	0.9297	
9	5866	DM-M10NS-452 T581-5	9/17/10	77.61	13.44	0.79	0.05	0.07	0.47	0.10	2.52	4.95	100.00	0.9284	
10	5623	EB-ASF-BM T562-2	5/19/08	75.54	14.61	1.13	0.11	0.08	0.52	0.23	1.94	5.83	99.99	0.9253	
11	5867	DM-M10NS-886 T581-6	9/17/10	77.82	12.96	0.99	0.03	0.08	0.41	0.08	2.41	5.23	100.01	0.9209	
12	5456	HL-NH06-T2 T538-7	4/13/06	77.92	13.09	0.73	0.04	0.09	0.48	0.06	3.01	4.58	100.00	0.9207	
13	2752	BUR-523.3		78.26	12.57	0.79	0.03	0.08	0.42	0.05	2.37	5.43	100.00	0.9175	
14	3557	MRT-3A T329-3	8/30/95	78.73	13.58	0.58	0.08	0.07	0.54	0.09	2.31	4.02	100.00	0.9168	
15	3558	MRT-3B T329-4	8/30/95	78.67	13.58	0.58	0.08	0.07	0.54	0.09	2.34	4.05	100.00	0.9162	
16	1448	126-1254 t115-12	1/28/85	77.26	12.70	0.91	0.08	0.08	0.48	0.14	2.67	5.68	100.00	0.9156	
17	5619	EB-ASH-28cl T561-1(pop1)	4/28/200	75.91	14.40	1.13	0.12	0.09	0.53	0.23	1.98	5.61	100.00	0.9153	
18	4948	SR-042102-1 T488-1	10/26/02	77.21	13.20	0.77	0.04	0.08	0.50	0.09	3.23	4.89	100.01	0.9150	
19	4646	JRK-DV-207 T442-9	8/3/00	77.13	13.08	0.76	0.04	0.08	0.48	0.06	3.03	5.34	100.00	0.9137	
20	1449	126-1265 t115-13	1/28/86	77.58	12.59	0.89	0.07	0.08	0.44	0.12	2.36	5.87	100.00	0.9133	
21	5533	RDO-091106g-djk T545-6(total)	1/17/07	77.07	12.98	0.84	0.09	0.07	0.49	0.15	2.18	6.15	100.02	0.9125	
22	5750	RN-Gunclub 1 T573-9	6/4/09	78.43	13.19	0.66	0.07	0.06	0.42	0.10	2.18	4.88	99.99	0.9121	
23	1440	03068506A SILICIC FR.T114-1	12/12/85	77.71	12.67	0.74	0.04	0.08	0.49	0.07	3.04	5.15	99.99	0.9113	
24	3739	FLV-SP-8A T347-1	11/96	77.00	13.31	0.71	0.04	0.08	0.46	0.05	3.75	4.58	99.98	0.9110	
25	1888	JT-NOVA-1600 T150-7	11/9/87	77.18	12.98	0.81	0.04	0.08	0.48	0.06	3.42	4.96	100.01	0.9108	
26	2728	BUR832		76.96	12.98	2.57	0.01	0.06	0.47	0.15	2.42	4.38	100.00	0.9107	
27	1887	JT-NOVA-1 T150-6	11/9/87	77.01	13.15	0.75	0.04	0.08	0.48	0.05	3.31	5.14	100.01	0.9104	
28	3496	JRK-DV-23 T323-6	5/6/95	77.38	13.18	0.71	0.04	0.08	0.48	0.07	3.73	4.33	100.00	0.9085	
29	3364	M94FI-143 T315-1	11/23/94	76.92	13.12	0.73	0.04	0.08	0.48	0.07	4.02	4.55	100.01	0.9083	
30	1842	FLV-19-WW T146-7	8/25/87	77.31	13.24	0.72	0.04	0.08	0.48	0.06	3.76	4.31	100.00	0.9077	
31	5041	JRK-DV-219B T496-6	3/17/03	76.78	13.16	0.74	0.04	0.08	0.48	0.07	3.17	5.49	100.01	0.9051	
32	3742	FLV-SP-8C MINOR T347-3	11/96	76.89	13.12	0.73	0.04	0.08	0.49	0.06	3.16	5.45	100.02	0.9028	
33	5544	WA3 Borchert White Ash #3/Sku		77.40	12.58	0.88	0.03	0.08	0.54	0.11	1.83	6.56	100.01	0.9027	
34	5057	EC-110-djk T497-9	4/23/03	77.14	12.59	0.84	0.04	0.08	0.45	0.07	2.41	6.39	100.01	0.9022	
35	4073	EL-68-MD MED FE (1) T374-4	11/97	76.87	12.27	2.08	0.12	0.09	0.47	0.35	2.75	5.00	100.00	0.9021	
36	5285	BTD-DV-01 T519-9	8/24/04	77.15	12.92	0.71	0.04	0.08	0.47	0.06	3.22	5.35	100.00	0.9014	
37	4950	SR-042102-3 T488-3	10/26/02	77.21	13.24	0.86	0.05	0.07	0.49	0.07	3.32	4.70	100.01	0.9014	

Listing of 37 closest matches for COMP. NO. 5881 for elements: **Al, Si, Ca, Mn, Fe**

	C.No	Sample Number	An. Date	SiO2	Al2O3	Fe2O3	MgO	MnO	CaO	TiO2	Na2O	K2O	Total,R	Sim. Co	Sample Location
1	5881	T-PKV-WMR-C T582-3	2/16/11	78.56	13.43	0.73	0.05	0.08	0.48	0.07	2.02	4.59	100.01	1.0000	
2	1842	FLV-19-WW T146-7	8/25/87	77.31	13.24	0.72	0.04	0.08	0.48	0.06	3.76	4.31	100.00	0.9912	Below Nomlaki, above Putah,Fish Lale
3	3364	M94FI-143 T315-1	11/23/94	76.92	13.12	0.73	0.04	0.08	0.48	0.07	4.02	4.55	100.01	0.9912	
4	3736	JRK-DV-SIX SP T346-6	11/96	76.39	13.46	0.73	0.04	0.08	0.47	0.07	3.27	5.49	100.00	0.9899	Type-Mesquite Spring
5	5041	JRK-DV-219B T496-6	3/17/03	76.78	13.16	0.74	0.04	0.08	0.48	0.07	3.17	5.49	100.01	0.9887	Mesquite Springs/Zabriskie Wash?
6	5564	M07-101b T548-2	5/29/07	78.35	13.47	0.74	0.04	0.08	0.46	0.07	2.73	4.07	100.01	0.9878	Mesquite Springs
7	3496	JRK-DV-23 T323-6	5/6/95	77.38	13.18	0.71	0.04	0.08	0.48	0.07	3.73	4.33	100.00	0.9878	Mesquite Springs
8	3742	FLV-SP-8C MINOR T347-3	11/96	76.89	13.12	0.73	0.04	0.08	0.49	0.06	3.16	5.45	100.02	0.9871	Rhyolite Ridge
9	1887	JT-NOVA-1 T150-6	11/9/87	77.01	13.15	0.75	0.04	0.08	0.48	0.05	3.31	5.14	100.01	0.9866	Death Valley, CA
10	5459	JC-NH06-T1 T538-5	4/13/06	78.76	13.19	0.75	0.04	0.08	0.49	0.06	3.24	3.40	100.01	0.9865	Noble Hills, Death Valley
11	3654	JRK-DV-71 T338-7	3/96	77.25	12.67	0.73	0.04	0.08	0.48	0.05	3.48	5.21	99.99	0.9853	Zabriskie Wash
12	5580	M07-101a T548-1	5/29/07	78.23	13.42	0.75	0.04	0.08	0.46	0.06	2.76	4.18	99.98	0.9853	Mesquite Springs
13	3250	EV-1 T306-1	5/27/94	76.46	13.15	0.71	0.04	0.08	0.48	0.07	3.55	5.47	100.01	0.9850	
14	1930	SC-45B T163-5	5/14/88	77.23	12.81	0.73	0.05	0.08	0.49	0.06	3.56	4.98	99.99	0.9833	
15	4646	JRK-DV-207 T442-9	8/3/00	77.13	13.08	0.76	0.04	0.08	0.48	0.06	3.03	5.34	100.00	0.9833	Mesquite Springs
16	4507	MNM-DV-11-FC T418-3	11/5/99	76.46	12.98	0.75	0.04	0.08	0.48	0.05	3.24	5.92	100.00	0.9826	Zabriskie Wash
17	2533	FLV 161-CS HI K FRACT	3/8/91	76.91	12.98	0.74	0.03	0.08	0.49	0.08	2.96	5.74	100.01	0.9823	
18	3100	DLS-413L T284-3	11/4/93	77.06	12.95	0.72	0.04	0.08	0.47	0.06	3.15	5.48	100.01	0.9821	
19	2051	CAES#2 1683.5 T171-7	9/5/88	79.67	12.63	0.73	0.01	0.08	0.49	0.06	4.19	2.14	100.00	0.9812	
20	5288	JRK-CIT-NOV-02 T519-6	8/24/04	76.99	12.95	0.73	0.04	0.08	0.46	0.07	2.98	5.70	100.00	0.9805	
21	3739	FLV-SP-8A T347-1	11/96	77.00	13.31	0.71	0.04	0.08	0.46	0.05	3.75	4.58	99.98	0.9804	
22	3101	DLS-413M T289-4	11/4/93	77.02	12.99	0.75	0.04	0.08	0.47	0.05	3.18	5.44	100.02	0.9800	
23	1440	03068506A SILICIC FR.T114-1	12/12/85	77.71	12.67	0.74	0.04	0.08	0.49	0.07	3.04	5.15	99.99	0.9797	
24	3778	JRK-DV-80 T352-10	12/96	76.82	12.72	0.75	0.04	0.08	0.48	0.06	2.84	6.21	100.00	0.9797	Zabriskie Wash
25	5285	BTD-DV-01 T519-9	8/24/04	77.15	12.92	0.71	0.04	0.08	0.47	0.06	3.22	5.35	100.00	0.9792	
26	3175	93SgFI-2 T300-5	2/13/94	76.35	13.11	0.74	0.04	0.08	0.46	0.07	2.80	6.35	100.00	0.9786	
27	3102	DLS-413X T289-5	11/4/93	77.03	12.99	0.72	0.04	0.08	0.46	0.07	3.21	5.40	100.00	0.9785	SE Nevada, below Putah Tuff
28	4948	SR-042102-1 T488-1	10/26/02	77.21	13.20	0.77	0.04	0.08	0.50	0.09	3.23	4.89	100.01	0.9747	
29	5033	JRK-DV-221 T495-9	3/17/03	76.82	13.15	0.77	0.04	0.08	0.46	0.06	3.07	5.55	100.00	0.9727	Mesquite Springs
30	155	JOD-9-7-81E, T43-8		77.15	12.83	0.76	0.04	0.08	0.46	0.07	3.52	5.10	100.01	0.9712	
31	5456	HL-NH06-T2 T538-7	4/13/06	77.92	13.09	0.73	0.04	0.09	0.48	0.06	3.01	4.58	100.00	0.9711	Noble hills, Death Valley
32	1888	JT-NOVA-1600 T150-7	11/9/87	77.18	12.98	0.81	0.04	0.08	0.48	0.06	3.42	4.96	100.01	0.9700	
33	3176	93SgFI-3 T300-6	2/13/94	76.36	13.11	0.76	0.04	0.08	0.45	0.07	2.94	6.19	100.00	0.9692	
34	1304	TRENCH *8 (B) bulk T100-15	7/2/85	77.07	12.78	0.71	0.06	0.08	0.45	0.12	3.70	5.04	100.01	0.9685	
35	3740	FLV-SP-8B T347-2	11/96	76.94	13.23	0.72	0.04	0.09	0.48	0.06	3.75	4.69	100.00	0.9679	
36	5275	GPS-018-04 T515-5	8/24/04	77.04	13.02	0.73	0.04	0.09	0.48	0.08	3.43	5.08	99.99	0.9678	
37	3178	ES93FI-29 T300-8	2/13/94	76.44	13.05	0.75	0.04	0.08	0.44	0.07	2.92	6.20	99.99	0.96	

Yellow highlighted samples correlate to Tuff of Mesquite Springs (3.28 Ma)
Gray highlighted samples correlate to Tuff of Zabriskie Wash (3.35 Ma)

APPENDIX D - TABLE D. TEPHROCHRONOLOGIC CORRELATIONS FOR SAMPLE T-PKV-WMR-D

Listing of 37 closest matches for COMP. NO. 5882 for elements: **Na, Mg, Al, Si, K , Ca, Ti, Fe**

	C.No	Sample Number	An. Date	SiO2	Al2O3	Fe2O3	MgO	MnO	CaO	TiO2	Na2O	K2O	Total,R	Sim. Co	Sample Locations
1	5882	T-PKV-WMR-D T582-4	2/16/11	78.38	13.95	1.15	0.22	0.08	0.87	0.19	2.64	2.52	100.00	1.0000	
2	5767	15-III-00-4 399-404cm T575-9	8/4/09	78.52	13.26	1.27	0.21	0.06	1.16	0.18	2.95	2.38	99.99	0.9182	
3	2209	GOLD #1 3200' T181A-3	12/22/88	76.80	13.43	1.13	0.21	0.08	0.90	0.19	4.27	2.99	100.00	0.9134	
4	3976	JRK-DV-104 T363-6	5/97	76.85	13.40	1.12	0.22	0.06	0.88	0.20	3.76	3.53	100.02	0.9087	Tuff of Artists Drive, Death Valley
5	3556	DCNT-2 T329-2	8/30/95	78.57	13.29	1.02	0.17	0.04	0.90	0.20	2.54	3.27	100.00	0.9074	
6	1886	JT-BPT-1 T150-1	11/9/87	76.37	13.59	1.13	0.22	0.08	0.90	0.18	4.23	3.30	100.00	0.9041	
7	309	RBW-78-1339C, T11-4		78.23	13.09	1.13	0.25	0.03	1.31	0.18	3.12	2.65	99.99	0.9010	
8	3980	JRK-DV-113 MAJOR T363-10	5/97	76.69	13.52	1.12	0.23	0.07	0.91	0.20	3.79	3.47	100.00	0.9009	Tuff of Artists Drive, Death Valley
9	1288	JY-84-27A T100-11	7/2/85	76.71	13.34	1.12	0.21	0.07	0.88	0.20	4.24	3.23	100.00	0.9006	
10	10	AXL-30k-160(1), T3,4		75.88	13.91	1.13	0.22	0.07	0.83	0.20	3.43	4.33	100.00	0.9004	
11	5397	CAES#1 1143 T530-3	9/7/05	76.60	13.41	1.11	0.21	0.07	0.88	0.20	4.32	3.18	99.98	0.9001	
12	1889	JT WALL ASH T150-8	11/9/87	76.19	13.66	1.15	0.22	0.08	0.92	0.21	4.33	3.25	100.01	0.8983	
13	220	MLG-2, T12-2		76.02	13.69	1.14	0.22	0.06	0.91	0.21	4.51	3.23	99.99	0.8961	
14	2215	CAES #1 1143 T181B-4	1/23/89	76.10	13.92	1.11	0.21	0.06	0.90	0.21	4.28	3.23	100.02	0.8946	
15	3981	JRK-DV-113 HI K fract T363-10	5/97	76.31	13.37	1.11	0.21	0.07	0.86	0.18	3.17	4.71	99.99	0.8944	
16	1726	SBCM1-72-10 T137-8	4/23/87	76.48	13.31	1.09	0.23	0.06	0.91	0.19	4.45	3.28	100.00	0.8940	
17	5720	JRK-DV-031308-1 T571-8	1/20/09	76.11	13.53	1.15	0.22	0.05	0.95	0.18	3.82	4.00	100.01	0.8906	Mesquite Springs
18	5706	JRK-DV-031208-2 T569-8(pop2)	1/8/09	76.56	13.27	1.15	0.22	0.06	1.07	0.19	3.65	3.83	100.00	0.8903	Tuff of Artists Drive (?)
19	2747	BUR-996		78.38	12.45	1.02	0.18	0.06	0.87	0.19	3.17	3.66	99.98	0.8899	
20	307	RBW-78-1339A, T11-2		78.00	13.06	1.14	0.25	0.03	1.25	0.21	2.98	3.08	100.00	0.8884	
21	3555	DCNT-1 T329-1	8/30/95	78.43	13.15	0.99	0.17	0.03	0.90	0.20	2.45	3.69	100.01	0.8879	
22	4851	jf-01-07 Perkins (F/C)		76.30	13.34	1.15	0.23	0.08	0.94	0.21	4.62	3.10	99.97	0.8876	
23	2669	GM-91-M1 T240-1	9/28/91	77.28	13.20	1.14	0.21	0.04	1.23	0.17	4.20	2.54	100.01	0.8876	
24	3876	GL2-4.40 MINOR2 T357-2	2/97	77.16	13.10	1.20	0.21	0.04	1.14	0.19	3.76	3.20	100.00	0.8861	
25	484	758-328(2), T15-2, low total		78.27	12.94	1.03	0.15	0.00	0.85	0.19	3.80	2.76	99.99	0.8861	
26	1520	EMER-1 T120-4	4/29/86	77.13	13.14	1.14	0.23	0.03	1.29	0.19	3.93	2.93	100.01	0.8850	
27	11	AXL-30k-160(2), T18-7		75.92	13.63	1.13	0.20	0.04	0.86	0.18	3.57	4.47	100.00	0.8846	
28	43	BUT-1, T8-9		76.38	13.58	1.06	0.21	0.05	0.83	0.20	4.14	3.55	100.00	0.8845	
29	1744	JY 84-27B T136-13	4/22/87	76.56	13.12	1.09	0.23	0.07	0.89	0.20	4.31	3.54	100.01	0.8842	
30	2186	CUB CK POND (bulk) T179-5	12/20/88	77.75	12.72	1.11	0.22	0.04	1.22	0.20	3.53	3.20	99.99	0.8834	
31	1169	JY-84-7 7-49-4 T87-14	12/24/84	76.67	13.07	1.09	0.22	0.06	0.87	0.22	4.36	3.44	100.00	0.8831	
32	1844	FLV-21-WW T146-9	8/25/87	77.21	12.88	1.10	0.22	0.05	0.99	0.21	3.97	3.36	99.99	0.8829	
33	483	758-328(1), T7-18, pd		78.42	13.01	1.02	0.16	0.03	0.82	0.19	4.04	2.31	100.00	0.8824	
34	2050	CAES#2 1644 T171-6	9/5/88	78.18	12.63	1.09	0.18	0.04	0.99	0.20	3.65	3.04	100.00	0.8812	
35	4914	CM-PETAT-1_-100+325 T483-1	10/26/02	77.17	13.05	1.32	0.21	0.08	1.21	0.19	4.05	2.73	100.01	0.8800	
36	1733	ASW 61185-25 T-136-2	4/22/87	77.78	12.97	1.19	0.17	0.05	0.84	0.17	3.34	3.48	99.99	0.8795	
37	219	MLG-1, T12-1		76.64	13.14	1.17	0.21	0.05	0.98	0.21	4.37	3.23	100.00	0.8793	

Listing of 37 closest matches for COMP. NO. 5882 for elements: **Mg, Al, Si, Ca, Ti, Fe** Date of Update: 3/28/11

	C.No	Sample Number	An. Date	SiO2	Al2O3	Fe2O3	MgO	MnO	CaO	TiO2	Na2O	K2O	Total,R	Sim. Co	Sample Location
1	5882	T-PKV-WMR-D T582-4	2/16/11	78.38	13.95	1.15	0.22	0.08	0.87	0.19	2.64	2.52	100.00	1.0000	
2	3976	JRK-DV-104 T363-6	5/97	76.85	13.40	1.12	0.22	0.06	0.88	0.20	3.76	3.53	100.02	0.9756	Tuff of Artists Drive, Death Valley
3	10	AXL-30k-160(1), T3,4		75.88	13.91	1.13	0.22	0.07	0.83	0.20	3.43	4.33	100.00	0.9753	
4	2209	GOLD #1 3200' T181A-3	12/22/88	76.80	13.43	1.13	0.21	0.08	0.90	0.19	4.27	2.99	100.00	0.9744	
5	1886	JT-BPT-1 T150-1	11/9/87	76.37	13.59	1.13	0.22	0.08	0.90	0.18	4.23	3.30	100.00	0.9742	Black Point Tuff, Death Valley
6	5720	JRK-DV-031308-1 T571-8	1/20/09	76.11	13.53	1.15	0.22	0.05	0.95	0.18	3.82	4.00	100.01	0.9673	Tuff of Artists Drive (?)
7	220	MLG-2, T12-2		76.02	13.69	1.14	0.22	0.06	0.91	0.21	4.51	3.23	99.99	0.9672	
8	1288	JY-84-27A T100-11	7/2/85	76.71	13.34	1.12	0.21	0.07	0.88	0.20	4.24	3.23	100.00	0.9670	
9	1889	JT WALL ASH T150-8	11/9/87	76.19	13.66	1.15	0.22	0.08	0.92	0.21	4.33	3.25	100.01	0.9669	Tucki Mountain, Death Valley
10	5397	CAES#1 1143 T530-3	9/7/05	76.60	13.41	1.11	0.21	0.07	0.88	0.20	4.32	3.18	99.98	0.9662	Bristol Dry Lake, Mojave, CA
11	1726	SBCM1-72-10 T137-8	4/23/87	76.48	13.31	1.09	0.23	0.06	0.91	0.19	4.45	3.28	100.00	0.9650	
12	3981	JRK-DV-113 HI K fract T363-10	5/97	76.31	13.37	1.11	0.21	0.07	0.86	0.18	3.17	4.71	99.99	0.9646	Tuff of Artists Drive, Death Valley
13	3980	JRK-DV-113 major T363-10	5/97	76.69	13.52	1.12	0.23	0.07	0.91	0.20	3.79	3.47	100.00	0.9640	Tuff of Artists Drive, Death Valley
14	11	AXL-30k-160(2), T18-7		75.92	13.63	1.13	0.20	0.04	0.86	0.18	3.57	4.47	100.00	0.9622	
15	2215	CAES #1 1143 T181B-4	1/23/89	76.10	13.92	1.11	0.21	0.06	0.90	0.21	4.28	3.23	100.02	0.9600	Bristol Dry Lake, Mojave, CA
16	1744	JY 84-27B T136-13	4/22/87	76.56	13.12	1.09	0.23	0.07	0.89	0.20	4.31	3.54	100.01	0.9582	
17	5706	JRK-DV-031208-2 T569-8(pop2)	1/8/09	76.56	13.27	1.15	0.22	0.06	1.07	0.19	3.65	3.83	100.00	0.9569	
18	43	BUT-1, T8-9		76.38	13.58	1.06	0.21	0.05	0.83	0.20	4.14	3.55	100.00	0.9547	
19	1169	JY-84-7 7-49-4 T87-14	12/24/84	76.67	13.07	1.09	0.22	0.06	0.87	0.22	4.36	3.44	100.00	0.9544	
20	4851	jf-01-07 Perkins (F/C)		76.30	13.34	1.15	0.23	0.08	0.94	0.21	4.62	3.10	99.97	0.9528	
21	247	ONT-1, T14-7		76.16	13.63	1.14	0.19	0.05	0.81	0.20	4.40	3.42	100.00	0.9475	
22	5480	FLV-119-WW(light) T539-8	5/25/06	76.75	12.91	1.17	0.18	0.05	0.90	0.19	3.33	4.53	100.01	0.9454	
23	219	MLG-1, T12-1		76.64	13.14	1.17	0.21	0.05	0.98	0.21	4.37	3.23	100.00	0.9416	
24	1844	FLV-21-WW T146-9	8/25/87	77.21	12.88	1.10	0.22	0.05	0.99	0.21	3.97	3.36	99.99	0.9414	
25	1556	WA 3-30 T127-1	7/18/86	76.48	13.28	1.20	0.20	0.05	0.92	0.21	4.06	3.60	100.00	0.9409	
26	5142	KT262-03-S3 T504-9	9/2/03	76.31	13.38	1.28	0.19	0.05	0.82	0.19	4.22	3.56	100.00	0.9396	
27	3515	JRK-DV-39	7/6/95	75.41	13.82	1.20	0.24	0.06	0.93	0.22	4.55	3.56	99.99	0.9378	
28	5065	SL-AS9-I T498-5	4/23/03	75.76	13.38	1.32	0.19	0.03	0.84	0.19	3.74	4.55	100.00	0.9377	
29	525	GPL-G, T53-2	03/25/83	76.95	12.97	1.10	0.22	0.03	1.15	0.19	3.91	3.49	100.01	0.9374	
30	4852	jf-01-07 (F/C) 2		76.41	13.36	1.04	0.23	0.08	0.94	0.21	4.62	3.11	100.00	0.9373	
31	2328	FLV-87-HT T192-6	6/1/89	75.68	13.42	1.25	0.21	0.05	0.85	0.23	3.61	4.70	100.00	0.9342	
32	1580	ASW 61186-3 T128-12	8/19/86	77.09	12.91	1.12	0.21	0.04	1.01	0.21	3.50	3.92	100.01	0.9339	
33	834	GS-80		75.84	13.44	1.16	0.19	0.05	0.86	0.23	4.11	4.11	99.99	0.9334	
34	1182	OP84-193B t89-12	2/28/85	77.28	12.77	1.09	0.19	0.05	0.98	0.19	4.07	3.38	100.00	0.9334	
35	3876	GL2-4.40 MINOR2 T357-2	2/97	77.16	13.10	1.20	0.21	0.04	1.14	0.19	3.76	3.20	100.00	0.9333	
36	5477	FLV-119-WW(dark) T539-7	5/25/06	76.85	12.91	1.16	0.18	0.05	0.88	0.17	3.18	4.62	100.00	0.9331	
37	2377	033089-H1M T202-8	1/7/90	76.21	13.23	1.11	0.20	0.04	0.89	0.23	3.59	4.49	99.99	0.9331	

Yellow highlighted samples correlate to Tuff of Artists Drive (>3.58 Ma, aka lower Nomlaki group)
Gray highlighted samples correlate to Nomlaki Tuff (3.27 Ma)

APPENDIX D - TABLE E. TEPHROCHRONOLOGIC CORRELATIONS FOR SAMPLE T-PKV-WMR-E

Listing of 37 closest matches for COMP. NO. 5883 for elements: **Na, Al, Si, K , Ca, Mn**

	C.No	Sample Number	An. Date	SiO2	Al2O3	Fe2O3	MgO	MnO	CaO	TiO2	Na2O	K2O	Total,R	Sim. Co	Sample Locations
1	5883	T-PKV-WMR-E T582-5	2/16/11	76.97	13.97	0.54	0.04	0.07	0.69	0.05	2.96	4.72	100.01	1.0000	
2	3720	EL-61-TC T344-4	11/96	77.34	13.34	0.81	0.14	0.07	0.69	0.11	2.49	5.01	100.00	0.9556	
3	205	LD-96, T3,4		76.62	13.27	0.92	0.05	0.07	0.66	0.08	3.54	4.79	100.00	0.9539	
4	3033	KIRK-1 crse T281-8	6/22/93	76.10	12.48	2.16	0.01	0.07	0.72	0.14	3.00	5.32	100.00	0.9524	
5	726	LD-96		77.04	13.01	0.89	0.05	0.07	0.65	0.08	3.50	4.70	99.99	0.9523	
6	5771	DW-182-GE-08 T569-4	1/8/2009	75.88	13.56	1.97	0.06	0.06	0.68	0.16	2.78	4.86	100.01	0.9516	
7	5146	DPB-10 T211-1	9/2/03	78.10	12.89	0.85	0.05	0.07	0.60	0.08	2.99	4.36	99.99	0.9486	
8	3981	JRK-DV-113 HI K fract T363-10	5/97	76.31	13.37	1.11	0.21	0.07	0.86	0.18	3.17	4.71	99.99	0.9471	
9	2007	FLV-59-CS T167-1	7/19/88	75.66	13.61	0.96	0.12	0.07	0.67	0.13	3.33	5.46	100.01	0.9469	
10	1950	WL-4-8B (21.275M) T162-5	5/14/88	76.67	13.13	0.82	0.06	0.07	0.65	0.12	3.47	5.01	100.00	0.9455	
11	1664	TPS-314 T132-7	10/21/86	76.37	14.02	0.64	0.09	0.06	0.70	0.08	3.44	4.60	100.00	0.9444	
12	1468	RABEK Y8 T115-6 CORR K	1/27/86	78.72	12.90	0.57	0.09	0.07	0.63	0.08	2.97	3.98	100.01	0.9423	
13	1452	RABEK Y8 T115-6	01/27/86	78.73	12.90	0.57	0.09	0.07	0.63	0.08	2.97	3.97	100.01	0.9420	
14	1668	LAKEVIEW-6 T132-11	10/21/86	76.51	13.75	0.77	0.07	0.07	0.56	0.08	3.38	4.82	100.01	0.9408	
15	2441	DPB-10 T211-1	8/14/90	77.90	12.89	0.84	0.06	0.07	0.60	0.08	3.17	4.39	100.00	0.9407	
16	5039	JRK-DV-227 T496-4	3/17/03	76.57	13.45	0.61	0.07	0.07	0.59	0.09	3.11	5.45	100.01	0.9384	
17	1568	WLC-85-2 (10.65M) T127-14	8/18/86	76.61	13.40	0.87	0.03	0.06	0.70	0.05	3.52	4.76	100.00	0.9383	
18	5028	JRK-DV-215 T495-4	3/17/03	76.49	13.46	0.63	0.07	0.07	0.58	0.09	3.00	5.61	100.00	0.9376	
19	1847	FLV-24-WW T146-12	8/25/87	76.71	13.02	0.67	0.07	0.07	0.63	0.08	3.18	5.58	100.01	0.9364	
20	438	9-85-2A, T6-1		77.06	12.66	0.54	0.02	0.07	0.74	0.04	3.07	5.79	99.99	0.9361	
21	4506	MNM-DV-10-FC T418-2	11/5/99	76.29	13.30	0.54	0.03	0.07	0.67	0.05	3.42	5.64	100.01	0.9361	
22	4502	MNM-DV-6-FC T417-8	11/5/99	76.28	13.20	0.52	0.03	0.07	0.68	0.06	3.38	5.78	100.00	0.9356	
23	4631	TRT-1 T441-6	6/29/00	76.94	13.30	0.60	0.07	0.07	0.57	0.08	3.24	5.13	100.00	0.9352	
24	1046	DSDP 36-10-2 SSA3, T78-5	07/18/84	77.04	13.17	0.81	0.02	0.06	0.67	0.03	3.50	4.69	99.99	0.9349	
25	4092	DF-2X-1-2 T375-9	11/97	76.68	13.54	0.52	0.05	0.07	0.76	0.05	3.81	4.51	99.99	0.9343	
26	1436	08088503 T114-7	12/12/85	77.53	12.69	0.70	0.06	0.07	0.58	0.09	3.14	5.13	99.99	0.9341	
27	4645	JRK-DV-206 T442-8	8/3/00	75.76	13.56	0.89	0.10	0.08	0.68	0.14	3.10	5.69	100.00	0.9333	
28	5641	JC-108-CH103 T563-6	9/25/08	77.27	14.18	0.76	0.03	0.06	0.64	0.05	2.76	4.25	100.00	0.9331	
29	4721	GH-93-1 T460-8	4/20/01	77.28	12.94	0.85	0.06	0.07	0.61	0.07	3.57	4.54	99.99	0.9329	
30	3719	EL-60-TC T344-3	11/96	77.35	13.29	0.83	0.15	0.08	0.69	0.13	2.47	5.02	100.01	0.9327	
31	10	AXL-30k-160(1), T3,4		75.88	13.91	1.13	0.22	0.07	0.83	0.20	3.43	4.33	100.00	0.9322	
32	5679	ALT-2A-N T567-1(Pop2)	1/8/09	74.24	12.90	2.68	0.08	0.07	0.66	0.22	2.92	6.23	100.00	0.9314	
33	3395	94CB 4054 T316-1	1/6/95	75.71	12.56	2.10	0.01	0.07	0.73	0.14	3.44	5.25	100.01	0.9312	
34	859	LM-15		77.08	13.23	0.80	0.13	0.06	0.78	0.10	3.21	4.61	100.00	0.9310	
35	2124	EUR-88-N50 T176-6	10/27/88	76.55	12.99	0.92	0.04	0.07	0.71	0.07	2.66	5.99	100.00	0.9305	
36	4845	OL-CST-1 HiFeCa T470-7	10/18/01	76.46	13.05	0.98	0.04	0.07	0.63	0.07	3.84	4.86	100.00	0.9304	
37	5030	JRK-DV-217 T495-6	3/17/03	76.76	13.39	0.55	0.06	0.07	0.54	0.09	2.95	5.60	100.01	0.9296	L. Badlands Tuffs 2.89-2.58 Ma

Listing of 37 closest matches for COMP. NO. 5883 for elements: **Al, Si, Ca, Mn, Fe** Date of Update: 3/28/11

	C.No	Sample Number	An. Date	SiO2	Al2O3	Fe2O3	MgO	MnO	CaO	TiO2	Na2O	K2O	Total,R	Sim. Co	Sample Location
1	5883	T-PKV-WMR-E T582-5	2/16/11	76.97	13.97	0.54	0.04	0.07	0.69	0.05	2.96	4.72	100.01	1.0000	
2	4506	MNM-DV-10-FC T418-2	11/5/99	76.29	13.30	0.54	0.03	0.07	0.67	0.05	3.42	5.64	100.01	0.9828	Corr. 9-85-2A; 3.14 ±0.15 Ma
3	4502	MNM-DV-6-FC T417-8	11/5/99	76.28	13.20	0.52	0.03	0.07	0.68	0.06	3.38	5.78	100.00	0.9769	Corr. 9-85-2A; 3.14 ±0.15 Ma
4	438	9-85-2A, T6-1		77.06	12.66	0.54	0.02	0.07	0.74	0.04	3.07	5.79	99.99	0.9675	Coso, K-Ar: 3.14±0.15 Ma, avg
5	4092	DF-2X-1-2 T375-9	11/97	76.68	13.54	0.52	0.05	0.07	0.76	0.05	3.81	4.51	99.99	0.9673	
6	1697	CNP-1-3 T135-2	1/16/87	76.78	13.38	0.52	0.04	0.07	0.80	0.04	3.83	4.55	100.01	0.9562	
7	1468	RABEK Y8 T115-6 CORR K	1/27/86	78.72	12.90	0.57	0.09	0.07	0.63	0.08	2.97	3.98	100.01	0.9523	
8	1452	RABEK Y8 T115-6	01/27/86	78.73	12.90	0.57	0.09	0.07	0.63	0.08	2.97	3.97	100.01	0.9523	
9	3597	EL-4-FL T333-2	3/96	76.21	13.14	0.56	0.04	0.07	0.59	0.06	3.50	5.83	100.00	0.9500	Corr Mt Jackson,NV ash 2.9 Ma
10	5649	VM26-136 386-387 T564-4	11/13/08	79.02	13.23	0.58	0.09	0.07	0.61	0.10	2.87	3.42	99.99	0.9472	
11	4505	MNM-DV-9-FC T418-1	11/5/99	76.47	13.06	0.53	0.02	0.08	0.65	0.03	3.56	5.60	100.00	0.9454	
12	5822	Guaytan3-19-1 T578-7	11/24/09	77.24	13.01	0.60	0.08	0.07	0.62	0.11	3.97	4.30	100.00	0.9453	
13	5030	JRK-DV-217 T495-6	3/17/03	76.76	13.39	0.55	0.06	0.07	0.54	0.09	2.95	5.60	100.01	0.9440	L. BadlandsTuffs 2.81-2.58 Ma
14	3841	SPT 91996-1 T355-3	1/97	75.72	13.52	0.68	0.06	0.07	0.71	0.07	2.33	6.85	100.01	0.9435	
15	5366	NA-30C T526-8	05/31/20	78.46	13.08	0.54	0.09	0.07	0.55	0.09	2.18	4.93	99.99	0.9429	
16	5823	Guaytan3-19-2 T578-8	11/24/09	77.27	13.01	0.58	0.08	0.07	0.59	0.11	4.03	4.26	100.00	0.9427	
17	4056	JRK-DV-115 T372-7	10/97	77.20	13.12	0.56	0.06	0.07	0.56	0.07	3.36	5.00	100.00	0.9424	
18	5648	VM17-18 370-371 T564-3	1/13/08	79.05	13.22	0.59	0.09	0.07	0.60	0.10	2.84	3.44	100.00	0.9410	
19	2012	SAFZ-3 T167-6	7/19/88	76.57	13.77	0.59	0.07	0.08	0.64	0.07	4.25	3.97	100.01	0.9397	
20	5039	JRK-DV-227 T496-4	3/17/03	76.57	13.45	0.61	0.07	0.07	0.59	0.09	3.11	5.45	100.01	0.9396	
21	5858	Guaytan(combo)		77.43	13.03	0.59	0.09	0.07	0.59	0.10	3.84	4.27	100.01	0.9394	
22	5651	RC9-26P 323-342 T564-6	11/13/08	78.97	13.23	0.61	0.10	0.07	0.61	0.09	2.89	3.43	100.00	0.9382	
23	4631	TRT-1 T441-6	6/29/00	76.94	13.30	0.60	0.07	0.07	0.57	0.08	3.24	5.13	100.00	0.9355	
24	1664	TPS-314 T132-7	10/21/86	76.37	14.02	0.64	0.09	0.06	0.70	0.08	3.44	4.60	100.00	0.9350	
25	1860	FLV-33-WW T147-7	9/30/87	76.87	12.95	0.64	0.07	0.07	0.62	0.12	2.69	5.96	99.99	0.9336	
26	3558	MRT-3B T329-4	8/30/95	78.67	13.58	0.58	0.08	0.07	0.54	0.09	2.34	4.05	100.00	0.9328	
27	3557	MRT-3A T329-3	8/30/95	78.73	13.58	0.58	0.08	0.07	0.54	0.09	2.31	4.02	100.00	0.9327	
28	5028	JRK-DV-215 T495-4	3/17/03	76.49	13.46	0.63	0.07	0.07	0.58	0.09	3.00	5.61	100.00	0.9310	
29	1337	BE-25 T106-2	8/29/85	77.14	12.68	0.56	0.07	0.07	0.54	0.10	1.40	7.44	100.00	0.9305	
30	5365	NA-51A T526-7	05/31/20	78.55	13.10	0.52	0.09	0.07	0.53	0.09	2.23	4.83	100.01	0.9297	
31	1847	FLV-24-WW T146-12	8/25/87	76.71	13.02	0.67	0.07	0.07	0.63	0.08	3.18	5.58	100.01	0.9295	
32	1667	TPS-317 T132-10	10/21/86	75.92	14.36	0.51	0.05	0.06	0.78	0.03	3.75	4.53	99.99	0.9291	
33	3536	TPSS-353 POP2 T326-8	7/6/95	76.80	13.20	0.47	0.05	0.06	0.67	0.06	3.35	5.36	100.02	0.9282	
34	5647	VM15-51 360-361 T564-2	11/13/08	77.82	13.94	0.63	0.09	0.06	0.74	0.08	2.80	3.85	100.01	0.9267	
35	1699	CNP-3-4 T135-4	1/16/87	76.81	13.27	0.52	0.06	0.06	0.80	0.06	3.83	4.60	100.01	0.9261	
36	1701	CNP-3-6 T135-6	1/16/87	76.59	13.45	0.55	0.05	0.06	0.83	0.03	3.86	4.58	100.00	0.9256	
37	1507	BE-249 T119-8	4/28/86	77.00	12.75	0.57	0.07	0.07	0.53	0.08	1.77	7.16	100.00	0.9256	

Yellow highlighted samples correlate to Coso tephra (3.14 ±0.15 Ma, K-Ar), possibly as young as ~2.6 to ~2.9 Ma, lower tuffs of Badlands.

APATITE (U-Th[Sm])/He DATA

	SAMPLE #	AGE (MA)	ERROR (MA)
1	SFSR01-1	10.8	0.65
	SFSR01-2	10.1	0.61
	SFSR01-3	14.2	0.85
12	SFSR12-1	7.4	0.44
15	SFSR15-1	35.6	2.13
	SFSR15-2	9.0	0.54
	SFSR15-3	8.7	0.52
16	SFSR16-1	-3.0	-0.18
	SFSR16-2	12.8	0.77
17	SFSR17-1	0.3	0.02
	SFSR17-2	5.4	0.33
20	SFSR20-1	5.3	0.32
	SFSR20-2	36.8	2.21
	SFSR20-3	2.9	0.17
22	SFSR22-1	3.4	0.21
26	SFSR26-1	6.4	0.38
35	SFSR35-1	-157.3	-9.44

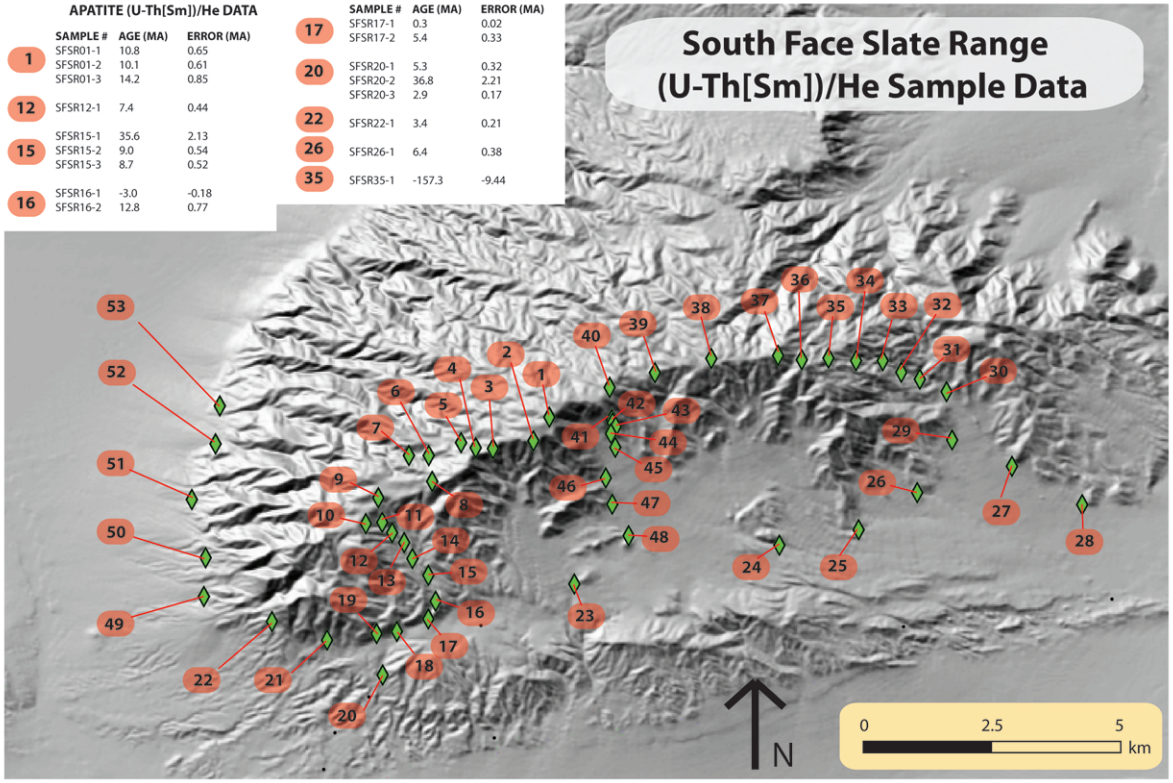

ZIRCON (U-Th[Sm])/He DATA

	SAMPLE #	AGE (MA)	ERROR (MA)
1	zSFSR01-1	44.7	3.58
	zSFSR01-2	55.4	4.43
	zSFSR01-3	45.9	3.67
2	zSFSR02-1	55.8	4.47
	zSFSR02-2	32.5	2.60
	zSFSR02-3	56.5	4.52
3	zSFSR03-1	32.0	2.56
	zSFSR03-2	43.1	3.44
	zSFSR03-3	50.7	4.05
4	zSFSR04-1	53.9	4.32
	zSFSR04-2	57.6	4.61
	zSFSR04-3	58.4	4.67
5	zSFSR05-1	61.0	4.88
	zSFSR05-2	51.2	4.09
	zSFSR05-3	48.5	3.88
6	zSFSR06-1	36.0	2.88
	zSFSR06-2	29.3	2.35
	zSFSR06-3	33.3	2.66
7	zSFSR07-1	52.3	4.18
	zSFSR07-2	50.0	4.00
	zSFSR07-3	49.0	3.92
8	zSFSR08-1	43.2	3.46
	zSFSR08-2	49.8	3.98
	zSFSR08-3	47.3	3.78
9	zSFSR09-1	29.2	2.34
	zSFSR09-2		Lost Data
	zSFSR09-3	43.1	3.44
10	zSFSR10-1	69.5	5.56
	zSFSR10-2	27.2	2.18
	zSFSR10-3	33.1	2.65
11	zSFSR11-1	46.8	3.74
	zSFSR11-2	49.6	3.97
	zSFSR11-3	46.7	3.74
12	zSFSR12-1	44.6	3.57
	zSFSR12-2	35.4	2.83
	zSFSR12-3	32.9	2.64
13	zSFSR13-1	62.6	5.01
	zSFSR13-2	45.8	3.66
	zSFSR13-3	49.3	3.94
14	zSFSR14-1	37.2	2.98
	zSFSR14-2	45.9	3.67
	zSFSR14-3	27.2	2.18
15	zSFSR15-1	44.5	3.56
	zSFSR15-2	41.3	3.30
	zSFSR15-3	44.8	3.58
16	zSFSR16-1	46.9	3.75
	zSFSR16-2	45.7	3.65
	zSFSR16-3	42.6	3.41
17	zSFSR17-1	49.7	3.97
	zSFSR17-2	52.1	4.17
	zSFSR17-3	39.7	3.18
18	zSFSR18-1	45.6	3.65
	zSFSR18-2	37.9	3.03
	zSFSR18-3	38.1	3.05
19	zSFSR19-1	46.9	3.75
	zSFSR19-2	43.1	3.45
	zSFSR19-3	40.7	3.25
20	zSFSR20-1	35.0	2.80
	zSFSR20-2	78.6	6.29
	zSFSR20-3	48.0	3.84
21	zSFSR21-1	40.5	3.24
	zSFSR21-2	33.9	2.71
	zSFSR21-3	32.9	2.63
22	zSFSR22-1	57.1	4.57
	zSFSR22-2	38.4	3.07
	zSFSR22-3	43.7	3.50
23	zSFSR23-1	51.0	4.08
	zSFSR23-2	46.7	3.74
	zSFSR23-3	55.0	4.40
24	zSFSR24-1	42.8	3.42
	zSFSR24-2	56.4	4.51
	zSFSR24-3	61.0	4.88
25	zSFSR25-1		No Data
	zSFSR25-2		No Data
	zSFSR25-3		No Data
26	zSFSR26-1	57.7	4.61
	zSFSR26-2	49.7	3.98
	zSFSR26-3	50.4	4.04
27	zSFSR27-1	60.0	4.80
	zSFSR27-2	56.9	4.55
	zSFSR27-3	61.4	4.91
28	zSFSR28-1	59.7	4.78
	zSFSR28-2	56.0	4.48
	zSFSR28-3	51.7	4.14
29	zSFSR29-1	51.9	4.15
	zSFSR29-2		Lost Data
	zSFSR29-3	47.6	3.81
30	zSFSR30-1		No Data
	zSFSR30-2		No Data
	zSFSR30-3		No Data
31	zSFSR31-1		No Data
	zSFSR31-2		No Data
	zSFSR31-3		No Data
32	zSFSR32-1		No Data
	zSFSR32-2		No Data
	zSFSR32-3		No Data
33	zSFSR33-1		No Data
	zSFSR33-2		No Data
	zSFSR33-3		No Data
34	zSFSR34-1		No Data
	zSFSR34-2		No Data
	zSFSR34-3		No Data
35	zSFSR35-1	42.4	3.39
	zSFSR35-2	45.1	3.61
	zSFSR35-3	48.4	3.88
36	zSFSR36-1		No Data
	zSFSR36-2		No Data
	zSFSR36-3		No Data
37	zSFSR37-1		No Data
	zSFSR37-2		No Data
	zSFSR37-3		No Data
38	zSFSR38-1	47.7	3.82
	zSFSR38-2	44.6	3.57
	zSFSR38-3	45.1	3.61
39	zSFSR39-1	66.2	5.29
	zSFSR39-2	63.5	5.08
	zSFSR39-3	67.9	5.43
40	zSFSR40-1	42.1	3.37
	zSFSR40-2	27.8	2.22
	zSFSR40-3	25.9	2.07
41	zSFSR41-1	49.3	3.94
	zSFSR41-2	48.2	3.85
	zSFSR41-3	62.4	5.00
42	zSFSR42-1	54.6	4.37
	zSFSR42-2	49.1	3.93
	zSFSR42-3	40.8	3.27
43	zSFSR43-1		No Data
	zSFSR43-2		No Data
	zSFSR43-3		No Data
44	zSFSR44-1		No Data
	zSFSR44-2		No Data
	zSFSR44-3		No Data
45	zSFSR45-1		No Data
	zSFSR45-2		No Data
	zSFSR45-3		No Data
46	zSFSR46-1		No Data
	zSFSR46-2		No Data
	zSFSR46-3		No Data
47	zSFSR47-1		No Data
	zSFSR47-2		No Data
	zSFSR47-3		No Data
48	zSFSR48-1		No Data
	zSFSR48-2		No Data
	zSFSR48-3		No Data
49	zSFSR49-1		No Data
	zSFSR49-2		No Data
	zSFSR49-3		No Data
50	zSFSR50-1		No Data
	zSFSR50-2		No Data
	zSFSR50-3		No Data
51	zSFSR51-1		No Data
	zSFSR51-2		No Data
	zSFSR51-3		No Data
52	zSFSR52-1		No Data
	zSFSR52-2		No Data
	zSFSR52-3		No Data
53	zSFSR53-1		No Data
	zSFSR53-2		No Data
	zSFSR53-3		No Data

Sample collection and processing by:
William Rittase (2010-2012)

Data reduction and interpretation by:
Dr. Danny Stockli
Dr. J. Douglas Walker

University of Kansas, Dept. of Geology

PLATES

PLATE 1

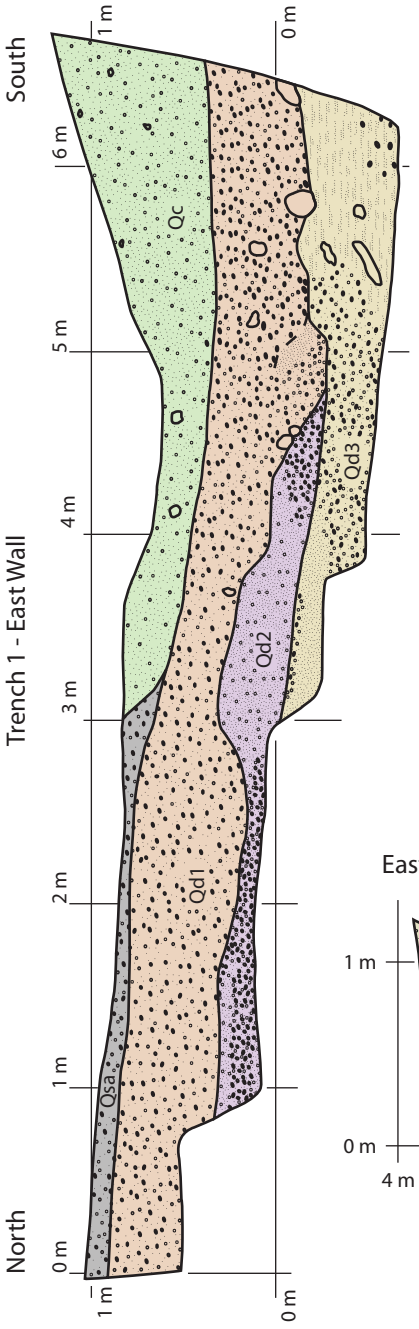

Qc -- Late Holocene shutter ridge colluvium; unconsolidated and unsorted coarse sand, silt and gravel (few clasts are >5 cm); most clasts are free of CaCO3, but ~10% have stage I petrocalcic horizons and are likely recycled from shutter ridge; open void spaces between gravel clasts; non-indurated; clasts are not imbricated; medium-gray/tan matrix color; 5-10 cm thick soil development.

Qsa -- Late Holocene soil development on Qd1 deposit; bioturbated zone 5-10 cm deep; incipient Av horizon.

Qd1 -- Younger subfacies of late Holocene debris flow (3.5-4 ka); moderately indurated, matrix-supported debris flow; poorly sorted coarse sand and gravel conglomerate (10% of clasts 5-10 cm across); poor bedding with scour beds common; medium-gray/light-tan color; stage I petrocalcic horizons; no salt shattering of metamorphic clasts.

Qd2 -- Older subfacies of late Holocene debris flow; slightly coarser sand/gravel; stage II petrocalcic horizons; no salt shattering of metamorphic clasts.

Qd3 -- Well-indurated, matrix-supported debris flow; poorly sorted gravels, sand & silt (with larger zones of arkosic sands and silt that are more med-tan/gray and retain moisture better); stage II & III petrocalcic development (slate & schist clasts display "salt shattering" and break easily).

Trench Scale:
~1 inch = 1 meter

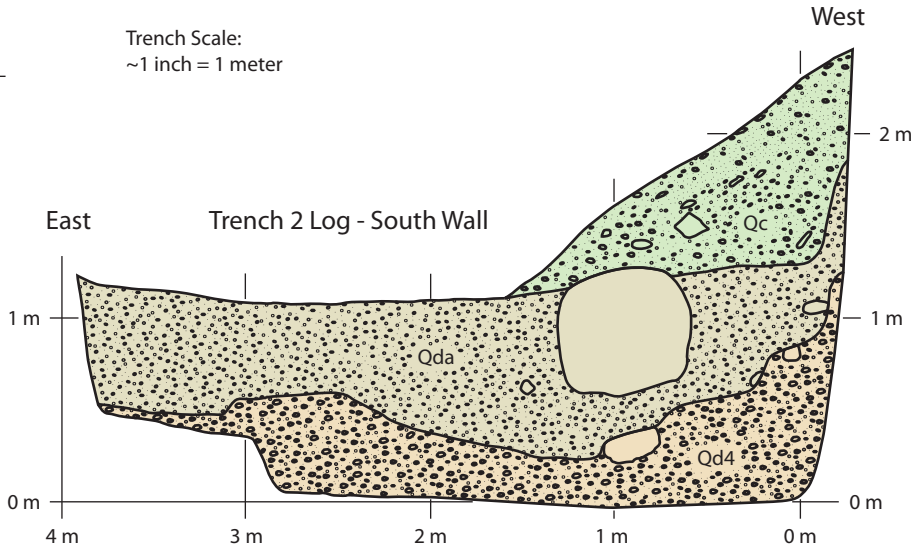

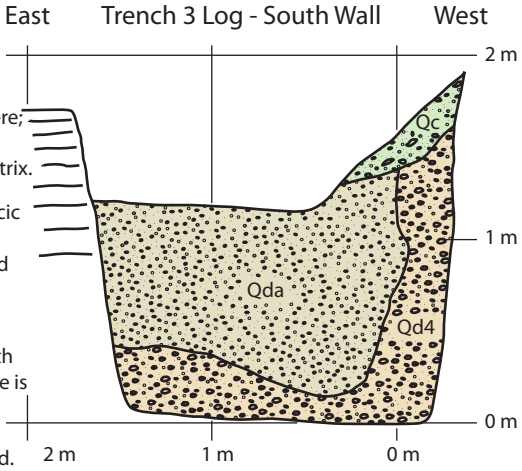

Qc -- Modern stream riser colluvium; open voids between gravel & boulder clasts; crude bedding & sorting on collapse/scree slopes, unsorted elsewhere; light tan/gray matrix color; no soil development; some clasts have stage I petrocalcic coating & are recycled from shutter ridge; weakly indurated matrix.

Qda -- Late Holocene alluvium (younger than Qd1 in trench 1); no petrocalcic development except for a few older, recycled clasts; poorly sorted, coarse gravel conglomerate with a few large boulders 20-100 cm across buttressed against western channel wall; no void spaces between clasts; good to poor bedding; weakly indurated matrix.

Qd4 -- Ca. 30 ka shutter ridge alluvium; matrix-supported fanglomerate with clasts 3-15 cm across; stage I & II petrocalcic horizons on clasts (deposit here is ~3 m below true surface and comprises a C soil horizon (i.e., weaker soil deveopment); no salt shattering of metamorphic clasts; weak to moderate matrix induration; light tan to gray color; poorly to unsorted; poorly bedded.